Secure Web Server System Resources Utilization

Liberios Vokorokos, Anton Baláž, Norbert Ádám

Technical University of Košice, Letná 9, 042 00 Košice, Slovakia,
liberios.vokorokos@tuke.sk, anton.balaz@tuke.sk, norbert.adam@tuke.sk

Abstract: One of the main goals of an operating system is the efficient usage of system resources and their management. Modern systems offer complex mechanisms for the management of these resources. Their system-wide use may be separated into multiple layers – from the lowest (the operating system kernel) to the highest (various virtualization techniques). Somewhere in the middle are the applications consuming these system resources. An example of such an application is the Apache web server. It implements some of the resource management mechanisms at application level. However, the system contains elements, the management of which is not possible at application level or its implementation has a significant overhead and may negatively affect the performance and secure usage of the server. The aim of the study is to create a more efficient resource management mechanism at the level of the Apache web server. The proposed architecture allows the treatment of possible security threats, such as DoS attacks, makes the use of system resources more efficient, thus – indirectly – it also addresses the environmental impacts of data centers. The reason for selecting the Apache web server as the referential implementation of the resource usage improvement are its market share and its open source nature, which renders making amendments to the server simple.

Keywords: security; system resources; management; Apache; cgroups; CGI

1 Introduction

System resource management is a topic often related to operating system mechanisms. Solving system resource management problems is therefore left over to the authors of operating systems or architects. Even though it is required – to a certain extent – that the operating system manages most of the system resources, there are cases, when the task of system resource management has to be left over to the application, or to ensure that the application increases the level of use of the allocated resources.

With today's web applications at hand, web servers often have to deal with enormous loads – millions of web content generation requests coming from their clients. Generating content has a price in terms of memory, computation time,

power, CPU time, etc., especially if one has to deal with extreme amount of requests. By improving resource management we may improve security, make the use of the resources more efficient and – in the end – decrease the power costs by improving system usage efficiency.

We know of experiments to improve the resource usage of web servers used in in-house solutions, producing certain results [1], nevertheless there is still room for improvement – both in the field of implementation or the results themselves. With the advent of new technologies, new approaches are being developed to improve and make the current resource management solutions more efficient.

This work describes the approaches in use, presents the new technologies available in the field of resource management, and – most importantly – implements an improvement in this field and proposes the implementation of such an extension of the Apache web server.

2 Efficient Use of System Resources

In modern operating systems, the use of system resources is considered to be a more or less solved problem. Resource management is being done efficiently at the lowest OS level by the kernel, which may be configured to a certain extent, depending on the system in use.

Recently, great effort has been put into higher level system resource management, mainly to separate programs executed at application level and the operating system itself. This field is represented by various virtualization technologies – for their application in modern systems, seen in the work G. Banga et al.

2.1 Virtualization and Separation

Virtualization is a method of executing various virtual environments (virtual machines) on a single physical machine.

The virtual environment is where the programs are executed; it behaves as a separate entity and represents a real computer system. The individual environments are mutually isolated and thus have no knowledge of the existence of similar environments, if multiple virtual environments are being executed simultaneously on a single physical machine. However, this kind of isolation requires full resource management, therefore in the text below we have described the approaches used in virtualization and resource management.

Virtualization is based on the principle of having virtual machine monitor software managing the allocation of computer resources to the respective virtual environments. This monitor is the abstraction layer between the hardware – the physical machine – and the given virtual environment. There are multiple types of

virtualization, depending on the executed virtual environment and the implementation of this monitor.

Kolyshkin described three basic virtualization principles, differing in the methods and conditions of execution of the virtual environments [1]. These are:

- Full virtualization or emulation
- Para-virtualization
- OS-level virtualization

Each of these approaches has its advantages and disadvantages, related to the execution performance of the given virtual environment. The respective virtualization approaches are thus compromises between performance and modifications made to the executed system.

2.2 OS-level Virtualization

Virtual environments using this approach are called containers – they represent the execution environment of the operating system [5]. Operating systems running on a single kernel are being executed in the individual containers. The resources are allocated to such environments upon creation and they are often altered dynamically during the execution.

Applications, as well as the individual environments behave as individual units, which may be isolated (seen from the other containers) [10]. Such isolation is not performed by virtualization of the whole operating system, just the mechanisms offered by the operating system itself (the kernel), which executes all containers. These mechanisms include process identifiers (PIDs), user identifiers (UIDs), shared memory, etc. Contexts and filters are created to perform the separation of the respective containers. Contexts represent the separation of the identifiers used in the said mechanisms: each container has its own context of identifiers, relevant only for it. On the other side, filters control the access of the respective containers to the kernel objects by controlling the privileges of the individual containers.

There are multiple container implementations available in operating systems running a Linux kernel. The most widely known is OpenVZ Linux VServer, while the newest addition to these is a solution called LXC Linux containers. They differ is the way they implement the container and resource management levels. To prevent attacks between the environments, the system must distribute the resources among the respective virtual environments securely.

These containers often implement processor time management in two levels [11]. One level is the CPU scheduler of the operating system. The second level is the scheduler of the respective implementation, which is either part of the amendments applied to the system or a separate entity, similar to the virtual machine monitor. CPU time scheduling is then done using known algorithms.

The remaining resources, such as physical memory, disk space, etc. may be managed in the respective containers separately by using the appropriate memory management mechanisms [16] or a resource driver may be introduced, such as a memory controller [17], which can limit the amount of memory available to certain application groups (e.g. to an application in the context of a specific container).

Interesting is the implementation of system resource limitations in LXC Linux containers. It uses various novel attributes of the Linux kernel, even a mechanism called Control Groups [9]. This allows setting constraints using control groups. The running processes (i.e. tasks) are then allocated to the respective groups as needed. The system kernel will then allocate the system resources in accordance with the rules specified in the respective groups.

From this point, the respective groups (cgroups) are treated as standard Linux processes. Thus, they form a certain hierarchy and the descendant groups in the hierarchy inherit the attributes, in this case the constraints of the parent groups. These group constraints are implemented by means of so-called subsystems. These are linked to the directory structure of the system. The whole directory structure of the link represents a hierarchy of constraints – it contains files of the constraint rule applicable to the individual subsystems. The basic subsystems, thus also the system resources, influenced by the cgroups are the following:

- CPU – controlling processor access of the tasks by using the CPU scheduler,
- CPUACCT – generates messages concerning the usage of CPU resources,
- CPUSET – assigns the individual processors and memory nodes to tasks,
- MEMORY – manages task memory constraints,
- BLKIO – manages I/O device data transfer constraints,
- NET_CLS – marks packets with identifiers for the network traffic controller,
- NET_PRIO – sets the network traffic priority in case of the network interfaces.

The newly created group is a directory in each of the subsystems in the directory structure. It also contains the files of the respective subsystems required to define new constraints, as well as the file with the identifiers of running processes belonging to the particular group.

Cgroups may be used even beyond the scope of virtualization tools to separate applications and thus this technique is an appropriate candidate for the implementation of the solution – our improvement to web server resource management.

The advantage of virtualization at the level of the operating system is the performance, comparable to that of native code execution. By removing the virtualization layer – the virtual machine monitor – the execution costs decrease.

The separation of the respective virtual environments is not as significant as with emulation or paravirtualization, but it is sufficient enough. The security of the system as such is ensured by the separation of the important applications into separate environments. Dynamic resource management allows runtime application migration.

A disadvantage may be the requirement of using the same kernel with the virtualized operating systems. Thus, in case of Linux only Linux systems may be virtualized.

3 The Solution Proposal

The proposed security improvement in server resource usage lies in ensuring a more strict allocation of the individual system resources to the processes executing the programs generating dynamic web server content. These are especially the programs using the Common Gateway Interface (CGI) protocol. Stricter system resource allocation allows more efficient system operation by defining system resource consumption constraints and thus achieves the required service quality. Strict allocation of processor time and memory to the respective processes helps solve possible Denial of Service (DoS) attacks, limit the impact of badly written web applications by using well-defined constraints to prevent any request from consuming all available system resources.

3.1 Design of Architecture

The goal is to limit the respective system resources as required, during the assignment of CGI programs to the respective processes or immediately after it. The reason of preferring such a direct assignment of resource constraints to processes before allocating the resources during process creation is the fact that the same process may be used for the sequential execution of multiple independent programs, using a process pool. In such a case the resource constraint of a single program would remain valid for other programs, if they were executed in the same process.

The respective CGI programs may be identified by the UID of the executed program at the time of system resource constraint allocation. Normally, the UID of the executed program (web) is identical to the one of the executed web server. The UID is altered using the suExec module. Using UIDs to identify the programs allows resource constraints to be assigned according to the user (web page), the program was executed by.

The proposed improvement is implemented as a server module. Due to the modular architecture of the web server, this module is connected to the web server architecture and the other modules, required for the correct function of this

module. This provides the following: a connection between the module and server functionalities; a mechanism to define, process and store the module configuration; the possibility to initialize the module upon server start-up. The architecture of the resulting solution is shown in Figure 1. The mod_cgrp module is the outcome of this work.

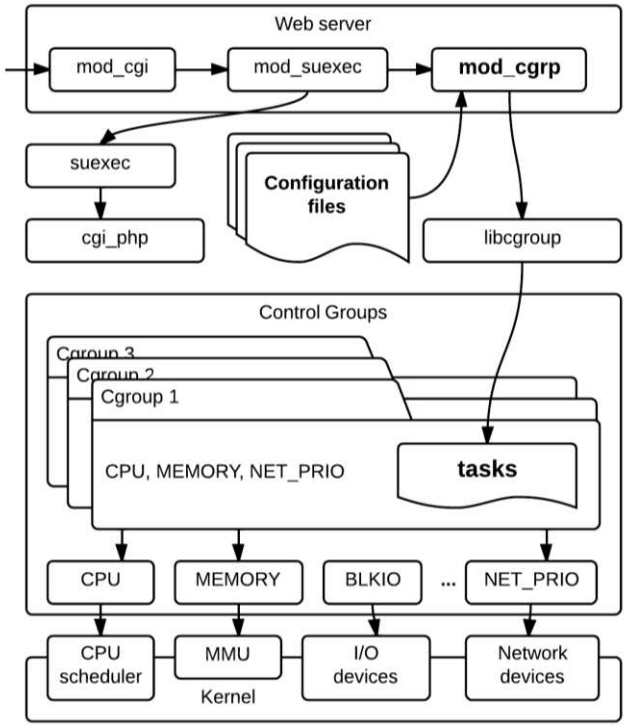

Figure 1
System architecture

Constraining system resources is provided by a system mechanism called Control Groups. This mechanism is supported by the kernel itself. Resource management is implemented by the control groups organized in the file system. The kernel allocates resources to the respective groups according to the group attribute settings.

The processes are identified by means of the configuration files. These contain the data required for the identification of the respective processes, as well as the processes, which have to be assigned to specific cgroups. These data are stored in data pair records. The first member of the pair is the PID of the process assigned to the constraint group. The other member of the pair is the identifier of the cgroup. Only a single constraint group may be assigned to a process having a specific PID.

3.2 Principles of Resource Constraint

Designed module assigns newly created processes to groups with limited privileges to consume specific system resources, as shown in Figure 2.

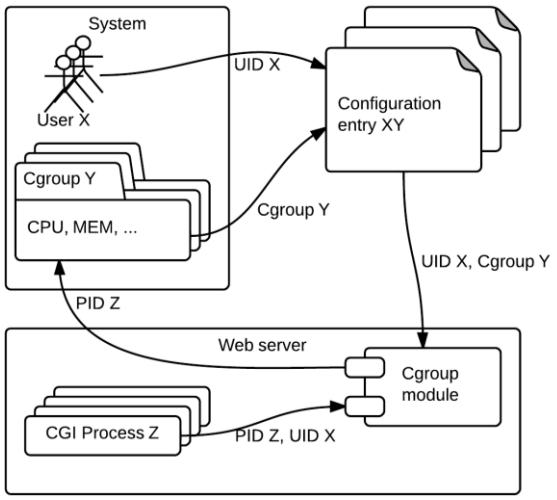

Figure 2
System resource assignment

The execution of the module starts with loading the configuration. Configuration processing is executed automatically by the web server upon its initialization, along with the other modules. Next, the UID of the executed process is retrieved. The server checks, if there is an entry in the configuration for the specified identifier. If the identifier in question is not present in any of the entries, the execution terminates. Otherwise, the ID of the process running the CGI program is retrieved. The module checks the existence of the constraint group stated in the configuration and as in case of the configuration itself, if the existence is not confirmed, the execution terminates and an error message is written to the log file. If the group exists, the retrieved process identifier is assigned to the particular group and the execution terminates with a message stating successful assignment of the process to the group with the given constraints.

4 Experimental Validation

To evaluate the reliability and functionality of the proposed and implemented solution, we have performed some measurements. These measurements focused on the performance and the correct server functionality during the use of the proposed module. The measurements were performed with the tools provided by the operating system and the web server itself.

The computer system used to perform the measurements was a HW system with the following parameters:

- Intel i3 processor working at 2.20 GHz,
- 4096 MB RAM system memory,
- 500GB hard drive spinning at 5400 RPM.

As to the software, the system was running a GNU/Linux Fedora 20 operating system with a 3.13.7 Linux kernel. The web server version number was 2.4.6.

The results of all measurements were recorded by redirecting the standard output of the *top* and Apache Benchmark (*ab*) tools to separate files. The stress testing of the respective resources was performed using a series of php scripts allocating small or large chunks of data (depending on the types of the measured resources) in cycles.

4.1 Module Performance

The following measurements focused on comparing the web server performance with various amounts of requests executed in parallel. Test performed with the *ab* program. The output of the program was – in addition to other things – information on the transfer time and the average time of execution of a single request. We have executed multiple measurements, with varying amounts of parallel requests. Each of these measurements was performed twice, with the module active and inactive. This way we could test the effect of the module on the performance of the web server.

Figure 3 and Figure 4 show that the presence of the module does not significantly impact the speed of request processing. Differences in server performance having the module inactive or active are negligible with low amounts of requests and increase along with the increasing the amount of the requests. The overall evaluation of the presence of the module when responding to the requests aimed at simple HTML or more complex CGI programs is positive. The module has no significant impact on the web server itself.

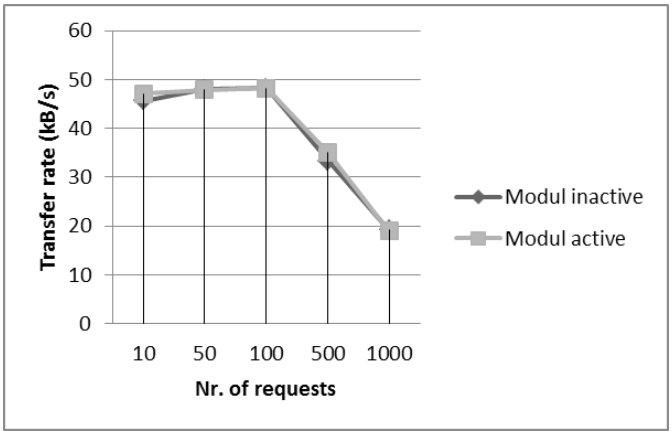

Figure 3
Transfer speed

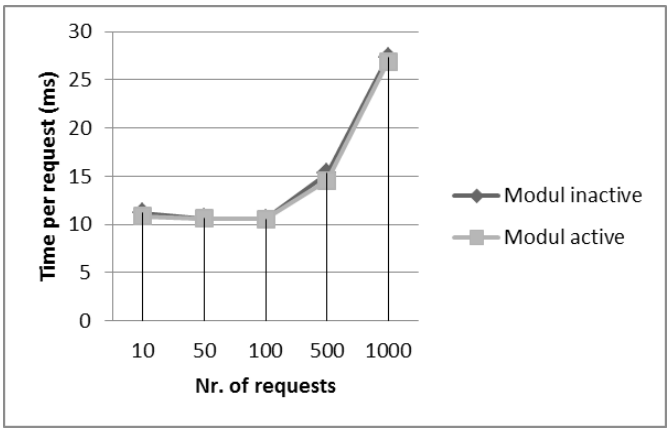

Figure 4
The average time spent by the execution of a single request

4.2 High System Utilization

In this section, we have focused the measurement efforts on comparing the activities of the web server with the module inactive and active, using requests of programs stressing selected system resources. Each measurement was performed individually, with the same program, specifically written for the given system resource. To gather the results we have used the *ab* toolset; we used the *top* program monitoring various system resources to create a specific number of requests.

The subsequent two measurements are aimed at CPU load. The created cgroup has been crafted to prevent the CPU load values from exceeding 50%. The executed program is a cycle, in which the number PI is allocated 3 million times as part of the Foo class. The chart in Figure 5 (with the module being inactive) shows the CPU load – three of the five processes cause CPU loads surpassing 50% during the execution.

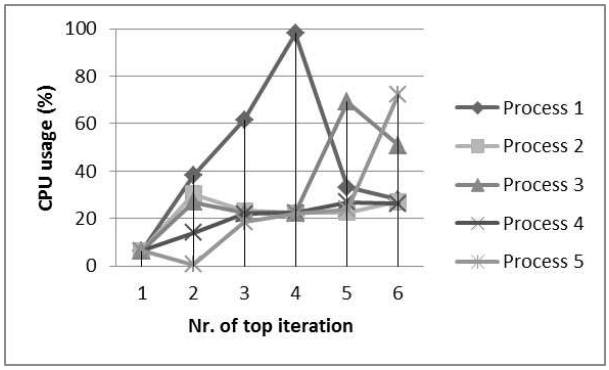

Figure 5
CPU time usage, with the module being inactive

Figure 6 (with the module being active) shows that none of the processes surpassed the 50% CPU load constraint. Each process utilizes approximately the same CPU time during execution and the remaining parts of the system do not degrade due to eventually malicious code.

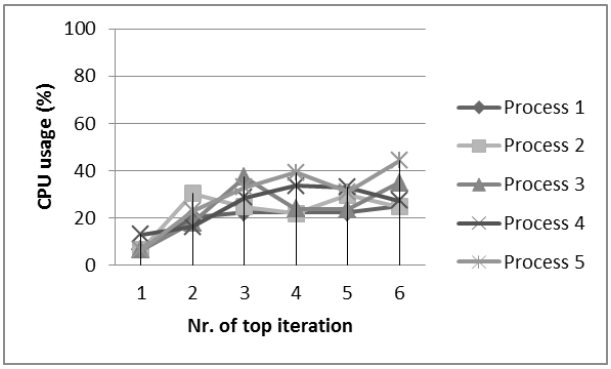

Figure 6
CPU time usage, with the module being active

The next measurement focused again on the CPU as a system resource. However, unlike the previous case focused on CPU time, this time we focused our measurements on one of the CPUs of a multiprocessor system. Again, we executed the same PHP program aimed at stress testing the system CPU. The test system contained multiple processors.

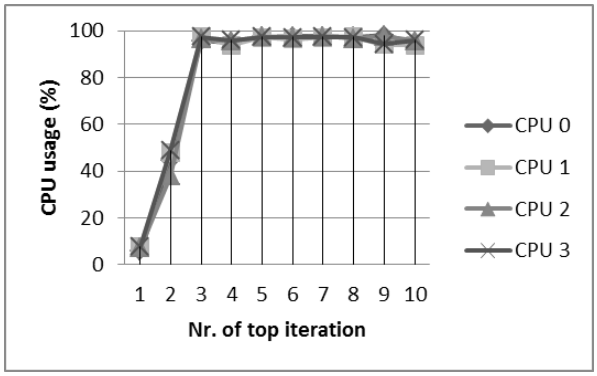

Figure 7
Multi-core CPU load, with the module being inactive

Figure 7 (with the module being inactive) shows the load of all processors in the system from the start of the execution of the respective CGI servers on the server. In this measurement, the server did not have the module functionality activated, so all four processors were loaded to almost 100%.

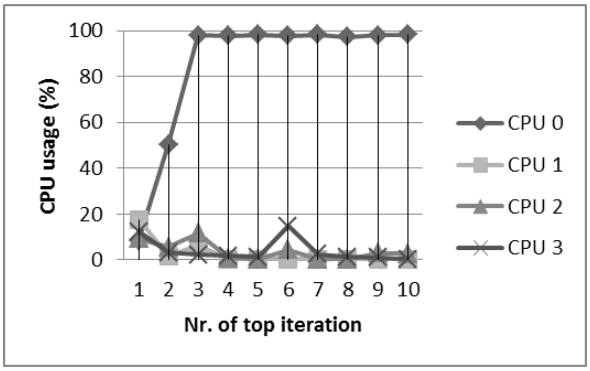

Figure 8
Multi-core CPU load, with the module being active

In the next measurement, the module was active and the cgroup was set up to allow the respective CGI processes of the given user (web) only to the CPU0 processor. As it is shown in the chart in Figure 8 (with the module being active), only the CPU0 processor was running. The other processors did not run the above malware; therefore their load did not exceed 20%.

The last server functionality measurement focused on memory as a system resource. Again, a special PHP script, representing malware was written, but this time it stressed the system memory. The program works again in cycles, but instead of a small number- PI, it allocates a number equal to the iteration multiplied by 100 and inserts it into a dynamic array.

The PHP interpreter contains mechanisms to limit the amount of memory allocated to the respective processes. This is 128 MB by default. To demonstrate the functionality and flexibility of the module configuration, we have altered this setting to 2 GB. There are plenty of languages – in addition to PHP – which may be used to run CGI programs and have no such limitation implemented.

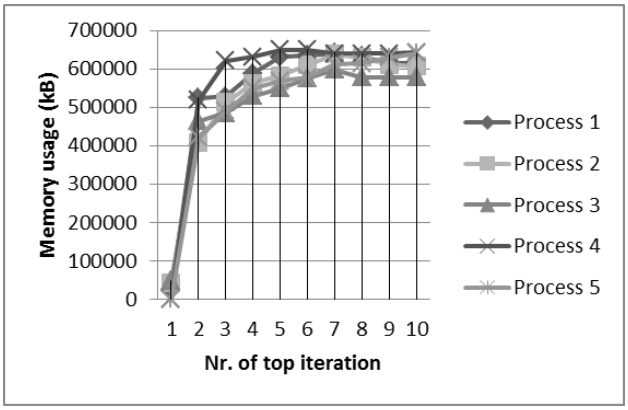

Figure 9
Memory usage, with the module being inactive

Figure 9 (with the module being inactive) shows the memory usage after loading the malicious program. The chart contains the first 10 iterations of the log of the *top* program. The chart shows that after the first iteration more than 600 MB of the memory of all processes was allocated. All 5 processes used all available system memory. If there are many client-side requests, the memory resources run out fast and the service is going to be unavailable.

In the second measurement focused on memory this module was active. A cgroup was set up to limit the maximum memory allocated to the process in this group. The constraint set up was 10 MB. The chart in Figure 10 showed the results of this measurement. As it is evident, none of the processes has produced a load greater than 10 MB to the physical memory of the system. The load was approx. 5 MB/process. The constraint was working well and we may state that this module setting is more flexible, since it may be used even for programs written in other languages than PHP. Moreover, we may define different constraints for different users (web sites).

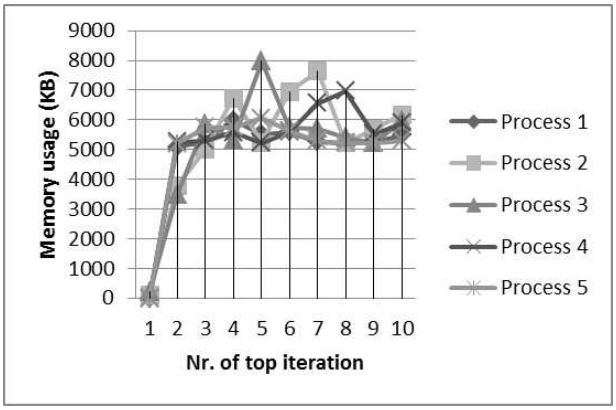

Figure 10
Memory usage, with the module being inactive

Conclusions

The output of this article is an efficient solution of using system resources. The solution designed and implemented at the level of a web server, allows limiting key system resources, such as CPU time and memory.

The system was subject of performance and functionality tests of the module with various configurations. The module as such does not degrade the performance too much to have a significant impact on the execution of the web server. Our tests showed that the module does not have any significant performance impact and all results achieved without the module stopped were approximately the same as those achieved with the module running.

As far as functionality tests are concerned, some attributes in the implementation have already been implemented but are not flexible enough or they do not cover all cases, in which insufficient resource management could affect the performance and stability of the whole system.

In addition to the tested resource constraints, cgroups provide significantly broader system resource configuration possibilities – other than CPU time and memory – therefore they provide a far better way of system resource management and a more stable environment for applications running on such a system, which provides further development possibilities in the proposed solution.

We may also state that the limitations, achievable by means of this resource management facility, are a more coherent and transparent configuration system applicable to various system resources, managed at a single place. It prevents configuration errors, eventual stability problems or various security threats to the system.

The work presented here, allows data centers to use their system resources more efficiently and securely, taking the costs related to power consumption into

account – being an important attribute of data centers, monitored not only to decrease operating costs but also the environmental impact.

Acknowledgements

This work was supported by the Slovak Research and Development Agency under the contract No. APVV-0008-10 and project KEGA 008TUKE-4/2013: Microlearning environment for education of information security specialists.

References

[1] Kolyshkin Kirill: Virtualization in Linux, OpenVZ Technical Report, Kirkland 2006

[2] Banga Gaurav, Druschel Peter, Mogul Jeffrey: Resource Containers: A New Facility for Resource Management in Server Systems. Proceedings of the Third Symposium on Operating Systems Design and Implementation (OSDI), New Orleans 1999

[3] Soltesz Stephen et al.: Container-based Operating System Virtualization: A Scalable, High-Performance Alternative to Hypervisors, ACM SIGOPS Operating Systems Review (EuroSys), Vol. 41, No. 3, New York 2007, pp. 275-287

[4] Singh Balbir, Srinivasan Vaidyanathan: Containers: Challenges with the Memory Resource Controller and its Performance, Proceedings of the Ottawa Linux Symposium, Vol. 2, Ottawa 2007, pp. 209-222

[5] Tomášek Martin: Computational Environment of Software Agents, Acta Polytechnica Hungarica, Vol. 5, No. 2, Budapest 2008, pp. 31-41

[6] Totok Alexander, Karamcheti Vijay: Optimizing Utilization of Resource Pools in Web Application Servers, Concurrency and Computation: Practice and Experience, Vol. 22, Danvers 2010, pp. 2424-2444

[7] Diao Yixin, Hellerstein Joseph, Parekh Sujay: Using Fuzzy Control to Maximize Profits in Service Level Management, IBM Systems Journal, Vol. 41, No. 3, New York, 2002, pp. 403-420

[8] Prpič Martin et al.: RedHat Enterprise Linux 6.5 GA Resource Management Guide [online], New York 2013, Available on: https://access.redhat.com/site/documentation/en-US/Red_Hat_Enterprise_Linux/6/pdf/Resource_Management_Guide/Red_Hat_Enterprise_Linux-6-Resource_Management_Guide-en-US.pdf [quoted: February 2, 2014]

[9] Mihályi Daniel, Novitzká Valerie: Towards the Knowledge in Coalgebraic Model of IDS, Computing and Informatics, Vol. 33, No. 1, Bratislava 2014, pp. 61-78

[10] Mihályi Daniel, Novitzká Valerie: What about Linear Logic in Computer Science?, Acta Polytechnica Hungarica, Vol. 10, No. 4, Budapest 2013, pp. 147-160

[11] Sitko Maroš, Madoš Branislav: Specialized Information System for Web Content Management, Computer Science and Technology Research Survey, Vol. 6, Košice 2012, pp. 364-370

[12] Barham Paul et al.: Xen and the Art of Virtualization, Proceedings of the Nineteenth ACM Symposium on Operating Systems Principles (SOSP), Bolton Landing 2003, pp. 164-177

[13] Sugerman Jeremy, Venkitachalam Ganesh, Lim Beng-Hong: Virtualizing I/O Devices on VMware Workstation's Hosted Virtual Machine Monitor, USENIX Annual Technical Conference, General Track, Boston 2001, pp. 1-14

[14] Gulati Ajay et al.: Cloud-Scale Resource Management: Challenges and Techniques, Proceedings of the 3rd USENIX Conference on Hot Topics in Cloud Computing, Portland 2011, p. 3

[15] Engler Dawson et al.: Exokernel: An Operating System Architecture for Application-Level Resource Management, ACM SIGOPS Operating Systems Review, Vol. 29, No. 5, New York 1995, pp. 251-266

[16] Seawright Love, Mackinnon Richard: VM/370—a Study of Multiplicity and Usefulness, IBM Systems Journal, Vol. 18, No. 1, Riverton 1979, pp. 4-17

[17] Vokorokos Liberios, Pekár Adrián, Ádám Norbert: Data Preprocessing for Efficient Evaluation of Network Traffic Parameters, Proceedings of 16th IEEE International Conference on Intelligent Engineering Systems (INES), Lisbon 2012, pp. 363-367

[18] Vokorokos Liberios, Baláž Anton, Trelová Jana: Distributed Intrusion Detection System using Self Organizing Map, Proceedings of 16th IEEE International Conference on Intelligent Engineering Systems (INES), Lisbon 2012, pp. 131-134

[19] Madoš, Branislav: Architecture of Multi-Core System-on-the-Chip with Data Flow Computation Control, International Journal of Computer and Information Technology (IJCIT) Vol. 3, No. 5 (2014), ISSN 2279-0764, pp. 958-965

Monte-Carlo Simulation of Helicopter Noise

József Bera[1] and László Pokorádi[2]

[1] Óbuda University, Doctoral School of Safety and Security Sciences, Népszínház u. 8, H-1081 Budapest, Hungary, e-mail: bera.jozsef@prosysmod.hu

[2] Óbuda University, Donát Bánki Faculty of Mechanical and Safety Engineering, Népszínház u. 8, H-1081 Budapest, Hungary, e-mail: pokoradi.laszlo@bgk.uni-obuda.hu

Abstract: Currently, applied flying noise investigation methods are done from energetic points of view, independent of other noise sources. These methods do not adequately accept the ground state of the environment and its changes. This paper proposes a new Monte-Carlo Simulation-based investigation method, to analyze changes of environment states when the number and characteristics of flying operations and noise levels fluctuate stochastically.

Keywords: environment protection; noise; helicopter; Monte-Carlo Simulation

1 Introduction

These days the number of flights over living spaces is increasing. Flight noise investigation is currently done from only energetic points of view, independent of other noise sources. Therefore, the ground state of the environment and its changes do not get enough attention, so flight noise, is analyzed as if it would create more noise sources.

The approaches mentioned above lack subjective observation. This is a big problem in the case of the noise, which is called energy pollution or disturbed transfer of energy [4] that usually generates an immediate reaction from the observers and the environment.

There is an important question. Which method is adaptable to depict correct changes of environment state when the numbers and characters of flying operations and related noise levels are different in time? This study proposes a new simulation method based on a Monte-Carlo Simulation to answer this question.

The Monte-Carlo Simulation is one of the most well-known parametric uncertainty investigation methods. There are several books and studies that mention the theory of the Monte-Carlo Simulation and its applications.

Newman and Barkema describe the Monte-Carlo Simulation and its application opportunities to investigate several scientific problems [10]. Pokorádi has summarized the theoretical background of the mathematical modeling of technical systems and processes [12].

In the study of Madić and Radovanović, an attempt was made to investigate the Monte-Carlo Method applicability for solving single-objective optimization problems [8]. Based on the results, they proposed a wider application of the Monte-Carlo Method for solving machining optimization problems because of its simplicity, efficiency and wide-ranging capabilities.

Morariu and Zaharia presented a calculation methodology of the testing duration of the products' reliability. Their proposed methodology and the accuracy of the results were verified by using the Monte-Carlo data simulation method [8].

Sobor et al. analyzed the evolution of jet passenger aircraft noise and uncertainty of its determination [13]. They used probability calculation analysis.

The Authors have investigated noise protection questions of helicopters and aerial and other types of transportation [1] [2] [3] [4] [5]. These publications showed measured data which are used in the Monte-Carlo Simulation (see Table 1).

The outline of the study is the following: Section 2 shows the model of flying noise emission. Section 3 depicts the Monte-Carlo briefly. Section 4 demonstrates an assessment method of helicopter noise emission used Monte-Carlo Simulation. Section 5 summarizes the study, outlines the prospective scientific work of the Authors.

2 Helicopter Noise Effect Model

The noise pressure L_{Aeq}, is mostly related to the changes of state of environment parameters. This noise pressure level which characterizes the observed influence of noise, is an equivalent parameter constituted by maximum and minimum sound pressures [4]. In case of aerobatic flies of helicopters uncertainties of equivalent noise pressures of maneuvers should be characterized by their distribution (see Figure 3).

The equivalent noise pressure is in accord with changes of pressure in the environment. But disturbance depends on time of noise effect too. Therefore, the duration of noise effect should be taken into account during the modeling of noise. The average noise load L_{AXj} of (the j^{th}) maneuver [dB] can be determined by the following equation:

$$L_{AX,j} = L_{Aeq,j} + 10 \cdot \lg \frac{\tau_j}{\tau_{ref}} \left[\text{dB}\right] \tag{1}$$

where:

$\tau_{j.}$ – time of (the j^{th}) maneuver [s]

L_{Aeqj} – equivalent noise pressure of (the j^{th}) maneuver [dB]

$\tau_{ref.}$ – reference time: 1 s

The authoritative acoustical pressure level occurred from aerobatics $L_{AM,re}$ can be determined by the following equation [4]:

$$L_{AM,re} = 10 \cdot \lg \frac{\tau_{ref}}{T_M} \sum_{j=1}^{M} 10^{0,1 \cdot L'_{AXj}} \left[\text{dB}\right] \tag{2}$$

where:

T_M – time of estimation [s]

M – number of flying maneuvers

The used time of estimation is 1800 s (30 min), because the average time of one aerobatic fly operation is 30 minutes.

The applications of equations (1) and (2) are in Hungary and in the European Union. These equations will be used during our investigation to estimate noise load of a helicopter aerobatics. In other words, equations (1) and (2) will be the model of the investigated helicopter flying operations. These equation determined by European and Hungarian regulations, therefore, the applied model has to be validated.

We can see that these equations compose a deterministic mathematical model of helicopter aerobatic noise. But the time of the maneuver is a variable parameter, that can be characterized by its distribution function (see Figure 4). The number of maneuvers is a fluent parameter too (see Figure 5). Therefore, in order to investigate this environmental protection problem (basically a deterministic model with stochastic input parameters) the Monte-Carlo Simulation should be used.

3 The Monte-Carlo Simulation

Monte-Carlo is one of the well-known classical simulation techniques. The name Monte-Carlo was applied to this class of mathematical methods by scientists working on the development of nuclear weapons during the Manhattan Project in Los Alamos [7]. All Monte-Carlo Simulations have the following common features:

1) A known *f(x)* probability density function over the set of system inputs.
2) Random sampling of inputs based on the distribution specified in feature 1) and simulation of the system under the selected inputs.
3) Numerical aggregation of experimental data collected from multiple simulations conducted according to feature 2) [6].

Numerical experiments of Monte-Carlo Simulation lead us to run the simulation on many sampled inputs before we can infer the values of the most interesting system performance measures.

At its heart it is a computational procedure in which a performance measure is estimated using samples drawn randomly from a population with appropriate statistical properties. The selection of samples, in turn, requires an appropriate random number generator. During our investigation the Hit and Miss (Acceptance–Rejection) Method will be used. This method, which is related to John von Neumann, contains random samplings from an appropriate distribution and subjecting it to a test to determine whether or not it will be acceptable for use.

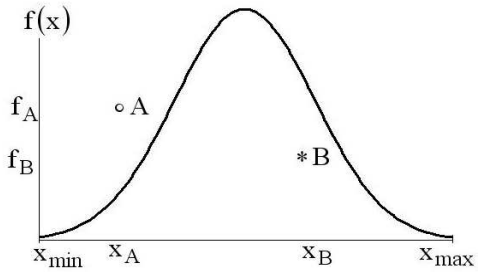

Figure 1
Illustration of Acceptance-Rejection Method

First, the *f(x)* probability density function and interval of the generated parameter should be determined (see Fig. 1). They can be defined by statistical Monte-Carlo Simulation of the pipeline system to investigate effects of the thermal water temperature of the real measured data or they can be assumed by preliminary experiences. Then two independent random values x from $[x_{min}; x_{max}]$ and y_x from (0; 1) intervals are generated and tested to see whether there are inequalities or not

$$y_x < f(x) \tag{1}$$

holds:

- If the inequality holds, then accept x as a variable generated from *f(x)* (see B point in Figure 1).
- If the inequality is violated, reject the pair x, y_x (see A point in Figure 1) and try again.

The Acceptance-Rejection Method can be executed simply and can generate random numbers to any kind of distribution [11].

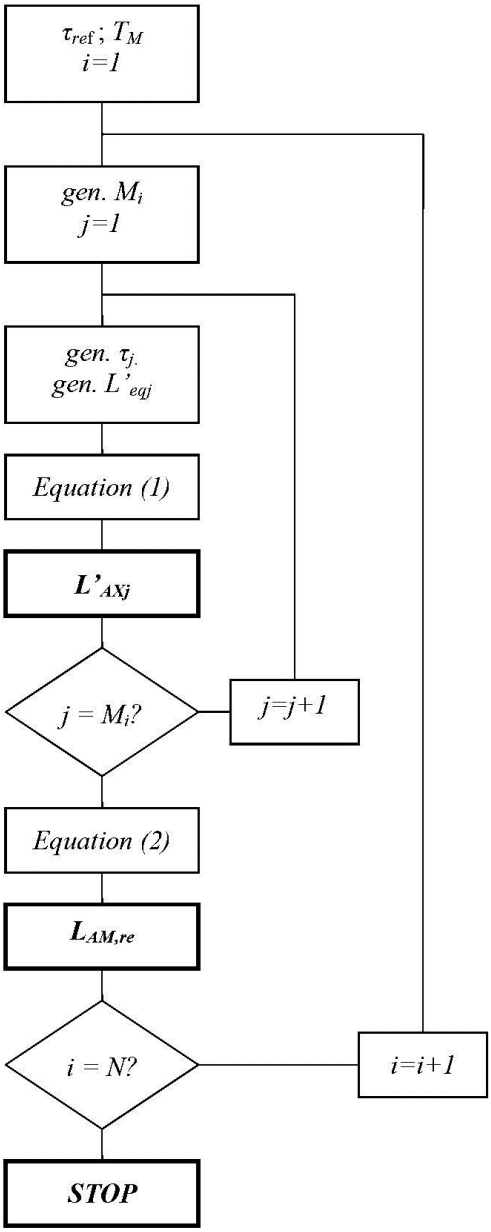

Figure 2
Block Diagram of the Monte-Carlo Simulation

4 Helicopter Noise Simulation

During the investigation of the equations (1) and (2) form the deterministic model which has been excited by different M numbers of maneuvers, τ time of maneuver and L'_{eq} equivalent noise pressure.

4.1 The Simulation

The block diagram of the simulation can be seen in Figure 2. The number of model generations N was 1500. The basic statistical data is shown by Table 1. Investigation of Sobor et al. showed that the change of equivalent noise depends on the differences of the independent parameters of noise events but it is independent of the type of their distributions [13]. During the simulation, the Acceptance-Rejection Method shown in Chapter 3 was used. The density functions were chosen by our measuring [1] and general engineering experiences (see Table 1 right column). The histograms of applied excitation values are shown by Figures 3-5.

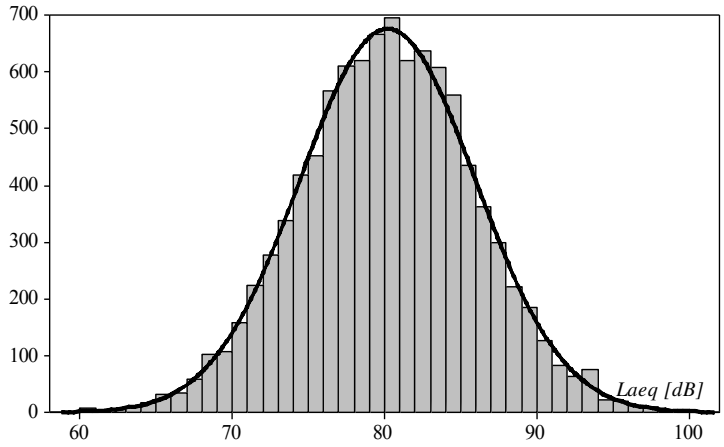

Figure 3
Histogram of Equivalent Noise Pressures (L_{Aeq})

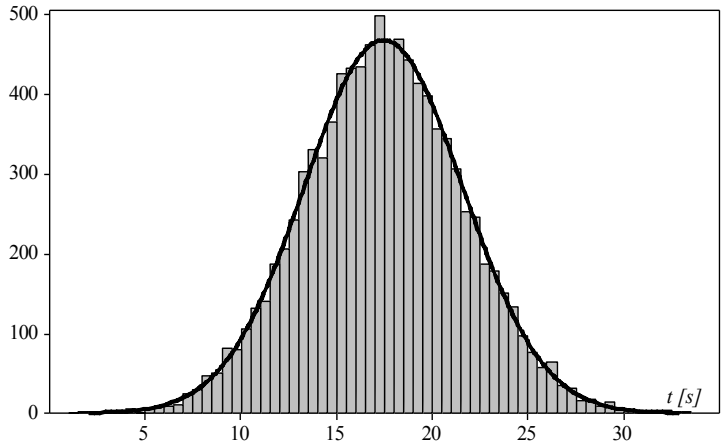

Figure 4
Histogram of Times of Maneuvers (t)

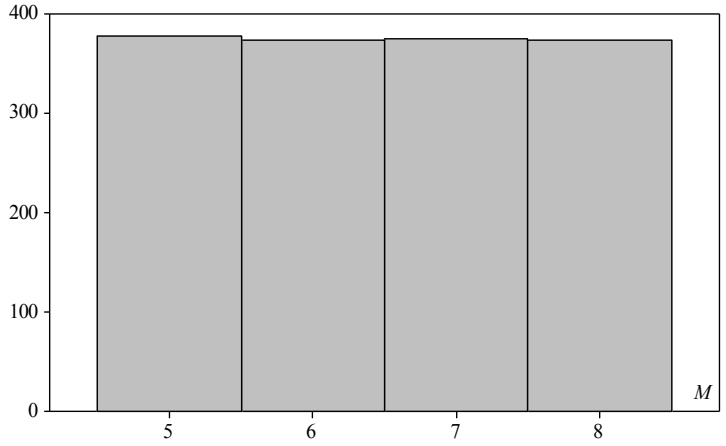

Figure 5
Histogram of Numbers of Maneuvers (M)

Table 1

Statistical Data of Excitation Values

	Min.	Mean	Max.	Dev.	Density Function
L'_{eq-m} [dB]	58.3	80.2	102.4		Normal
L'_{eq-ex} [dB]	58.6	80.2	101.1	5.75	
M_{-m} [-]	5	6.5	8		Uniform
M_{-ex} [-]	5	6.497	8	1.12	
τ_{-m} [s]	1.5	17.5	33.5		Normal
τ_{-ex} [s]	1.52	17.44	33.35	4.14	

4.2 Results and Discussion

From the results of the simulation, the following conclusions can be deduced:

1. The Monte-Carlo Simulation can be used to analyze noise effects of helicopter aerobatics.
2. The noise pressure L_{Aeq} and acoustical pressure level $L_{AM,re}$, as unique limits, are inappropriate to investigate subjective noise observations and to make decisions that satisfy the condition of compromises. Additional indicators should be introduced for correct assessment.
3. Due to uncertainties of environmental factors affecting the noise transmission measured values can have significant differences.

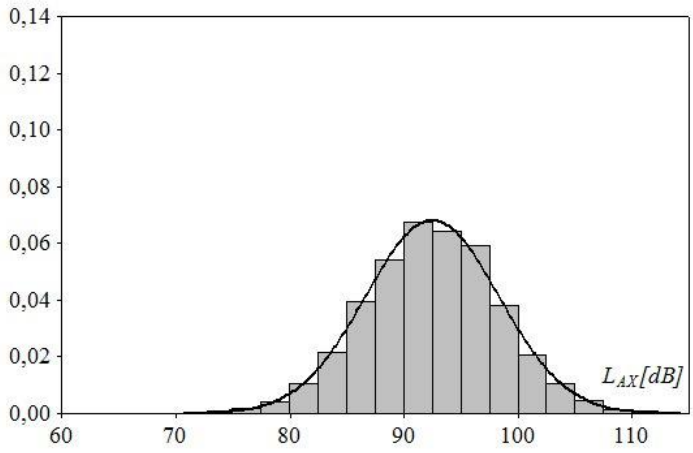

Figure 6

Density Function of Average Noise Loads (L_{AX})

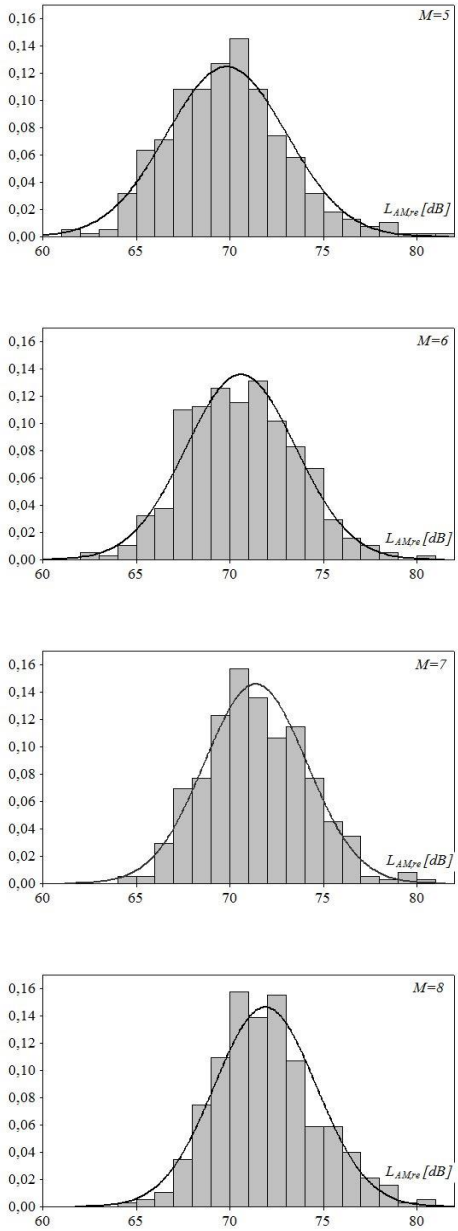

Figure 7
Density Functions of Authoritative Acoustical Pressure Levels
in Cases of Different Numbers of Maneuvers ($L_{AM,re}$)

4. The duration of the maneuvers resultant in the L_{AX} values used in valuation interval increased to +10 dB (see Figures 3 and 6). Namely, we consider 10 dB higher values of the assessment. It suggests focusing on the level of disturbance.

5. Figure 8 shows consequence of the preferably determined time of estimation. Based on these results, we draw the conclusion, that the distribution function is shifted towards lower noise levels and a narrower range of 60 to 80 dB added values.

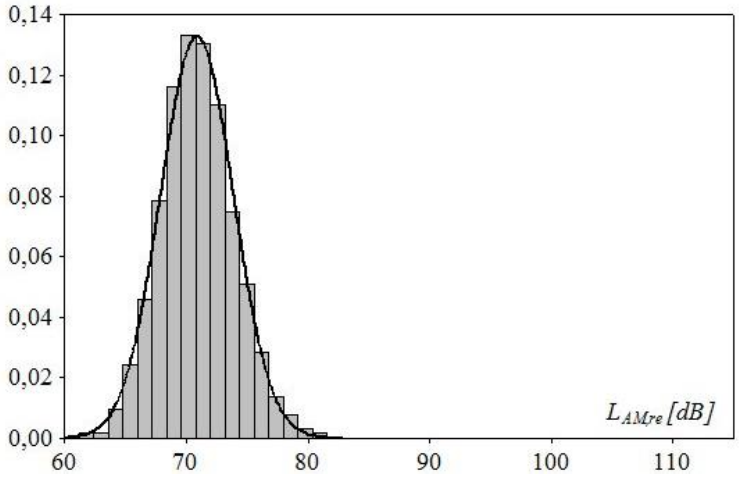

Figure 8
Density Function of Authoritative Acoustical Pressure Level ($L_{AM,re}$)

6. The number of maneuvers determines the total duration of noisy periods and its ratio to the quiet period. This is significant because the exposure time (durations of maneuvers) play a central role in reducing noise levels. So, the importance of number and times of maneuvers should be highlighted in the evaluation process.

7. The applied model should be set up to following points of view:

   - The measured noise pressure L_{Aeq} shows a short period in the change of environment status based on the maximum and minimum sound pressure level values.
   - The time of estimation T_M equal to the duration of aerobatic flying operation allows for a more realistic analysis and more effective decisions.

8. For realistic results, the measured pressure levels and their distributions have to be investigated, instead of, the average noise parameters.

Conclusions and Future Work

This paper proposed a Monte-Carlo Simulation-based method to investigate the noise load of helicopter aerobatics.

The research work and its results demonstrate that parameters of environmental systems are uncertain. Applying only unique key numbers to depict environmental problems and their comparison with threshold values are not allowed. The density functions of environmental system parameters should be used to investigate different loads of environment.

During prospective scientific research, related to this field of environmental protection and applied mathematics, the Authors would like to develop other methodologies to model and investigate the environmental effects of aviation and other means of transport.

References

[1] Bera J. – Pokorádi L.: Actual Question of Measuring of the Aircraft Noise, The Challenge of Next Millennium on Hungarian Aeronautical Sciences (12th Hungarian Days of Aeronautical Sciences), pp. 114-123

[2] Bera J. – Pokorádi L.: Industrial Helicopter Application and its Noise Protection Problems, Proceedings of the 12th Mini Conference on Vehicle System Dynamics, Identification and Anomalies, Budapest, November 8-10, 2010, ISBN: 978 963 313 058 2, pp. 343-350

[3] Bera J. – Pokorádi L.: Noise Protection Investigation of Heliports, Proceedings of the 11th Mini Conference on Vehicle System Dynamics, Identification and Anomalies, Budapest, 10-12 November, 2008, (ISBN 978 963 313 011 7), pp. 577-581

[4] Bera J. – Pokorádi L.: Theory and Practice of Helicopter Noise, Campus Kiadó, Debrecen, 2010, 192 p. (in Hungarian)

[5] Bera J.: Noiseprotectional Design of Heliports, Repüléstudományi Közlemények Különszám, 2007. április, Szolnok (CD-version) (in Hungarian) http://www.szrfk.hu/rtk/kulonszamok/2007_cikkek/bera_jozsef.pdf.

[6] Guizani, M., Rayes, A., Khan, B., Al-Fuqaha, A., Network Modeling and Simulation, A Practical Respective, John Wiley & Sons, Chichester, 2010, p. 281

[7] Kalos M. H. and P. A. Whitlock Monte-Carlo Methods. Second Edition 2008 WILEY-VCH Verlag GmbH & Co. KGaA, Weinheim

[8] Miloš Madić; Miroslav Radovanović, Possibilities of Using The Monte-Carlo Method for Solving Machining Optimization Problems, Facta Universitatis, Mechanical Engineering Vol. 12, No. 1, 2014, pp. 27-36

[9] Morariu Cristin Olimpiu, Sebastian Marian Zaharia, A New Method for Determining the Reliability Testing Period Using Weibull Distribution, Acta Polytechnica Hungarica, Vol. 10, No. 7, 2013, pp. 171-186

[10] Newman M. E. J., Barkema G. T.: Monte-Carlo Methods in Statistical Physics, Oxford University Press Inc., New York, 1999, p. 475

[11] Pokorádi László, Molnár Boglárka, Monte-Carlo Simulation of the Pipeline System to Investigate water Temperature's Effects, Polytechnical University of Bucharest. Scientific Bulletin. Series D: Mechanical Engineering 73:(4) pp. 223-236 (2011)

[12] Pokorádi, L.: Systems and Processes Modeling, Campus Kiadó, Debrecen, 2008, p. 242 (in Hungarian)

[13] Sobor Á. et. al.: The Evolution of the Equivalent Noise Level of Aircraft Depending on Spreading of the Route, Kép és Hangtechnika XXVIII. pp. 190-192 (in Hungarian)

A Fuzzy Expert System for Industrial Location Factor Analysis

Aleksandar Rikalovic, Ilija Cosic

Department of Industrial Engineering and Management, Faculty of Technical Sciences, University of Novi Sad, Trg Dositeja Obradovica 6, 21000 Novi Sad, Serbia; e-mail: a.rikalovic@uns.ac.rs, ilijac@uns.ac.rs

Abstract: The identification of a new industrial location requires consideration of a complex set of factors in the decision making process. These factors are generally described with a number of different indicators, expressed in quantitative and/or qualitative ways, thus resulting in a nonlinear optimization problem. Besides, some of the input data are imprecise, incomplete or not totally reliable. Therefore, it is necessary to interpret, standardize and fuse data in specific factors suitable for comparison. To take into account all of these aspects above and allow for identification of an optimal solution by reasoning on available information, this paper proposes the use of an expert system for industrial location factor analysis. Management of uncertainty is an important issue in the design of expert systems, since data maybe indefinite, inaccurate and ambiguous. Fuzzy logic provides an approach to data fusion and reasoning for uncertain data by using the human expert knowledge. The proposed expert system is based on Fuzzy Inference Systems (FIS), which solve the nonlinear optimization problem by using the available knowledge. Results show that the proposed approach obtains accurate results in industrial location factor analysis, similar to those devised by experts of the field.

Keywords: expert system; fuzzy logic; fuzzy inference system (FIS); decision support system (DSS); industrial location; factor analysis

1 Introduction

One of the most important and far-reaching strategic decisions faced by industry managers is deciding where to locate new industrial facilities [1]. The industrial location problem can be represented as a selection process of potential sites in order to satisfy all applied to requirements in the best possible way. Industrial location decision making must consider a wide range of quantitative and qualitative factors in order to coordinate socio-economic benefits and environmental sustainability [2]. Besides, increasing complexity is undoubtedly a relevant characteristic of today's international economy with many variables affecting location decision making: this is therefore, becoming a key issue in the

firm strategies [3]. Goals considered in the selection process may be non-linearly related to the factors thus leading to a nonlinear optimization problem with respect to the each goal [4].

In many situations, we cannot consider only one criterion because several conflicting objectives usually need to be considered in decision making [5]. Industrial location is therefore multi-objective [6] and multi-criteria problem [7]. Multi-criteria decision making (MCDM) techniques have been used to solve various facility location problems [8, 9]. However, these techniques, assume data homogeneity, which is unrealistic in many decision making situations such as industrial location problems. To allow for comparing the various goals and avoid biases due data representation in MCDA it is necessary to normalize and standardize all input data in a range suitable for processing before applying the multi-criteria analysis [10, 11]. Industrial location analysis traditionally uses qualitative and quantitative tools such as checklists, dimensional analysis evaluation techniques and multivariate statistical analysis to deal with multi-criteria analysis [12, 13].

Unfortunately, the above approaches are not sufficient in today's rapidly changing and highly uncertain environment, where strategic decisions on industrial location have an extremely complex and imprecise nature [14]. Managers are in fact making difficult and important decisions concerning industrial locations on the weak base of imprecise information and incomplete knowledge [15]. Besides, traditionally data are collected and treated as directly-measurable quantities for location selection, even though may be affected by some uncertainty due to the measurement process [16]. However, several characteristics of the location problem can be described only in a qualitative way by using the natural language, which is intrinsically approximate and imprecise representation of the information [17]. The challenge is how to bring quantitative and qualitative (linguistic) data into the same analytic methodology [18]: applying fuzzy logic seems to be the most appropriate method to incorporate all of these factors in the strategic decision making [19].

The industrial location problem requires complex knowledge management and analysis. The need of an appropriate support to human decision makers is due to four kinds of limits: cognitive, economic, time and competitive demands [20]. Usually previous experience or expert knowledge is used to design decision support systems [21]. To develop an intelligent decision support system for industrial location factor analysis, we need a holistic view of the various factors as well as of data and knowledge management (reasoning techniques) based on an expert system.

To address all of the above aspects in a comprehensive, homogeneous framework, we propose a hierarchical technique, based on a fuzzy expert system, which uses a set of Fuzzy Inference Systems (FIS) to interpret, standardize and fuse heterogeneous data in order to estimate normalized industrial location factors.

This paper is organized as follows: in Section 2, we summarize the industrial location process, the typical industrial location factors and data representation, pointing out the role of the fuzzy representation in the decision support systems. In Section 3 we present the innovative methodology for industrial location factor analysis. Section 4 presents the implementation of the methodology in Vojvodina, Serbia as the study case to show the implementation choices. Section 5 shows examples of experimental results, and Section 6 some derives conclusions and directions for future research.

2 Background

The industrial location selection process requires the analysis and the possible optimization of a complex set of factors involving economic, social, technical, environmental and political issues. Due to the complexity of the task, the site selection process is divided into two phases: selection of a macro-location (i.e., the municipality) followed by the selection of a micro-location (i.e., the specific location) [12]. Zelenovic [13] also distinguish macro and micro location and proposing process consisting of four phases: selection of continent, selection of country, selection of municipality, and finally selection of the specific location.

A large amount of information must be accumulated to aid in the decision-making process. Many of factors have to be considered in the industrial location selection process, as social and environmental aspects have received more emphasis in the process and are supported by legislations and regulations [22]. The number and the types of factors affecting the location selection vary in each case, and they often can be hundreds. The most commonly used industrial location factors are linked in Table 1 [23].

Table 1
Typical industrial location factors

Grouped Factors	***Factors***
Transportation	*Highway facilities, railroad facilities, waterway transportation, airway facilities, trucking services, shipping cost of raw material, cost of finished goods transportation, shipping cost of raw material, warehousing and storage facilities.*
Labor	*Low cost labor, attitude of workers, managerial labor, skilled labor and wage rates, unskilled labor, unions, and educational level of labor.*
Raw Materials	*Proximity to supplies, availability of raw materials, nearness to component parts, availability of storage facilities for raw materials and components and location of suppliers.*

Markets	*Existing consumer market, existing producer market, potential consumer market, anticipation of growth of markets, marketing services, favorable competitive position, population trends, location of competitors, future expansion opportunities and size of market.*
Industrial Site	*Accessibility of land cost of industrial land, developed industrial park, space for future expansion, availability of lending institution, closeness to other industries.*
Utilities	*Attitude of utility agents, water supply, wastewater, cost and quality, disposable facilities of industrial waste, availability of fuels, cost of fuels, availability of electric power and availability of gas.*
Government Attitude	*Building ordinances, zoning codes, compensation laws, insurance laws, safety inspections and stream pollution laws.*
Tax Structure	*Industrial property tax rates, state corporate tax structure, tax free operations, and state sales tax.*
Climate and Ecology	*Amount snow fall, percent rain fall, living conditions, relative humidity, monthly average temperature, air pollution and ecology.*
Community	*Reputation of local authorities, colleges and research institutions, attitude of community residents, quality of schools, religious facilities, library facilities, recreational facilities, attitude of community leaders, medical facilities, hotels and motels.*

Quantitative methods for data analysis can be used if all these data are quantitative. However, many data are qualitative in nature and presented in various linguistic forms [1]. From the viewpoint of incorporating qualitative factors in the location decision, the most widely used techniques are the weighted checklist approach [24] and the fuzzy logic [25].

In the literature, fuzzy logic has been used extensively in decision support systems, for strategic planning, in industrial organizations to model Fuzzy Inference System (FIS) [15]. Fuzzy Inference Systems are, in fact, methods for mapping an input space to an output space by using fuzzy logic [26]. Due their intuitive handling and simplicity, FIS have been applied in a wide range of fields, such as control, decision support, image processing, and expert systems [27]. The strength of FIS relies on two important characteristics. First, they are able to handle linguistic concepts. Second, they are universal approximators able to perform nonlinear mappings between inputs and outputs [28]. The fuzzy rules of the system make use of fuzzy linguistic terms described by membership functions [29]. These functions capture the human expert's conception of the linguistic terms. Fuzzy rules take the form IF *(conditions)* THEN *(actions)*. Where *conditions* and *actions* are linguistic values applied to input and output variables respectively.

3 Methodology

In this section we introduce an innovative methodology for industrial location analysis. The proposed expert system manages and explores the knowledge in this specific application by reasoning on a database of facts by means of suitable inference rules. Fuzzy logic is applied to the decision support system for factors analysis providing a formal methodology to capture valid patterns for uncertainty reasoning. The proposed comprehensive, homogeneous framework uses a set of Fuzzy Inference Systems to interpret, standardize and fuse heterogeneous data in order to estimate normalized industrial location factors.

The FIS for industrial location factor analysis is divided into three main components: the fuzzifier, the knowledge management and the defuzzifier (Figure 1). The fuzzifier and the defuzzifier convert external information in fuzzy quantities and vice versa. The knowledge management uses the fuzzy rules of the knowledge base that allows for approximate reasoning [30].

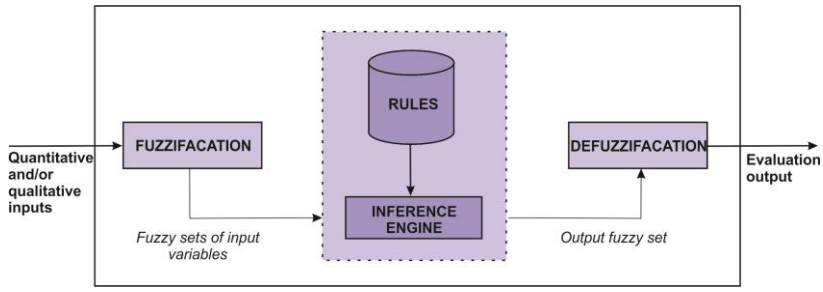

Figure 1
Fuzzy Expert System

For fuzzification of quantitative variables we used trapezoidal membership functions while triangular membership functions are used for qualitative inputs [31]. To interpret the inputs we defined boundaries and level of uncertainty in the membership functions.

The rule based system is provided by the expert of the field to combine and process fuzzy data and derive the desired knowledge about the envisioned environment. We developed suited fuzzy rules to generate normalized outputs for the industrial location selection problem.

In the literature, there are different approaches for the FIS design and implementation. The Mamdani's fuzzy inference method [31] is the most used. This method is characterized by the following fuzzy rule schema:

$$\text{IF } (x \text{ is } A) \text{ THEN } (y \text{ is } B)$$

where A and B are fuzzy sets defined on the input and output domains, respectively. The if-part of the rule "x *is* A" is called the antecedent, while the

then-part of the rule "*y is B*" is called the consequent [32]. If there are more input variables in the antecedent they are joined by the OR and AND operators.

In Mandami's FIS, the antecedents and the consequents of the rules are expressed as linguistic constraints [31]. As a consequence, this kind of FIS provides an intuitive technique to represent the knowledge base, which is easy to understand and maintain. This approach is therefore, widely used in decision support systems [34].

In the expert system proposed in this paper all designed FIS are based on the same defuzzification module, where output is normalized and represented in the range [0, 10] suitable for multi-criteria analysis. The output is given by a set of five triangular membership functions representing the linguistic properties: *insufficient*, *regular*, *satisfactory*, *good* and *excellent* (Figure 2). In the final step of the defuzzification process we used the centroid rule [31].

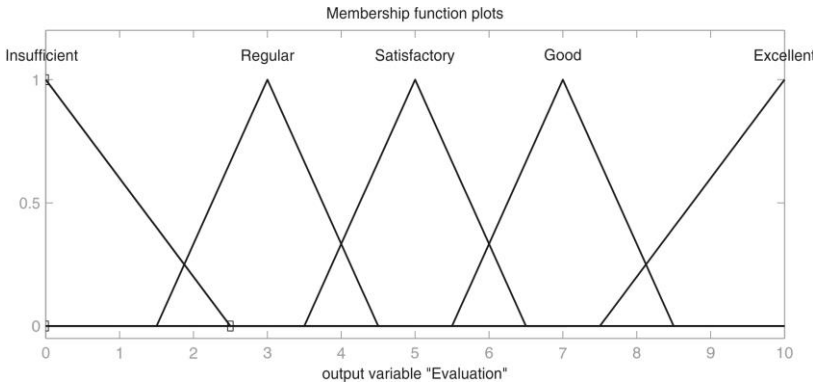

Figure 2
Triangular MFs

The FIS's of the proposed expert system for industrial location factor analysis, has been implemented and tested by using MATLAB, by exploiting the fuzzy descriptions and processing made available by the Fuzzy System Toolbox.

4 Implementation

In this section we describe the implementation of the proposed fuzzy expert system for industrial location analysis whose general structure has been introduced in Section 3. To test the efficiency and the effectiveness of the proposed approach we implemented the Fuzzy Inference Systems for the study case of Vojvodina, a region in Serbia. We focused on four typical industrial location factors for municipality selection: *airway facilities*, *reputation and efficiency of local authorities*, *utilities* and *ecology*. We designed four Fuzzy

Inference Systems to interpret, standardize and fuse heterogeneous data, in order to estimate the normalized industrial location factors. In the following we will analyze each of the FIS systems.

4.1 Airway Facilities

To design Fuzzy Inference System for the factor *airway facilities,* we used one input variable: *distance from the airport*. We considered this quantitative input variable defined in the range from 0 to 150 km. Linguistically, we represented it with five triangular membership functions: *very close*, *close*, *acceptable*, *faraway* and *very far away* (Figure 3).

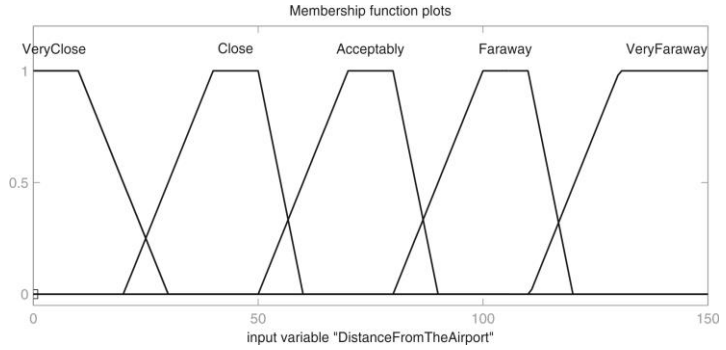

Figure 6
Membership functions for input variable distance from the Airport

The knowledge base for the factor *airway facilities* includes the following IF-THEN rules:

1) IF *(DistanceFromTheAirport is VeryClose)* THEN *(Evaluation is Excellent)*;

2) IF *(DistanceFromTheAirport is Close)* THEN *(Evaluation is Good)*;

3) IF *(DistanceFromTheAirport is Acceptably)* THEN *(Evaluation is Satisfactory)*;

4) IF *(DistanceFromTheAirport is Faraway)* THEN *(Evaluation is Regular)*;

5) IF *(DistanceFromTheAirport is VeryFaraway)* THEN *(Evaluation is Insufficient)*.

In Figure 4 we report the output resulting from the application of these IF-THEN rules, with the membership function given above.

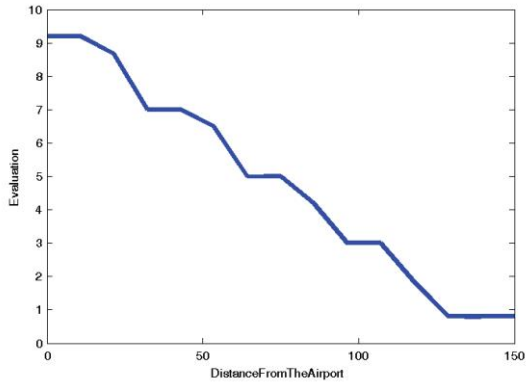

Figure 4
Output surface for the FIS airway facilities

4.2 Reputation and Efficiency of Local Authorities

To design Fuzzy Inference System for factor *reputation and efficiency of local authorities* we used two input variables: *number of investment* and *business environment*. For the quantitative input variable *number of investment* we defined range from 0 to 20 investments. Linguistically, we represented it with triangular membership functions: *very small number*, *small number*, *average number*, *high number* and *very high number* (Figure 5).

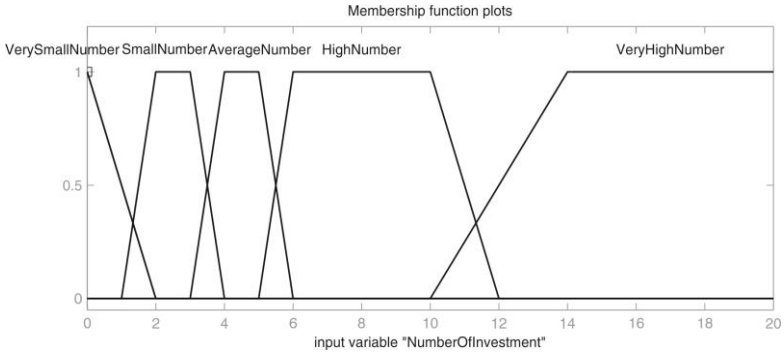

Figure 5
Membership functions for input variable number of investment

For the qualitative input variable *business environment* are defined in the range from 1 to 5 and linguistically represented trapezoidal membership functions: without certificate, in the certification process, certificate candidate and certified (Figure 6).

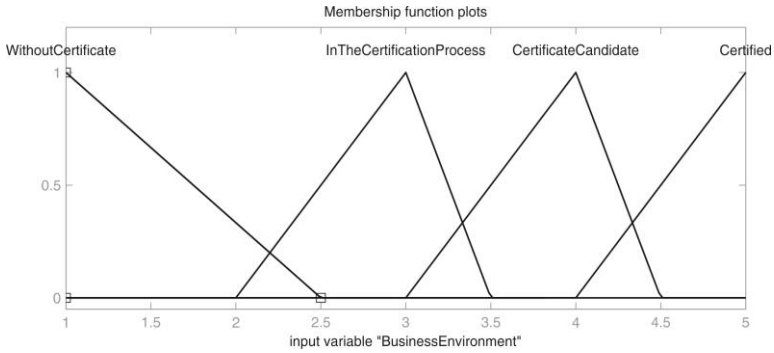

Figure 6
Membership functions for input variable business environment

The knowledge base for the factor *reputation and efficiency of local authorities* includes the following IF-THEN rules joined by AND operators:

1) IF *(NumberOfInvestment is VerySmallNumber)* AND *(BusinessEnvironment is WithoutCertificate)* THEN *(Evaluation is Insufficient)*;

2) IF *(NumberOfInvestment is SmallNumber)* AND *(BusinessEnvironment is InTheCertificationProcess)* THEN *(Evaluation is Regular)*;

3) IF *(NumberOfInvestment is AverageNumber)* AND *(BusinessEnvironment is CertificateCandidate)* THEN *(Evaluation is Satisfactory);*

4) IF *(NumberOfInvestment is HighNumber)* AND *(BusinessEnvironment is Certified)* THEN *(Evaluation is Good)*;

5) IF *(NumberOfInvestment is VeryHighNumber)* AND *(BusinessEnvironment is Certified)* THEN *(Evaluation is Excellent)*;

6) IF *(NumberOfInvestment is VeryHighNumber)* AND *(BusinessEnvironment is CertificateCandidate)* THEN *(Evaluation is Excellent)*;

7) IF *(NumberOfInvestment is VeryHighNumber) AND (BusinessEnvironment is InTheCertificationProcess)* THEN *(Evaluation is Good)*;

8) IF *(NumberOfInvestment is VeryHighNumber)* AND *(BusinessEnvironment is WithoutCertificate)* THEN *(Evaluation is Satisfactory)*;

9) IF *(NumberOfInvestment is VerySmallNumber)* AND *(BusinessEnvironment is InTheCertificationProcess)* THEN *(Evaluation is Insufficient)*;

10) IF *(NumberOfInvestment is SmallNumber)* AND *(BusinessEnvironment is WithoutCertificate)* THEN *(Evaluation is Regular)*;

11) IF *(NumberOfInvestment is VerySmallNumber)* AND *(BusinessEnvironment is Certified)* THEN *(Evaluation is Regular)*;

12) IF *(NumberOfInvestment is VerySmallNumber) AND (BusinessEnvironment is CertificateCandidate)* THEN *(Evaluation is Regular)*;

13) IF *(NumberOfInvestment is HighNumber)* AND *(BusinessEnvironment is CertificateCandidate)* THEN *(Evaluation is Good)*;

14) IF *(NumberOfInvestment is SmallNumber) AND (BusinessEnvironment is CertificateCandidate)* THEN (Evaluation is Satisfactory);

15) IF *(NumberOfInvestment is SmallNumber)* AND *(BusinessEnvironment is Certified)* THEN *(Evaluation is Satisfactory)*.

In Figure 7 we report the output resulting from the application of these IF-THEN rules, with the membership function given above.

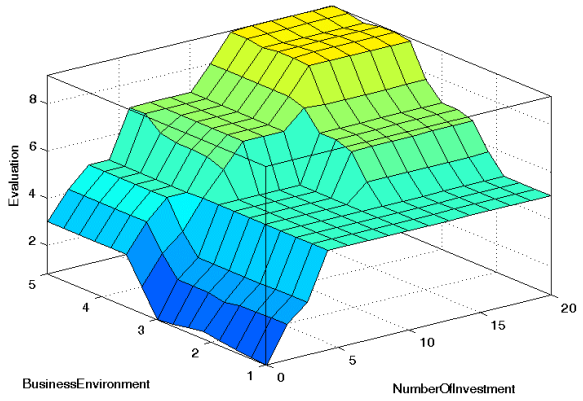

Figure 7
Output surface for the FIS reputation and efficiency of local authorities

4.3 Utilities

To design a Fuzzy Inference system for the factor *utilities,* we used four input variables: *industrial property tax*, *price of water*, *price of the wastewater* and *price of garbage*. For quantitative variable input *industrial property tax* we defined range from 0 to 150 (RSD), for *price of water* and *price of the wastewater* range from 0 to 150 (RSD/m^3) and *for price of garbage* range from 0 to 50 (RSD/m^3). Linguistically, we represented it with five triangular membership functions: *very small price*, *small price*, *acceptable price*, *high price* and *very high price* (Figures 8, 9, 10, 11).

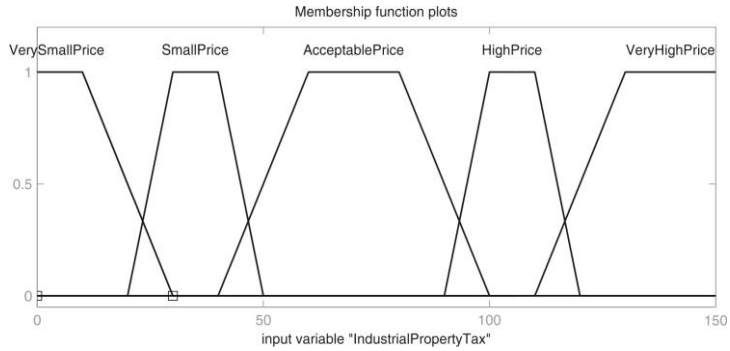

Figure 8
Membership functions for input variable industrial property tax

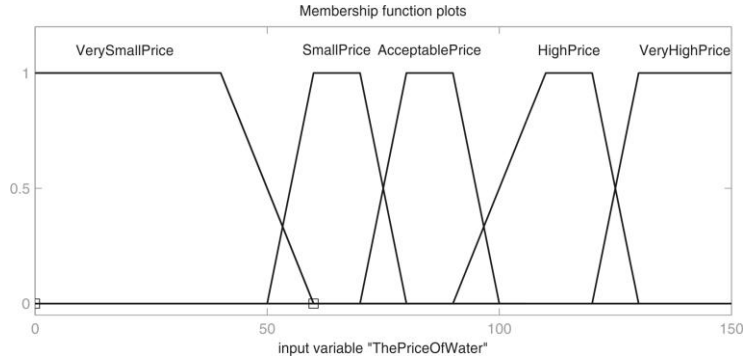

Figure 9
Membership functions for input variable price of water

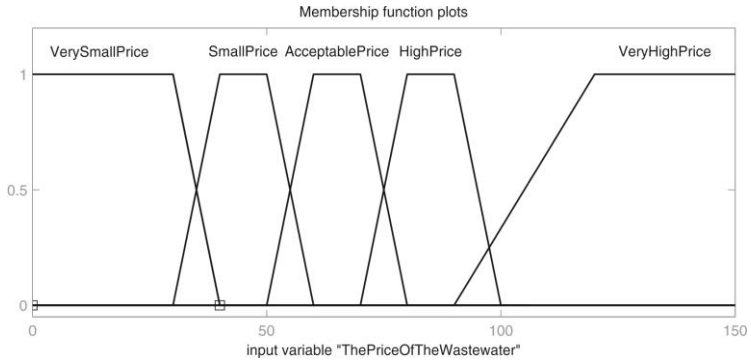

Figure 10
Membership functions for input variable price of the wastewater

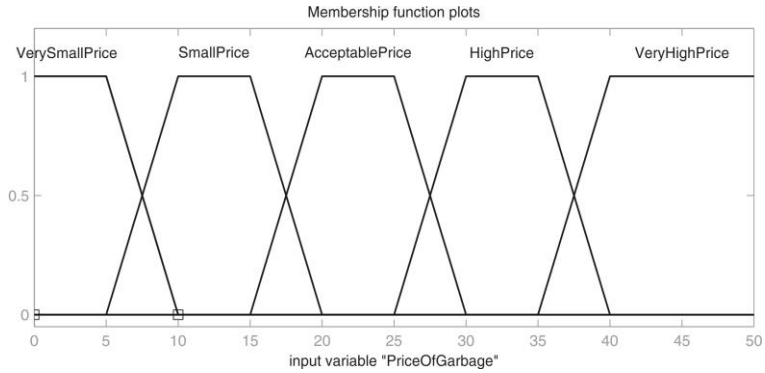

Figure 11
Membership functions for input variable price of garbage

The knowledge base for the factor *utilities* includes the following IF-THEN rules joined by OR operators:

1) IF *(IndustrialPropertyTax is VerySmallPrice)* OR *(ThePriceOfWater is VerySmallPrice)* OR *(ThePriceOfTheWastewater is VerySmallPrice)* OR *(PriceOfGarbage is VerySmallPrice)* THEN *(Evaluation is Excellent);*

2) IF *(IndustrialPropertyTax is SmallPrice)* OR *(ThePriceOfWater is SmallPrice)* OR *(ThePriceOfTheWastewater is SmallPrice)* OR (*PriceOfGarbage is SmallPrice)* THEN *(Evaluation is Good)*;

3) IF *(IndustrialPropertyTax is AcceptablePrice)* OR *(ThePriceOfWater is AcceptablePrice)* OR *(ThePriceOfTheWastewater is AcceptablePrice)* OR *(PriceOfGarbage is AcceptablePrice)* THEN *(Evaluation is Satisfactory)*;

4) IF *(IndustrialPropertyTax is HighPrice)* OR *(ThePriceOfWater is HighPrice)* OR *(ThePriceOfTheWastewater is HighPrice)* OR *(PriceOfGarbage is HighPrice)* THEN *(Evaluation is Regular)*;

5) IF *(IndustrialPropertyTax is VeryHighPrice)* OR *(ThePriceOfWater is VeryHighPrice)* OR *(ThePriceOfTheWastewater is VeryHighPrice)* OR *(PriceOfGarbage is VeryHighPrice)* THEN *(Evaluation is Insufficient).*

In Figure 12 we report the output resulting from the application of these IF-THEN rules, with the membership functions given above.

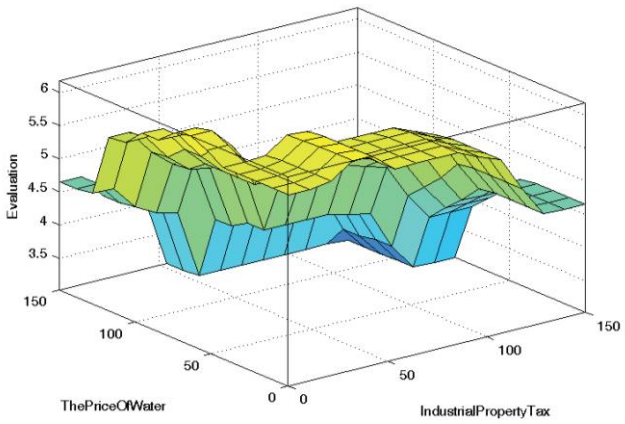

Figure 12
Output surface for the FIS utilities

4.4 Ecology

To design the fuzzy inference system for the factor *ecology,* we used one input variable: *environmental assessment*. We considered this quantitative input variable defined in the range from 1 to 4. Linguistically, we represented it with five membership functions: *degraded environment*, *endangered environment*, *quality environment* and *very quality environment* (Figure 13).

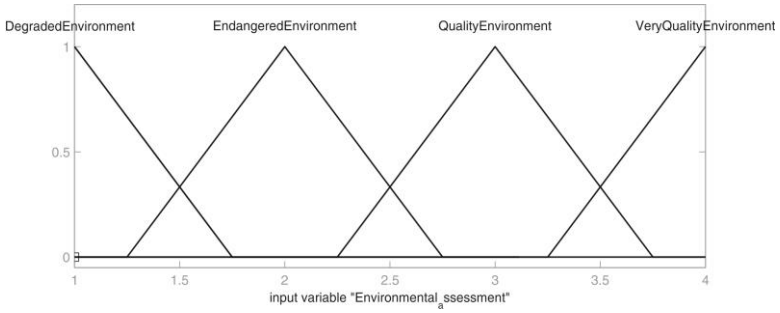

Figure 13
Membership functions for input variable Environmental assessment

Knowledge Base for the factor *ecology* includes the following IF-THEN rules:

1) IF *(EnvironmentalAssessment is DegradedEnvironment)* THEN *(Evaluation is Insufficient)*;

2) IF *(EnvironmentallAssessment is EndangeredEnvironment)* THEN *(Evaluation is Regular)*;

3) IF *(EnvironmentalAssessment is QualityEnvironment)* THEN *(Evaluation is Good)*;

4) IF *(EnvironmentalAssessment is VeryQualityEnvironment)* THEN *(Evaluation is Excellent)*.

In Figure 7 we report the output resulting from the application of IF-THEN rules, with the membership functions given above.

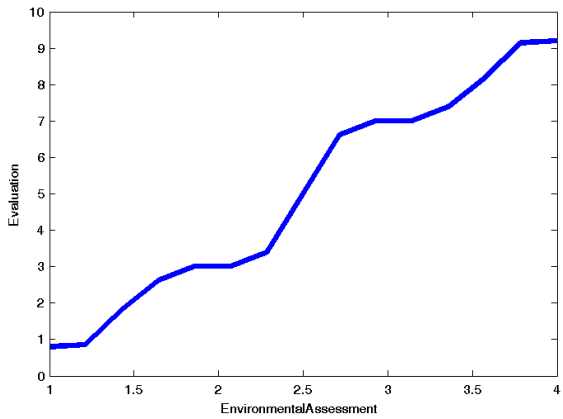

Figure 14
Output surface for the FIS Ecology

5 Experimental Results

In this section we report the final results produced by the use of the fuzzy expert system for industrial location analysis. By combining the IF-THEN rules we obtain the evaluation of the each municipality and its suitability as industrial location, by considering the factors described in Section 4. We provided results for all the 45 municipalities of the study case. The outputs are standardized in the range [0,10], where 0 means not suitably and 10 full suitability for industrial location. In Figure 15 we show example of the inference rules and the results for the factor *airway facilities* for Pecinci municipality. The evaluation of the suitability for the Pecinci municipality is between *good* and *excellent* with grade 7.98. In Figure 16 show an example for factor *reputation and efficiency of local authorities* for Indjija municipality. The Evaluation of the suitability for the Indjija municipality is *excellent* with grade 9.2.

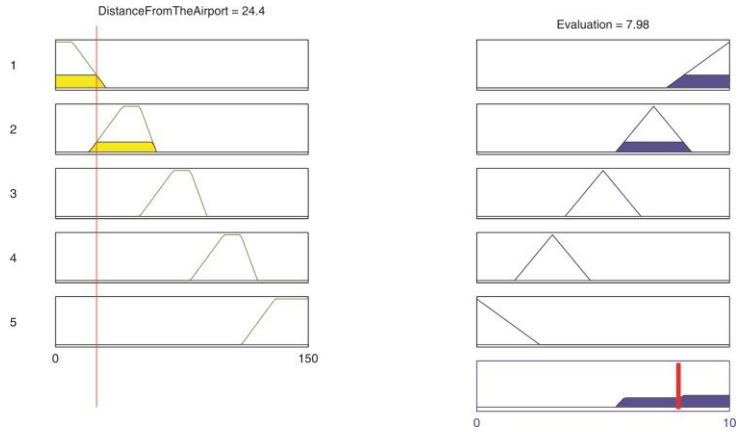

Figure 15
Combination of the defined rules and results for the factor airway facilities for Pecinci municipality

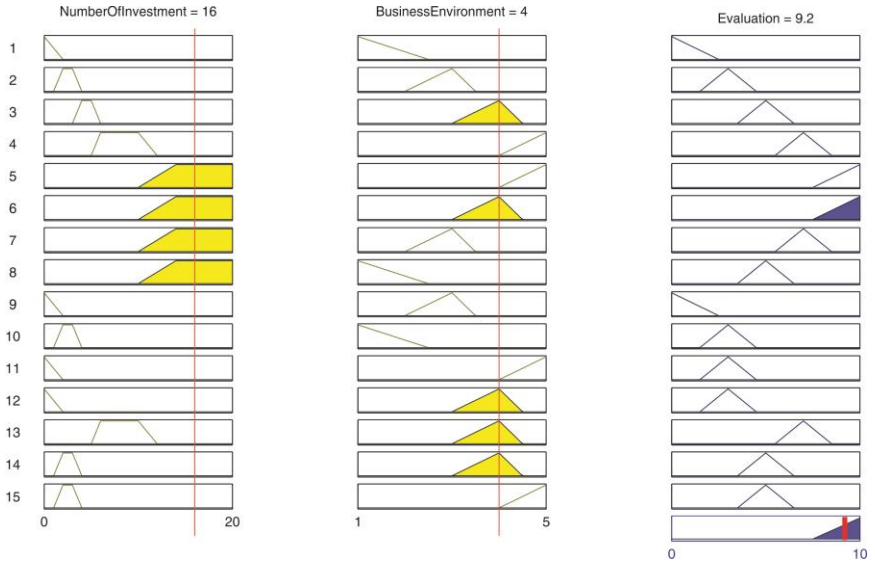

Figure 16
Combination of the defined rules and results for the reputation and efficiency of local authorities for Indjija municipality

In Figure 17 we show combination of the defined rules and results for the factor *utilities* for Zrenjanin municipality as example. Evaluation of suitability for Zrenjanin municipality is between *satisfactory* and *good* with grade of 5.59. In Figure 18 we show example of output results for the factor *ecology* for Kikinda municipality. Evaluation of suitability for Kikinda municipality is *insufficient*, with grade 0.8.

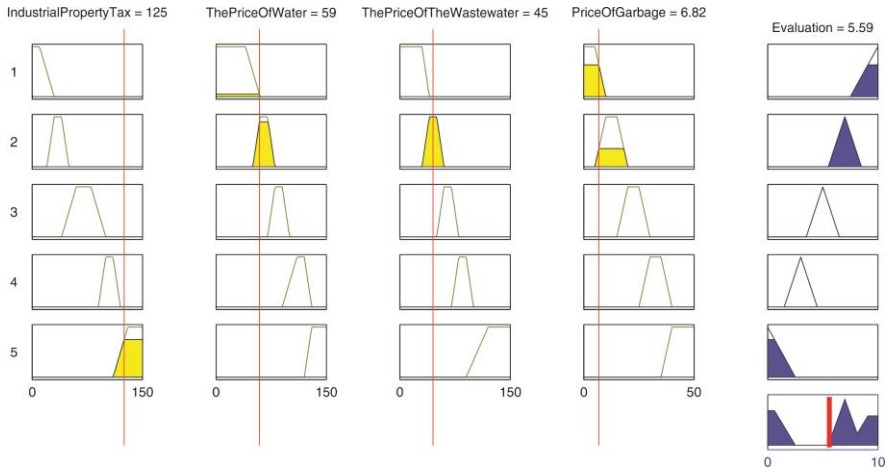

Figure 17

Combination of the defined rules and results for the factor utilities for Zrenjanin municipality

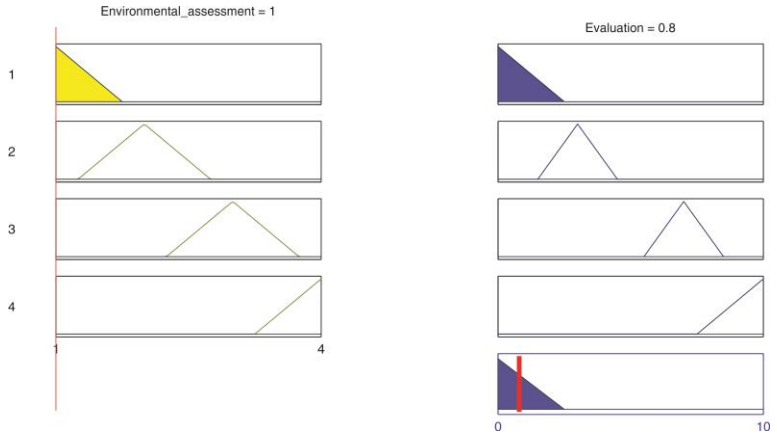

Figure 18

Combination of the defined rules and results for the factor ecology for Kikinda municipality

All results for the 45 municipalities were obtained in the same manner as in the given examples and show the different suitability of the municipality for each various factors.

Conclusion

An expert system for industrial location factor analysis, composed of various Fuzzy Inference Systems, addressing specific aspects, has been developed to manage uncertainty, standardization and fusion of data in a homogeneous framework. We used fuzzy logic in the decision support system for factors analysis as methodology to capture valid patterns for reasoning about uncertainty

of quantitative and qualitative data. The presented methodology can be used for various factors and in different regions by tailoring the membership functions and the IF-THEN rules to the specific case.

The FIS for comprehensive industrial location factor analysis presented in this paper has been tested: results are equivalent to those derived by experts in the field. In further research, we will explore the connection between multi-criteria decision analysis and fuzzy expert systems.

References

[1] R. Bhatnagara, A. S. Sohalb, Supply Chain Competitiveness: Measuring the Impact of Location Factors, Uncertainty and Manufacturing Practices, Technovation, No. 25, pp. 443-456, 2005

[2] M. Reisi, L. Aye, A. Soffianian, "Industrial Site Selection by GIS in Isfahan," 19th Iran International Conference on Geoinformatics, 2011

[3] L. A. Sabater, A. A. Tur, J. M. Navarro, Industrial Location, Spatial Discrete Choice Models and the Need to Account for Neighbourhood Effects, 3rd World Conference of the Spatial Econometrics Association, Barcelona Spain, 8-10 July 2008

[4] Z. M. Shen, C. Coullard, M. S. Daskin, A Joint Location-Inventory Model. Transportation Science 37(1), pp. 40-55, 2003

[5] D. Queiruga, G. Walter, J. G. Bention, and T. Spengler, "Evaluation of Sites for the Location of WEEE Recycling Plants in Spain," Waste Management, Vol. 11, pp. 181-190, 2006

[6] S. Carver, Integrating Multi-Criteria Evaluation with Geographical Information Systems. International Journal of Geographical Information Systems, 5, pp. 321-339, 1991

[7] W. Atthirawong and B. MacCarthy, "An Application of Analytical Hierarchy Process to International Location Decision Making," presented at 7th Annual Cambridge International Manufacturing Symposium: Restructuring Global Manufacturing, Cambridge. England: University of Cambridge, pp. 1-18, 2002

[8] M. Badri, "Combining the Analytic Hierarchy Process and Goal Programming for Global Facility Location- Allocation Problem", Int. J. Production Economics, 62, pp. 237-248, 1999

[9] J. Korpela, and M. Tuominen, "A Decision Aid in Warehouse Site Selection", Int. J. Production Economics, 45, pp. 169-180, 1996

[10] H. Voogd, Multicriteria Evaluation for Urban and Regional Planning. Pion, Ltd., London, 1983

[11] J. R. Eastman, Idrisi for Windows, Version 2.0: Tutorial Exercises, Graduate School of Geography – Clark University, Worcester, MA., 1997

[12] D. Zelenovic, "Location of Production Systems," in The Design of Production Systems, 2nd ed. Novi Sad: Faculty of Technical Sciences, pp. 373-394, 2003

[13] U. Bankhofer, Industrial Location Management. Wiesbaden: German university-Verlag, 2001

[14] Ghazinoory, S. Zadeh and Memariani, A. Fuzzy SWOT Analysis. Journal of Intelligent & Fuzzy Systems, No. 18, pp. 99-108, 2007

[15] I. Rawabdeha, A. Al-Refaie and H. Arabiyatd, Developing a Fuzzy Logic Decision Support System for Strategic Planning in Industrial Organizations, Advanced Technology & Science, IJISAE, 1(2), pp. 14-23, 2013

[16] P. Rezaei, K. Rezaie, S. N. Shirkouhi and M. R. J. Tajabadi, Application of Fuzzy Multi-Criteria Decision Making Analysis for Evaluating and Selecting the Best Location for Construction of Underground Dam, Acta Polytechnica Hungarica, Vol. 10, No. 7, 2013

[17] R. Tanscheit, Sistemas Fuzzy. Rio de Janeiro: Departamento de Engenharia Elétrica, PUC- Rio, 2004

[18] J. Malczewski, GIS and Multicriteria Decision Analysis, John Wiley and Sons, Toronto, 1999

[19] K. Culo and Skendrovic, V. A Fuzzy Logic Approach to Decision Making. A proceeding of 7th OTM Conference Preliminary Program, Croatia, 2006

[20] C. W. Holsapple and A. B. Whinston, Decision Support Systems: A Knowledge-based Approach, West Publishing Company, Minneapolis, 1996

[21] N. E Matsatsinis, M. Doumpos and C. Zopounidis, Knowledge Acquisition and Representation for Expert Systems in the Field of Financial Analysis, Expert Systems With Applications, Vol. 12, No. 2, pp. 247-262, 1997

[22] R. L. Keeney, Siting Energy Facilities. New York: Academic Press, 1980

[23] M. A. Badri, "Dimensions of Industrial Location Factors: Review and Exploration," Jornal of Business and public affairs Volume 1, Issue 2, 2007

[24] R. Tanscheit, Sistemas Fuzzy. Rio de Janeiro: Departamento de Engenharia Elétrica, PUC- Rio, 2004

[25] C. Dhaya and G. Zayaraz, Pondicherry Engineering College, Puducherry, International Journal of Advanced Science and Technology Vol. 49, December, 2012

[26] G. Chen, Introduction to Fuzzy Sets, Fuzzy Logic, and Fuzzy Control Systems. Hoboken, NJ: CRC Press, 2000

[27] T. J. Ross, Fuzzy Logic with Engineering Applications, 2nd ed. Chichester: Wiley, 2004

[28] G. Serge (2001) Designing Fuzzy Inference Systems from Data: Interpretability oriented Review, IEEE Transactions on Fuzzy Systems, Vol. 9, No. 3, pp. 426-442, 2001

[29] T. J. Ross., Fuzzy Logic with Engineering Applications, International Edition, McGraw-Hill, Inc, 1997

[30] E. Czogala and J. Leski, Fuzzy and Neuro-Fuzzy Intelligent Systems, ser. Studies in Fuzziness and Soft Computing. Springer, Vol. 47, 2000

[31] E. Mamdani and S. Assilian, "An Experiment in Linguistic Synthesis with a Fuzzy Logic Controller," Int. Journ. of Man-Machine Studies, Vol. 7, No. 1, pp. 1-13, 1975

[32] A. Provotar, A. Lapko, and A. Provotar, "Fuzzy Inference Systems and their Applications," Cybernetics and Systems Analysis, Vol. 49, No. 4, pp. 517-525, 2013

[33] L. A. Zadeh, "Toward a Theory of Fuzzy Information Granulation and its Centrality in Human Reasoning and Fuzzy Logic," Fuzzy Sets and Systems, Vol. 90, No. 2, pp. 111-127, 1997

[34] R. Abrahart, L. See, and D. Solomatine, Building Decision Support Systems Based on Fuzzy Inference, in Practical Hydroinformatics, ser. Water Science and Technology Library, Eds., Vol. 68, pp. 215-228, 2008

Application Benchmark of Three Micro Hole Machining Processes for Manufacturing the Nozzle of a Medical Water Jet Machine

Vilmos Csala, Tibor Szalay, Balázs Farkas, Sándor Markos

Department of Manufacturing Science and Engineering, Budapest University of Technology and Economics, Műegyetem rkp. 3, H-1111 Budapest, Hungary, csala@manuf.bme.hu, szalay@manuf.bme.hu, farkasb@manuf.bme.hu, markos@manuf.bme.hu

Abstract: Micro hole machining refers to the process of drilling holes with a diameter of less than 1 millimeter. This paper compares three commonly used technologies: mechanical drilling, laser machining and electrical discharge machining. All of these techniques were analyzed based on an experimental measurement of dimensional accuracy, circularity, burr formation and the image of the internal surface. The most significant criterion of analysis is surface quality, as the main purpose of the examination was to find the most precise process. In addition, a detailed cost analysis, pertaining to machining time, the tools and machines was performed. The experiment utilized a high precision lathe, an Nd:YAG laser and an electrical discharge machine. The final results revealed the micro drilling process as the one with the most promising parameters. Therefore, it was suggested for industrial applications. However, once the economic factors were not taken into account, the EDM also became a more attractive option, based on good technical and quality parameters.

Keywords: micro manufacturing; drilling; EDM; laser machining

1 Introduction

Nowadays, the machining of micro holes is in high demand, when it comes to industrial applications. Although there are numerous challenges and difficulties related to such technologies, machining holes with a diameter of less than 1 millimeter or even 100 μm is considered to be common practice in medical device production, in the automotive industry and in other state of the art technologies. Additionally, manufacturing miniature parts or features, have a tradition and several technologies are known that can successfully accomplish the task, such as, laser machining or EDM. The most important difference in today's production practice, is that we need to manufacture a high volume of these parts, and we also need to retain this ability in the serial production. Fortunately, more and more

companies provide this technology, resulting in a rapid development of micro-scale parts machining. [1, 2]

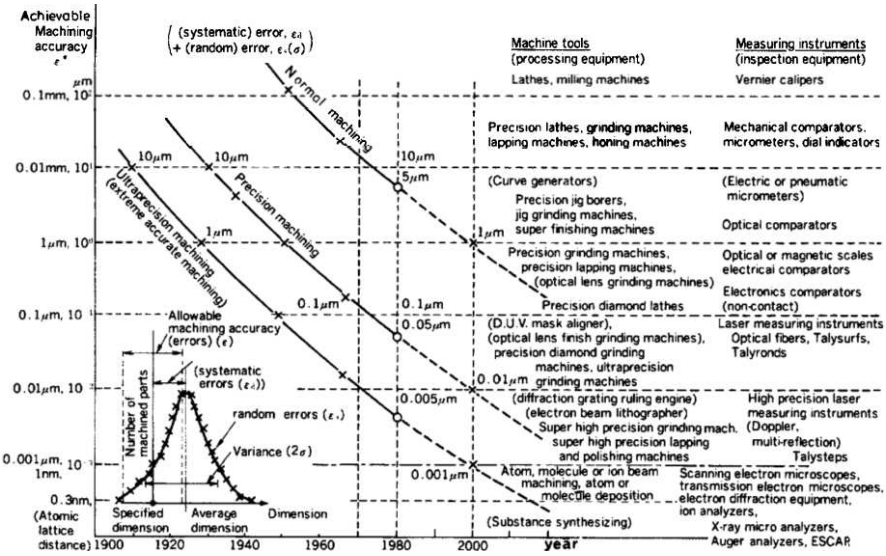

Figure 1

Taniguchi's prognosis [4]

According to Taniguchi's prediction, machining parts and details in the micron range, using traditional cutting operations will become available at the beginning of the 21st Century [3]. (Figure 1) The curves in Figure 1, display the manufacturing capability of the available technologies as a function of achievable accuracy, dating as far back as 1940. As Taniguchi describes in the figure, the size of the micro machining end product is around 100 μm. Table 1 summarizes the most frequently used machining operations as well as the minimum sizes that can be produced by using them.

Table 1

Size limit of technologies [1]

Machining operation	**Achievable size**
Micro-molding	500 μm
Micro-pressing	50 μm
Micro-milling and grinding	25 μm
Stereolitography	12 μm
Micro-EDM	5 μm
Ion-beam machining	0.2 μm

Our motivation to compare the most frequently used micro-hole machining operations by experimental means originated from our strong interest in a company dealing with the production of medical devices. This particular firm has

developed medical water jet machining devices for surgical applications. The general structure of the machining device can be observed in Figure 2. Medical devices need to conform to some extreme requirements. First of all, the device must be controlled with high precision; moreover, both the cutting fluid and the material of the nozzle must be bio-compatible. In medical water jet machining, saline is the most commonly used working fluid, while the nozzle is usually made of metal or metal alloys, such as alumina, titanium and platinum. In order to provide the necessary fluid velocity for cutting, the diameter of the nozzle must be between 0.1 – 0.15 mm so we created the test part that can be seen on Figure 3 [5].

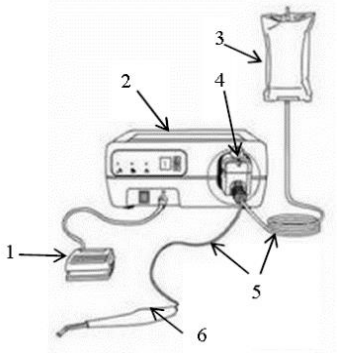

1. pedal (switching on-off the device)
2. motor/generator
3. saline
4. pump piston
5. rubber tubing
6. cutting nozzle

Figure 2
The medical water jet machine

Our investigations were aimed at selecting a suitable technology for the medical water jet machining device's cutting nozzle production. In the end, stainless steel was chosen as test material and experiments were carried out, where drilling was limited to electrical-discharge machining and laser machining trials. By varying the machining parameters, we measured the form and diameter accuracy, the burr formation, the hole's surface roughness, as well as the machining time. Based on our experimental results, we made a suggestion concerning the most suitable technology.

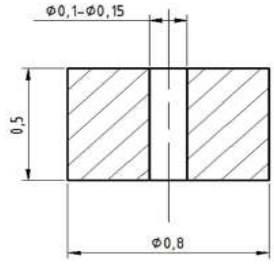

Figure 3
The cutting nozzle

2 Examination of the Holes

First, it is essential to clarify the definition of relevant methods and equipment. The microscopic images were taken by the Dino-Lite Pro AM3013T digital microscope that has a magnification factor of 500x.

Dimensional accuracy. The investigation was carried out by the microscope's computer program called DinoCapture. After calibrating the software, the diameter of the holes was measured manually by selecting the program option that makes it possible to mark some edge points of the hole in the microscopic images. Afterwards, the program automatically calculated its diameter.

Circularity. Precise results can be obtained by using e.g. coordinate measuring machine probes with a very small spherical tip. [6] In the absence of such a device, the measurement of the circularity was once again carried out by DinoCapture. 3-3 points have been marked within both the inner and the outer circle of the entrance and the difference between the two radiuses has yielded the circularity results. This method is merely suitable for providing an approximation of the true values as the inner and the outer circles are not concentric. However, the effect of this limitation is negligible. The circularity was graded on a scale ranging from 1 to 5 where:

1: value of the circularity $\leq$5 µm

2: value of the circularity $\leq$10 µm

3: value of the circularity $\leq$15 µm

4: value of the circularity $\leq$20 µm

5: value of the circularity $\leq$25 µm

Burr formation. The burr formation was examined by analyzing the microscopic images. Previous research [7] has established the basic burr types in conventional drilling. The shape of the burrs can be uniform (a)(b), crown (d) and transient (c). The transient burr is halfway between the uniform and the crown burr. (Figure 4)

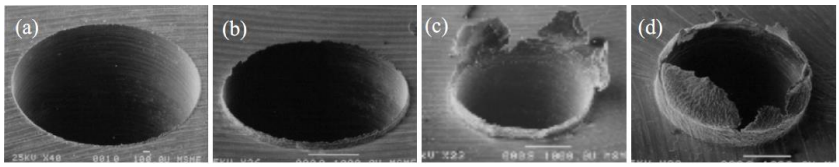

Figure 4
Drilling burr types [7]

Quality of the internal surface. In order to be able to measure the internal surface, the holes had to be cut in half. The examination of the internal surface quality was carried out by a scanning electron microscope (Philips XL 30 SEM) in a laboratory belonging to the Department of Material Science and Engineering (Figure 5).

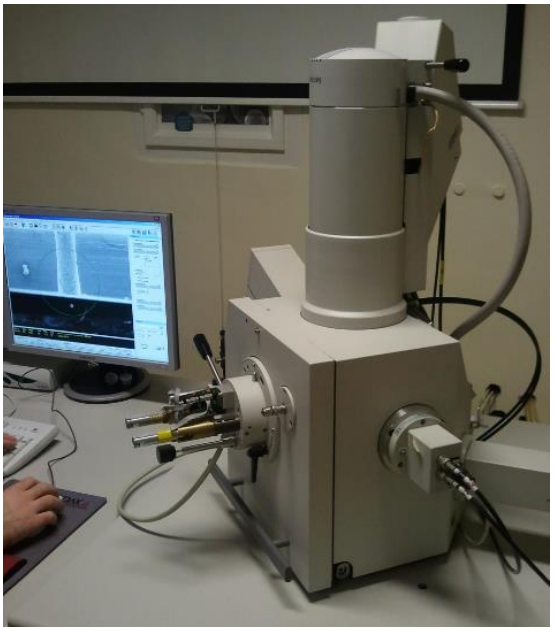

Figure 5
Scanning Electron Microscope

It was not a goal of these experiments and measurements to investigate the machinability parameters [8,9] (e.g. energetics, tool wear or tool life) Nevertheless, the authors consider further machinability research of micro drilling to be one of the primary focus areas of their team's activities.

3 Machining Experiments

3.1 Micro-Drilling

Although mechanical drilling is a traditional cutting technology and as such, its parameters, results as well as the overall process are investigated extensively on a macro level, the micro-drilling process has several modifying factors and we also concluded our results based on this latter approach. When it comes to micro-drilling, there are plenty of additional influencing parameters to be taken into account. These include, but are not limited to, the remarkably high spindle revolution (between 1-12 x 104 min^{-1}), the stability of the spindle and the high cutting forces resulting from a relatively big edge radius (see Figure 6) [10, 11].

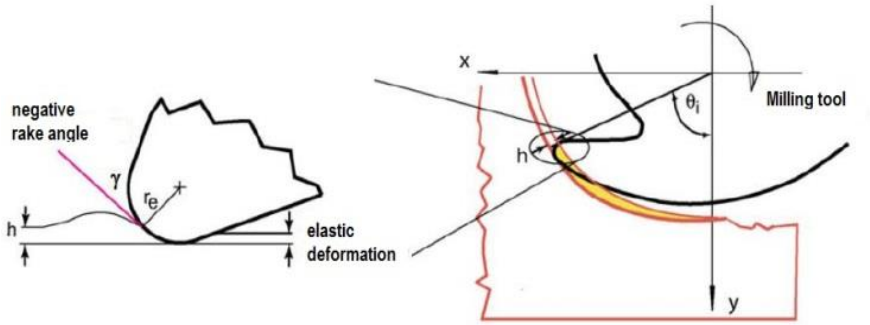

Figure 6

Elastic deformation in micro-drilling as a consequence of the low chip thickness - edge radius ratio

The drilling experiments were carried out in a laboratory owned by the Department of Manufacturing Science and Technology. The machine tool was a high precision lathe called Csepel Ultraturn1. This machine tool is equipped with an additional high speed spindle with a maximum rotational speed of 60000 min^{-1}. Table 2 shows the measured positioning capability of this machine. [12] Figure 7 depicts the machining environment of the micro-drilling experiments.

Table 2

Accuracy of Csepel machine tool

UP 1 lathe (Csepel Ultraturn)	[mm]
Axial error of the spindle	0.001
Radial error of the spindle	0.001
Positioning unit in z direction	0.0001
Positioning unit in x direction	0.0001
Positioning accuracy	0.001
Repeatability	0.001

Figure 7

The Csepel Ultraturn machine tool

During the experiments, SECO tools, an SD22 center drill and an SD26 micro-drill were used. The appropriate tools were chosen after comparing the choice of the main producers and distributors based on the price and technology descriptions.

The experiments also required the use of ASTM 316 (EN 1.4401) stainless steel sheets, the cutting speed and the feed of which were often altered. The detailed parameters of the experiments can be found in Table 3. Figure 8 shows some of the holes corresponding to the numbers presented in the experiment plan (Table 3); the apostrophes indicate the cases where the pilot drill was broken and thus it could not be used.

Table 3
Plan for the micro-drilling experiments

Plan for the experiments					
No.	**Diameter [mm]**	**Cutting speed [m/min]**	**revolution number [min^{-1}]**	**feed [mm/rev.]**	**feed rate [mm/min]**
1	0.15	4.712	10000	0.001	10
2	0.15	4.712	10000	0.002	20
3	0.15	4.712	10000	0.003	30
4	0.15	9.425	20000	0.001	20
5	0.15	9.425	20000	0.002	40
6	0.15	9.425	20000	0.003	60
7	0.15	14.137	30000	0.001	30
8	0.15	14.137	30000	0.002	60
9	0.15	14.137	30000	0.003	90

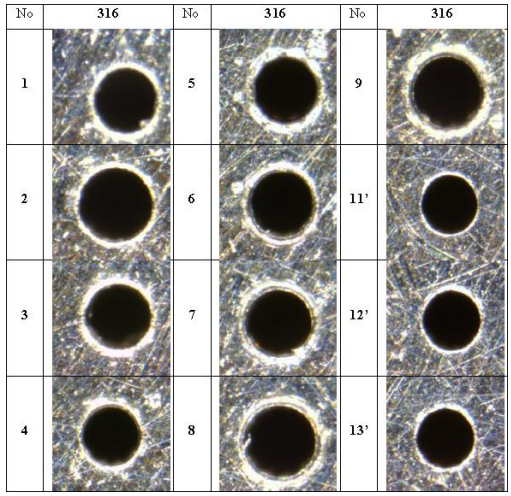

Figure 8
Results of the drilling experiments

Machining time. Machining times depend on the speed and the feed. The shortest time was 8 seconds, whereas the longest was 18 seconds.

Dimensional accuracy. The diameters of the micro-holes are summarized in Table 4. The numbering of the holes in this table is in correspondence with that in Table 3 (the experiment plan).

Table 4 shows that the variation of the parameters did not have a significant influence on the results. However, there are a few exceptions; whenever the pilot drill was not used, the diameter was smaller compared to its size without the pilot drill.

Table 4
Diameter of the micro-holes

Micro-drilling			
No.	**316**	No.	**316**
1	Ø0.152 mm	**7**	Ø0.156 mm
2	Ø0.152 mm	**8**	Ø0.154 mm
3	Ø0.156 mm	**9**	Ø0.152 mm
4	Ø0.154 mm	**11'**	Ø0.148 mm
5	Ø0.155 mm	**12'**	Ø0.148 mm
6	Ø0.158 mm	**13'**	Ø0.146 mm

Circularity. Table 5 demonstrates that the circularity values are appropriate. They refer back to the graded scale (1 to 5) developed earlier in the paper for the purpose of categorizing the approximate circularity values. In Table 5, all the values are between 1 and 2, but we can see that without the use of the pilot drill, we got 2 as a result in each case.

Table 5
Circularity of micro-holes

Micro-drilling			
No.	**316**	No.	**316**
1	2	**7**	2
2	1	**8**	1
3	1	**9**	2
4	1	**11'**	2
5	2	**12'**	2
6	2	**13'**	2

Burr formation. Figure 9 shows the exits of micro-drilling. When the cutting speed and the feed were increased, there was also a noticeable surge in burr formation, mostly resulting in the appearance of transient burrs. This time, however, the use of the pilot drill did not have an impact on the results.

Images of the internal surface. As shown in Figure 10, the surface got the most scratches when we used a minimal cutting speed combined with a maximum feed. Increasing the feed led to further deterioration of the surface quality.

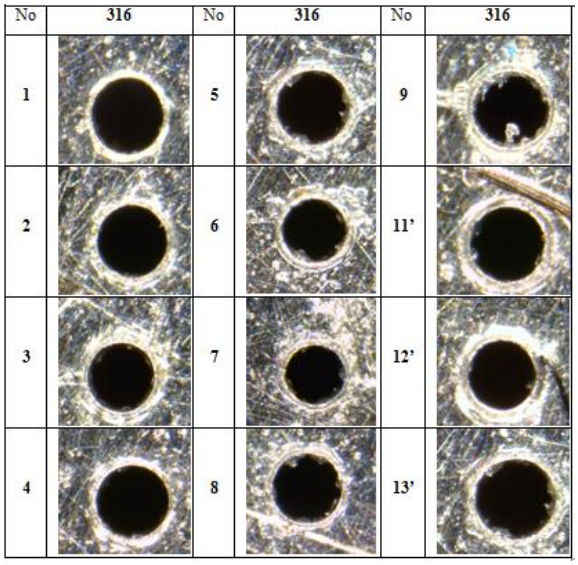

Figure 9
Exit of micro-drilling

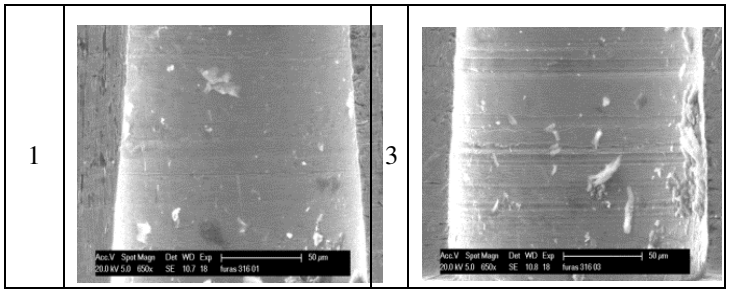

Figure 10
SEM images of micro-drilling

3.2 Laser Drilling

The laser drilling experiments were carried out in the laboratory of the Department of Material Science and Engineering. We used the LASAG KLS 246-FC 40 Nd:YAG laser cutting machine that has an average power of 15 W with a maximum exciting frequency of 5000 Hz. Its minimal focal diameter is 0.03 mm. Therefore it is suitable for producing a hole with a diameter of 0.15 mm. In hole machining application We used a circular trajectory cutting method in the hole machining process. The hole creation strategy can be observed in Figure 11, where the cutting starts out from the center point (1) then an inner circle is applied for roughing (2) and finally, the requested diameter is finished by creating a second circle (3). The machining environment can be seen in Figure 12.

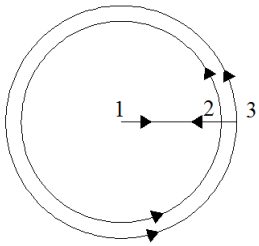

Figure 11
Circular cutting trajectory

During the experiments we varied the pulse time, the frequency, the average power and energy level, as well as the pressure of the oxygen inlet. Table 6 demonstrates the plan for the laser drilling experiments. As Figure 13 reveals, the quality of the laser cutting is lower than that of the micro-drilling operation in terms of form and diameter accuracy. There are only a few holes that fall within the acceptable range of parameters.

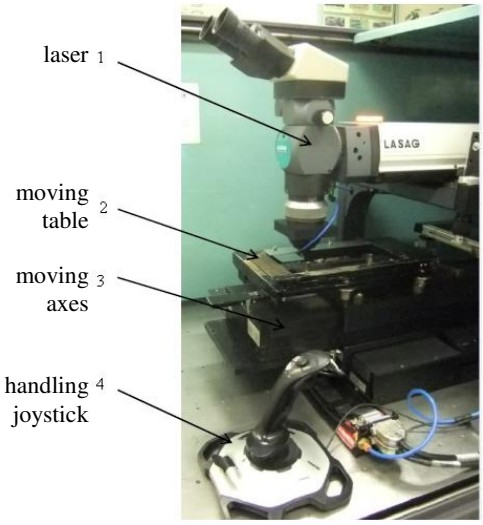

Figure 12
The laser drilling environment

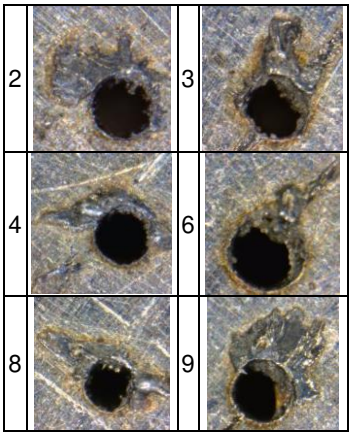

Figure 13
Results of laser drilling

Table 6
The plan for the laser drilling experiments

Plan for the experiments in laser drilling								
No. of holes	**Voltage [v]**	**Pulse time [ms]**	**Frequency [Hz]**	**Cutting speed [m/s]**	**Acceleration [m/s^2]**	**Average power [W]**	**Average energy [mJ]**	**Pressure of oxygen [bar]**
1 - 3	350	0.1	500	1	0.5	15	36	4
4 - 6	350	0.1	500	1	0.5	15	36	5
7 – 9	350	0.1	500	1	0.5	15	36	6
10 – 12	350	0.05	900	1	0.5	13-14	15.3	4
13 – 15	350	0.05	900	1	0.5	13-14	15.3	5
16 - 18	350	0.05	900	1	0.5	13-14	15.3	6

The machining took around 2 seconds.

Dimensional accuracy. The diameter values of the micro holes can be found in Table 7 A). As the frequency was gradually increased, the diameters of the holes became more and more accurate. However, the pressure of the oxygen inlet did not influence the results.

Table 7
Diameter and the circularity of the micro-holes

Laser-drilling				
A) Diameter			B) Circularity	
No.	**316**		No.	**316**
3	Ø0.192 mm		**3**	4
6	Ø0.204 mm		**6**	4
9	Ø0.206 mm		**9**	3
12	Ø0.174 mm		**12**	4
14	Ø0.166 mm		**14**	3
18	Ø0.170 mm		**18**	3

Circularity. The circularity values are displayed in Table 7 B). When the power was at a high level, the pressure of the oxygen inlet did not have a particular influence on the results. However, in cases when the power was low, the frequency was high and the pressure of the oxygen inlet was increased, the overall quality of the circularity was improved. Thus, based on the values in the table, the quality of the circularity is inappropriate.

Burr formation. Figure 13 illustrates the appearance of burrs at the entrance of laser-drilled hole. The burr was generated when the laser beam slammed into the material and the material melted. A higher power level leads to similarly increased burr formation.

Images of the internal surface. Figure 14 depicts the internal surfaces. Since the material has also melted all along the internal surface, the quality level is inappropriate.

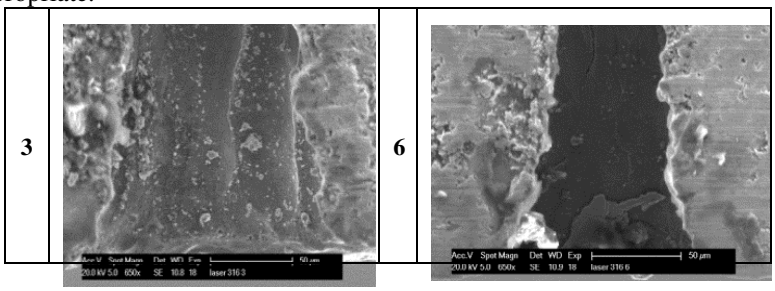

Figure 14
SEM images of laser drilling

3.3 Micro-EDM

As before, the micro electrical discharge machining experiments were carried out in a laboratory belonging to the Department of Manufacturing Science and Technology. Figure 15 shows that we used the Sarix SX100 micro EDM machine tool. The diameter of the applied electrode was Ø 0.15 mm and made of CKi08 material (Sarix regularly used this electrode material that contains 92% WC and 8% Co). During the hole drilling process, we varied the pulse time, the voltage and the frequency. The plan for the micro-EDM experiments can be seen in Table 8. The applied parameters were chosen based on previous experiences and on state of the arts research literature [13].

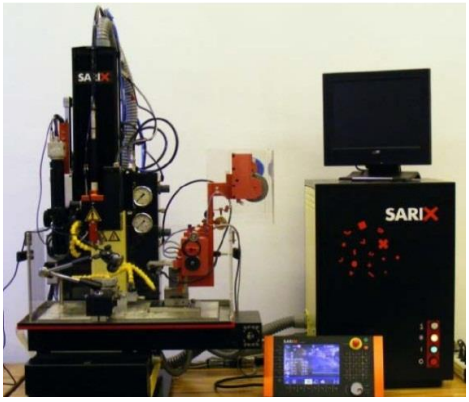

Figure 15
Sarix micro-EDM machine

Table 8
Plan for the micro-EDM experiments

Plan for the experiment in micro-EDM						
No.	**Frequency [Hz]**	**Voltage [V]**	**Current [A]**	**Pulse time [ms]**	**Spark-gap [µm]**	**Gain**
1	100	80	80	4	72	10
2	100	90	80	4	72	10
3	100	100	80	4	72	10
4	120	80	80	4	72	10
5	120	90	80	4	72	10
6	120	100	80	4	72	10
7	150	80	80	4	72	10
8	150	90	80	4	72	10
9	150	100	80	4	72	10

Figure 16 displays some of the results of the machining experiments. The form accuracy of the holes is comparable with that obtained by micro-drilling. In terms of cost and machining time, however, this technology is not the most efficient one.

Machining times were a subject to set discharge parameters. The shortest time was 8 minutes, while the longest lasted for 36 minutes. These times could be reduced by using optional machining parameters.

Dimensional accuracy. The diameters of the micro holes are fully appropriate. There are two outliers (2 and 3) as shown in Table 9.

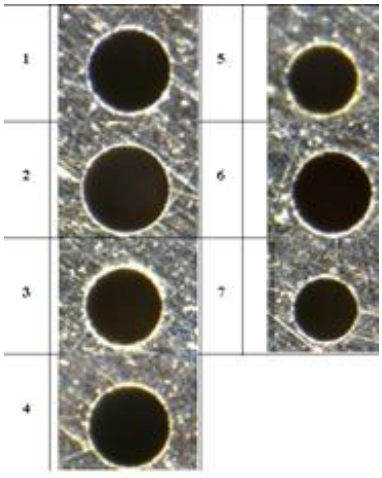

Figure 16
Holes machined by micro-EDM

Table 9
Diameters of the micro-holes

Micro-EDM			
No.	**316**	No.	**316**
1	Ø0.152 mm	**5**	Ø0.148 mm
2	Ø0.186 mm	**6**	Ø0.140 mm
3	Ø0.178 mm	**7**	Ø0.142 mm
4	Ø0.142 mm		

Circularity. The circularity of the micro holes is excellent when using the micro-EDM technology as the values are less than 5 micron. (Table 10)

Table 10
Circularity of the micro-holes

Micro-EDM							
No.	**316**	No.	**316**	No.	**316**	No.	**316**
1	1	**3**	1	**5**	1	**7**	1
2	1	**4**	1	**6**	1		

Burr formation. One of the primary advantages of this technology is that there are no visible burrs at either the entrance or the exit.

Images of the internal surface. No obvious differences can be detected between the pictures. Craters can be observed on all of the internal surfaces of the holes. (Figure 17)

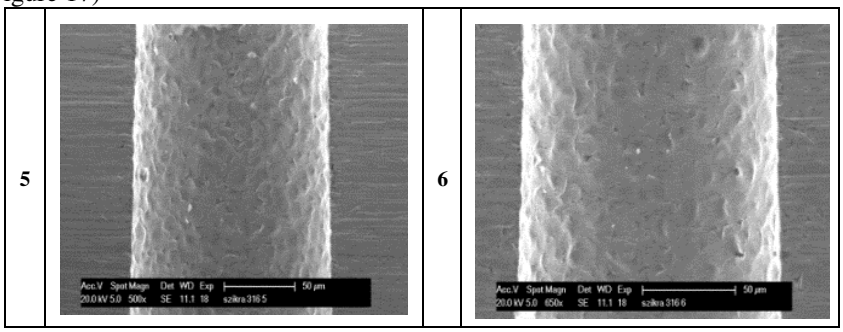

Figure 17
SEM images of micro-EDM

Conclusions

Three different technologies were tested based on the following dimensions: form (1), diameter (2), accuracy and surface roughness (3), burr formation (4), machining time (5), machining time (6), availability of technology (7), opportunities in terms of medical application (8) and accessibility of skilled staff (9).

In Table 11 we evaluate these parameters on a scale of 1 to 5, where 1 is the worst and 5 is the best value. The scores are based on the outcomes of our experiments and their sum determines the overall "quality" of the particular technology. Using this framework for evaluation, we suggest the adoption of the micro drilling technology for industrial application. The second best option is the micro-EDM method, while laser drilling is the least applicable option from the three evaluated.

Table 11
Evaluation of the investigated technologies

Point of view	Micro-drilling	Laser drilling	Micro-EDM
1	4	1	5
2	5	3	4
3	5	1	3
4	2	1	5
5	4	5	1
6	3	5	1
7	5	5	5
8	5	5	5
9	2	4	4

In the near future, we intend to carry out further micro drilling experiments using different types of tools and materials in order to eventually select the optimal parameters. Additionally, we aim to investigate the forces, vibrations and noises produced during the course of these experiments.

Moreover, it is among our future plans to explore the possible methods of burr removal. For instance, they can be removed mechanically using smaller tools - preferably with sharp edges. A major disadvantage of this method is the great manual effort that is required to succeed. If the design is more complex, electropolishing is a more preferred burr removal technology. [14]

Our third main goal is to ascertain the numerical values related to surface roughness. Due to the small diameter of the holes, determining these values is in fact a fairly challenging task. Although a conventional reference-plane surface measuring machine might be able to provide us with the sought data, the process is by no means simple. First of all, the holes and the measuring stylus need to face the same direction. If this condition is not fulfilled, the values will be incorrect. To guarantee that the directions are the same, the sides of the work piece have to be made accurate by grinding. There exist two other relevant technologies that are used to examine the quality of the holes' internal surface. The first one is the atomic force microscope AFM [15] and the second solution takes the form of a 3D optical surface profiler. The latter technology has already been used in a previous research paper titled Zygo NewView. [16]

Acknowledgement

This research was initiated an industrial demand that aimed to compare the application of hole making technology in micro machining range. The work reported in the paper has been developed within the framework of the project „Talent care and cultivation in the scientific workshops of BME". Said project is supported by the grant TÁMOP-4.2.2.B-10/1--2010-0009. This research paper is partially subsidized by the Hungarian Scientific Research Fund and it is registered

under the project number OTKA 101703. The results of this analysis are used in the international bilateral project "Multi-sensors based intelligent tool condition monitoring in mechanical micro-machining", the project number of which is TÉT_10-1-2011-0233. The research and the dissemination of its results gained the support of the CEEPUS III. HR0108 project.

References

[1] John Shanahan (Product Manager of. Makino): Trends in Micro Machining Technologies, EDM Today (2004)

[2] Alaattin Kaçal, Ferhat Yildirim: High Speed Hard Turning of AISI S1 (60WCrV8) Cold Work Tool Steel, Acta Polytechnica Hungarica, Vol. 10, No. 8 (2013) pp. 169-186

[3] Wit Grzesik: Adwanced Machining Processes of Metallic Materials, Elsevier (2008)

[4] Norio Taniguchi: Current Status in, and Future Trends of, Ultraprecision Machining and Ultrafine Materials Processing, CIRP Annals, Manufacturing Technology Vol. 32/2 (1983) pp. 573-582

[5] Vilmos Csala: Application of Micro-Drilling Technology – in Hungarian, BSc Thesis, BME (2012)

[6] Chen-Chun Kao, Albert j Shih: Form measurement of micro-holes. Measurement Science and Technology.18 (2007) pp. 3603-3611

[7] Boris Stirn, Kiha Lee, David A. Dornfeld. Burr Formation in Micro-Drilling. Proceedings of the American Society for Precision Engineering/Virginia (2001)

[8] János Kundrák, Zoltán Pálmai: Application of General Tool-life Function under Changing Cutting Conditions, Acta Polytechnica Hungarica, Vol. 11, No. 2 (2014) pp. 61-76

[9] Richárd Horváth, Ágota Drégelyi-Kiss, Gyula Mátyási: Application of RSM Method for the Examination of Diamond Tools, Acta Polytechnica Hungarica, Vol. 11, No. 2 (2014) pp. 137-147

[10] Pei Yongchen, Tan Qingchang, Yang Zhaojun. A Study of Dynamic Stresses in Micro-Drills under High-Speed Machining. International Journal of Machine Tools & Manufacture. Volume 46, Issue 14 (2006), pp. 1892-1900

[11] Varga, Gy., Dudas, I.: Modelling of Vibration of Twist Drills when Environmentally Friendly Drilling, International Journal of Mathematical Science, Vol. 6, No. 3-4 (2007) pp. 319-338, ISSN: 0972-754X

[12] Csepel UP1 report of the measured accuracy, Csepel Művek Szerszámgépgyár

[13] K. H Ho, S. T Newman: State of the Art Electrical Discharge Machining, International Journal of Machine Tools and Manufacture, Volume 43, Issue 13 (2003) pp. 1287-1300

[14] T. Gietzelt, L. Eichhorn. Mechanical Micromachining by Drilling, Milling and Slotting // Micromachining Techniques for Fabrication of Micro and Nano Structures, 1 (2012) pp. 159-182

[15] Xianghua Wang, Giuseppe Yickhong Mak,Hoi Wai Cho. Laser Micromachining and Micro-Patterning with a Nanosecond UV Laser // Micromachining Techniques for Fabrication of Micro and Nano Structures, 1 (2012) pp. 85-109

[16] Eberhard Bamberg, Sumet Heamawatanachai. Orbital Electrode Actuation to Improve Efficiency of Drilling Micro-Holes by Micro-EDM // Journal of Materials Precessing Technology 209 (2009) pp. 1826-1834

Analysis of the Impact of Front and Back light on Image Compression with SPIHT Method during Realization of the Chroma Key Effect in Virtual TV Studio

Branimir Jakšić[1], Boris Gara[2], Mile Petrovic[1], Petar Spalevic[1], Ljubomir Lazic[3]

[1] Faculty of Tehnical Sciences, Kneza Milosa 7, 38220 Kosovska Mitrovica, Serbia, branimir.jaksic@pr.ac.rs, mile.petrovic@pr.ac.rs, petar.spalevic@pr.ac.rs

[2] Ministry of Interior Republic of Serbia, Kneza Milosa 101, 11000 Belgrade, Serbia, boris.gara@mup.gov.rs

[3] State University of Novi Pazar, Vuka Karadzica bb, 36300 Novi Pazar, Serbia, llazic@np.ac.rs

Abstract: In this paper analysis of the impact of front and back light on compression of static image necessary for realization of the chrome-key effect in virtual TV studio is presented. For image compression SPIHT method is used. The analysis is performed for the fixed value of front light and variable values of the back light. Compression is applied to different values of the bit per pixel (bpp). The quality of compressed images is rated based on the values MSE, SNR and PSNR. The obtained values are displayed in tables and graphics. Based on these graphics a comparison between compressed images with different levels of front and back lights was made and it is given a level of image brightness produces the best results. It was found how the quality of compression varies with the changing brightness of images at different bit per pixel.

Keywords: chroma key; front light; back light; SPIHT method; bit per pixel (bpp); mean square error (MSE); signal to noise ratio (SNR); peak signal to noise ratio (PSNR)

1 Introduction

Chroma key process in television replaces studio set design and reduces the overall costs of the production of the program. It is a way of mixing two video signals, in which the solid background color of a video signal (signal with the live picture from the scene) is replaced by another video signal. Replacement is done by a fast switching circuit that alternately turns on and of a video signal from foreground (FG) and a video signal of the new background (BG). The process of

changing the background is called keying [1, 2]. Inserting a video signal of the new background in a monochrome background of the foreground, is made at the time of scanning, on the border between the object or the participants in the foreground and the background. In this way it creates the impression that the objects of the foreground are in a scene that comes from some other source. One color background can be of any color, provided that the color is not on objects or participants in the front of the stage [3]. Today, blue or green color are used for the background.

Chroma key procedure gives satisfactory results for static scenes (news programs, panel discussions, weather, etc.), but when it comes to shooting scenes with dynamic movements of participants, it does not follow changes in the of angle of shooting, the transition from zoom to the total, or movement from one camera to another, and it is disturbing the real relationship between the participants and the objects of the scene and the sense of space and depth in images is lost.

Because of this, the range of chroma key effect is limited to static relationship with the foreground. Therefore, when a natural relationship of the background and foreground in television production is desired, producers are using a virtual studio [4, 5].

2 Virtual TV Studio

Virtual TV studio provides a natural relationship between the participants and the scenery. Therefore, real-time corrections of the scenery can be generated from computers and coordinates obtained depending on the position of the camera, and ultimately result in the creation of the foreground. In this way the logical relationship between the set and the participants is preserved, and there is also a sense of depth in the images. In virtual studio it is possible to generate scenery that is in the foreground, and that can be opaque or translucent (transparent). Computer-generated scenery has the visual appearance of real decor in the background, and in this way it is possible to create a variety of decors, even surreal decors, so there is a visual impression that the TV studio is a lot larger than it is. Software packages 3D Studio Max, Maya, SoftImage and LightWave are used when we want to create a computer-generated scenery [6, 7].

Virtual studio technology is based on an already described chroma key procedure. In chroma key procedure static two-dimensional computer generated graphics are used for scenery, and those graphics are inserted as a background image. But it does not follow the changes of angle of shooting, transition from zoom to total or movement from one camera to another, and results in a disruption of the real relationship between the participants and the scenery. In virtual studio, data on the position of the camera are processed in the computer and real-time adjustments on the position of the generated 3D graphics and animations are made, based on the

data from the camera. Therefore, the naturalness is retained, there is an illusion of spaciousness and logical relationship between participants and objects in the video signal of live image and scenery is reatined [8].

A studio which implements virtual studio is generally L-shaped or U-shaped, and the newest studios are circular. Scene (walls and floors) should be uniformly colored blue or green while the side walls and places where the wall crosses into the floor should be rounded, to avoid creating unwanted shadows. Blue or green screen can also be used. Diffuse lighting is mostly used, to awoid creation of create shadows. Participants are in nearly empty space, usually with no or only a few real elements in the studio, and the other scenery is generated in a pre-production by a computer and is then combined with the video signal from the camera.

Main equipment of the virtual television studio consists of a camera with CCU (Camera Control Unit), sensors for determining the position of the camera, a computer with high processing power, a chroma keyer and a delay line. Block diagram of a virtual studio with three cameras is shown in Figure 1.

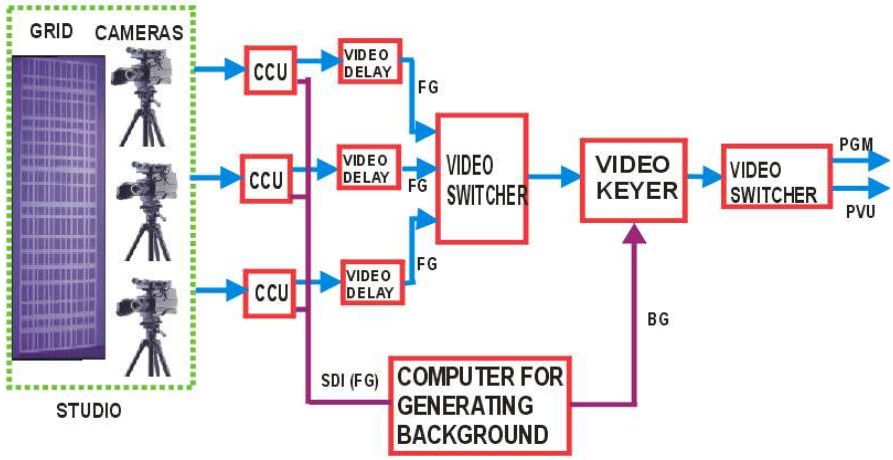

Figure 1
Block diagram of a virtual studio with multiple cameras

The video signal from the camera that captures the foreground, through delay lines is fed to chroma keyer. Information from sensors that determines the position of the camera is fed to a computer with large processing power, on the basis of which real-time correction of the generated scenery is done, and then the corrected information is transmitted to chroma keyer where the two images are combined. The computer has a video output for preview, a video input, an audio input and output, a delay-line for video and audio signals. Supports SD and HD standards, PAL and NTSC formats. The computer is controlled by a software suite that consists of an active relational database for fast and easy visualization (rendering)

of the graphics. All individual set designes have their own separate database. Data on the position of the camera during shooting allows computers to, after data processing, adjust the position of the generated graphics for scenery, so you can maintain the illusion of spaciousness and naturalness.

Manufacturers have developed various methods for determining the position of the camera and the measurements of basic movements that each camera can make (pan, tilt, displacement along the x, y, z axes, zoom and focus). Pan sets the horizontal movement, tilt determines the vertical movement, zoom enlarges or reduces the actual size of the image or the frame and the focus determines the sharpness of the image.

In Pattern System (recognizable grid), a grid is drawn (network) in blue or green chroma key background that lies behind the performers (Figure 1). The grid is drawn in a lighter shade of blue or green. The video signal from the camera is led to the computer with a special video processor and sophisticated software that determines the exact location and orientation of the camera from the video signal, including settings for zoom and focus. Depending on the system, the process of re-calculating the position of the camera lasts from 1 to 3 frames.Chroma key process insertion of a new signal can be done with any color in the background, provided that the color is not on the objects and the participants in the front of the stage. For the background color saturated blue and saturated green are used, and, in special cases, pink [9].

3 Lighting

The biggest challenge when setting up a scene (bluescreen or greenscreen) is setting the light and avoiding shadows because we have to achieve a uniform new color of the background. Shadows can cause appearance of the darker background color, which will not be registered when the background is changing. In order to obtain a better quality of recording it is necessary to make a difference in color (in color coordinates) between the subject and the background, so as to increase the difference between the color of the background or subject. For lighting it is usually the same setting as the default setting for the recording that includes three lights (front, side and back) [10].

Front (direct, main, critical) light is set in the direction of the camera, in the angle of 0° - 30° on each side, with vertical angle of approximately 45°. This angle highlights the greater part of the face, the smaller part remains in the shadows. It should be somewhere between hard and soft light. Too strong or too soft light is generally undesirable for most subjects. In the studio this "golden mean" is achieved by a Fresnel light [11] [12].

For the side light, the supplementary light is placed at angles from 45° to 90° on either side of the camera, or 90° from the main light, but the safest place to be is at 45° from the camera. It needs to be less saturated than the main light and softer. The main and supplementary light should be in the ratio 2:1 (2000 lx : 1000 lx). It eliminates shadows that come from the main light.

Background sidelight is placed on the side of the subject to be shot, from 90° to 135° on each side and is used to illuminate the space background and to get the depth and separation. The intensity of the background light should be about 2/3 of the intensity of the main light elements in the scene. This ensures that the central subject is separated from the background [11] [13].

In Figure 2 types of lights in the implementation of the virtual TV studios are shown.

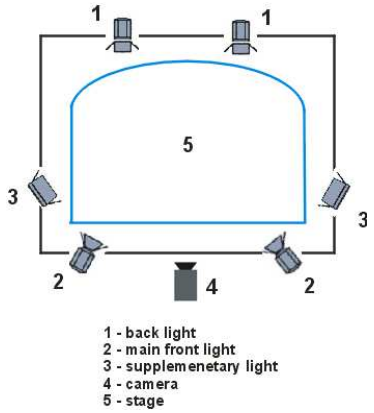

Figure 2

Types of lights in the implementation of the virtual TV studios

The light sources are characterized by the color temperature. Color temperature (°K) is the temperature to which the black body should be heated - (a light source) so its color is colorimetric most similar to the color of the secondary sources of daylight.

The intensity of light (luminous intensity I) falling on a surface depends on the strength of the light source, and the distance between the source and the area to be illuminated.

Luminous intensity (intensity of the light source, cd, I) is the amount of light energy that a point source of light emits per second in one direction given by unit of spatial angle.

Brightness (luminance intensity, lx, E) is the amount of light energy that per second falls on a unit area. Units are lux (lx) and foot-candle (fc). Lux and foot candle are units of volume illumination. The difference is that the lux is metric and foot-candle Saxon measure [14].

4 Realization of the TV Studio

Analysis compression is performed over images obtained in the TV studio with area of 12x8 = 96 m^2 and a height of 4.5 m. Dimension of the blue background is 8 x 3,5 m. Disposition of the lights in relation to the object in the scene is shown in Figure 3.

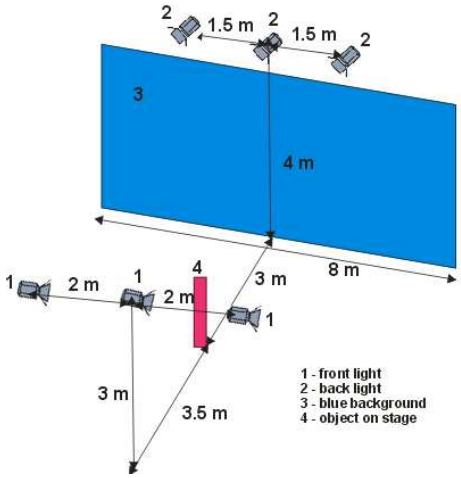

Figure 3
Disposition of the lighting in TV studio

Number of the front and the back lights is 3, and all lights are set at an angle of 45° to the horizontal plane. Horizontal distance between the front and back light is 6.5 m. The spacing between the back lights is 1.5 m and they are placed at a height of 3 m in relation to the scene. Devices for the formation of the back lights Reflector. Flourescent soft lights 2 lamps 55 W, 3200 K were used. The front lights are mounted at a height of 3 meters in relation to the scene, and the spacing between them is 2 m. As a devices for the formation of the front light Fresnel Reflectors lens (150 mm Fresnel lens and G22 lamp holder, halogen lamp 1000 W, 3200 K) were used.

For the color temperature control an instrument was used to measure the color temperature Minolta Color Meter II. For the control of the light intensity digital luxmeter VDVM1300 was used.

In this analysis, the object that is being filmed is at a distance of 3 m from the background (and the back light) and 3.5 m from the front light. For filming the object in the scene a digital camera Canon EOS 550D was used. It is set at a distance of 2 m from the object.

In practical cases the object in the scene can be placed at any distance between the front and the back lights.

5 SPIHT Compression Algorithm

Development of digital images led to the appearance of several methods to store digital pictures. In order to reduce the size of storage needed for high resolution still digital images, it is necessary to perform compression and thus reduce the file size. Compression is the process of eliminating data redundancy or converting data into a form that occupies less storage space.

The JPEG (Joint Photographic Experts Group) method is a standard procedure for image compression. It is an established method for the compression of both B/W and coloured images in real (natural) scenes. It is used for the compression of natural images and paintings, but it is not efficient for the compression of text images, freehand and technical drawings. Together with GIF, JPEG is the most popular format for transferring images over the Internet due to a satisfactory compression ratio and support by all web browsers for these file formats.

EZW (Embedded Zero-tree Wavelet) algorithm enables the progressive transmission of a compressed image. By using this algorithm, it is possible to stop the encoding process at any moment when the desired bit-rate is achieved. In the wavelet decomposition, the image is divided into sets of frequency/spatial hierarchical sub-bands. The important premise of the zero-tree algorithm is that substantial redundancy exists between the "parent" and "child" samples within the sub-band hierarchy [15].

EZW algorithm has very good performance (peak signal to noise ratio - PSNR) compared to other compression algorithms with low bit-rates. It keeps significant coefficients in all levels. The main drawback of the EZW algorithm is its complexity which impacts calculation resources [16, 17].

The EZW algorithm is used as a base for development of large number of similar compression methods. One of the most popular methods is SPIHT (Set Partitioning In Hierarchical Trees). In the original EZW method, arithmetic coding of the bit streams was essential to compress the ordering information as conveyed by the results of the significance tests.

Unlike the EZW, SPIHT doesn't use arithmetic coding. The subset partitioning is so effective and the significance information so compact that even binary un-coded transmission achieves similar or better performance than EZW. The reduction in complexity from eliminating the arithmetic encoder is significant.

The algorithm is introduced by Said and Pearlman [18] for the compression of still images. This method gives better results for larger compression ratios than EZW. The term "Hierarchical Trees" points to quad trees that consist of "parent" and "child" nodes as defined in EZW. Set Partitioning is the operation that divides wavelet coefficients from quad trees into partitions.

The algorithm selects the coefficients $c_{i,j}$ such that, with n decremented in each pass, the coefficients are distributed into three ordered lists - List of Insignificant Sets (LIS), List of Insignificant Pixels (LIP) and List of Significant Pixels (LSP).

After initialization, the following steps are iterated: sorting pass, refinement pass and quantization step update. Through those steps the appropriate significance, sign and most significant bits are sent to the decoder or stored on file.

6 The Measures of Compression Quality

Three of the most used measures for the comparison of image quality are the mean square error (MSE), signal to noise ratio (SNR) and peak signal to noise ratio (PSNR).

A method for the estimation of image quality is needed in order to give a view about how "lossy" compression methods modify image quality. We may treat an image as a matrix whose elements are image pixels.

The estimation process is then based on the calculation of distances between appropriate elements of input and output matrices. In this way, not only comparison of quality of different compression methods is enabled, but also comparison of the results of the same method using different compression ratios.

We denote the matrix A at the input of the compression system with elements a_{ij}, with $i \in \{1...M\}$, $j \in \{1...N\}$, where M is the number of image elements in the vertical and N is the number of image elements in horizontal direction [19]. MxN is the total number of image elements.

The output of the compression system is the matrix A' with elements a'_{ij}. The distance between the elements of matrices A and A' represents the error or the loss of image quality. Usually, the error is larger for higher compression ratios. A user can set the compression ratio according to the desired image quality, and hence directly influence the data size of the compression image [19].

The total reconstruction error is defined as:

$$E = \sum_{i=0}^{m-1} \sum_{j=0}^{n-1} \left\| a_{ij} - a'_{ij} \right\|^2 \tag{1}$$

The distance between matrices A and A' is frequently calculated using the Mean Square Error:

$$MSE = \frac{1}{MxN} \sum_{i=0}^{m-1} \sum_{j=0}^{n-1} \left\| a_{ij} - a'_{ij} \right\|^2 \tag{2}$$

where MxN is the total number of image pixels, and the sum is applied to all image elements.

The amplitudes of image elements are in the range $[0,2^n-1]$, where n is the number of bits needed for binary representation of amplitude of each element in the original image. MSE does not consider amplitudes of image elements (it only considers differences between amplitudes) and it is the reason for introducing the Peak Signal to Noise Ratio:

(3)

The variable MAX_I is the maximum amplitude value of image element (pixel). When the amplitude of the image pixel is represented by B bits, MAX_I is 2^B-1

7 System Model

For the analysis we have used uncompressed images with original resolution of 1600x1200 pixels, and analysis was carried out in the previously described virtual studio.

The images are illuminated with different lighting intensity of front and back studio lights. Image analysis is divided into three blocks. The first is for the case of fixed front light at 200 lx, the other for a fixed at 800 lx, and the third for the fixed at 1400 lux. For all three cases the back light is changed in the range of 200 to 1400 lx. In Figure 4, Figure 5 and Figure 6 are given the appearance of images that have been subjected to compression.

Figure 4

Appereance of images obtained for front light at 200 lx and back light: a) 200 lx, b) 400 lx, c) 600 lx, d) 800 lx, e) 1000 lx, f) 1200 lx, g) 1400 lx

Figure 5

Appereance of images obtained for front light at 800 lx and back light: a) 200 lx, b) 400 lx, c) 600 lx, d) 800 lx, e) 1000 lx, f) 1200 lx, g) 1400 lx

Figure 6

Appereance of images obtained for front light at 1400 lx and back light: a) 200 lx, b) 400 lx, c) 600 lx, d) 800 lx, e) 1000 lx, f) 1200 lx, g) 1400 lx

Figure 7, Figure 8 and Figure 9 shows the appearance histograms of images obtained in a Virtual TV studio.

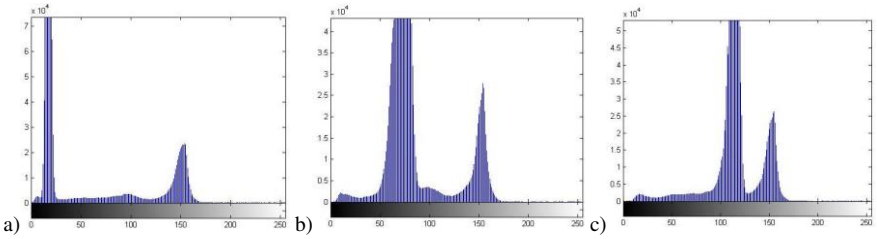

Figure 7

Histograms of images obtained for front light at 200 lx and back light: a) 200 lx, b) 800 lx, c) 1400 lx

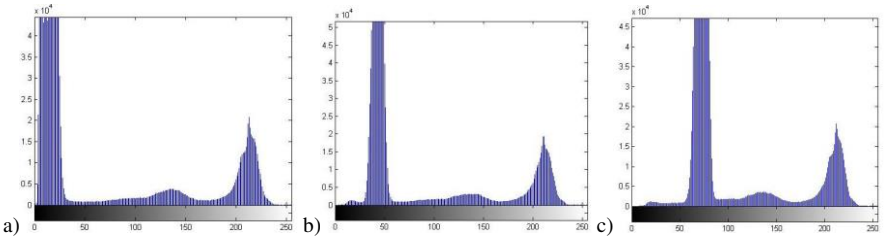

Figure 8

Histograms of images obtained for front light at 800 lx and back light: a) 200 lx, b) 800 lx, c) 1400 lx

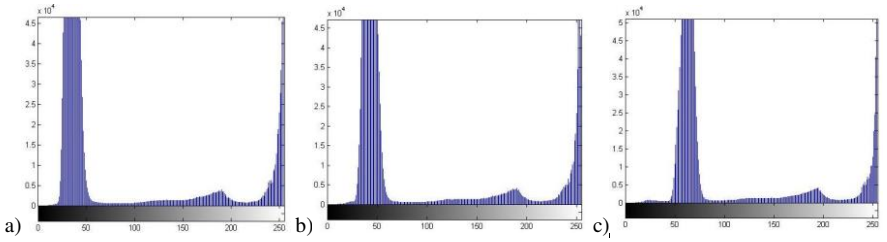

Figure 9

Histograms of images obtained for front light at 1400 lx and back light: a) 200 lx, b) 800 lx, c) 1400 lx

Figure 10 shows an example of the realization of chroma key effect in the case of the front and back lighting with intensity of 1400 lx.

Image compression is performed in the software package Matlab 7.0 using module for compression with SPIHT algorithm. Ten transfer rates are applied: 0.05 0.1, 0.2, 0.3, 0.4, 0.5, 0.7, 1.0, 1.5 and 3.0 bits / element images (bpp). Based on the differential between the original and reconstructed images, following values were computed: middle squared error (MSE), ratio signal / noise (SNR) and peak signal / noise ratio (PSNR).

Figure 10

An example of the realization of chroma key effect with the front and back light of 1400 lx

8 Analysis Results

The values of MSE, SNR and PSNR for different speeds of transfer and for different degrees of studio lighting for front and back lights are given in Table 1, Table 2 and Table 3, respectively.

Table 1

MSE values for compression images with different values of the front and back lights

front light [lx]	back light [lx]	bpp									
		0.05	0.1	0.2	0.3	0.4	0.5	0.75	1	1.5	3
200	200	4.6	2.9	2.1	1.7	1.4	1.2	0.8	0.5	0.3	0
	400	5.9	4.6	3.5	2.9	2.4	2.1	1.5	1	0.5	0.1
	600	6.4	4.8	3.6	3	2.5	2.1	1.5	1	0.5	0.1
	800	7.3	5.9	4.6	3.9	3.4	2.9	2	1.5	0.7	0.1
	1000	8	6.4	5	4.3	3.7	3.1	2.2	1.6	0.8	0.1
	1200	8.5	6.7	5.3	4.4	3.8	3.3	2.3	1.7	0.8	0.1
	1400	8.9	7.2	5.7	4.8	4.2	3.6	2.5	1.9	0.9	0.1
800	200	5.8	3.2	2.1	1.6	1.3	1	0.7	0.5	0.2	0
	400	6	3.4	2.3	1.8	1.5	1.3	0.8	0.6	0.3	0
	600	6.1	3.9	2.8	2.3	1.9	1.6	1.1	0.7	0.4	0.1
	800	6.7	4.2	3	2.5	2.1	1.8	1.2	0.8	0.4	0.1
	1000	6.5	4.3	3.1	2.5	2.1	1.8	1.3	0.8	0.4	0.1
	1200	6.8	4.4	3.2	2.6	2.2	1.8	1.3	0.9	0.5	0.1
	1400	7	4.6	3.3	2.7	2.3	1.9	1.4	0.9	0.5	0.1
1400	200	6.1	3.4	2.3	1.8	1.4	1.2	0.8	0.5	0.3	0
	400	6.1	3.6	2.4	1.9	1.5	1.3	0.9	0.6	0.3	0
	600	6.6	3.7	2.4	1.9	1.6	1.3	0.9	0.6	0.3	0
	800	6.2	3.7	2.6	2.1	1.7	1.4	0.9	0.6	0.3	0
	1000	6.3	3.9	2.7	2.2	1.8	1.5	1	0.7	0.3	0
	1200	6.7	4.2	2.9	2.4	2	1.7	1.1	0.7	0.4	0
	1400	6.7	4.3	3	2.4	2	1.7	1.2	0.8	0.4	0

Table 2

SNR values for compression images with different values of the front and back lights

front light [lx]	back light [lx]	bpp									
		0.05	0.1	0.2	0.3	0.4	0.5	0.75	1	1.5	3
200	200	27.9	29.9	31.3	32.3	33.1	33.8	35.7	37.2	40.3	48.4
	400	25.7	26.9	28.2	29	29.8	30.5	32	33.6	36.4	45.3
	600	22.6	23.6	24.7	25.4	26.1	26.7	28.3	29.6	32.9	41.3
	800	21.1	22	23	23.7	24.4	25	26.6	27.8	31.1	39.5
	1000	20	21.2	22.3	23.1	23.8	24.5	25.9	27.5	30.4	39.2
	1200	20.2	21.1	22.2	22.9	23.6	24.3	25.8	27.1	30.3	38.9
	1400	19.9	20.8	21.9	22.6	23.3	24	25.4	26.8	30	38.6
	200	30.4	33.1	35	36.2	37.1	38	39.9	41.5	44.7	52.6
	400	29.7	32	33.6	34.7	35.6	36.3	38.1	39.7	42.7	51

800	600	28.7	30.7	32.1	33	33.8	34.5	36.1	37.9	40.6	49.1
	800	28.3	30.3	31.7	32.6	33.4	34.1	35.7	37.4	40.2	48.8
	1000	27.9	29.8	31.2	32.1	32.8	33.5	35.1	36.8	39.6	48.2
	1200	27.3	29.2	30.6	31.5	32.3	33	34.5	36.2	39.1	47.8
	1400	26.6	28.4	29.8	30.7	31.4	32.1	33.7	35.3	38.2	46.9
1400	200	31.1	33.6	35.3	36.4	37.3	38.1	40	41.7	44.9	53.2
	400	30.8	33.2	34.9	35.9	36.8	37.5	39.4	41.1	44.2	52.6
	600	30.6	33.2	34.9	36	36.9	37.6	39.4	41.2	44.2	52.7
	800	30.5	32.8	34.4	35.4	36.2	36.9	38.7	40.5	43.5	52.1
	1000	30.1	32.2	33.8	34.7	35.6	36.3	38	39.9	42.8	51.5
	1200	29.9	31.9	33.5	34.4	35.2	35.9	37.6	39.5	42.4	51.2
	1400	29.4	31.3	32.8	33.7	34.5	35.3	37	38.8	41.8	50.6

Table 3

PSNR values for compression images with different values of the front and back lights

front light [lux]	back light [lux]	bpp									
		0.05	0.1	0.2	0.3	0.4	0.5	0.75	1	1.5	3
200	200	41.5	43.5	44.8	45.9	46.7	47.4	49.3	50.8	53.8	62
	400	40.4	41.6	42.7	43.5	44.3	45	46.4	48	50.8	59.7
	600	40.1	41.3	42.6	43.4	44.2	44.9	46.4	48	50.8	59.7
	800	39.5	40.4	41.5	42.2	42.9	43.5	45	46.4	49.5	58.1
	1000	39.1	40.1	41.1	41.8	42.5	43.2	44.7	46	49.2	57.8
	1200	38.8	39.9	40.9	41.7	42.3	43	44.5	45.8	49.1	57.5
	1400	38.6	39.6	40.6	41.3	41.9	42.5	44.1	45.4	48.7	57.1
800	200	40.5	43.1	44.9	46.2	47.1	47.9	49.9	51.4	54.7	62.6
	400	40.3	42.8	44.4	45.5	46.4	47.1	49	50.5	53.5	61.8
	600	40.2	42.2	43.6	44.5	45.4	46	47.6	49.4	52.1	60.6
	800	40	41.9	43.3	44.2	45	45.7	47.3	49	51.8	60.4
	1000	39.9	41.8	43.3	44.1	44.9	45.6	47.2	48.8	51.7	60.3
	1200	39.8	41.7	43.1	44	44.8	45.5	47	48.7	51.6	60.2
	1400	39.7	41.5	42.9	43.8	44.5	45.2	46.8	48.4	51.3	60
1400	200	40.3	42.8	44.5	45.6	46.5	47.3	49.2	50.9	54.1	62.4
	400	40.3	42.6	44.3	45.4	46.3	47	48.8	50.5	53.6	62
	600	40.2	42.5	44.2	45.3	46.2	46.9	48.7	50.5	53.5	61.9
	800	40.1	42.4	44.1	45	45.9	46.6	48.4	50.2	53.2	61.8
	1000	39.9	42.2	43.8	44.8	45.6	46.3	48.1	49.9	52.9	61.6
	1200	39.9	41.9	43.5	44.4	45.2	45.9	47.6	49.5	52.4	61.2
	1400	39.8	41.8	43.3	44.3	45.1	45.8	47.5	49.3	52.3	61.2

In the given tables it is shown that the MSE values decrease and the values of SNR and PSNR increase with increasing bpp for all images with different lighting conditions.

Graphic display of changes PSNR with increasing speeds of transfer due to compression in the case of fixed front light at 200 lx, 800 lx to 1400 lx are shown in Figure 11, Figure 12 and Figure 13, respectively.

From the graphics shown in Figure 11, Figure 12 and Figure 13 it can be seen that the PSNR increases with increasing bpp. At lower values of bpp, PSNR values for different intensity of brightness are approximately the same. With increasing intensity of front light PSNR is also increasing. Growth of the PSNR for increasing intensity of back light is much more pronounced than for the lower value of fixed front light. At higher values of fixed front light, difference between PSNR for different values of the intensity of the back light is smaller.

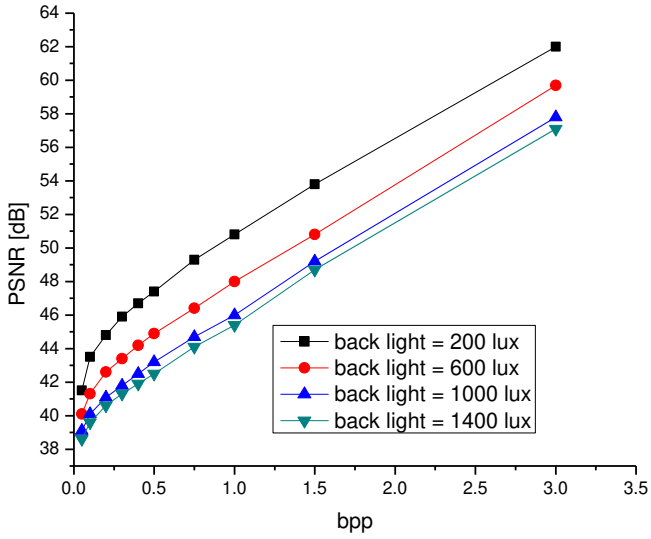

Figure 11
Change of PSNR for different values of bpp with fixed front light = 200 lx

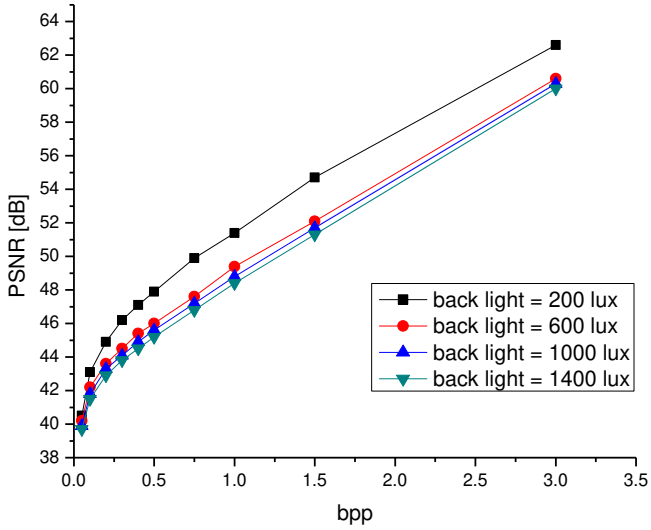

Figure 12
Change of PSNR for different values of bpp with fixed front light = 800 lx

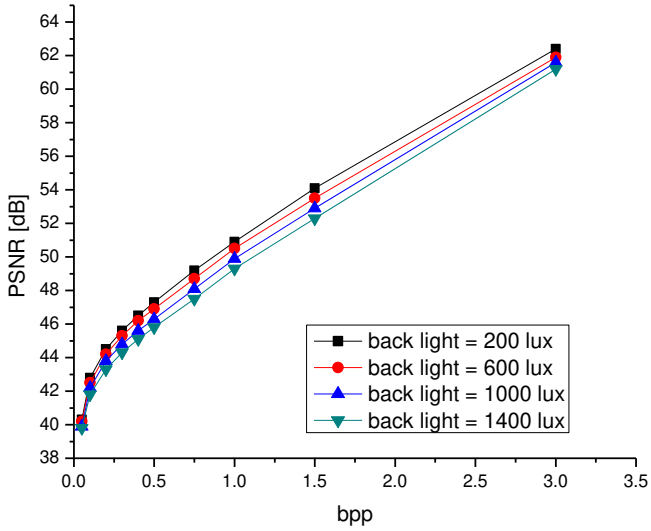

Figure 13
Change of PSNR for different values of bpp with fixed front light = 1400 lx

Figure 14 shows the change of PSNR with increasing intensity of the back light, for different intesities of the front light and the bit per pixel image (bpp).

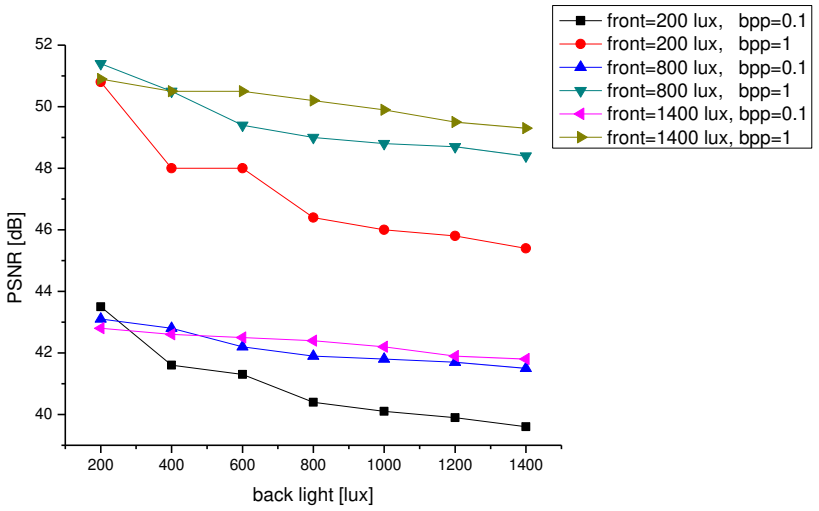

Figure 14
PSNR change for different strengths of the front ligh

Figure 14 shows that with increasing intensity back light PSNR is decreasing for any value of bpp and front light. Fastest decrease is achieved with lower values of the front light, while for the biggest values decrease of the PSNR is less pronounced. Higher PSNR values are obtained for higher values of the front light, while lower values of the front light give a lower PSNR values.

Conclusions

The quality of compressed images needed for the realization of the effect of chroma key is a very important feature, because its quality, depends on successful realization of chroma key effect. One of the most important factors in the realization of chroma key effect in virtual TV studio is disposition of spotlights and intensity of studio lighting.

Based on the obtained results it can be concluded that the quality of the images compressed with SPIHT method is better for higher values of bpp (bit per pixel image) than for the lower. With increasing intensity of front light the quality of compressed image increases. Quality improvement of compression is much more pronounced with higher intensity of back light than at lower levels of fixed front light. With increasing intensity of the back light quality of compression decreases for any value of bpp and front light. Better quality of compression is obtained at higher values of the front light. Applied analysis and obtained results can be used in the realization of virtual digital multimedia TV studios to obtain quality compressed images.

Acknowledgement

This work was done within the research project of the Ministry of Science and Technological Development of Serbia III47016 and TR35026.

References

[1] M. Moshkowitz: *The Virtual Studio: Technology and Techniques*, Focal Press 2000

[2] G. Thomas: *Prompting Guide for Chroma keying*, US Patent, No. 5, 1998

[3] S. Göbel, C. Geiger, C. Heinze, D. Marinos, *A Virtual Archery Simulator*, Advanced Visual Interfaces, Rome, Italy, ACM, 2010, pp. 337-340

[4] D. Hughes: *Virtual studio technology*, 1996

[5] M. Rotthaler: *Virtual Studio Technology: An Overview of the Possible Applications in Television Programme Production*, EBU Technical Review, 1996

[6] O. Grau, T. Pullen, G. A. Thomas: *A Combined Studio Production System for 3-d Capturing of Live Action and Immersive Actor Feedback*, IEEE Transactions on Circuits and Systems for Video Technology 14, March 2004, pp. 370-380

[7] O. Grau: *3d Sequence Generation from Multiple Cameras*, International workshop on multimedia signal processing 2004, Siena, Italy, September 2004

[8] J. Herder, M. Wilke, J. Heimbach, S. Göbel, D. Marinos, *Simple Actor Tracking for Virtual TV Studios Using a Photonic Mixing Device*, 12th International Conference on Human and Computer, Hamamatsu/Aizu Wakamatsu/Duesseldorf, December, 2009

[9] M. Petrovic, B. Jaksic, P. Spalevic, I. Petrovic, V. Dakovic: *The Analysis Background on the Effect of Chroma-Key in Virtual TV Studio*, INFOTECH 12, Jahorina, Bosnia and Herzegovina, 2012, pp. 937-941

[10] I. Schiller, R. Koch, *Data Structures for Capturing Dynamic Sceneswith a Time-of-Flight Camera*, Dynamic 3D Imaging Workshop at DAGM 2009, Dyn3D, LNCS 5742, Jena, Germany, September 2009, pp. 42-57

[11] D. Lyver and G. Swainson: *Basics of Video Lighting*, 2nd ed, Oxford, England, 1999

[12] I. Schiller, B. Bartczak, F. Kellner, R. Koch, *Increasing Realism and Supporting Content Planning for Dynamic Scenes in a Mixed Reality System incorporating a Time-of-Flight Camera*, Journal of Virtual Reality and Broadcasting, Vol. 7, No. 4, 2010

[13] B. Fitt, J. Thornley: *Lighting Technology: a Guide for the Entertainment Industry*, 2nd ed, Elsevier, 2001

[14] N. Mobsby: *Lighting Systems for TV Studios*, Entertainment Technology Press Ltd, 2001

[15] S. Vijayarani, M. Vinupriya, *Performance Analysis of Canny and Sobel Edge Detection Algorithms in Image Mining*, International Journal of Innovative Research in Computer and Communication Engineering, Vol. 1, No. 8, 2013

[16] N. I. Glumov, A. V. Kuznetsov, *Analysis of Images for Local Artificial Changes with JPEG Compression Properties*, Pattern Recognition and Image Analysis, Vol. 22, No. 1, March 2012, pp. 210-214

[17] L. Malnar, B. Kosović, J. Batan: *Image Compression using EZW Algorithm*, ZESOI, Zagreb, Croatia, 2007 (in Croatian)

[18] S. Ilic, M. Petrovic, B. Jaksic, P. Spalevic, Lj. Lazic, M. Milosevic, *Experimental Analysis of Picture Quality after Compression by Different Methods*, Przegląd elektrotechniczny, ISSN 0033-2097, R. 89 NR 11, 2013

[19] M. Jančić: *The Norms for Image Compression*, FER, Zagreb, Croatia, 2002 (in Croatian)

Compressive Properties of Commercially Available PVC Foams Intended for Use as Mechanical Models for Human Cancellous Bone

Ákos Oroszlány, Péter Nagy, József Gábor Kovács

Department of Polymer Engineering, Faculty of Mechanical engineering,
Budapest University of Technology and Economics
Műegyetem rkp. 3, H-1111 Budapest, Hungary
akos.oroszlany@audi.hu, nagy@pt.bme.hu, kovacs@pt.bme.hu

Abstract: Compressive properties of three commercially available rigid polyvinyl chloride (PVC) foams intended for use as possible model material for human cancellous bone were investigated. Quasi-static compression tests were performed on PVC foam blocks of different densities (0.10, 0.13 and 0.20 g/cm^3) with a crosshead speed of 0.15 mm/sec to determine the compressive Young's modulus, the yield strength and the energy absorbed until yield. The results were compared with data obtained on human cancellous bone and polyurethane (PUR) foams. Results showed that according to their Young's modulus and yield strength the investigated 0.1 and 0.13 g/cm^3 PVC foams are suitable as mechanical model material for Osteoporotic cancellous bone, while 0.20 g/cm^3 PVC foam is suitable as model material for normal bone. According to the energy absorbed until yield the 0.10 g/cm^3 PVC foams are suitable as mechanical model material for Osteoporotic(OP) cancellous bone. For the modeling of normal bone both the 0.13 and 0.20 g/cm^3 PVC foams are suitable. Based on these results, it can be concluded that the examined PVC foams may prove suitable as a model material for OP and normal cancellous bone.

Keywords: PVC foam; compressive properties; synthetic bone; human cancellous bone; Osteoporotic bone; cross-linking

1 Introduction

Cadaveric bone tissue is widely used for biomechanical tests and in medical implant-related research. Biological samples have a high variance in mechanical properties, caused by age, weight, sex and physical characteristics. This complicates the comparative testing of medical implants, and requires a higher number of test specimens. To reduce the high variance of properties between test specimens, the samples must be carefully selected. For these reasons the comparability and reproducibility of the results achieved often demands a larger number of test specimens. Comparative testing of orthopedic implants in human

cadavers is very limited not only because of biological but of ethical, and economical reasons, too [1-4].

Animal models provide a possible solution for biomedical research, since the healing of fractures and bone defect repair can be investigated. The use of living animal models have been disputed over the last 150 years. Animal models are simplified representations of the actual system of interest; they possess the same or similar functions and structures as the system under study. Biomedical studies using animal models may offer advantages over human cadavers, since the models are often simpler to control and manipulate, and ethical concerns may be less troublesome to address. The number of test specimens must still be large for reasons of comparability and reproducibility. When selecting an animal model bone phenotype, cross-species biomechanical properties should also be considered. Since there are no established standards, and there is a wide variety of bone shapes and sizes, a large number of variables must be considered when establishing mechanical testing procedures. The need for control groups, the care of animals etc. make animal models expensive, and should only be used when studying biological processes in the body. Because of these considerations, it is desirable to refine and reduce the use of animals and to find alternative models [5-8].

Synthetic materials offer a wide range of possibilities as bone model materials. The major advantage of synthetic materials is that they can be engineered to meet certain requirements, and will have constant material properties. The cellular structure of foams resembles that of cancellous bone and their mechanical properties like strength and stiffness are also similar to those of cancellous bone. They provide an uncontaminated, clean test environment, which makes them the ideal choice when biological processes in the body are not part of the research. For this reason they can be used effectively in the development of bone fixating implants, since the measurement results are not affected by the biological diversity of even one species. Biomechanical measurements performed with the help of synthetic materials are easy to control, repeat and compare [6, 9].

Synthetic whole bones are widely used for the testing of fracture reconstruction systems in cases when anatomic correspondence is of concern. Such systems are used for example in the reconstruction of human long bones, spine and vertebra. Heier et al. compared replicate femurs and tibias made of short-glass-fiber-reinforced (SGFR) epoxy, and fiberglass-fabric-reinforced (FFR) epoxy to model human femurs under bending, axial, and torsional loads [10]. Sommers et al. studied an osteoporotic long-bone model and validated surrogate models for normal bone. They found that validated surrogate models for osteoporotic bone were also needed because of the differences between the two models [11]. Johnson et al. prepared synthetic thoracic vertebrae from open-cell rigid foam to study their morphological and mechanical (static, dynamic) properties. Their research showed that synthetic open-cell foam vertebrae with a fiberglass resin cortex offers an alternative to human vertebral bone in static and dynamic

biomechanical experiments [12]. Wähnert et al. prepared a distal femur model from 0.15 g/cm^3 density PUR foam to model osteoporotic bone. Their results showed that their method for customizing artificial bones could provide suitable results, although it disregarded cortical bone [13].

The whole bone model is not always in *in vitro* biomechanical tests, in most cases it is enough to use a part of the bone (eg. only the femoral head instead of the whole femur). In practice, several materials have been used as model material for bones. Filled epoxy resins, glass or carbon fiber composites, or solid polyurethane (PUR) are all used to substitute cortical bone [9]. For the modeling of cancellous bone mostly rigid or semi-rigid porous polymeric foams are used. Szivek et al. studied several PUR mixtures for the substitution of cellular bone. They measured the elastic modulus, yield and compressive strength of different, closed cell PUR foams, and concluded that with appropriate ratios of isocyanate to polyol a porous bone-like foam structure can be achieved. The mechanical properties of such foams are reproducible and could resemble those of human bone [14-15]. Thompson et al. studied under torsion and axial loading the shear and compressive properties of four types of rigid polyurethane foams, which are sold for biomechanical tests. They concluded that these foams may be used to simulate the elastic but not the failure properties of cancellous bone [16]. Shepherd et al. compared the compressive properties of three kinds of PUR foam to that of normal and osteoporotic human bone. In their study they measured the Young's modulus (E), yield strength (σ_y) and energy absorbed utill yield (ΔE_y) of the studied foams. They concluded that the 0.16 g/cm^3 foam could substitute osteoporotic human bones during *in vitro* testing of biomedical implants in cases when fracture stress is of concern. The 0.32 g/cm^3 foam could substitute normal human bones in the same situation. Furthermore, neither of the studied PUR foams should be used when energy dissipation or fatigue is of concern [17]. Although PUR foams are widely used as bone model material, Shikimani et al. used polycarbonate (PC) plates and compared their results with measurements made on the mandibular bone of dogs [18-19]. Palissery et al. studied cross-linked, closed-cell PVC foam as the potential model material for cancellous bone for *in vitro* biomechanical tests of orthopedic devices. In their work, they studied the cyclic tension and compression behavior of the PVC foam applying 1/3 of the ultimate strength in each cycle. In their work they concluded that the performance of PVC foam during tension and compression testing is qualitatively similar to that of cancellous bone. Furthermore, bone model material should be selected based not only on similar static behavior, but also on similar compression/tension strength ratio and similar fatigue properties as well, particularly with respect to material property degradation [20].

The aim of this paper was to determine whether PVC foams could also be suitable for the mechanical modeling of normal and OP bone. Suitability was determined by the method developed by Li and Aspden [21] for the comparison of cancellous bone of patients with osteoporosis or osteoarthritis. Li and Aspden compared the Young's modulus, yield strength, and energy absorbed until yield as a function of

the density of the studied bone samples. Shepherd et al. [17] used the same method in their study on commercially available PUR foams used as a mechanical model for OP human bones. We used this method since both Shepherd and Apsden used the same method during their research, which enables us to compare our result not only to human bone, but also to PUR. Determining such mechanical properties may help us to select the relevant PVC foams as appropriate models in studies about the mechanical evaluation of implant performance.

2 Methods and Materials

2.1 Materials

Closed-cell, cross-linked PVC foams with a density of 0.10, 0.13 and 0.20 g/cm^3 were examined in this study. The results were compared with those of PUR foams of a density of 0.09, 0.16 and 0.20 g/cm^3 studied by Shepherd et al [17] and human bones studied by Li and Aspden [21]. The mechanical properties of the PVC foams used for this study and those of the PUR foams used by Shepherd are listed in Table 1, as provided by the manufacturer. Shepherd used the 0.16 and 0.20 g/cm^3 PUR foams to model low and medium density cancellous bone, and the open-cell rigid 0.09 g/cm^3 PUR foam to model very low density cancellous bone. To facilitate comparison, the PVC foams were selected to have similar density, compressive and tensile strength to the PUR foams studied by Shepherd. All PVC foams were delivered by Alcan Airex AG free of charge for research purposes in block form, with dimensions of 400×800×30 mm.

Table 1
Material properties as provided by the manufacturers

Foam	Material	Density [g/cm^3]	Compressive strength [MPa]	Young's modulus [MPa]	Tensile strength [MPa]
Sawbones®	PUR	0.09	0.6	16	1.0
Sawbones®	PUR	0.16	2.2	58	2.1
Sawbones®	PUR	0.32	8.4	210	5.6
AIREX® C70.90	PVC	0.10	1.9	125	2.7
AIREX® C70.130	PVC	0.13	2.8	170	3.8
AIREX® C70.200	PVC	0.20	5.2	280	6.0

Using a fine saw blade on a jigsaw machine, cube-shaped specimens were machined with nominal dimensions of 10×10×10 mm. The size of each specimen was measured and recorded with a Mitutuyo Digimatic digital caliper and the actual dimensions of the specimens were used for calculation. Six blocks were prepared from each PVC foam.

2.1 Method

The quasi-static unconstrained compression tests were conducted on a Zwick Z005 materials testing machine fitted with a load cell of 1000 N, and a self-aligning compression plate (Fig. 1). The use of a self-aligning compression plate was necessary so that the compression would be uniaxial and no buckling of the specimens would occur because of shape inaccuracies.

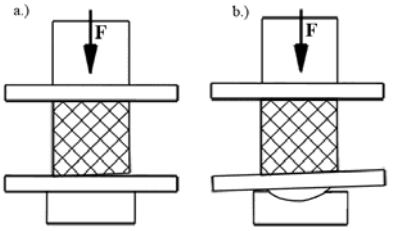

Figure 1
Measurement setup: a) Parallel plate, b) Self-aligning compression plate

Engineering stress was calculated with formula 1.

$$\sigma(x) = \frac{F(x)}{A_0}, \tag{1}$$

where $\sigma(x)$ is the engineering stress [MPa] as a function of the crosshead displacement (x) of the machine, $F(x)$ is the force [N] recorded by the load cell as a function of the crosshead displacement of the machine and A_0 is the original cross-sectional area [mm^2] of the PVC foam block. In order to simplify the evaluation process, a fifth grade polynomial was fitted to the results of the stress-strain curve. This polynomial was used for the calculation of the absorbed energy and the first derivative needed for the calculation of the Young modulus. formula 2 is the typical form of a fifth grade polynomial.

$$\sigma(x) = C_5 x^5 \pm C_4 x^4 \pm C_3 x^3 \pm C_2 x^2 \pm C_1 x \pm C_0, \tag{2}$$

where x is the crosshead displacement in [mm]. C_i-s are the constants specific to each measured foam block, where $i=\{0, 1, 2, 3, 4, 5\}$.

The engineering strain was calculated by dividing the displacement of the machine crosshead (at each data point) by the initial height of the PVC foam block (formula 3.)

$$\varepsilon = \frac{\Delta h}{h_0} \tag{3}$$

where ε is the engineering strain [%], Δh is the displacement [mm] of the machine crosshead and h_0 is the initial height [mm] of the PVC foam block.

The yield strength was calculated according to the method described by Li and Apsden [21] and used by Shephard et al. [17] for the study of commercially available PUR foams as mechanical model material for OP human bones. Li and Apsden defined the yield strength as the stress at which Young's modulus is reduced to 97% of its original value. In this work, the yield strength was calculated according to formula 4.

$$\sigma_y = \sigma(x = \varepsilon_y) \tag{4}$$

where σ_y is the yield strength [MPa], ε_y is the strain at yield.

Young's modulus was calculated with formula 5.

$$E(x) = \sigma'(x) \tag{5}$$

where *E(x)* is Young's modulus [MPa] as a function of the crosshead displacement, *σ'(x)* is the first derivative of the stress-strain curve as a function of the crosshead displacement of the machine.

The energy absorbed until yield was calculated by integrating the polynomial equation of the engineering stress-strain curve between the limit of zero and the strain point at which the yield strength was determined (Eq. 6).

$$\Delta E_y = \int_0^{\varepsilon_y} \sigma(x)dx \tag{6}$$

where ΔE_y is the energy absorbed until yield [kJ/m^3], ε_y is the strain at yield, and *σ(x)* is the fifth grade polynomial fitted to the stress-strain curve.

3 Results and Discussion

Six cube-shaped specimens were machined with nominal dimensions of 10×10×10 mm from each studied PVC foam. The size of each specimen was measured and recorded and in the evaluation of the measurements the actual size of the specimens were used for calculation. Statistical comparisons were made using a two-sample t-test with a significance level set at 0.05.

Results

Figure 2 shows two characteristic stress-strain and modulus-strain curves from the compression testing of two PVC foam blocks. Figure 2a shows the characteristic stress-strain curves of a 0.20 g/cm^3 and 0.10 g/cm^3 density foam blocks. The expression for Young's modulus of the material is given by the gradient of the curve. Figure 2b shows Young's modulus as a function of the strain. Young's modulus was determined as the maximum value of the curve in Figure 2b. The

yield point was defined as the stress at the end of the peak region, when Young's modulus is reduced by 3%.

Figure 2a and 2b have the same strain axes to allow easy comparison. The curves on the figure are typical of those obtained in this study. The energy absorbed until yield is the area under the stress-strain curve up to the yield point (hatched area on Figure 2a for the 0.20 g/cm^3 density PVC foam).

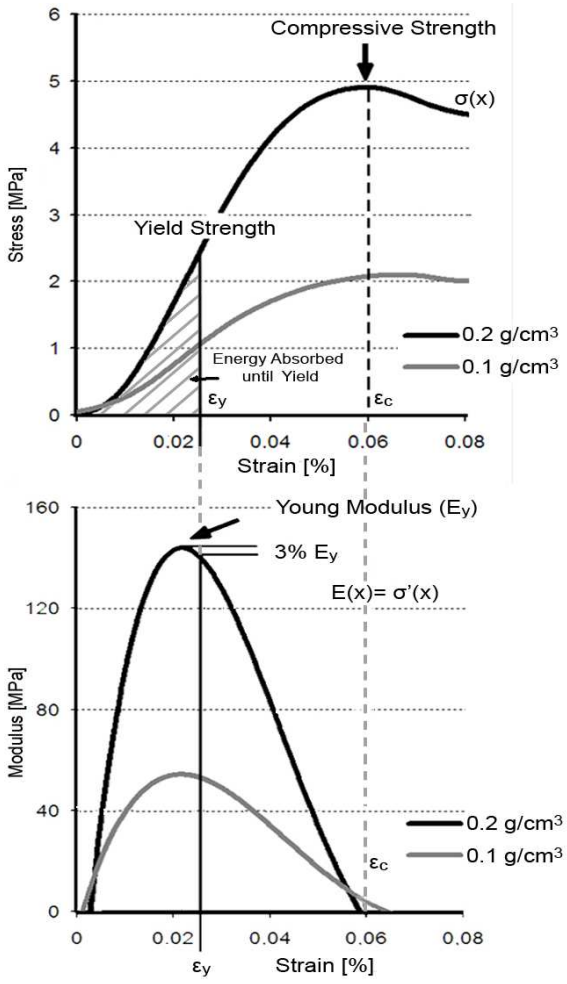

Figure 2

Characteristic Stress-strain and Young's modulus curves of high and low density PVC foams. (a) Stress-strain curves of low and high density PVC foams, (b) Young's modulus determined as the gradient of the curve. The yield point is defined as the point at which Young's modulus decreases to 97% of its maximum value. The area under the stress-strain curve up to the yield point is defined as the energy absorbed until yield.

Table 2 summarizes the results for the three studied PVC foams and compares their values with those obtained by Shepherd et al. and Li and Apsden. The values compared are Young's modulus, yield strength and energy absorbed until yield.

Table 2

Compression testing results of human bone, PUR and PVC foams.

Results of foams are given as mean± standard deviation. The results for bones are given as mean and min-max of measurement range.

	Material	Young's modulus [MPa]	Yield strength [MPa]	Energy absorbed until yield [kJ/m^3]
Shepherd et al. [16]	0.09 g/cm^3 PUR	0.7±0.2	0.03±0.01	1.0±0.5
	0.16 g/cm^3 PUR	42.0±3.0	1.1±0.1	10.0±3.0
	0.32 g/cm^3 PUR	146±6	3.7±0.9	30.0±6.0
Aspden and Li [21]	OP bone	247 (50-410)	2.5 (0.6-5.8)	16.3 (2-52)
	Normal bone	310 (40-460)	3.3 (0.4-9.0)	21.8 (2-90)
Our results	0.10 g/cm^3 PVC	53.7±5.0	1.3±0.1	17.8±1.5
	0.13 g/cm^3 PVC	66.4±5.1	2.2±0.1	42.4±6.0
	0.20 g/cm^3 PVC	123.2±14.9	3.0±0.1	41.2±11.4

Discussion

The purpose of the study was to determine whether closed-cell, cross-linked PVC foams could be suitable for the mechanical modeling of normal and OP bone. The method used was first published by Li and Aspden for the comparison of cancellous bone of patients with osteoporosis or osteoarthritis [21]. Shepherd et al. used the same method in their study on commercially available PUR foams as mechanical model materials for OP human bones [17]. Using exactly the same method as Li and Aspden, and Shepherd et al. provides a unique opportunity to compare the studied mechanical properties of human bone, PUR and PVC foams. Such comparative studies for different bone model materials are extremely rare, since different research groups use different methods for the validation of their material.

The 0.10 g/cm^3 PVC foam was used to model very low density cancellous bone the same way as the 0.09 g/cm^3 PUR foam studied by Shepherd et al. The PVC foam is much stronger than the PUR foam, and the results suggest that it could model severely osteoporotic bones. The Young's modulus of this material is close to the lower limit of the modulus of the OP bone. The yield strength is one-half of the average value for osteoporotic bone, but it is within the limits measured by Aspden and Li. The lightest foam's absorbed energy until yield is practically equal to that of the OP bone. According to these results the lowest density closed-cell, cross-linked, PVC foam studied in this paper is suitable as a mechanical model material for severely osteoporotic cancellous bone.

In terms of yield strength and Young's modulus, the 0.13 g/cm^3 PVC foam is a more suitable model material for osteoporotic cancellous bone than the 0.10 g/cm^3 PVC foam. In contrast to the 0.10 g/cm^3 density PVC foam and the 0.16 g/cm^3 PUR material studied by Shepherd et al., the yield strength of this PVC foam matches that of the osteoporotic human cancellous bone, although its Young's modulus is still at the lower end of the range of human osteoporotic bone's Young's modulus.

The results for the 0.20 g/cm^3 PVC foam quantitatively match those for the 0.32 g/cm^3 PUR material, and those for normal human bone. This makes it a suitable material for the modeling of normal human cancellous bone during *in vitro* biomechanical tests.

Previous papers used different methods to study possible substitute materials for human cancellous bone during *in vitro* biomechanical tests. Fatigue tests on rigid PUR foams showed that these materials do not model the behavior of cancellous bone precisely under dynamic and cyclic loading [9, 22]. Fresh animal and human bone (both cortical and cancelous) have viscoelastic properties that make their properties and behavior unique [23-25]. PVC foams have also displayed such properties, which could make them a better model material for trabecular bone during *in vitro* biomechanical tests [20, 26, 27].

The results of this paper indicate that cross-linked, closed-cell PVC foams could be more suitable for the modeling of human cancellous bone than currently used PUR foams. Based on Young's modulus, yield strength and energy absorbed until yield, they represent human cancellous bone better than PUR foams. Their viscoelastic, and energy absorbing properties also make them a more suitable material for the modeling of cancellous bone.

The different test specimen geometry used in our study does not affect the properties measured since these were calculated from the original cross section of the specimens. Furthermore, our test specimens and those of Aspden et al. and Shepherd et al. have comparable dimensions and cross section/height aspect ratios. Keaveny et al., and Pilkey et al. showed in their works that much higher cross section/height aspect ratio is needed for a significant difference in measurement results [28, 29].

In this paper we compared the Young's modulus, yield strength and energy absorbed until yield of three cross-linked, solid, closed-cell PVC foams, with those of rigid closed-cell and open-cell PUR foams, and osteoporotic and normal density bones. Our results indicate that further comparative research would be needed on these materials. Not only compressive but bending and tensile tests would be needed, and fatigue behavior should also be compared under different loads. Any similarities found between the mechanical properties of PVC foam and cancellous bone would strengthen the case that PVC foams are suitable as a human cancellous bone model.

Conclusions

From the results of the above-mentioned and discussed measurements, the following conclusions can be drawn:

- The investigated cross-linked, rigid cellular PVC foams are adequate model materials for osteoporotic and normal cancellous human bone.
- Based on Young's modulus and yield strength, the investigated 0.1 and 0.13 g/cm^3 PVC foams are suitable as mechanical model materials for osteoporotic cancellous bone.
- Based on Young's modulus and yield strength, the investigated 0.20 g/cm^3 PVC foam is suitable as a model material for normal bone.
- Based on energy absorbed until yield, the 0.10 g/cm^3 PVC foam is a suitable mechanical model material for osteoporotic cancellous bone. For the modeling of normal bone, both the 0.13 and 0.20 g/cm^3 PVC foams are suitable.

In summary, it can be concluded that according to the results of this research, cross-linked closed-cell rigid PVC foams are suitable as mechanical model materials for human cancellous bone.

Acknowledgement

This paper was supported by the János Bolyai Research Scholarship of the Hungarian Academy of Sciences. The authors would like to thank Arburg Hungaria Ltd. for the injection molding machine.

This work is connected to the scientific program of the "Development of quality-oriented and harmonized R+D+I strategy and functional model at BME" project. This project is supported by the New Széchenyi Plan (Project ID: TÁMOP-4.2.1/B-09/1/KMR-2010-0002).

The work reported in this paper has been performed in the framework of the project "Talent care and cultivation in the scientific workshops of BME" project. This project is supported by the TÁMOP - 4.2.2.B-10/1-2010-0009 grant.

This work was supported by the Hungarian Scientific Research Fund (OTKA PD 105995)

References

[1] E. M. Meslin, K. A. Quaid: Ethical Issues in the Collection, Storage, and Research Use of Human Biological Materials; Journal of Laboratory and Clinical Medicine, 144, 5, 2004, 229-234

[2] C. E. Dunham, S. E. Takaki, J. A. Johnson, C. E. Dunning: Mechanical Properties of Cancellous Bone of the Distal Humerus; Clinical Biomechanics, 20, 8, 2005, 834-838

[3] E. Perilli, M. Baleani, C. Öhman, R. Fognani, F. Baruffaldi, M. Viceconti: Dependence of Mechanical Compressive Strength on Local Variations in Microarchitecture in Cancellous Bone of Proximal Human Femur; Journal of Biomechanics, 41, 2, 2008, 438-446

[4] H. Follet, K. Bruyère-Garnier, F. Peyrin, J. P. Roux, M. E. Arlot, B. Burt-Pichat, C. Rumelhart, P. J. Meunier: Relationship between Compressive Properties of Human Os Calcis Cancellous Bone and Microarchitecture Assessed from 2D and 3D Synchrotron Microtomography; Bone, 36, 2, 2005, 340-351

[5] H. Brockstedt, M. Kassem, E. F. Eriksen, L. Mosekilde, F. Melsen: Age- and Sex-related Changes in Iliac Cortical Bone Mass and Remodelling; Bone, 14, 4, 1993, 681-691

[6] M. A. K. Liebschner: Biomechanical Considerations of Animal Models used in Tissue Engineering of Bone; Biomaterials, 25, 9, 2004, 1697-1714

[7] P. Buma, W. Schreurs, N. Verdonschot: Skeletal Tissue Engineering - from *in Vitro* Studies to Large Animal Models, Biomaterials; 25, 9, 2004, 1487-1495

[8] K. A. Athanasiou, A. Agarwal, A. Muffoletto, F. J. Dzida, G. Constantinides, M. Clem: Biomechanical Properties of Hip Cartilage in Experimental Animal Models; Clinical Orthopaedics and Related Research, 316, 7, 1995, 254-266

[9] Y. H. An, R. A. Draughn: Mechanical Testing of Bone and the Bone–Implant interface, CRC Press, London, 2000, Chapter 10.: Synthetic materials and structures used as models for bone

[10] A. D. Heiner, T. D. Brown: Structural Properties of a New Design of Composite Replicate Femurs and Tibias; Journal of Biomechanics, 34, 6, 2001, 773-781

[11] M. B. Sommers, D. C. Fitzpatrick, S. M. Madey, C. V. Zanderschulp, M. Bottlang: A Surrogate Long-Bone Model with Osteoporotic Material Properties for Biomechanical Testing of Fracture Implants; Journal of Biomechanics, 40, 15, 2007, 3297-3304

[12] A. E. Johnson, T. S. Keller: Mechanical Properties of Open-Cell Foam Synthetic Thoracic Vertebrae; Journal of Materials Science: Materials in Medicine, 19, 3, 2008, 1317-1323

[13] D. Wähnert, K. L. Hoffmeier, Y. Stolarczyk, R. Fröber, G. O. Hofmann, T. Mückley: Evaluation of a Customized Artificial Osteoporotic Bone Model of the Distal Femur; Journal of Biomaterials Applications, 26, 4, 2011,451-464

[14] J. A. Szivek, M. Thomas, J. B. Benjamin: Characterization of a Synthetic Foam as a Model for Human Cancellous Bone; Journal of Applied Biomaterials, 4, 3, 1993, 269-272

[15] J. A. Szivek, J. D. Thompson, J. B. Benjamin: Characterization of Three Formulations of a Synthetic Foam as Models for a Range of Human Cancellous Bone Types; Journal of Applied Biomaterials, 6, 2, 1995, 125-128

[16] P. Patel, D. Shepherd, D. Hukins: Compressive Properies of Commercially Available Plyurathane Foams as Mechanical Models for Osteoporotic Human Cancellous Bone; BMC Musculoskeletal Disorders; 9, 10, 2008, 137-144

[17] M. S. Thompson, I. D. McCarthy, L. Lidgren, L. Ryd: Compressive and Shear Properties of Commercially Available Polyurethane Foams; Journal of Biomechanical Engineering – ASME, 125, 5, 2003, 732-734

[18] Y. Shikinami, M. Okuno: Bioresorbable Devices Made of Forged Composites of Hydroxyapatite (HA) Particles and Poly-L-lactide (PLLA): Part I. Basic Characteristics; Biomaterials, 20, 9, 1999, 859-877

[19] Y. Shikinami, M. Okuno: Bioresorbable Devices Made of Forged Composites of Hydroxyapatite (HA) Particles and Poly-L-lactide (PLLA): Part II. Practical Properties of Miniscrews and Miniplates; Biomaterials, 22, 23, 2001, 3197-3211

[20] V. Palissery, M. Taylorm, M. Browne: Fatigue Characterization of a Polymer Foam to Use as a Cancellous Bone Analog Material in the Assessment of Orthopaedic Devices; Journal of Material Science: Materials in Medicine, 15, 1, 2004, 61-67

[21] B. Li, R. M. Aspden: Composition and Mechanical Properties of Cancellus Bone from the Femoral Head of Patients with Osteoporosis or Osteoarthritis; Journal of Bone and Mineral Research, 12, 4, 1997, 641-651

[22] L. J. Gibson, M, F, Ashby: Cellular Solids Structure and Properties, Cambridge University Press, Cambridge, 1999

[23] T. P. M. Johnson, S. Socrate, M. C. Boyce: A Viscoelastic, Viscoplastic Model of Cortical Bone Valid at Low and High Strain Rates; Acta Biomaterialia, 6, 10, 2010, 473-4080

[24] R. M. Guedes, J. A. Simoes, J. L. Morais: Viscoelastic Behaviour and Failure of Bovine Cancellous Bone under Constant Strain Rate; Journa of Biomechanics, 36, 1, 2006, 49-60

[25] J. F. Mano: Viscoelastic Properties of Bone: Mechanical Spectrospcopy Studies on a Chicken Model; Materials Science and Engineering C, 25, 2, 2005, 145-152

[26] K. Kanny, H. Mahfuz, L. A. Carlsson, T. Thomas, S. Jeelani: Dynamic Mechanical Analyses and Fexural Fatigue of PVC Foams; Composite Structures, 58, 2, 2002, 175-183

[27] G. T. Lim, V. Altstädt, F. Ramsteiner: Understanding the Compressive Behavior of Linear and Cross-linked Poly(vinyl chloride) Foams; Journal of Cellular Plastics, 45, 9, 2009, 419-439

[28] T. M. Keaveny, T. P. Pinila, R. P. Crawford, D. L. Kopperdahl, A. Lou: Systematic and Random Errors in Compression Testing of Trabecular Bone; Journal of Orthopaedic Research, 15, 1, 1997, 101-110

[29] W. B. Lievers, S. D. Waldman, A. K. Pilkey: Minimizing Specimen Length in Elastic Testing of End-constrained Cancellous Bone; Journal of the Mechanical Behavior of Biomedical Materials, 3, 2010, 22-30

A Preliminary Study of the Application of the P-graph Methodology for Organization-based Multiagent System Designs: Assessment

Juan C. García-Ojeda[1,2], Botond Bertok[2], Ferenc Friedler[2], Andres Argoti[3] and L. T. Fan[3]

[1]Department of Systems Engineering, Autonomous University of Bucaramanga, Av. 42 No 48-11, El Jardín, Bucaramanga, Santander 680003, Colombia, E-mail: jgarciao@unab.edu.co

[2]Department of Computer Science and Systems Technology, University of Pannonia, Egyetem u. 10, H-8200 Veszprém, Hungary, E-mail: {bertok, friedler}@dcs.vein.hu

[3]Department of Chemical Engineering, Kansas State University, 1005 Durland Hall, Manhattan, Kansas 66506, U. S. A. E-mail:{argoti,fan}@ksu.edu

Abstract: At the outset, the design of an organization-based multiagent system is modeled according to the framework of Organization Model for Adaptive Complex Systems (OMACS). Subsequently, this design model is transformed into a process-network model. Eventually, the resultant process-network model in conjunction with the P-graph-based methodology give rise to: (i) the maximal structure of the process network, comprising all the feasible combinations of structures, i.e., OMACS-based design configurations, capable of yielding the specified products from the specified raw material; (ii) every feasible structure for the process of interest; and (iii) the optimal structure of the network, i.e., the optimal OMACS-based design configuration. Finally, in light of the tenet of a modeling-transformation-evaluation paradigm, an appraisal is made of the feasibility as well as the flexibility and cost of the optimal OMACS-based design configuration obtained.

Keywords: Organization-based Multiagent System Design; Model Transformation; Process Synthesis; P-graph Framework; OMACS Framework

1 Introduction

Designing and implementing large, complex, and distributed systems by resorting to autonomous or semi-autonomous agents that can reorganize themselves by cooperating with one another represent the future of software systems [4]. A set of methodologies [21], a selection of design processes [3], and a collection of frameworks [4], [5], [6], [7], [8], [16], [23], [27], [35], [36] are available in the

literature to provide the basis for constructing sophisticated autonomous multiagent organizations. Moreover, a set of metrics and methods have been suggested with the intention of providing useful information about key properties (e.g., complexity, flexibility, self-organized, performance, scalability, and cost) of these multiagent organizations [24], [26], [31], [33].

The above-mentioned methodologies, processes, frameworks, and procedures, nevertheless, do not offer techniques for identifying the number of feasible configurations[1] that can be synthesized, or designed, from a set of heterogeneous agents. This is an important issue when designing a multiagent system because of the nature of the environments where it operates (dynamic, continuous, and partially accessible) [29]. The multiagent system must be adaptive (self-organized) to adjust its behavior to cope with the dynamic appearance and disappearance of goals (tasks), their given guidelines, and the overall goal of the multiagent system [29], [30]. To address such an issue, i.e., identifying feasible agent´s configurations, we propose a novel approach based upon previous work on organization-based multiagent systems [4] and the P-graph methodology [10].

The current contribution describes the deployment of the P-graph methodology for synthesizing organization-based multiagent systems based upon the OMACS framework. The remainder of the current contribution comprises: an outline of the OMACS framework (Section 2); a brief description of the P-graph methodology (Section 3); the motivational example for undertaking the work (Section 4); a procedure for transforming an organization-based multiagent system design into a process-synthesis problem (Section 5); a description of the mathematical programming model for synthesizing organization-based multiagent systems (Section 6); the preliminary results of the proposed approach (Section 7); and finally, the conclusions as well as the proposed future work (Section 8).

2 The Framework of Organization Model for Adaptive Computational Systems: OMACS

The Framework of Organization Model for Adaptive Computational Systems (hereafter, OMACS) defines the entities in standard multiagent systems and their relationship as a tuple $O_{OMACS} = \langle G_{OMACS}, R_{OMACS}, A_{OMACS}, C_{OMACS}, \Phi, P_{OMACS}, \Sigma,$ *oaf, achieves, capable, requires, possesses, potential*$\rangle$, and it is also represented via an UML[2]-based organizational meta-model (see Figure 1) [4]. These are briefly described in what follows.

[1] These feasible configurations may be seen as agent´s organizations or agents' teams [4].

[2] Unified Modeling Language (UML) is a standardized general-purpose modeling language in the field of object-oriented software engineering.

The organization, O_{OMACS}, is composed of four entities including G_{OMACS}, R_{OMACS}, A_{OMACS}, and C_{OMACS}. G_{OMACS} defines the goals of the organization (i.e., overall functions of the organization); R_{OMACS} defines a set of roles (i.e., positions within an organization whose behavior is expected to achieve a particular goal or set of goals). A_{OMACS} is a set of agents, which can be either human or artificial (hardware or software) entities that perceive their environment (Σ – domain model) and can perform actions upon it. In order to perceive and to act, the agents possess a set of capabilities (C_{OMACS}), which define the percepts/actions at their disposal. Capabilities can be soft (i.e., algorithms or plans) or hard (i.e., hardware related actions). P_{OMACS} formally specifies rules that describe how O_{OMACS} may or may not behave in particular situations.

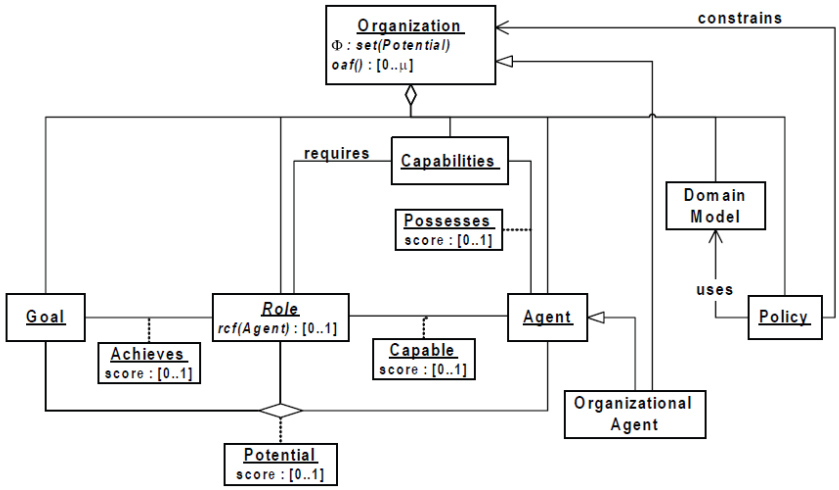

Figure 1
OMACS Meta-model [4]

In addition, OMACS defines a set of functions – *achieves*, *requires*, *possesses capable*, *potential*, *oaf*, and ϕ – to capture the different relations among the entities. *achieves*, a function whose arguments are a goal in G_{OMACS} as well as a role in R_{OMACS} that generates an output which is a positive real number greater than or equal to 0 and less than or equal to 1 (*achieves*, R_{OMACS} *x* $G_{OMACS} \rightarrow [0,1]$, defines the extent of achievement of a goal by a role); *possesses*, a function with an agent in A_{OMACS} and a capability in C_{OMACS} as inputs yields a positive real number in the range of [0,1] (possesses, A_{OMACS} *x* $C_{OMACS} \rightarrow [0,1]$, defines the quality of an agent´s capability); requires, a function that assumes a role in R_{OMACS}, thereby yielding a set of capabilities required to play that role (*requires*, $R_{OMACS} \rightarrow \rho(C_{OMACS})$, defines the set of capabilities required to play a role[3]); *capable*, a function whose inputs are an agent in A_{OMACS} and a role in R_{OMACS} and generates an

[3] ρ denotes power set.

output, which is a positive real number greater than or equal to 0 and less than or equal to 1 (*capable*, A_{OMACS} *x* $R_{OMACS} \rightarrow [0,1]$, defines how well an agent can play a role), thus giving rise to

$$capable(a,r) = \begin{cases} 0 & if \prod_{c \in requires(r)} possesses(a,c) = 0 \\ \frac{\sum_{c \in requires(r)} possesses(a,c)}{|requires(r)|} & elsewhere; \end{cases} \quad (1)$$

potential, a function with an agent in A_{OMACS}, a role in R_{OMACS}, and a goal in G_{OMACS} as inputs yields a positive real number in the range of [0,1], thus yielding

$$potential(a, r, g) = achieves(r, g) * capable(a, r) \quad (2)$$

(*potential*, A_{OMACS} *x* R_{OMACS} *x* $G_{OMACS} \rightarrow [0,1]$, defines how well an agent can play a role to achieve a goal), and assignment set, ϕ, the set of agent-role-goal tuples $<a, r, g>$, indicating that agent $a \in A_{OMACS}$ has been assigned to play role $r \in R_{OMACS}$ in order to achieve goal $g \in G_{OMACS}$ (ϕ is a subset of all the potential assignments of agents to play roles to achieve goals). Finally, the selection of ϕ from the set of potential assignments is defined by the organization's reorganization function, *oaf*, that assumes a set of assignments in ϕ, thereby yielding a positive real number in the range of $[0,\infty]$ (*oaf*, $\rho(\phi) \rightarrow [0,\infty]$, defines the quality of a proposed set of assignments, i.e., *oaf* computes the goodness of the organization based on ϕ), thus resulting in

$$oaf = \sum_{<a_i,r_j,g_j> \in \phi_{OMACS}} potential(a_i, r_j, g_j). \quad (3)$$

3 Process Network Synthesis

In a process system, raw materials are consumed through various transformations (e.g., chemical, physical, and biological) to desired products. Vessels where these transformations take place are called operating units of the process. A given set of operating units with likely interconnections can be portrayed as a network.

The desired products can be also manufactured via some sub-networks of the above-mentioned network. Thus, a given network may give rise to a variety of processes, or process networks, producing the desired products, and each of such process networks corresponds to a sub-network, that can be considered regarded as its structure. Energy and raw material consumption strongly depend on the selection of a process structure; thus, the optimal design of such a process structure, i.e., the process network synthesis (PNS), or process synthesis in short, has both environmental and economic implications [14].

A number of methods has been developed for process synthesis [28]. These methods can be classified according to whether they are based on heuristics or algorithms, i.e., mathematical programming approaches. The majority, if not all, of these methods, however, may not be sufficiently effective for PNS of a realistic or industrial scale, process because of its combinatorial complexity arising from the involvement of a large number of interconnected loops [14]. To cope with this, an innovative approach based on P-graphs (process graphs), which are unique, mathematically rigorous bipartite graphs, has been proposed to facilitate the process network synthesis [10]. The P-graphs are capable of capturing not only the syntactic but also semantic contents of a process network. Subsequently, an axiom system underlying the P-graph framework is constructed to define the combinatorial feasible process-network structures. The analysis and optimization of properties of such structures are performed by a set of efficient combinatorial algorithms: MSG [9], SSG [9], and ABB [13].

3.1 Process Graph (P-graph)

The mathematical definition of a P-graph and a process structure represented by it are elaborated below [10].

Finite set M, containing materials, and finite set O, containing operating units, are given such that

$$O \subseteq \rho(M) \times \rho(M) \tag{4}$$

Thus, a P-graph can be defined to be a pair, (M,O), as follows:

The vertices of the graph are the elements of

$$V = M \times O \tag{5}$$

Those belonging to set M are of the M-type vertices, and those belonging to set O are of O-type vertices. The arcs of the graph are the elements of

$$A = A_1 \cup A_2 \tag{6}$$

where

$$A_1 = \{(X,Y) \mid Y = (\alpha,\beta) \in O \text{ and } X \in \alpha\} \tag{7}$$

and

$$A_2 = \{(Y,X) \mid Y = (\alpha,\beta) \in O \text{ and } X \in \beta\} \tag{8}$$

In these expressions, X designates an M-type vertex; Y, an O-type vertex; α a set of M-type vertices from which arcs are directed into the O-type vertices; and, β a set of M-type vertices to which arcs are directed out of the O-type vertices.

For illustration let M be a set of materials, $M=\{A,B,C,D,E,F\}$, and O be a set of operating units given by $O=\{(\{B,A\},\{A\}),(\{D,E\},\{B,C\}),(\{F\},\{A,C\}),(\{F\},\{A,C\})\}$. It is not difficult to validate that sets M and O satisfies constraint (1), i.e., (M,O) is a P-graph, as depicted in Figure 2.

3.2 Solution Structures

The materials and operating units in a feasible process structure must always conform to certain combinatorial properties. For example, a structure containing no linkage between a raw material and a final product is unlikely to represent any practical process. Hence, it is of vital importance to identify the general combinatorial properties to which a structure must conform. More important, the properties identified should be satisfied by the structure of any feasible solution of the synthesis problem. In other words, those and only those structures satisfying these properties can be feasible structures of a process: no other structures or constraints need to be considered in synthesizing the process.

A set of axioms has been constructed to express necessary and sufficient combinatorial properties to which a feasible process structure should conform. Next, each axiom is stated: (S1) Every final product is represented in the graph; (S2) A vertex of the *M*-type has no input if and only if it represents a raw material; (S3) Every vertex of the *O*-type represents an operating unit defined in the synthesis problem; (S4) Every vertex of the *O*-type has at least one path leading to a vertex of the *M*-type representing a final product; and, (S5) If a vertex of the *M*-type belongs to the graph, it must be an input to or output from at least one vertex of the *O*-type in the graph.

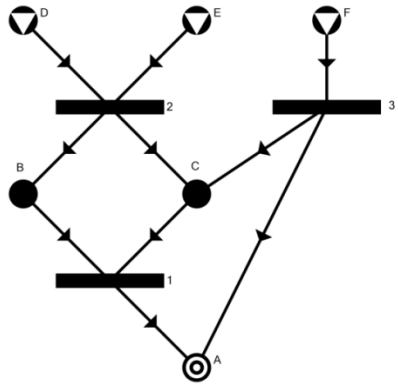

Figure 2

P-graph *(M,O)* where *A*,*B*,*C*,*D*,*E*, and *F* are materials, and *1*,*2*, and *3* are the operating units: ▽ represents raw materials or input elements of the whole process; ● symbolizes intermediate-materials or elements, emerging between the operating units; and ◎ represents products or outputs of the entire process

If a P-graph of a given synthesis problem, *(P,R,O)*[4], satisfies theses axioms, it is defined to be a solution-structure of the problem.

[4] Where $P \subseteq M$ is the set of product, $R \subseteq M$ is the set of raw materials, and O the set of operating units.

3.3 Algorithms MSG, SSG, and ABB

Both the P-graph representation of a process network and the set of five axioms for solution structures, i.e., combinatorial feasible networks, render it possible to fashion the three mathematically rigorous algorithms: MSG, SSG, and ABB. The algorithm MSG (Maximal-Structure Generation) generates the maximal structure (super-structure) of a process synthesis network. Also, the algorithm SSG (Solution-Structure Generation) generates the set of feasible process structures from the maximal structure, which leads to the algorithm ABB (Accelerated Branch and Bound) for computing the n-best optimal solution structure [9], [10], [11], [12], [13].

4 Motivational Example: Cooperative Robotic Search Team System

To demonstrate the application of the P-graph framework for assessing the design of OMACS-based multiagent systems, a survey is given of a simplified Cooperative Robotic Search Team[5] (CRST) system [20], [33]. Essentially, we are to design a team of robots whose goal is to search for different areas of a given location on a map. The team should be able to search any area of the given location even when faced with failures of individual robots or specific capabilities of those robots. This implies that the team must be able to: (1) assign areas based on individual team member´s reliability; (2) recognize when a robot is unable to perform adequately its duties; and (3) reorganize the team to allow it to achieve its goals in spite of individual failures.

4.1 Overview of CRST Organization

For illustration, it is presumed that four goals be achieved by the CRST. In other words, $G = \{g_1, g_2, g_3, g_4\}$ where g_i for $1 \leq i \leq 4$ signifies "search area i." In the CRST, two roles are identified, i.e., $R = \{r_1, r_2\}$ where r_1 and r_2 represent the Searcher and Patroller roles, respectively. In particular, role $r_1$requires the Sonar, Movement, and GPS capabilities for achieving goals g_1, g_2, g_3, and g_4. Likewise, role r_2 requires the Movement, GPS, and Range Finder capabilities for achieving the same goals as those of role r_1. Moreover, for each goal, g_j, an achieve value is assigned. This achieve value defines the extent of achievement of a goal by a role. Both, the *requires* and *achieves* relations can be formally stated as: *requires* = $\{(r_1,\{c_1, c_2, c_3\}),(r_2,\{c_2, c_3, c_4\})\}$ and *achieves* = $\{(r_1, g_1, 0.2), (r_1, g_2, 0.4), (r_1, g_3, 0.8), (r_1, g_4, 1.0), (r_2, g_1, 1.0), (r_2, g_2, 0.7), (r_2, g_3, 0.4), (r_2, g_4, 0.1)\}$.

[5] Although the CRST presented in this paper has been simplified (due to space constraint), it is still interesting enough to illustrate our work.

Also, four capabilities are specified. They are Sonar (c_1), Movement (c_2), GPS (c_3), and Range Finder (c_4). c_1 captures information about all objects around agent a_i (in a 360° view). c_2 allows agent a_i to move in any direction, north, south, east, or west (up, down, left, or right). c_3 provides the ability to read the absolute position of agent a_i in the environment. Finally, c_4 renders it possible for agent a_i to measure the distance of the closest object directly in front of it.

In addition, three different agents are modeled; they are a_1, a_2, and a_3. Specifically, agent a_1 possesses capabilities c_1, c_2, c_3, and c_4 while both agents a_2 and a_3 possess capabilities c_2, c_3, and c_4. The possesses relationship is formulated as follows: *possesses = {(a_1,c_1,0.3), (a_1,c_2,0.5), (a_1,c_3,0.3), (a_1,c_4,0.3), (a_2,c_2,0.7), (a_2,c_3,0.5), (a_2,c_4,0.7), (a_3,c_2,0.4), (a_3,c_3,0.9), (a_3,c_4,0.2)}*.

Additionally, the cost of each individual agent a_1, a_2, and a_3 is \$850, \$900, and \$950, respectively (see Figure 3).

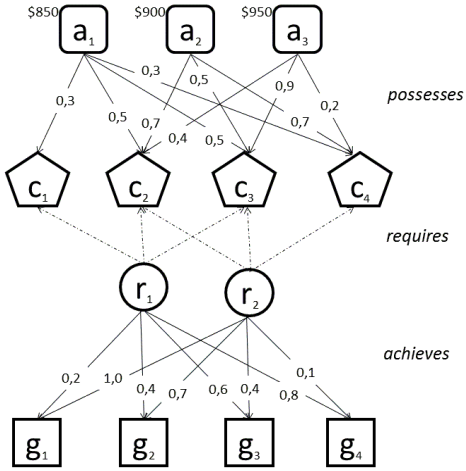

Figure 3

Overview of the CRST Organization. The boxes at the top of the diagram represent agents identified by their types, circles represent the roles, pentagons represent capabilities, and squares are system's goals. The arrows between the entities represent functions/relations *achieves*, *requires*, and *possesses*

5 Algorithm OMACStoPNS

Algorithm OMACStoPNS comprises two mayor parts, the initialization and the construction parts. The initialization part (statements *st1*, *st2*, *st3*, and loop *lp1*) specifies the sets of available raw materials and desired products to be manufactured as well as their parameters. The construction part (loop *lp3*) specifies the set of candidates operating units as well as their parameters (see Figure 3).

input: $G_{OMACS}, A_{OMACS}, R_{OMACS}, achieves, requires, possesses$
comment: G_{OMACS} defines the goals of the organizations, R_{OMACS} defines a set of roles, A_{OMACS} is a set of agents, $achieves$ defines the extent of achievement of a goal by a role, ($G_{OMACS} \times R_{OMACS} \rightarrow [0 \dots 1]$) $possesses$ defines the quality of an agent´s capability ($A_{OMACS} \times C_{OMACS} \rightarrow [0 \dots 1]$), and $requires$ defines the set of capabilities required to play a role ($R_{OMACS} \rightarrow \wp(C_{OMACS})$). The $capable$ function ($A_{OMACS} \times R_{OMACS} \rightarrow [0 \dots 1]$)
output: sets P, R, O
comment: $R \subset M, P \subset M, R \cap P = \emptyset$
begin
comment: initialization part of the algorithm;
st1: $M := M \cup \{oaf\}$;
st2: $P := P \cup \{oaf\}$;
st3: $U_{oaf} := \infty; L_{oaf} := 0; c_{oaf} := 1;$
lp1: **for** $a_i \in A_{OMACS}$ **do**
begin
$R := R \cup \{a_i\}; M := M \cup \{a_i\}; U_{a_i} := \infty; L_{a_i} := 0; c_{a_i} := cost(a_i);$
end;
comment: construction part of the algorithm;
lp2: **for** $g_i \in G_{OMACS}$ **do**
begin
$M := M \cup \{g_i\}; g_{i\_oaf} := \{\{g_i\}, \{oaf\}\}; O := O \cup \{g_{i\_oaf}\};$
$U_{g_{i\_oaf}} := \infty; L_{g_{i\_oaf}} := 0; c_{g_{i\_oaf}} := 0;$
$a_{g_i, g_{i\_oaf}} := 1; a_{g_{i\_oaf}, oaf} := 1;$
end;
lp3: **for** $a_i \in A_{OMACS}$ **do**
begin
$Capabilities_{a_i} := \emptyset;$
for $\langle a', c, value' \rangle \in possesses$ **do**
begin
if $a' = a_i$ **then**
$Capabilities_{a_i} := Capabilities_{a_i} \cup \{c\};$
end;
end;
for $\langle r_k, \wp(c) \rangle \in requires$ **do**
begin
if $\wp(c) \subseteq Capabilities_{a_i}$ **then**
$aux := \emptyset;$
for $\langle r'', g_j, value'' \rangle \in achieves$ **do**
begin
if $r_k = r''$ **then**
$M := M \cup \{a_i\_r_k\_g_j\}; a_i\_r_k\_g_j := \{\{a_i\_r_k\_g_j\}, \{g_j\}\};$
$aux := aux \cup \{a_i\_r_k\_g_j\}; O := O \cup \{a_i\_r_k\_g_j\};$
$U_{a_i\_r_k\_g_j} := \infty; L_{a_i\_r_k\_g_j} := 0; c_{a_i\_r_k\_g_j} := 0;$
$a_{a_i\_r_k\_g_j, a_i\_r_k\_g_j} := 1; a_{a_i\_r_k\_g_j, g_j} := value'';$
$a_{a_i, a_1\_r_k} = 1; a_{a_i\_r_k, a_i\_r_k\_g_j} := capable(a_i, r_k);$
end;
if *aux is not empty* **then**
$a_i\_r_k := \{\{a_i\}, \{aux\}\}; O := O \cup \{a_i\_r_k\};$
$U_{a_i\_r_k} := 1; L_{a_i\_r_k} := 0; c_{a_i\_r_k} := 0;$
end;
end;
end;

Figure 4
Algorithm OMACStoPNS written in Pidgin Algol

Each agent a_i in A_{OMACS}, is transformed into raw material r and added to set R (loop *lp1*); as such, Axiom (S2) is satisfied. Algorithm OMACStoPNS generates the resources, R_{a_i}; R_{a_1}, R_{a_2}, and R_{a_3}. Furthermore, lower bound L_{a_i}, upper bound

U_{a_i}, and cost c_{a_i}, are set for each resource, R_{a_i}; as such, algorithm OMACStoPNS specifies the total amount of available resources for the motivational problem (see Table 1). Thus, only a single product, *oaf*, is specified and added to set *P* (statements *st1*, *st2*, and *st3*); as such, Axiom (S1) is automatically satisfied. Note that this is analogous to the notion of the goodness of the organization based on the quality of a proposed set of assignments. In other words, the set of agent-role-goal tuples $\langle a_i, r_k, g_j \rangle$ indicates that agent $a_i \in A_{OMACS}$ has been assigned to play role $r_k \in R_{OMACS}$ in order to achieve goal $g_j \in G_{OMACS}$. For outcome *oaf*, algorithm OMACStoPNS sets lower bound L_{oaf}, upper bound U_{oaf}, and cost c_{oaf}; as such, the amount of product to be manufactured for meeting the demand of the problem is specified (see Table 2).

Table 1
Resources to be considered in process synthesis for the example

Resource R_j	Lower bound R_j	Upper bound R_j	Cost c_j
a_1	0	∞	0
a_2	0	∞	0
a_3	0	∞	0

Table 2
Targets to be considered in process synthesis for the example

Target P_j	Lower Bound L_j	Upper Bound U_j	Cost c_jc$_j$
oaf	0	∞	1

Subsequently, algorithm OMACStoPNS systematically specifies the operating units in loops *lp2* and *lp3*, representing organizational assignments, as described in section 3; as such, Axioms (S3) and (S4) are satisfied. First, the algorithm loops through every goal $g_j \in G$. Each goal g_j is transformed into material *m* for inclusion in set *M*. Algorithm OMACStoPNS generates materials M_{g_j}; M_{g_1}, M_{g_2}, M_{g_3}, and M_{g_4}. Note that material M_{g_j} represents the goals to be accomplished by the organization. This gives rise to the creation of operating unit *o* for inclusion in set *O* for each g_j. Algorithm OMACStoPNS generates operating units Og_{j_oaf}. Additionally, lower bound $L_{g_{j\_oaf}}$, upper bound $U_{g_{j\_oaf}}$, cost $c_{g_{j\_oaf}}$, and a_{ji}, the consumption rate of entity m_j by operating unit o_i are set for each operating unit $O_{g_{j\_oaf}}$; as such, algorithm specifies the goals to be achieved by the system (see Table 1).

Afterwards, algorithm OMACStoPNS loops through every agent $a_i \in A$. Consequently, for each agent a_i, algorithm OMACStoPNS checks whether a_i is capable of playing a given role r_k in *R*. If so, algorithm OMACStoPNS searches for every g_j in *G*, such that g_j is achieved by r_k. As a result, algorithm OMACStoPNS generates materials $M_{a_{i\_}r_{k\_}g_j}$; $M_{a_{1\_}r_{1\_}g_1}$, $M_{a_{1\_}r_{1\_}g_2}$, $M_{a_{1\_}r_{1\_}g_3}$, $M_{a_{1\_}r_{1\_}g_4}$, $M_{a_{1\_}r_{2\_}g_1}$, $M_{a_{1\_}r_{2\_}g_2}$, $M_{a_{1\_}r_{2\_}g_3}$, $M_{a_{1\_}r_{2\_}g_4}$, $M_{a_{2\_}r_{2\_}g_1}$, $M_{a_{2\_}r_{2\_}g_2}$, $M_{a_{2\_}r_{2\_}g_3}$, $M_{a_{2\_}r_{2\_}g_4}$,

$M_{a_3\_r_2\_g_1}$, $M_{a_3\_r_2\_g_2}$, $M_{a_3\_r_2\_g_3}$, and $M_{a_3\_r_2\_g_4}$. Subsequently, for each agent a_i, role r_k, and goal g_j, two operating units o are created and added to set O. One indicates that agent a_i is capable of playing role r_k; the second implies that agent a_i has been assigned to play role r_k in order to achieve goal g_j. Accordingly, algorithm OMACStoPNS generates the operating units $O_{a_i\_r_k}$ and $O_{a_i\_r_k\_g_j}$. Moreover, lower bounds $L_{a_i\_r_k}$ and $L_{a_i\_r_k\_g_j}$; upper bounds $U_{a_i\_r_k}$ and $U_{a_i\_r_k\_g_j}$; and costs $c_{a_i\_r_k}$ and $c_{a_i\_r_k\_g_j}$; and the consumption flow rate of material m_j, a_{ji}, by operating unit o_i, are set for each of operating units $O_{a_i\_r_k}$ and $O_{a_i_r_k_g_j}$$\mathrm{O_{a_i_r_k_g_j}}$; as such, algorithm specifies whether agent a_i has been assigned to play role r_k in order to achieve goal g_j (see Table 3). As a result, the execution of loop *lp3* assures that Axiom (S5) is satisfied by the maximal structure. Figure 5 displays the maximal structure of the motivational example generated by algorithm MSG.

Table 3

Operating units to be considered in process synthesis for the example*

Operating Unit O_i	**Input Material m_j**	**Output Material m_j**	**Lower bound L_i**	**Upper bound U_i**	**Cost c_i**
g_1_oaf	g_1 (1)	oaf (1)	0	∞	0
g_2_oaf	g_2 (1)	oaf (1)	0	∞	0
g_3_oaf	g_3 (1)	oaf (1)	0	∞	0
g_4_oaf	g_4 (1)	oaf (1)	0	∞	0
$a_1\_r_1\_g_1$	$a_1\_r_1\_g_1$(0.433)	g_1(0.2)	0	∞	0
$a_1\_r_1\_g_2$	$a_1\_r_1\_g_2$(0.433)	g_2(0.4)	0	∞	0
$a_1\_r_1\_g_3$	$a_1\_r_1\_g_3$(0.433)	g_3(0.6)	0	∞	0
$a_1\_r_1\_g_4$	$a_1\_r_1\_g_4$(0.433)	g_4(0.8)	0	∞	0
$a_1\_r_2\_g_1$	$a_1\_r_2\_g_1$(0.433)	g_1(1.0)	0	∞	0
$a_1\_r_2\_g_2$	$a_1\_r_2\_g_2$(0.433)	g_2(0.7)	0	∞	0
$a_1\_r_2\_g_3$	$a_1\_r_2\_g_3$(0.433)	g_3(0.4)	0	∞	0
$a_1\_r_2\_g_4$	$a_1\_r_2\_g_4$(0.433)	g_4(0.1)	0	∞	0
$a_2\_r_2\_g_1$	$a_2\_r_2\_g_1$(0.633)	g_1(1.0)	0	∞	0
$a_2\_r_2\_g_2$	$a_2\_r_2\_g_2$(0.633)	g_2(0.7)	0	∞	0
$a_2\_r_2\_g_3$	$a_2\_r_2\_g_3$(0.633)	g_3(0.4)	0	∞	0
$a_2\_r_2\_g_4$	$a_2\_r_2\_g_4$(0.633)	g_4(0.1)	0	∞	0
$a_3\_r_2\_g_1$	$a_3\_r_2\_g_1$(0.5)	g_1(1.0)	0	∞	0
$a_3\_r_2\_g_2$	$a_3\_r_2\_g_2$(0.5)	g_2(0.7)	0	∞	0
$a_3\_r_2\_g_3$	$a_3\_r_2\_g_3$(0.5)	g_3(0.4)	0	∞	0
$a_3\_r_2\_g_4$	$a_3\_r_2\_g_4$(0.5)	g_4(0.1)	0	∞	0
$a_1\_r_1$	a_1	$a_1\_r_1\_g_1$(0.433), $a_1\_r_1\_g_2$(0.433), $a_1\_r_1\_g_3$(0.433), $a_1\_r_1\_g_4$ (0.433)	0	1	0

$a_1\_r_2$	a_1	$a_1\_r_2\_g_1(0.433)$, $a_1\_r_2\_g_2(0.433)$, $a_1\_r_2\_g_3(0.433)$, $a_1\_r_2\_g_4$ (0.433)	0	1	0
$a_2\_r_2$	a_2	$a_2\_r_2\_g_1(0.633)$, $a_2\_r_2\_g_2(0.633)$, $a_2\_r_2\_g_3(0.633)$, $a_2\_r_2\_g_4$ (0.633)	0	1	0
$a_2\_r_2$	a_3	$a_3\_r_2\_g_1(0.5)$, $a_3\_r_2\_g_2(0.5)$, $a_3\_r_2\_g_3(0.5)$, $a_3\_r_2\_g_4$ (0.5)	0	1	0

* The numbers in the brackets are the flow rates, a_{ji}, of the input and output materials relative to the unit capacity of each operating unit.

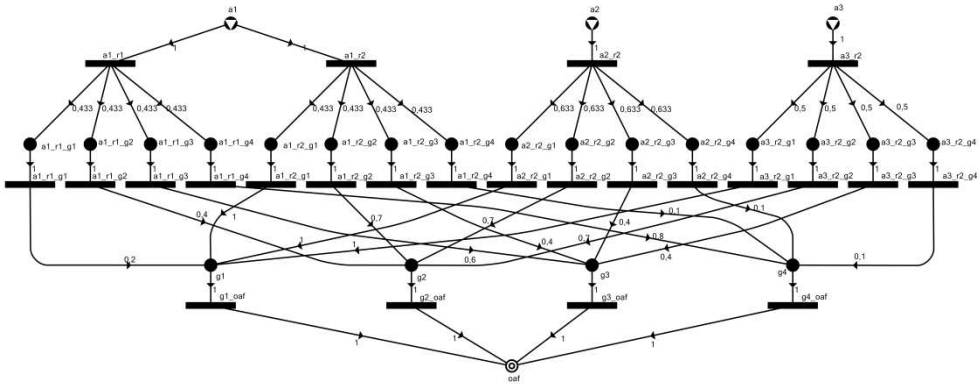

Figure 5
Maximal structure for the hypothetical example to illustrate the solution-structure generation with algorithm MSG

6 Mathematical Programming Model

Unlike any of the available algorithmic methods for computing the quality of a proposed set of assignments based upon OMACS, i.e., agents, $a_i \in A_{OMACS}$, assigned to play roles, $r_k \in R_{OMACS}$, in order to achieve goals, $g_j \in G_{OMACS}$, where no mathematical programming model is derived due to the approach adopted, i.e., step-by-step computation [4], [20], [30], [33], [37], [38]; we propose a simple mathematical programming model, which is derived from the maximal structure, generated by algorithm MSG, and does not impair the optimality of the resultant solution.

In the present work, a mixed-integer linear programming (MILP) model has been formulated, which at the very least yields a solution identical with those conventional OMACS-based assignment algorithms [37], [38].

Let M denote the set of entities; P, the set of products, where $P \subseteq M$; R, the set of initially available resources, where $R \subseteq M$; and O, the set of activities, where $O = \rho(M) \times \rho(M)$. The relations between entities and activities are denoted by a_{ji}

which gives the difference between the production and consumption rate of entity M_j by activity O_i, where $M_j \in M$ and $O_i \in O$. Also given are lower bound L_{O_i} and upper bound U_{O_i} for the volume of each activity O_i, as well as its cost c_{O_i}. In addition, lower bound L_{R_j} and upper bound U_{R_j} are specified for each resource R_j. In addition, lower bound L_{P_j} and upper bound U_{P_j} are defined for each product P_j. Moreover, two classes of variables are involved in the mathematical programming model. One class consists of binary variables, each denoted by $y_{O_i} \in \{0,1\}$ expressing the absence (0) or the existence (1) of operating unit O_i; and the other, continuous variables, each denoted by x_{O_i} expressing the size or capacity of operating unit O_i relative to the unit size. If operating unit O_i is included in the network, as indicated by $y_i = 1$, the concomitant continuous variable, x_{O_i}, can be any real value in the range of 0 to the upper limit for the capacity of operating unit O_i. Thus, $x_{O_i} \leq y_{O_i} U_i$, where U_i is the upper limit for the capacity; if such an upper limit does not exist, the U_i can be any large number L. Finally, z, maximal, is the objective value. The resultant MILP model is given in the following.

$$z = max\left(\sum_{P_j \in M \cap P}\left(c_{P_j} * \sum_{O_i \in O} a_{ij} * x_{O_i}\right)\right) \tag{9}$$

subject to (10)

$$M = \bigcup_{(\alpha_i,\beta_i) \in O} \alpha_i \cup \beta_i$$

$$0 \leq x_{O_i}, L_{O_i} \leq x_{O_i} \leq U_{O_i} \qquad \forall O_i \in O \tag{11}$$

$$L_{P_j} \leq \sum_{O_i \in O} a_{ij} * x_{O_i} \leq U_{P_j} \qquad \forall P_j \in M \cap P \tag{12}$$

$$L_{R_j} \leq \sum_{O_i \in O} a_{ji} * x_{O_i} \leq U_{R_j} \qquad \forall R_j \in M \cap R \tag{13}$$

$$L_{M_j} \leq \sum_{O_i \in O} a_{ji} * x_{O_i} - \sum_{O_i \in O} a_{ij} * x_{O_i} \leq U_{M_j} \qquad \forall M_j \in M \backslash (R \cup P) \tag{14}$$

$$x_{O_i} \leq y_{O_i} L \tag{15}$$

$$y_{O_i} \in \{0,1\} \tag{16}$$

The maximal structure serves as the input to the generation and solution of the MILP model by algorithm ABB [13]. It yields the optimal network and a finite number of *n*-best suboptimal networks in ranked order. Algorithm ABB has identified a total of 65535 structures[6,7] in less than 75 seconds on an Intel(R) Core(TM) i5 CPU @ 3.20 GHz. Table 4 shows 10 feasible solutions for the example. Algorithms MSG and ABB have been executed by software PNS Studio [32].

Table 4
Subset of Feasible Solutions (less than 1%) generated by algorithm

Sol. #	**agent's organization assignment set, ϕ**	**oaf value**	**Agents' cost ($)**
1	$\{\langle a_1,r_1,g_1\rangle,\langle a_1,r_1,g_2\rangle,\langle a_1,r_1,g_3\rangle,\langle a_1,r_1,g_4\rangle,$ $\langle a_1,r_2,g_1\rangle,\langle a_1,r_2,g_2\rangle,\langle a_1,r_2,g_3\rangle,\langle a_1,r_2,g_4\rangle,$ $\langle a_2,r_2,g_1\rangle,\langle a_2,r_2,g_2\rangle,\langle a_2,r_2,g_3\rangle,\langle a_2,r_2,g_4\rangle,$ $\langle a_3,r_2,g_1\rangle,\langle a_3,r_2,g_2\rangle,\langle a_3,r_2,g_3\rangle,\langle a_3,r_2,g_4\rangle\}$	4,3112	2700
1280	$\{\langle a_1,r_2,g_1\rangle,\langle a_1,r_2,g_2\rangle,\langle a_1,r_2,g_3\rangle,\langle a_1,r_2,g_4\rangle,$ $\langle a_2,r_2,g_1\rangle,\langle a_2,r_2,g_2\rangle,\langle a_2,r_2,g_3\rangle,\langle a_2,r_2,g_4\rangle,$ $\langle a_3,r_2,g_1\rangle,\langle a_3,r_2,g_2\rangle,\langle a_3,r_2,g_3\rangle,\langle a_3,r_2,g_4\rangle\}$	3,4452	2700
3204	$\{\langle a_1,r_1,g_1\rangle,\langle a_1,r_1,g_2\rangle,\langle a_1,r_1,g_3\rangle,\langle a_1,r_1,g_4\rangle,$ $\langle a_1,r_2,g_1\rangle,\langle a_1,r_2,g_2\rangle,\langle a_1,r_2,g_3\rangle,\langle a_1,r_2,g_4\rangle,$ $\langle a_2,r_2,g_1\rangle,\langle a_2,r_2,g_2\rangle,\langle a_2,r_2,g_3\rangle,\langle a_2,r_2,g_4\rangle\}$	3,2112	1750
7813	$\{\langle a_1,r_1,g_1\rangle,\langle a_1,r_1,g_2\rangle,\langle a_1,r_1,g_3\rangle,\langle a_1,r_1,g_4\rangle,$ $\langle a_1,r_2,g_1\rangle,\langle a_1,r_2,g_2\rangle,\langle a_1,r_2,g_3\rangle,\langle a_1,r_2,g_4\rangle,$ $\langle a_3,r_2,g_1\rangle,\langle a_3,r_2,g_2\rangle,\langle a_3,r_2,g_3\rangle,\langle a_3,r_2,g_4\rangle\}$	2,9186	1800
19883	$\{\langle a_2,r_2,g_1\rangle,\langle a_2,r_2,g_2\rangle,\langle a_2,r_2,g_3\rangle,\langle a_2,r_2,g_4\rangle,$ $\langle a_3,r_2,g_1\rangle,\langle a_3,r_2,g_2\rangle,\langle a_3,r_2,g_3\rangle,\langle a_3,r_2,g_4\rangle\}$	2,4926	1850
25400	$\{\langle a_1,r_2,g_1\rangle,\langle a_1,r_2,g_2\rangle,\langle a_1,r_2,g_3\rangle,\langle a_1,r_2,g_4\rangle,$ $\langle a_2,r_2,g_1\rangle,\langle a_2,r_2,g_2\rangle,\langle a_2,r_2,g_3\rangle,\langle a_2,r_2,g_4\rangle\}$	2,3452	1750
36779	$\{\langle a_1,r_2,g_1\rangle,\langle a_1,r_2,g_2\rangle,\langle a_1,r_2,g_3\rangle,\langle a_1,r_2,g_4\rangle,$ $\langle a_3,r_2,g_1\rangle,\langle a_3,r_2,g_2\rangle,\langle a_3,r_2,g_3\rangle,\langle a_3,r_2,g_4\rangle\}$	2,0526	1800

[6] It is important to point out that only 77% of the structures, i.e., 50626, are feasible assignments for the problem. OMACS model imposes that a feasible assignment set is based on the current set of goals required to be achieved by the system [4]. For example, assignment set $\phi = \{<a_1,r_1,g_1>,<a_1,r_1,g_3>,<a_2,r_2,g_4>,<a_3,r_2,g_4>\}$ is a valid assignment; however it is unfeasible for the motivational example: goal g_2 will never be achieved.

[7] Algorithm SSG has identified 65535 structures in 4.662 s without computing the optimal and sub-optimal assignments.

45654	$\begin{Bmatrix}\langle a_1,r_1,g_1\rangle,\langle a_1,r_1,g_2\rangle,\langle a_1,r_1,g_3\rangle,\langle a_1,r_1,g_4\rangle,\\ \langle a_1,r_2,g_1\rangle,\langle a_1,r_2,g_2\rangle,\langle a_1,r_2,g_3\rangle,\langle a_1,r_2,g_4\rangle\end{Bmatrix}$	1,8186	850
57730	$\{\langle a_2,r_2,g_1\rangle,\langle a_2,r_2,g_2\rangle,\langle a_2,r_2,g_3\rangle,\langle a_2,r_2,g_4\rangle\}$	1,3926	900
62333	$\{\langle a_3,r_2,g_1\rangle,\langle a_3,r_2,g_2\rangle,\langle a_3,r_2,g_3\rangle,\langle a_3,r_2,g_4\rangle\}$	1,1	950

7 Assessment of Organization-based Multiagent System Designs

To empirically evaluate the flexibility of the different agent-based organization designs identified by algorithm ABB, we have developed a simulation that steps through the CRST application. To measure the flexibility, the approach deployed in [33] is followed; specifically, capability failure has been simulated. At each step in the simulation, a randomly selected system goal, i.e., g_1, g_2, g_3, and g_4, is achieved. Subsequently, the best available assignment is calculated (see Eq. 2). The best assignment defines how well an agent, $a_i \in A_{OMACS}$, can play a role (see Eq. 1), $r_k \in R_{OMACS}$, to achieve a goal, $g_j \in G_{OMACS}$. Afterwards, one of the capabilities possessed by a robot is randomly selected and tested to see if it has failed. A predefined capability failure rate (0 – 100%) indicates if the selected capability has failed. Once failed, a capability is assumed to remain so for the life of the system. In addition, reorganization is performed to assign available robots to available goals and to de-assign robots if their capabilities have failed, and thus, they are no longer able to play their assigned roles.

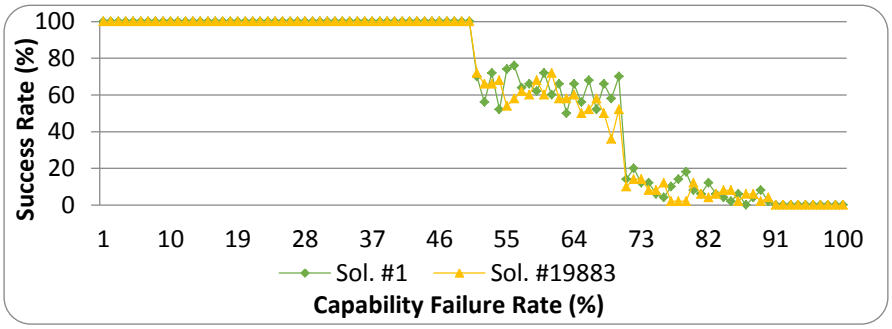

Figure 6
Comparison of Sol. #1 and Sol. # 19883

Each agent-based organization (see Section 6) has been simulated for failure rates ranging from 0 to 100% for 1000 system executions. The comparison of Figures 6 and 7 reveals a difference among the agent-based organization configurations, thereby rendering it possible to offer significant remarks about the claim, "the

higher the organization score (i.e., the oaf function), the better the performance of the organization."[36]. First, it is not always the rule that the higher the oaf function score, the better the performance of the agent-based organization. For instance, Figure 6 displays a scenario where an agent-based organization, i.e., Sol. # 19883, with an oaf value of ϕ = 2.4926 and the cost of $1850 performing equally well when compared to the best agent organization, i.e., Sol. # 1, with an oaf value of ϕ = 4.3112 and the cost of $2700.

Moreover, Figure 7 demonstrates another scenario where an agent-based organization, i.e., Sol. #7183, with an oaf value of ϕ = 2.9186 and the cost of $1800, is outperformed[8] by other agent-based organizations, i.e., Sol. #25400 and Sol. #57730, with oaf values of ϕ = 2.3452 and ϕ = 1.3926 whose costs are $1800 and $900, respectively.

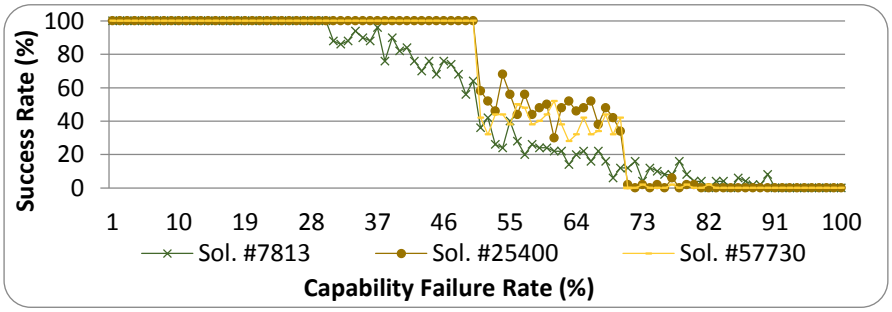

Figure 7
Comparison of Sol. #7813, Sol. #25400, and Sol. #57730

Conclusions and Future Work

In this work we have introduced an algorithmic method for assessing the n-best organizational-based multiagent system design based upon the OMACS framework. The method has been crafted by transforming an organizational-based multiagent system design into a *PNS* problem and solving the resultant problem by the algorithms and the software of the P-graph framework.

The potential of the proposed method has been illustrated by solving an example in which the optimal and suboptimal organizational-based multiagent system designs in ranked order emerge by defining its cost (in terms of the oaf function, i.e., ϕ; see Eq. 3), as the objective function. However, an optimal solution does not always capture the expected behavior of the organizational-based multiagent system design. Thus, additional research is needed to explore the combinations of the P-graph framework with other techniques (e.g., system reliability [16], self-organization [25], complex systems [34], genetic algorithms [1]), which can

[8] This behavior emerges when the capability failure rate ranges from 30% through 70%.

effectively capture the expected behavior of an organizational-based multiagent system in the design phase.

Finally, we propose the construction of a computational tool for transforming OMACS organizational-based multiagent systems into PNS problems and integrating it into existing tools [17], [18]. Our efforts will be the subject of future contributions in this research area; as well, its application in other domains [2], [15].

Acknowledgments

The first author would like to thank Virag Varga for her kind support in the definition of the mathematical model.

In memoriam, Prof. L. T. Fan (1929-2014)

References

[1] Arezki Mellal, M., Adjerid, S., Benazzouz, D., Berrazouane, S., Edward J. Williams, E. J. Optimal Policy for the Replacement of Industrial Systems Subject to Technological Obsolescence – Using Genetic Algorithm. Acta Polytechnica Hungarica, 10(1), 197-208 (2013)

[2] Barrera-Sanabria, G., Arenas-Seleey, D., García-Ojeda, Juan C., Méndez-Ortiz, F. Designing Adaptive Educational Web Sites: General Framework. In Proceedings of the IEEE International Conference on Advanced Learning Technologies, ICALT 2004, pp. 973-977, IEEE Computer Society, Joensuu, Finland (2004)

[3] Cossentino, C., Hilaire, V., Molesini, A., Seidita, V.: Handbook on Agent-Oriented Design Processes. An IEEE-FIPA Standard Compliant Description Approach. Springer-Verlag, Berlin (2014)

[4] DeLoach, S. A., Oyenan, W. H., Matson, E. T.: A Capabilities-based Model for Artificial Organizations. Journal of Autonomous Agents and Multiagent Systems. 16(1), 13-56 (2008)

[5] Dignum, V., Vázquez-Salceda, J., Dignum, F.: Omni: Introducing Social Structure, Norms and Ontologies into Agent Organizations. In: Bordini, R. H. *et al.* (eds.) PROMAS 2004, LNAI 3346, pp. 181-198, Springer-Verlag, Berlin Heildeberg (2005)

[6] Dignum, V. A.: Model for Organizational Interaction: Based on Agents, Founded in Logic. PhD Dissertation, Utrecht University (2004)

[7] Ferber, J., Gutknecht, O.: A Meta-Model for the Analysis and Design of Organizations in Multiagent Systems. In Proceedings of the 3rd International Conference on Multi Agent Systems, pp. 128-135, IEEE Computer Society, Washington, DC (1998)

[8] Fortino, G., Russo, W.: ELDAMeth: An Agent-oriented Methodology for Simulation-based Prototyping of Distributed Agent Systems. Information and Software Technology. 54(6), 608-624 (2012)

[9] Friedler, F., Tarján, K., Huang, Y. W. and Fan, L. T.: Combinatorial Algorithms for Process Synthesis. Computers Chem. Engng. 16, S313-320 (1992)

[10] Friedler, F., Tarján, K., Huang, Y. W. and Fan, L. T.: Graph-Theoretic Approach to Process Synthesis: Axioms and Theorems. Chem. Engng. Sci. 47, 1972-1988 (1992)

[11] Friedler, F., Tarján, K., Huang, Y. W., Fan, L. T.: Graph-Theoretic Approach to Process Synthesis: Polynomial Algorithm for Maximal Structure Generation. Computers Chem. Engng. 17, 929-942 (1993)

[12] Friedler, F., Varga, J. B., Fan, L. T.: Decision-Mapping for Design and Synthesis of Chemical Processes: Applications to Reactor-Network Synthesis. In: Biegler, L., Doherty, M. (eds.) AIChE Symposium Series, Vol. 91, pp. 246-250, American Institute of Chemical Engineers, New York (1995)

[13] Friedler, F. Varga, J. B., Feher, E., Fan, L. T.: Combinatorially Accelerated Branch-and-Bound Method for Solving the MIP Model of Process Network Synthesis. In: Floudas, C. A., Pardalos, P. M. (eds.) Global Optimization, Computational Methods and Applications, State of the Art, pp. 609-626, Kluwer Academic Publishers, Dordrecht, Netherlands (1996)

[14] Friedler, F., Fan, L. T., Imreh, B.: Process Network Synthesis: Problem Definition. Networks. 28, 119-124 (1998)

[15] Garcia-Ojeda, J. C., B. Bertok, F. Friedler. "Planning Evacuation Routes with the P-Graph Framework," *Chemical Engineering Transactions*, 29, 1531-1536 (2012)

[16] García-Ojeda, J. C., DeLoach, S. A., Robby, Oyenan, W. H., Valenzuela, J. O-MaSE: A Customizable Approach to Developing Multiagent Development Processes. In: Michael Luck, Lin Padgham (Eds.): Agent-oriented Software Engineering VIII, 8th International Workshop, AOSE 2007, Honolulu, HI, USA, May 14, 2007, Revised Selected Papers, LNCS 4951, 1-15, Springer-Verlag: Berlin (2008)

[17] García-Ojeda, J. C., DeLoach, S. A., Robby: AgentTool III: From Process Definition to Code Generation. In: Proceedings of the 8th international Conference on Autonomous Agents and Multiagent Systems - Volume 2, pp. 1393-1394, Budapest, Hungary (2009)

[18] García-Ojeda, J. C., DeLoach, S. A., Robby: AgentTool Process Editor: Supporting the Design of Tailored Agent-based Processes. In: Proceedings of the 2009 ACM Symposium on Applied Computing, pp. 707-714, Honolulu, Hawaii (2009)

[19] Garro, A., Tundis, A.: A Model-based Method for System Reliability Analysis. In: Proceedings of the 2012 Symposium on Theory of Modeling and Simulation - DEVS Integrative M&S Symposium (TMS/DEVS 2012), Article No 2, Society for Computer Simulation International, San Diego, CA (2012)

[20] Harmon, S. J., DeLoach, S. A., Robby, Caragea, D.: Leveraging Organizational Guidance Policies with Learning to Self-Tune Multiagent Systems. In: Proceedings of the Second IEEE International Conference on Self-Adaptive and Self-Organizing Systems, pp. 223-232, IEEE Computer Society, Venice, Italy (2008)

[21] Henderson-Sellers, B., Giorgini, P.: Agent-oriented Methodologies. Idea group Inc. Hershey, PA (2005)

[22] Horváth, A.: Investigation of Failure Systems. Acta Polytechnica Hungarica, 5(2), 127-132 (2008)

[23] Hübner, J. F., Sichman, J. S., Boissier, O.: Developing Organised Multiagent Systems using the MOISE+ Model: Programming Issues at the System and Agent Levels. *Int. J. Agent-Oriented Softw. Eng.* 1(3), 370-395 (2007)

[24] Jin, Y., Levitt, R. E.: The Virtual Design Team: A Computational Model of Project Organizations. Computational & Mathematical Organization Theory. 2(3), 171-196 (1996)

[25] Kauffman, S.: At Home in the Universe: The Search for the Laws of Self-Organization and Complexity. Oxford University Press, Oxford (1995)

[26] Klügl, F.: Measuring Complexity of Multiagent Simulations – An Attempt Using Metrics. In Dastani, M. *et al.* (eds.) LADS 2007, LNAI 5118, pp. 123-138, Springer-Verlag, Berlin Heildeberg (2006)

[27] Kota, R., Gibbins, N. and Jennings, N. R.: A Generic Agent Organisation Framework for Autonomic Systems. In: 1st International ICST Workshop on Agent-based Social Simulation and Autonomic Systems (ABSS 2009), 09-11 Sep, Limassol, Cyprus. pp. 203-219 (2009)

[28] Minoux, M.: Networks Synthesis and Optimum Network Design Problems: Models, Solution Methods and Applications. Networks, 19, 313-360 (1989)

[29] Nair, R., Tambe, M., Marsella, S.: Team Formation for Reformation. In: Proceedings of the AAAI Spring Symposium on Intelligent Distributed and Embedded Systems, pp. 52-56, AAAI Press, Menlo Park, CA (2002)

[30] Oyenan, W. H., DeLoach, S. A., Singh, S.: An Organizational Design for Adaptive Sensor Networks. In: 2010 IEEE/WIC/ACM International Conference on Web Intelligence and Intelligent Agent Technology WI-IAT, pp. 239-242, IEEE computer Society, Toronto, Canada (2010)

[31] Picard, G., Mellouli, S., and Gleizes, M.: Techniques for Multiagent System Reorganization. In: Dikenelli, O. *et al.* (eds.) ESAW 2005, LNAI 3963, pp. 142-152, Springer-Verlag, Berlin Heidelberg (2006)

[32] P-graph – PNS studio, http://www.p-graph.com

[33] Robby, DeLoach S. A., and, Kolesnikov, V. A.: Using Design Metrics for Predicting System Flexibility. In: Baresi, L. *et al.* (eds.) FASE 2006. LNCS, Vol. 3922, pp. 184-198. Springer-Verlag, Berlin Heidelberg (2006)

[34] Serugendo, G. D. M, Gleizes, M. P., Karageorgos, A.: Self-Organisation and Emergence in Mas: An Overview. Informatica 30(1), 45-54 (2006)

[35] Sims, M., Corkill, D., Lesser, V.: Automated Organization Design for Multiagent Systems. Auton. Agents and Multiagent Syst 16(2), 151-185 (2008)

[36] Vazquez-Salceda, J., Dignum, F.: Modelling Electronic Organizations. In Mark, V. *et al.* (eds.) Multiagent Systems and Applications III, LNAI 2691, pp. 584-593 Springer-Verlag, Berlin Heidelberg (2003)

[37] Zhong, C., DeLoach, S. A.: An Investigation of Reorganization Algorithms. In: 2006 International Conference on Artificial, pp. 514-517, CSREA Press (2006)

[38] Zhong, C.: Integrating Humans into and with Computing Systems. Ph.D. Dissertation, Kansas State University (2010)

Placement Optimization of Reference Sensors for Indoor Tracking

Károly Farkas

Budapest University of Technology and Economics
Magyar tudósok krt. 2, H-1117 Budapest, Hungary
e-mail: farkask@hit.bme.hu

Abstract: Location-based applications and services are becoming widespread with the proliferation of smart mobile devices. They require position tracking which is still a challenge today in the indoor environment. Different wireless technologies and localization techniques can be used to obtain the position estimation. One possibility is deploying cheap ZigBee sensors as reference points and using triangulation to compute the position of the visiting node. This technique requires the reception of a wireless signal of at least three reference sensors with well-known positions everywhere within the covered area. In this paper, we propose OptiRef, our simulated annealing based method to find, in a given area, the optimal number and placement of the reference sensors to be used for indoor positioning. Our method has O(n) complexity and shows linear run-time behavior. We investigate the performance of OptiRef via simulations focusing on ZigBee technology, although our method is generic and can be used with any kind of wireless technologies. The resulted reference point setup(s) can be considered as a good starting point for real environment design.

Keywords: Indoor localization; ZigBee; Triangulation; Simulated annealing; MATLAB

1 Introduction

Using some location-aware service is more and more common during our daily routines. Such services are based on location tracking. Collecting the location data is straightforward in open-air environments, e.g., via a GPS (Global Positioning System) receiver. However, indoor position tracking is a more challenging issue and still an actual research topic today. Several technologies and systems have been proposed and developed for indoor location sensing [1-3]. One possible approach is deploying cheap ZigBee (IEEE 802.15.4) sensors as reference points into the indoor area and using triangulation technics to derive the position of the visiting node.

Triangulation methods estimate the target location based on the geometric properties of triangles [1]. They have two variants, such as lateration and angulation. Lateration derives the position by measuring the object's distances from multiple reference points. However, instead of measuring the distance directly some other characteristics are usually measured, such as received signal strengths (RSS), time of arrival (TOA) or time difference of arrival (TDOA). Then, the distance is derived by computing the attenuation of the emitted signal strength or by multiplying the radio signal velocity and the travel time. On the other hand, angulation locates an object by computing angles relative to multiple reference points. Regardless the applied variant of triangulation, the indispensable requirement for computing the location estimation is to receive the signal of at least three reference points everywhere within the given area.

In this paper, we investigate how to place wireless reference points (ZigBee sensors) to perceive the signal with strong enough strength of at least three sensors everywhere within the given indoor territory, but keep the number of deployed sensors as low as possible. Hence, the overall cost of the indoor positioning system and its operation expenses can be kept low. We propose OptiRef, a simulated annealing based algorithm to find the optimal number and placement of the reference points in a given area. Our method has *O(n)* complexity and finds a solution, a good approximation of the global optimum, with linear run-time behavior. Furthermore, we have developed a simulation tool in the MATLAB [4] environment. We used this tool to implement OptiRef together with the ITU indoor wireless propagation model [5] simulating ZigBee signal propagation and to investigate the algorithm's behavior. Note, that our method is generic and can be used with any other wireless technologies (eg., Wi-Fi, Bluetooth, UWB). However, in this paper we focus our investigations on ZigBee sensors. Moreover, the reference point setup(s) given back by OptiRef can be considered as a good starting point for real environment design.

The rest of the paper is structured as follows. In Section 2, we briefly overview related approaches. OptiRef is proposed and described in Section 3, and we present its evaluation via simulations in Section 4. Finally, we give a short summary and sketch our future plans in Section 5.

2 Related Work

In the last years, several wireless technologies and systems have been proposed for indoor positioning [1-3]. One of them is the UWB (Ultra-Wide Band) technology which offers the highest accuracy, but it is quite an expensive solution still today. Cellular (mobile telephony) systems are also capable of providing positioning information, but their accuracy are low, and usually falls in the range of 50 m–100 m, which is appropriate only for cell based positioning.

On the other hand, most of the wireless positioning systems operate in the license free ISM (Industrial, Scientific and Medical) radio band and are based on Wi-Fi (eg., [6-8]), Bluetooth (eg., [9-11]) or ZigBee (eg., [12-14]) technologies. They use different methods for deriving the location information. For instance, location fingerprinting [1] is also a widely applied technique besides triangulation. In this case, signal fingerprints are collected in advance at a number of positions in the given area and later compared to the actual measurements. The location belonging to the best fit is selected as the position estimate. Unfortunately, none of these works investigate in a systematic way how to place the reference points optimally. Rather, they either use a pre-established infrastructure, or the placement is based on some heuristics or experimental results.

Considering the problem of optimal reference point placement, only minimum literature has been published so far to the best of our knowledge. The location optimization of Wi-Fi access points (AP) for fingerprint based positioning is a similar issue which has been investigated in some recent works. Baala et al. in [15] showed via measurements that the number and placement of the APs can have substantial impact on the position accuracy. But the authors do not propose a systematic way for finding an optimal AP deployment, rather the results are based on experiments. Zhao et al. in [16] proposed an AP location optimization method based on the Differential Evolution algorithm. In this method, the Euclidean distance of the RSS array between all the sampling points is maximized, by which the positioning accuracy can be improved. Unfortunately, the model does not take into account the effect of walls, doors and other obstacles. He at al. in [17] proposed a rapid and optimal AP deployment scheme based on genetic algorithm, which maximizes the signal space Euclidean distance between the APs. The simulation results pointed out that "the more the better" rule does not necessarily hold, though the number of APs usually increases with the size of the target area. Similarly to the previous work, the authors used a simple signal propagation approach and did not consider the attenuation effects of the indoor environment. Fang and Lin in [18] presented a framework for linking the placement of APs and the positioning performance. Their algorithm aims at choosing a proper set of APs' locations so that the signal is maximized and the noise is minimized simultaneously. The location system is developed in a real-world environment collecting realistic measurements. However, collecting and comparing the measurement results of the different AP setups can be a cumbersome task especially in a large area to be covered.

OptiRef is a simulation based method and can complement the measurement based approaches by considerably reducing the reasonable reference point setups to be considered. In this sense, the outcome of OptiRef is a good starting point for further, real environment investigations. For example, one can deploy a setup resulted by OptiRef, create the signal map of the territory by measurements, and refine the placement of the reference points based on the measured signal map.

3 Reference Point Placement

The triangulation method is a commonly used technique for positioning purposes in wireless environment. However, it demands the fulfillment of some basic requirements. Thus, the indispensable condition for triangulation is to receive the signal of at least three reference points everywhere within the given indoor area.

3.1 Optimization of Reference Point Setup

Finding the optimal number and positions of the reference points, which still satisfies the condition above, in real environment is a challenging task for analytical methods, because the propagation characteristics of wireless signals are too complex to be realistically modeled. Nevertheless, in order to find a setup with minimum number of reference sensors an obvious approach is to analyze and compare all the possible setups. Unfortunately, in real world this process is almost impossible to be accomplished, therefore simulations and optimization methods are to be used.

Actually, the number of reference sensor position combinations is infinite because the territory, where the sensors can be deployed, is continuous and contains infinite number of points available for sensor deployment. To handle this problem, we assume that the reference sensors can be located only in discrete points of the territory map. If the density of these points is high enough the original situation can be approximated well. For example, if we consider a 106 m × 102 m indoor territory (eg., a parking garage) where the sensors can be placed into the junctions of a grid with 10 cm grid distance, then the number of possible reference point locations is 1,081,200. Figure 1 illustrates this scenario but showing a grid with around 12 m grid distance for better visibility (the thick blue lines on the map represent walls). Of course, in a real environment it can happen that not all the grid points are valid locations for sensor deployment, and these points can be eliminated from the investigations.

Unfortunately, analyzing all the possible reference sensor setups with a brute force algorithm cannot be accomplished due to the huge number of location setup combinations. In the previous example, $2^{1081200}$ different sensor location setups exist that cannot be processed in acceptable time. To solve this problem, alternative solutions are required.

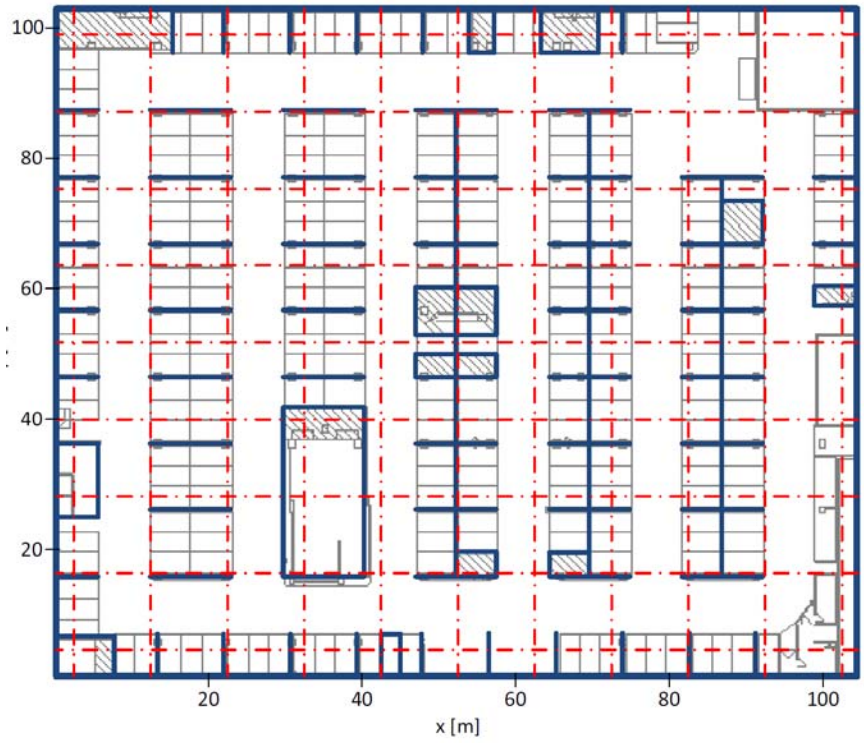

Figure 1
Territory map with a grid representing the possible reference sensor locations

3.2 OptiRef Algorithm

We propose OptiRef, our top-down reference point placement algorithm to find the optimal reference sensor location setup(s).

We start with a simple method. The initial step is to place a reference sensor in every discrete grid junction point of the territory map and compute the coverage area of each sensor using a wireless signal propagation model. In real environment, this can be almost any point of the continuous space, but we consider only discrete points with high density, equals to the map resolution in our simulations, in order to make the calculations possible. The next step is to determine the number of perceived reference sensors, using the previously computed coverage maps, in each point of the territory where the visiting node can be located, and thus to verify the fulfillment of the criterion. If there is no point on the map where the number of perceived reference sensors is less than three, than one sensor can be removed randomly. The next step is to check the criterion again.

If the number of perceived sensors still fulfills it in each point of the territory, then another sensor can be removed randomly and so on, otherwise the algorithm stops. This simple method provides a solution, but in most of the cases not an optimal one.

This method can be modeled in a tree graph, where the states represent by binary numbers all the possible reference point combinations. After serializing the grid (creating from the 2D grid a 1D sequence by writing down the rows of the grid one after the other) the binary number determines which sensor is part of the given setup. The root state (every digit is a 1) is the initial setup containing in every grid junction point a reference sensor. The states one level below represent the setups where a reference sensor is deployed in all but one grid junction point, or from a different viewpoint one sensor is removed compared to the parent state, and so on. For instance, 1011..1 means that the reference sensor in the second position is removed compared to the initial setup. Figure 2 illustrates this graph containing the possible reference point combinations. Note, that the Hamming distance between the neighboring levels is one, and the graph consists of n levels if the number of possible reference point locations (grid junction points) is n.

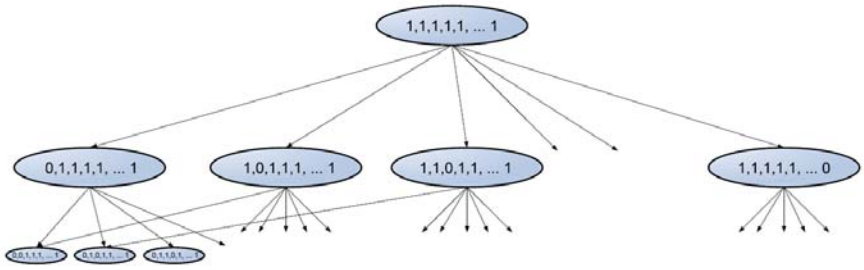

Figure 2
Graph representation of the possible reference sensor setups

With the graph representation we can originate our task in a graph theory problem. Thus, our goal is to find the state with the longest distance from the root, in which state the three perceivable reference sensors criterion still holds. On each level of the tree, the number of removed reference points is the same, therefore the deeper we are in the tree the less reference points are needed to cover the served territory. However, this "longest path" task is an NP-complete problem in graph theory [19].

Numerous heuristic optimization algorithms were developed to find the global optimum for such NP-complete problems, like hill climbing, swarm intelligence, integer linear programming, simulated annealing, etc. For our case, we propose simulated annealing to approximate the optimal reference point setup. Simulated annealing is a generic probabilistic algorithm for global optimization [19]. It tries to locate a good approximation of a given function's global optimum in a large search space even for NP-complete problems.

OptiRef extends the above-mentioned simple reference point placement method with the simulated annealing algorithm. Hence, a previously removed reference point can be put back again with some probability. This probability is given in Equation 1:

$$\exp\left(-\Delta E / T\right), \tag{1}$$

where ΔE stands for the cost function difference of the two neighboring reference sensor setups in question and parameter T is called temperature. The cost function, in our case, is the number of reference points in the given graph state. T is the sum of the number of perceived reference sensors for each position on the territory map. This number is decreasing as more and more sensors are removed (we are deeper in the graph), that can be interpreted as "cooling" in the context of simulated annealing. The possibility of putting a previously removed reference sensor back prevents the method from being stuck in a local minimum that is worse than the global one. Algorithm 1 shows the pseudo-code of the OptiRef algorithm's main steps.

Algorithm 1 OptiRef Algorithm

```
initialization (add all ref. points, compute the coverage maps, set counter)
While counter > 0      # counter is the step limit, linearly dependent on n
    Choose neighbor state randomly (put back or remove a ref. point)
        Case putback
            putbackRef() with Pr (exp(ΔE/T))
        Case remove
            removeRef() with Pr (1− exp(ΔE/T))
            If perceivedRefs < 3 (check the criterion)
                restoreRef() (restore the removed ref. point)
    counter = counter − 1
```

The time required to get an appropriate reference point setup is an important issue that is affected by the complexity of the algorithm used. To find the global optimum with a brute force method all the possible reference point setups must be investigated. Thus, it has an $O(2^n)$ complexity, where n is the number of possible reference point locations. In case of the OptiRef algorithm, a step limit, linearly dependent on n, is used to determine how many times reference point can be removed or put back which limits the running time of the algorithm, too. Hence, our method, having $O(n)$ complexity, is able to find a good approximation of the global optimum in real time showing linear run-time behavior.

4 Evaluation

The proposed OptiRef algorithm was evaluated via simulations. The simulation environment, the obtained results and some concluding remarks are presented in the following.

4.1 Simulation Environment

We have used the MATLAB [4] environment to develop our simulation tool. In this tool, we implemented first the ITU indoor wireless signal propagation model [5] that we applied in our simulations. The site-general ITU indoor model predicts the propagation path loss according to Equation 2:

$$L = 20 \cdot \log(f) + N \cdot \log(d) + Lf(k) - 28dB, \tag{2}$$

where L is the total path loss (dB), f is the frequency (MHz), N is the distance power loss coefficient, d is the distance between the transmitter and the receiver (m), $Lf(k)$ is the floor penetration loss factor and k is the number of floors between the transmitter and the receiver.

In our investigations, we used only a single floor environment, a sector on one level of a parking garage. However, the ITU indoor signal propagation model is applicable also in a multi floor environment setting the $Lf(k)$ parameter accordingly, that can be useful for the investigation of other indoor positioning based applications, too.

We selected the model and the simulation parameters according to the recommendations in [5] taking into account the properties of the simulated scenario (a parking garage). These parameters are: frequency, N, $Lf(k)$, transmitter antenna gain, receiver antenna gain and transmitted power. We set the default values of these parameters to 2.4 GHz, 27, 10, 5 dB, 2 dB, and 30 mW, respectively.

In wireless positioning systems, the RSS determines the range within the positioning service can be provided. If the signal is weak and the RSS is too low, the reference sensor is not perceived by the visiting terminal and cannot be used for positioning purposes. Thus, in order to determine the reference point coverage area we have introduced the terminal sensitivity parameter (-80 dB). If the received signal strength is lower than the terminal sensitivity, the terminal is out of the reference point's range.

In the simulator, we implemented not just our simulated annealing based OptiRef algorithm, but also a brute force method. In cases, when the number of possible reference point positions is not too high the brute force method is a better choice providing always the global optimal solution. However, due to the NP-completeness of the problem finding the optimal reference sensor topology with

the brute force method in real scenarios is usually not possible. In OptiRef, we set the step limit counter value as 10 times the number of the possible reference point positions giving the possibility to the algorithm not to get stuck in a local optimum. Table 1 summarizes the parameter settings we used in our simulations.

Table 1
Simulation parameter settings

Wireless signal propagation model		
ITU indoor		
Frequency	*N*	*Lf(k)*
2.4 GHz	27	10
Tx antenna gain	**Rx antenna gain**	**Tx power**
5 dB	2 dB	30 mW
Terminal sensitivity		
-80 dB		
Step limit of OptiRef (counter)		
10 × no. of the possible reference point positions		

Moreover, the simulated area (map) has to be loaded at the beginning of the simulation process into our simulation tool. A .bmp image file can be used to determine the simulated environment by defining the rooms, walls, pillars, etc.

We ran the simulations on a Dell Inspiron 14z laptop equipped with Intel Core i5 2430M CPU@2.4 GHz, 4 GB RAM and MS Windows7 (64bit) operating system.

4.2 Simulation Results

In order to analyze the performance of our method we ran a number of simulations. Hence, we compared the simulation running times of OptiRef and the brute force algorithm first. Then we investigated the outcomes of OptiRef after several runs in case of a given scenario to see how close the resulted reference point numbers are to each other and how the simulation run-times vary. Next, we took a closer look at one simulation outcome and examined the coverage map of the resulted reference point setup. And finally, we investigated how the resulted reference point numbers change if the initial criterion is modified.

4.2.1 OptiRef vs. Brute Force

In the first simulation round, we compared our OptiRef algorithm to the brute force method and investigated their limitations. We used a simple indoor map with no walls and obstacles.

In Figure 3, the average simulation run-times are shown, which were measured in function of the number of possible reference point positions and iterated 10 times for each setup, together with their 95% confidence intervals. We increased the number of possible reference point locations to see the scalability of OptiRef. In case of the brute force algorithm, we could not complete all of these simulations because they would have required too much time. Thus, we could investigate the required run-time of the brute force method only up to 20 possible reference point positions.

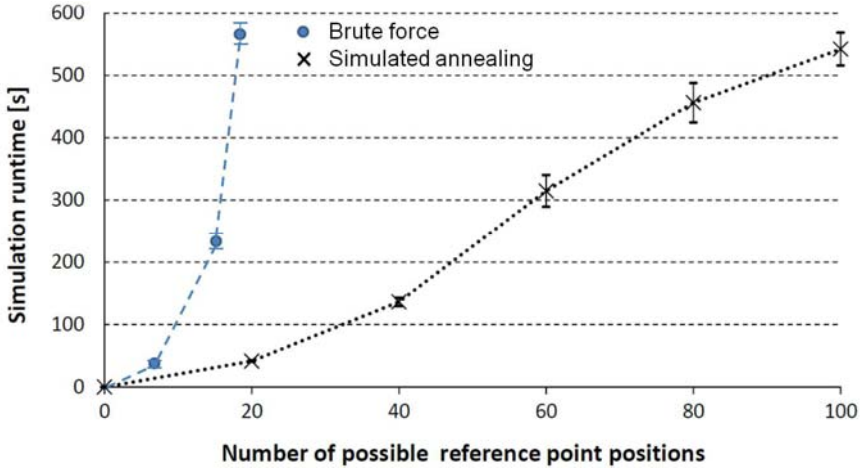

Figure 3
Simulation time vs. number of possible reference point positions in case of OptiRef and the brute force algorithm

The obtained results support that OptiRef scales well with the number of possible reference point positions showing a linear run-time increase. On the contrary, in case of the brute force algorithm the simulation run-time increases exponentially, as expected. Thus, in bigger scenarios with hundreds or thousands possible reference sensor locations the brute force method is practically unusable.

4.2.2 Performance of OptiRef

In the second round, we investigated further our OptiRef algorithm in a 106 m × 102 m territory, where the grid distance was around 12 m. The used territory map is illustrated in Figure 1. In our case, the number of possible reference point locations was 78 meaning 2^{78} different sensor topology setups. Of course, the grid density can be increased for the price of increased simulation run-time.

We repeated the simulation 10 times investigating the simulation run-time, consisting of the coverage map computation and the simulated annealing algorithm, and the resulted number of required reference points. The results are

collected in Table 2. The mean simulation run-time was 457.46 seconds, from which the time needed for the coverage map calculations is notable (456.87 sec), while only 0.59 seconds were required for the simulated annealing algorithm. This result is in line with our expectations. The coverage map calculation is time consuming especially when we have a huge number of reference sensors. On the other hand, the simulated annealing algorithm requires only some comparisons and a more or less random decision which can be carried out quickly.

Table 2
Mean run-time of 10 OptiRef simulations using the same scenario

	Total sim. time [sec]	**Coverage map calc. time [sec]**	**Sim. annealing alg. time [sec]**	**No. of required ref. points**
Mean & std.	457.46 ± 5.22	456.87 ± 5.15	0.59 ± 0.09	30.2 ± 1.8

Note, that simulated annealing randomly chooses the neighbor states in the graph, therefore in case of several optimal solutions the resulted reference sensor setup can be different in consecutive simulation runs, even if the input parameters are the same. An output of the simulation is presented in Figure 4 where the selected reference point locations and RSS values are illustrated. The colors represent the highest RSS value in the given point of the territory which usually, but not necessarily, belongs to the closest reference sensor in the vicinity of the measurement.

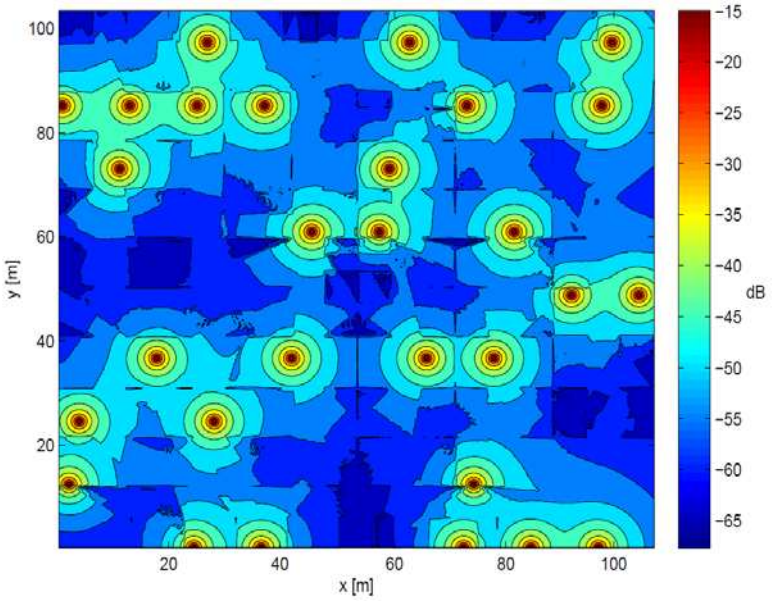

Figure 4
Selected reference point locations and RSS values using OptiRef

29 reference points were the minimum still enough to cover the territory by satisfying the perceivability criterion. However, we can never be sure that we found a global optimal solution (or reached only a local optimum), but repeating the simulation increases its probability. In normal scenarios, a simulation running time takes some hundred (see Table 2) or probably some thousand seconds (depending on the grid density) on a usual computer, so iterating the simulation a couple of hundred times should not cause any problem today.

Analyzing several simulation outcomes we can notice that the algorithm locates the reference points in the border areas in most of the cases and only few sensors are placed in the center. The reason is that the perceivability criterion is censorious at the boundaries of the map; hence more sensors must be deployed at the edges of the territory.

4.2.3 Coverage Map

In the third round, we examined the reference sensor coverage density achieved by our OptiRef algorithm. The developed simulation tool makes it possible to analyze the number of perceived reference points in the served territory. If the RSS is higher than the terminal sensitivity (-80 dB), the reference point is assumed to be available for positioning purposes. Figure 5 summarizes the number of available reference sensors considering all the measurement points. Figure 6 illustrates the same on the territory map (the different numbers are represented by different colors) in case of a given reference sensor setup.

We can see, that some parts of the territory, mainly the center areas, are covered by 10-12 reference sensors, while the terminals visiting the border areas can receive the signal of only few sensors. Nevertheless, our perceivability criterion still holds everywhere in the territory.

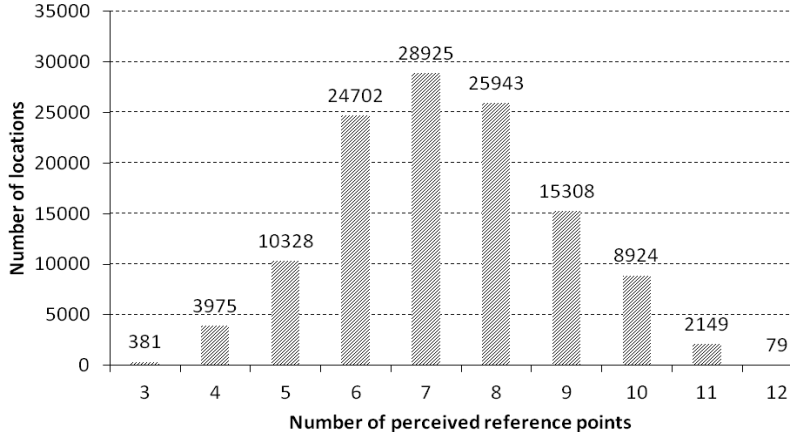

Figure 5
Number of reference points available for positioning

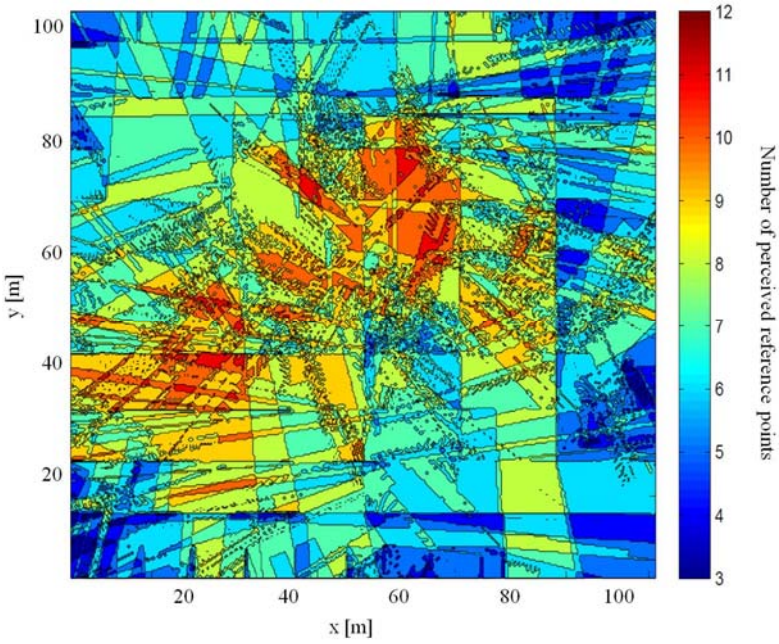

Figure 6
Map representation of the number of reference points available for positioning

4.2.4 Impact of the Criterion Change

In the forth round, we investigated the impact of changing the perceivability criterion. The perceivability of at least three reference sensors is a strict minimum requirement. However, by increasing the number of available reference sensors in a given point of the map the position estimation accuracy can be improved. We have analyzed the total number of required reference points if the minimum criterion of perceivable sensors is increased. The simulations were iterated 20 times and the results are shown in Figure 7 using the same territory map with the same 78 possible reference point locations, as in the previous experiments.

As it is expected, the number of required reference points for the positioning system is increasing if more than three sensors must be perceived in any point of the territory. As we noted before, the location and the number of reference points returned by OptiRef may vary due to the randomness of the simulated annealing algorithm. In Figure 7 the average, the minimum and the maximum number of required reference points are depicted using the same simulation setup. Although the differences are not significant, it is recommended to iterate the algorithm in order to find a sensor topology close to the global optimum.

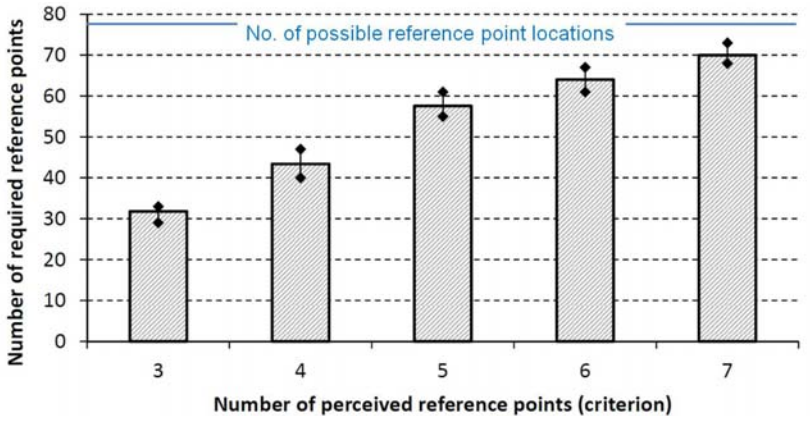

Figure 7
Number of reference points required to fulfill the perceivability criterion

4.2.5 Discussion

From the evaluation results we can see that OptiRef provides a solution for a given scenario within an acceptable time, if the number of possible reference point locations (grid density) is not too big (falls in the range of some hundreds). However, there is no guarantee that the resulted solution is a global optimal one. Hence, it is recommended to iterate the simulation to increase the probability of finding a global optimum. OptiRef is scalable, the simulation running time is linearly dependent on n, the number of grid points (potential reference sensors) in the given area. Moreover, OptiRef is flexible and can easily handle if the perceivability criterion changes. The simulation run-time does not increase in this case either because the time consuming part (coverage map calculations) does not change and it is performed only once in the initial phase.

An interesting issue is to think about how close to reality the simulation results are. In our case, it depends on the used wireless signal propagation model to a great extent. We ran also some simulations using a modified version of the free-space propagation model [5] and we introduced some wall attenuation (4dB) in computing the path loss. With this model we got slightly different results, the minimal reference point setup contained 25 sensors in case of the same scenario. Nevertheless, the signal propagation model can be easily replaced and using more realistic model results in solution closer to the real environment optimum.

Conclusions

In this paper, we investigated the issue of ZigBee reference sensor placement optimization for indoor positioning. Hence, we examined how to place the reference points to perceive the signal of at least three reference sensors everywhere within the given indoor territory, but keep the number of deployed

sensors as low as possible. We proposed OptiRef, a simulated annealing based method to find a good approximation of the optimal solution. OptiRef has *O(n)* complexity and shows linear run-time behavior. Furthermore, we have developed a simulation tool in MATLAB environment for the given problem. We used this tool to implement OptiRef together with the ITU indoor wireless signal propagation model and to investigate the algorithm's behavior.

By minimizing the amount of required reference points the cost of deployment and operation expenses can be reduced, while at the same time still providing an efficient positioning system. OptiRef and the developed simulation tool are generic and they can be useful in planning radio-based positioning systems not just focusing on ZigBee technology. The simulator is adaptable to different wireless technologies by adjusting the signal propagation parameters or even by replacing the propagation model. The reference point setup(s) resulted by OptiRef can be considered as a good starting point for real environment design.

As future work, we plan to further investigate the performance and limitations of OptiRef. We will collect real measurements and compare them with our simulation results. Moreover, in some scenarios it can be desirable to deploy such a reference point setup in which the sensors form a connected wireless sensor network. We plan to extend our algorithm to satisfy this condition, too.

Acknowledgement

The publication was supported by the EITKIC 12-1-2012-0001 project, which is supported by the Hungarian Government, managed by the National Development Agency, financed by the Research and Technology Innovation Fund and was performed in cooperation with the EIT ICT Labs Budapest Associate Partner Group (www.ictlabs.elte.hu). Károly Farkas has been partially supported by the Hungarian Academy of Sciences through the Bolyai János Research Fellowship. The author would like to acknowledge the support and help of Árpád Huszák and Győző Gódor in this work.

References

[1] H. Liu, H. Darabi, P. Banerjee, and J. Liu, "Survey of Wireless Indoor Positioning Techniques and Systems," IEEE Transactions on Systems, Man, and Cybernetics, Part C: Applications and Review, Vol. 37, No. 6, pp. 1067-1080, Nov. 2007

[2] Y. Gu, A. Lo, and I. Niemegeers, "A Survey of Indoor Positioning Systems for Wireless Personal Networks," IEEE Communications Surveys and Tutorials, Vol. 11, No. 1, pp. 13-32, 2009

[3] H. Koyuncu and S. H. Yang, "A Survey of Indoor Positioning and Object Locating Systems," International Journal of Computer Science and Network Security, Vol. 10, No. 5, pp. 121-128, May 2010

[4] MathWorks, “MATLAB and Simulink for Technical Computing,” 2012, www.mathworks.com

[5] J. S. Seybold, Introduction to RF Propagation. John Wiley & Sons, Inc., Sep. 2005

[6] P. Bahl and V. N. Padmanabhan, “RADAR: An In-Building RF-based User Location and Tracking System,” in Proceedings of the 19th IEEE International Conference on Computer Communications (INFOCOM 2000) Vol. 2, Tel Aviv, Israel, Mar. 2000, pp. 775-784

[7] M. Youssef, A. Agrawala, and A. Udaya Shankar, “WLAN Location Determination via Clustering and Probability Distributions,” in Proceedings of the First IEEE International Conference on Pervasive Computing and Communications (PerCom 2003) Dallas-Fort Worth, TX, USA, Mar. 2003, pp. 143-150

[8] T. King, S. Kopf, T. Haenselmann, C. Lubberger, and W. Effelsberg, “COMPASS: A Probabilistic Indoor Positioning System Based on 802.11 and Digital Compasses,” in Proceedings of the First ACM International Workshop on Wireless Network Testbeds, Experimental evaluation and CHaracterization (WiNTECH 2006) Los Angeles, CA, USA, Sep. 2006, pp. 34-40

[9] A. Genco, “Three Step Bluetooth Positioning,” in Proceedings of the First International Conference on Location- and Context-Awareness (LoCA'05) Oberpfaffenhofen, Germany, May 2005, pp. 52-62

[10] M. Rodriguez, J. P. Pece, and C. J. Escudero, “In-Building Location Using Bluetooth,” in Proceedings of the International Workshop on Wireless Ad-hoc Networks (IWWAN 2005) London, UK, May 2005

[11] S. Kawakubo, A. Chansavang, S. Tanaka, T. Iwasaki, K. Sasaki, T. Hirota, H. Hosaka and H. Ando, “Wireless Network System for Indoor Human Positioning,” in Proceedings of the 1st Inernational Symposium on Wireless Pervasive Computing (ISWPC 2006), Phuket, Thailand, Jan. 2006, pp. 1-6

[12] O. Hernandez, V. Jain, S. Chakravarty and P. Bhargava, “Position Location Monitoring - Using IEEE 802.15.4/ZigBee technology,” Beyond Bits, Vol. 4, pp. 67-73, Summer 2009

[13] K. Maneerat and C. Prommak, “On the Analysis of Localization Accuracy of Wireless Indoor Positioning Systems using Cramer’s Rule,” World Academy of Science, Engineering and Technology (WASET) - Online Special Issue, Vol. 60, pp. 202-207, Apr. 2011

[14] S.-H. Fang, C.-H. Wang, T.-Y. Huang, C.-H. Yang and Y.-S. Chen, "An Enhanced ZigBee Indoor Positioning System with an Ensemble Approach," IEEE Communications Letters, Vol. 16, No. 6, pp. 564-567, Apr. 2012

[15] O. Baala, Y. Zheng and A. Caminada, "The Impact of AP Placement in WLANbased Indoor Positioning System," in Proceedings of the Eighth International Conference on Networks (ICN'09) Cancun, Mexico, Mar. 2009, pp. 12-17

[16] Y. Zhao, H. Zhou and M. Li, "Indoor Access Points Location Optimization Using Differential Evolution," in Proceedings of the International Conference on Computer Science and Software Engineering (CSSE 2008), Vol. 1, Wuhan, China, Dec. 2008, pp. 382-385

[17] Y. He, W. Meng, L. Ma and Z. Deng, "Rapid Deployment of APs in WLAN Indoor Positioning System," in Proceedings of the 6th International ICST Conference on Communications and Networking in China (CHINACOM 2011) Harbin, China, Aug. 2011, pp. 268-273

[18] S.-H. Fang and T.-N. Lin, "A Novel Access Point Placement Approach for WLANBased Location Systems," in Proceedings of the IEEE Wireless Communications and Networking Conference (WCNC 2010) Sydney, Australia, Apr. 2010, pp. 1-4

[19] D. Karger, R. Motwani and G. Ramkumar, "On Approximating the Longest Path in a Graph," Algorithmica, Vol. 18, No. 1, pp. 82-98, 1997

On Two Modifications of $E_r/E_s/1/m$ Queuing System Subject to Disasters

Michal Dorda, Dusan Teichmann

VSB − Technical University of Ostrava, Faculty of Mechanical Engineering, Institute of Transport, 17. listopadu 15, 708 33 Ostrava-Poruba, Czech Republic, e-mail: michal.dorda@vsb.cz, dusan.teichmann@vsb.cz

Abstract: The paper deals with modelling a finite single-server queuing system with the server subject to disasters. Inter-arrival times and service times are assumed to follow the Erlang distribution defined by the shape parameter r or s and the scale parameter rλ or sμ respectively. We consider two modifications of the model − server failures are supposed to be operate-independent or operate-dependent. Server failures which have the character of so-called disasters cause interruption of customer service, emptying the system and balking incoming customers when the server is down. We assume that random variables relevant to server failures and repairs are exponentially distributed. The constructed mathematical model is solved using Matlab to obtain steady-state probabilities which we need to compute the performance measures. At the conclusion of the paper some results of executed experiments are shown.

Keywords: $E_r/E_s/1/m$; queuing; disasters; method of stages; balking; Matlab

1 Introduction

Queuing theory is a useful tool which enables us to find characteristics of queuing systems. We can meet queuing systems in many sectors, for example in informatics, telecommunications, transport or economics. In general, a queuing system represents a system which serves customers coming into the system. There are a lot of possible ways to classify queuing systems − for example according to the type of the input process (Poisson, *k* Erlang etc.), the service discipline (FCFS, LCFS, priority queues etc.), the capacity of the queue intended for waiting customers (systems which do not permit waiting for the service, finite capacity or the infinity capacity of the queue) and so on. Another criterion of the queuing system's classification is whether failures of servers are considered in the model. For a lot of queuing systems which have already been modelled it is assumed that no failures of servers can occur. Such queuing systems represent the first group of queuing systems often called reliable queuing systems. The second group of queuing systems is represented by the so-called unreliable queuing systems or queuing systems subject to server breakdowns.

Failures of the server have an obvious impact on the performance measures of the studied queuing system. It is clear, for example, that the mean number of the customers in the service for an unreliable queuing system should be less than the value of the same performance measure for a corresponding queuing system which is not subject to breakdowns. A lot of policies have been developed; the policies determine what happens with the customer being served when the server breaks down. In this paper we consider that failures of the server cause emptying of the queuing system; meaning that all customers in the system leave it without being served. Moreover, each customer coming into the system when the server is broken down is not willing to wait and leaves the system (or is rejected). Such type of server failures are often called disasters or catastrophes.

Some authors have already modelled queuing systems with server failures having the character of disasters or catastrophes. Krishna Kumar et al. [1] solved an M/M/1 queuing system. Catastrophes of the server occur according to the Poisson process when the server is busy. Whenever a catastrophe occurs the system empties instantly and all newly arriving customers are lost during the server repair. Sudhesh [2] studied a similar M/M/1 queue which differs in the fact that customers entering the system become impatient when the server is down. The authors of papers [1] and [2] executed transient analysis of the systems, which means they derived formulas for system state probabilities as functions of the time t. Yechiali [3] examined an M/M/c queue with random disastrous failures which cause all present customers to be lost. Customers entering the system during repairing of the server are considered to be impatient.

Queuing systems in which inter-arrival and service times are considered to follow the Erlang distribution have already been studied in the past. But in comparison with queues assuming exponential or general distributed inter-arrival and service times, the models of queuing systems under the assumption of the Erlang distribution are not so common, especially in the case of being subject to breakdowns.

Let us look at some models of reliable queuing systems in which the Erlang distribution is assumed. Plumchitchom and Thomopoulos [4] studied a single-server queuing system with Erlang distributed inter-arrival and service times. Wang and Huang [5] modelled a finite M/E_k/1 queuing system with a removable server (the server is turned off and turned on depending on the number of customers in the system). The authors further presented a cost function to determine the optimal policy. Cost and profit analysis for an M/E_k/1 queuing system with removable service station was carried out by Mishra and KumarYadav [6]. Yu et al. [7] developed a model of an M/E_k/1 queuing system with no damage service interruptions − it is assumed that after the first phase of service the service process can be interrupted with given probability. Binkowski and McCarragher [8] employed an E_r/E_k/1/N queuing system to model the operation of a mining stockyard. An optimal management problem of the N-policy M/E_k/1 queuing system with a removable service station under steady-state

condition was solved by Pearn and Chang [9]. In the paper [10] written by El-Paoumy and Ismail a solution of a finite $M^X/E_k/1/N$ with bulk arrivals, balking and reneging is demonstrated. The matrix-geometric solution of the $M/E_k/1$ queue with balking and state-dependent service was demonstrated by Yue et al. [11]. Shawky [12] considered a single-channel service time Erlangian queue with finite source of customers, one server, finite storage capacity and balking and reneging. Adan et al. [13] analysed an $E_k/E_r/c$ queuing system.

Some authors solved queues subject to failures under the assumption of the Erlang distribution which was most often applied to model service times. An $M/E_k/1$ queue with server vacation was studied by Jain and Agrawal [14]. The authors further assumed that the server can break down when it is busy and the Poisson arrival rate is state dependent. Wang and Kuo [15] solved an $M/E_k/1$ machine repair problem − several identical machines operating under the care of an unreliable service station. The authors employed matrix geometric method to derive the steady-state probabilities and developed the steady-state profit function to find out the optimum number of machines. Kumar et al. [16] considered an $M^X/E_k/1$ two-phase queuing system with a single removable server and with gating, server start-up and unpredictable breakdowns.

In this paper we will focus on finite single-server queuing systems with the server subject to disasters, where inter-arrival times and service times follow Erlang distribution. Further we will assume that times between failures and times to repair are exponentially distributed. We employed a "direct" approach to model the queuing systems consisting of creating a state transition diagram, on the basis of the diagram we derive a linear equation system describing the system and the equation system is solved numerically using suitable software; in the paper we give a hint for solving in Matlab [17]. We hope that this paper makes the solving of finite Erlang distributed queuing systems possible primarily to non-mathematicians who are not able to employ the most advanced mathematical methods used for analytical solving of queuing systems.

The rest of the paper is organized as follows. In Section 2 we will discuss the necessary assumptions. In Section 3 we will present the mathematical model and its solving using Matlab. In Section 4 we will present results of some numerical experiments we did with the proposed model. Please note that the paper is an extended version of our conference paper presented at the conference Mathematical Methods in Economics 2012 [18].

2 General Assumptions and Notations

Let us consider a single-server queuing system with a finite capacity equal to m, where $m>1$; that means the system has the capacity of m places for customers − single place in the service and $m-1$ places intended for the waiting of customers.

Customers waiting in the queue are served one by one according to the FCFS service discipline.

Let inter-arrival times follow the Erlang distribution with the shape parameter $r \geq 2$ and the scale parameter $r\lambda$; therefore the mean inter-arrival time is then equal to $\frac{r}{r\lambda} = \frac{1}{\lambda}$. Service times are also Erlang distributed with the shape parameter $s \geq 2$ and the scale parameter $s\mu$; thus the mean service time is equal to $\frac{s}{s\mu} = \frac{1}{\mu}$. We apply the Erlang distribution because it is able to model time duration of a lot of practical processes in comparison with the exponential distribution, which is often used. On the other hand, using the Erlang distribution brings some complications in modelling the system. However, single-server queues with the Erlang distribution of inter-arrival times or service times are still solvable using conventional methods.

Let us assume that the server is successively failure-free (or available) and under repair. We will assume two modifications. For the first modification we consider that failures of the server can occur when the server is idle or busy − we say that server failures are operate-independent. In the case of the second modification we assume that failures of the server are so-called operate-dependent, which means the server can break down only when it is servicing a customer. Let us assume for both modifications that repair of the server is started immediately after breakdowns, and it immediately starts to operate when repaired.

Now it is necessary to make some assumptions about failure frequency. Due to the fact that our modifications differ in assumptions about the occurrence of server failures we have to make different suppositions for individual modifications of the studied system. Assuming ergodicity (the system has the finite capacity), all of the possible states of the system can be summarized into three states:

- The idle state − no customer is in the system (the system is empty) and the server is not broken down (is in working condition). Let us denote the equilibrium probability that the server is idle P_{idle}.
- The busy state − i customers are in the system, where $i \in \{1,\ldots,m\}$; that means a customer is in the service and $(i-1)$ customers are waiting in the queue. The equilibrium probability that the system is found in the busy state is denoted with P_{busy}.
- The down state − no customer is in the system (as we are considering disasters) and the server is broken down and under repair; let us denote the equilibrium probability of this state P_{down}.

As these states are mutually exclusive and exhaustive, the sum of these probabilities has to be equal to 1:

$$P_{idle} + P_{busy} + P_{down} = 1. \tag{1}$$

Let us start with the first modification. The server is successively available and broken down. Let the times the server is available be exponentially distributed with the parameter η meaning that the mean time the server is available equals the reciprocal value of the parameter η. Times to repair are exponentially distributed as well, but with the parameter ζ; the mean time to repair therefore equals to $\frac{1}{\zeta}$. It is clear that the server's steady-state availability A (the ratio of time the server is available in expected value) is equal to:

$$A = \frac{\frac{1}{\eta}}{\frac{1}{\eta}+\frac{1}{\zeta}} = \frac{\zeta}{\eta+\zeta} = P_{idle} + P_{busy} \tag{2}$$

and the server's steady-state unavailability U (the ratio of time the server is broken down in expected value) is:

$$U = 1 - A = \frac{\eta}{\eta+\zeta} = P_{down}\,. \tag{3}$$

And now we have to use similar assumptions about the second modification. Let us assume that times of overall server working between failures are exponentially distributed with the parameter η; the mean time of overall server working between failures is then equal to the reciprocal value of the parameter η. Times to repair are exponentially distributed as well, but with the parameter ζ; the mean time to repair is therefore equal to $\frac{1}{\zeta}$ as well.

To express the server's steady-state availability it is necessary to realize that in this modification the server failures are not as frequent as in the first modification for the same value of the parameter η. The value η has to be multiplied by a coefficient expressed by ratio $\frac{P_{idle}+P_{busy}}{P_{busy}}$ which takes into account the fact that the ratio of time the server is idle has no impact on failure frequency. Now, for the server's steady-state availability we can write:

$$A = \frac{\frac{P_{idle}+P_{busy}}{P_{busy}}\cdot\frac{1}{\eta}}{\frac{P_{idle}+P_{busy}}{P_{busy}}\cdot\frac{1}{\eta}+\frac{1}{\zeta}} = \frac{\zeta\cdot\left(P_{idle}+P_{busy}\right)}{\eta\cdot P_{busy}+\zeta\cdot\left(P_{idle}+P_{busy}\right)} = P_{idle}+P_{busy}\,. \tag{4}$$

Realizing that $P_{down} = 1-\left(P_{idle}+P_{busy}\right)$ and substituting it into (4) we can derive an expected formula in the form:

$$P_{down} = \frac{\eta}{\zeta}\cdot P_{busy} = U\,. \tag{5}$$

As far as the behaviour of customers at the moment of the failure is concerned, we will assume that the system empties after every breakdown of the server; and the system is empty when the server is down − i.e. failures represent so-called disasters (or catastrophes) in the system.

Let us mention an example of such queuing system from railway transport. Marshalling yards represent important nodes on each railway net because they carry out inbound freight trains classification according to directions of individual wagons and form new outbound freight trains. Such yards are usually equipped with corresponding infrastructure consisting of reception sidings, a hump, sorting sidings and so on. The process of freight trains classification is carried out via the hump − a train of wagons is shunted from an arrival track over the hump and individual wagons (or set of wagons) are classified onto sorting sidings according to their directions.

The hump can be considered to be the server, the inbound freight trains represent customers and the classification process is their service. However, the infrastructure belonging to the hump can break down from time to time. For example, some switches of the ladder below the hump can be broken down so wagons cannot be classified over the hump. In such cases we must carry out the classification process in a different way without using the hump.

Another example of such queuing system could be a gas station that is open non-stop. The station is equipped with one gas pump. Drivers arrive at the gas station in order to pump and pay. However, the gas station is a technical device so it can be subject to breakdowns. Because the gas station has only one gas pump, no driver can be served and therefore drivers do not arrive at the station when the gas pump is closed (under repair). Also all drivers who are at the station when the gas pump breaks down leave the station to pump somewhere else.

As we stated before, the failures of the server have an impact on performance measures, therefore it is important to incorporate the failures in mathematical models of such queuing systems in order to get non-biased results.

3 Mathematical Model

To model the studied queuing system we applied the method of stages (see for example Kleinrock [19]). The method utilizes the fact that the Erlang distribution with the shape parameter r or s and the scale parameter $r\lambda$ or $s\mu$ is a sum of r or s independent exponential distributions with the same parameter $r\lambda$ or $s\mu$. The process of each customer's arrival consists of r exponential phases and the customer enters the system (or is rejected when the system is full) after finishing the last phase. Analogously, the service of each customer consists of s exponential phases and the customer leaves the system after finishing the last phase. Because the duration of all phases is exponentially distributed, the queue can be modelled

by a Markov chain. The reason for using the Erlang distribution is that this distribution is more general than the exponential distribution, which cannot be used in many practical examples; the Erlang distribution can be used to model random variables with a coefficient of variation less than 1.

Let us consider a random variable $K(t)$ being the number of the customers found in the system, a random variable $I(t)$ being the number of finished phases of customer's arrival, a random variable $J(t)$ being the number of finished phases of customer's service and a random variable $F(t)$ being the number of broken servers at the time t. On the basis of the assumptions established in Section 2 it is clear that $\{K(t), I(t), J(t), F(t)\}$ constitutes a Markov chain with the state space

$$\Omega = \{(k,i,j,f), k=0, i=0,\ldots,r-1, j=0, f=0,1\} \cup$$
$$\cup \{(k,i,j,f), k=1,\ldots,m, i=0,\ldots,r-1, j=0,\ldots,s-1, f=0\}.$$

Let us note that the first subset contains all the idle and down states and the second subset the busy states. The system is found in the state (k,i,j,f) at the time t if $K(t)=k$, $I(t)=i$, $J(t)=j$ and $F(t)=f$; let us denote the corresponding probability $P_{(k,i,j,f)}(t)$. Complex information about Markov chains can be found for example in Bolch et al. [20].

Now we would like to set up the mathematical model of the system. At first, let us establish a group of variables α_k, where $k=0,1,...,m$. The variable α_k for $k=0,1,...,m$ can take its value from the set $\{0,1\}$. The variables enable us to create the general model for both modifications (we can even create other modifications of the studied system using the variables, for example a modification in which the server breaks down only when the system is full). The variables will be used as a multiplier of the failure rate η. For the first modification we have $\alpha_k=1$ for $k=0,1,...,m$; that means the server can break down when idle ($k=0$) or busy ($k=1,...,m$). For the second modification we have $\alpha_0=0$ (the server can not break down when idle) and $\alpha_k=1$ for $k=1,...,m$ (the server can break down when busy).

Now we can illustrate the queuing model graphically on a state transition diagram (Figure 1). The vertices represent the particular states of the system and the directed edges indicate the possible transitions with the corresponding rates.

Please note that in Figure 1 only those states are depicted which are necessary for the formation of an equation system. Due to the fact that some edges lead from nowhere or point to nowhere in Figure 1, let us comment on such examples:

- The all red edges should point to states (0,0,0,1) up to (0,r−1,0,1) (the down states). But we did not draw all of them to these states because it would make the diagram more chaotic.
- Some green and blue edges are duplicated because the states to which the edges point or from which they lead are not depicted in Figure 1. For example, the green edge exiting the state (0,0,0,0) leads to the state (0,1,0,0), which is not depicted in Figure 1. On the other hand, the green edge leading to the state (0,i,0,0) exits the state (0,i−1,0,0), which is not

depicted either. The blue edge exiting the state (1,0,0,0) leads to the state (1,0,1,0) (not depicted) and the blue edge leading to the state (1,0,j,0) exits the state (1,0,j−1,0) (not depicted too).

- Some diagonal green edges lead from nowhere or point to nowhere for the same reason. For example the green edge exiting the state (1,r−1,0,0) leads to the state (2,0,0,0) (not depicted) and the green arc leading to the state (k,0,0,0) exits the state (k−1,r−1,0,0) (not depicted).

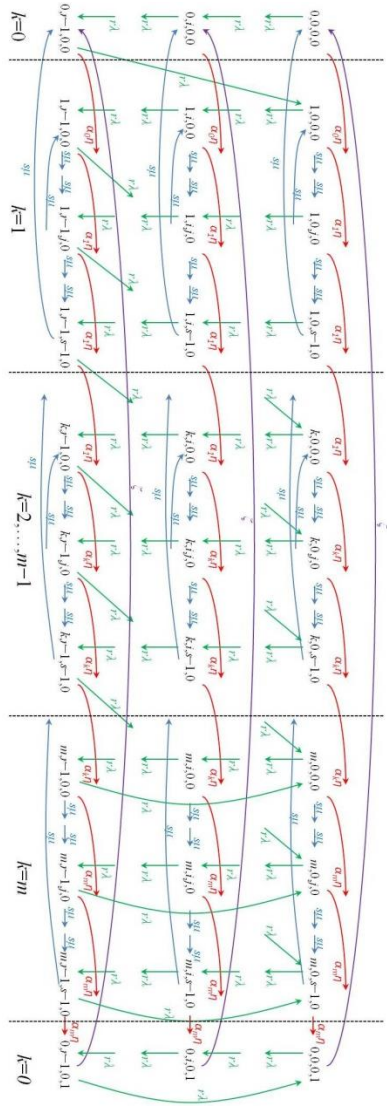

Figure 1
The state transition diagram

An original file containing the diagram can be downloaded from a web-page with the supplementary material − see [21].

Now we apply the global balance principle, which states that for each set of states X the flow out of the set X is equal to the flow into the set X (see Adan and Resing [22]). On the basis of the state transition diagram we are able to write the finite linear equation system of the steady-state balance equations in the form:

$$\left(r\lambda+\alpha_0\eta\right)\cdot P_{(0,0,0,0)}=s\mu\cdot P_{(1,0,s-1,0)}+\zeta\cdot P_{(0,0,0,1)}, \tag{6}$$

for $i=1,\ldots,r-1$:

$$\left(r\lambda+\alpha_0\eta\right)\cdot P_{(0,i,0,0)}=r\lambda\cdot P_{(0,i-1,0,0)}+s\mu\cdot P_{(1,i,s-1,0)}+\zeta\cdot P_{(0,i,0,1)}, \tag{7}$$

for $k=1,\ldots,m-1$:

$$\left(r\lambda+s\mu+\alpha_k\eta\right)\cdot P_{(k,0,0,0)}=r\lambda\cdot P_{(k-1,r-1,0,0)}+s\mu\cdot P_{(k+1,0,s-1,0)}, \tag{8}$$

for $k=1,\ldots,m-1, i=1,\ldots,r-1$:

$$\left(r\lambda+s\mu+\alpha_k\eta\right)\cdot P_{(k,i,0,0)}=r\lambda\cdot P_{(k,i-1,0,0)}+s\mu\cdot P_{(k+1,i,s-1,0)}, \tag{9}$$

for $j=1,\ldots,s-1$:

$$\left(r\lambda+s\mu+\alpha_1\eta\right)\cdot P_{(1,0,j,0)}=s\mu\cdot P_{(1,0,j-1,0)}, \tag{10}$$

for $k=1,\ldots,m, i=1,\ldots,r-1, j=1,\ldots,s-1$:

$$\left(r\lambda+s\mu+\alpha_k\eta\right)\cdot P_{(k,i,j,0)}=r\lambda\cdot P_{(k,i-1,j,0)}+s\mu\cdot P_{(k,i,j-1,0)}, \tag{11}$$

for $k=2,\ldots,m-1, j=1,\ldots,s-1$:

$$\left(r\lambda+s\mu+\alpha_k\eta\right)\cdot P_{(k,0,j,0)}=r\lambda\cdot P_{(k-1,r-1,j,0)}+s\mu\cdot P_{(k,0,j-1,0)}, \tag{12}$$

$$\left(r\lambda+s\mu+\alpha_m\eta\right)\cdot P_{(m,0,0,0)}=r\lambda\cdot P_{(m-1,r-1,0,0)}+r\lambda\cdot P_{(m,r-1,0,0)}, \tag{13}$$

for $j=1,\ldots,s-1$:

$$\left(r\lambda+s\mu+\alpha_m\eta\right)\cdot P_{(m,0,j,0)}=r\lambda\cdot P_{(m-1,r-1,j,0)}+r\lambda\cdot P_{(m,r-1,j,0)}+s\mu\cdot P_{(m,0,j-1,0)}, \tag{14}$$

for $i=1,\ldots,r-1$:

$$\left(r\lambda+s\mu+\alpha_m\eta\right)\cdot P_{(m,i,0,0)}=r\lambda\cdot P_{(m,i-1,0,0)}, \tag{15}$$

$$\left(r\lambda+\zeta\right)\cdot P_{(0,0,0,1)}=r\lambda\cdot P_{(0,r-1,0,1)}+\alpha_0\eta\cdot P_{(0,0,0,0)}+\eta\cdot\sum_{k=1}^{m}\sum_{j=0}^{s-1}\alpha_k\cdot P_{(k,0,j,0)}, \tag{16}$$

for $i=1,\ldots,r-1$:

$$\left(r\lambda+\zeta\right)\cdot P_{(0,i,0,1)}=r\lambda\cdot P_{(0,i-1,0,1)}+\alpha_0\eta\cdot P_{(0,i,0,0)}+\eta\cdot\sum_{k=1}^{m}\sum_{j=0}^{s-1}\alpha_k\cdot P_{(k,i,j,0)}. \tag{17}$$

Subtracting the probability on the left side of each equation (6) − (17) we got an equation system which can be written in the matrix form:

$$\mathbf{0} = \mathbf{Q}^T \cdot \mathbf{P},$$

where $\mathbf{Q}^T$ is the transposed infinitesimal generator matrix containing the transition rates of the Markov process and $\mathbf{P}$ is the unknown steady-state probability vector.

Because the matrix $\mathbf{Q}^T$ is singular (the equation set is not linearly independent and one equation is redundant), it is necessary to incorporate the normalization condition in the form:

$$\sum_{i=0}^{r-1}\sum_{f=0}^{1} P_{(0,i,0,f)} + \sum_{k=1}^{m}\sum_{i=0}^{r-1}\sum_{j=0}^{s-1} P_{(k,i,j,0)} = 1. \tag{18}$$

3.1 Solving Equation System using Matlab and Performance Measures

We got the equation system of $m \cdot r \cdot s + 2r + 1$ linear equations formed by equations (6) up to (18). The number of the unknown stationary probabilities is equal to $m \cdot r \cdot s + 2r$.

To solve the corresponding equation system we can omit an equation, for example equation (6). Numerical solving of the system can be performed using Matlab. However, the applied state description in the form of (*k*,*i*,*j*,*f*) is four-dimensional and is very good for the formation of the equation system but is absolutely unsuitable for the computations in Matlab. Therefore we are obliged to establish an alternative one-dimensional state description in the following form:

- The states (*k*,*i*,*j*,*f*) for *k*=1,...,*m*, *i*=0,...,*r*−1, *j*=0,...,*s*−1 and *f*=0 can be denoted using a single value $(k-1)\cdot r \cdot s + j \cdot r + i + 1$,
- The states (*k*,*i*,*j*,*f*) for *k*=0, *i*=0,...,*r*−1, *j*=0 and *f*=0,1 can be denoted using a single value $m \cdot r \cdot s + f \cdot r + i + 1$.

Applying the alternative one-dimensional state description we are able to transform the equation system in the form we need for using Matlab (we have to work with matrices). In Matlab we solve the linear system in the form:

$$\mathbf{B} = \mathbf{A} \cdot \mathbf{P},$$

where $\mathbf{B} = [0;\ldots;1;\ldots;0]^T$, where the value 1 is in the row $m \cdot r \cdot s + 1$ (in the case that we omit the equation corresponding to the steady-state probability $P_{(0,0,0,0)}$), $\mathbf{A}$ we get from the matrix $\mathbf{Q}^{\mathrm{T}}$ in which the row $m \cdot r \cdot s + 1$ is substituted by the row matrix $[1;1;\ldots;1]$ and $\mathbf{P}$ is the unknown steady-state probability vector.

After numerical solving of the equation system rewritten in the matrix form we obtain the stationary probabilities we need in order to compute performance measures of the studied system.

On the basis of the known stationary probability vector **P**, the steady-state probability that the server is idle is equal to:

$$P_{idle} = \sum_{i=0}^{r-1} P_{(0,i,0,0)}\,, \tag{19}$$

the steady-state probability that the server is busy can be expressed by the formula:

$$P_{busy} = \sum_{k=1}^{m}\sum_{i=0}^{r-1}\sum_{j=0}^{s-1} P_{(k,i,j,0)} \tag{20}$$

and for the equilibrium probability that the server is down it holds:

$$P_{down} = \sum_{i=0}^{r-1} P_{0,i,0,1}\,. \tag{21}$$

Now let us consider three performance measures − the mean number of the customers in the service *ES*, the mean number of the customers waiting in the queue *EL* and the mean number of the broken servers *EF*. All of them can be computed according to the formula for the mean value of discrete random variable, where the random variable $S \in \{0,1\}$ is the number of customers in the service, $L \in \{0, m-1\}$ the number of waiting customers and $F \in \{0,1\}$ the number of broken servers.

For the performance measures we can write following formulas:

$$ES = P_{busy}\,, \tag{22}$$

$$EL = \sum_{k=2}^{m}(k-1)\cdot\sum_{i=0}^{r-1}\sum_{j=0}^{s-1} P_{(k,i,j,0)}\,, \tag{23}$$

$$EF = P_{down}\,. \tag{24}$$

The Matlab script (m.file) with defined function enabling computation of equilibrium probabilities (19), (20) and (21) and performance measures (22), (23) and (24) is published online − see [21].

4 Results of Experiments

We performed several experiments with both modifications to demonstrate solvability of the presented model and to obtain some graphical dependencies. Applied values of the model parameters are summarized in Table 1.

Table 1

Summary of applied values of the model parameters

Parameter	m [-]	r [-]	$r\lambda$ [h^{-1}]	s [-]	$s\mu$ [h^{-1}]	η [h^{-1}]	ζ [h^{-1}]
Value	5	2	18	2	20	0.01 up to 0.1 with step 0.01	0.1 up to 1.0 with step 0.1

Substituting the values summarized in Table 1 into the model rewritten in Matlab we are able to compute the steady-state probabilities of the system states and on the basis of them we get the performance measures *ES*, *EL* and *EF* using formulas (22), (23) and (24).

The values of the mean number of the customers in the service *ES* are listed in Table 2. The upper value corresponds to the queuing system with operate-independent server failures, the lower value to the queue with operate-dependent server failures. The data from Table 2 are further shown in Figure 2, the left graph corresponds to the operate-independent modification and the right graph to the operate-dependent modification of the studied queuing system.

Comparing the values with each other we can see that increasing value of the parameter η causes the decrease of the performance measure *ES*. It is an expected fact because with increasing value of the parameter η server failures are more frequent. On the other hand, increasing value of the parameter ζ brings about the increase of the measure *ES*. This dependency could also be logically expected because increasing value of ζ causes shorter times to server repair. Let us note that the values of *ES* are greater for the second modification than for the first modification; it is also logical because it has to hold that the failure frequency of the operate-dependent modification is lower than the failure frequency of the operate-independent modification. The failure frequency of the operate-dependent modification was equal to the failure frequency of the operate-independent modification only in the case that the P_{idle} would be equal to zero.

Table 2

The mean number of the customers in the service *ES*

η / ζ	0.10	0.20	0.30	0.40	0.50	0.60	0.70	0.80	0.90	1.00
0.01	0.769	0.806	0.819	0.825	0.829	0.832	0.834	0.835	0.837	0.837
	0.780	0.812	0.823	0.828	0.832	0.834	0.836	0.837	0.838	0.839
0.02	0.704	0.768	0.792	0.804	0.812	0.817	0.821	0.824	0.826	0.828
	0.722	0.779	0.799	0.810	0.817	0.821	0.825	0.827	0.829	0.830

0.03	0.648	0.733	0.766	0.784	0.795	0.803	0.808	0.812	0.816	0.818
	0.673	0.748	0.777	0.793	0.802	0.809	0.814	0.817	0.820	0.822
0.04	0.601	0.701	0.743	0.765	0.779	0.789	0.796	0.801	0.806	0.809
	0.630	0.720	0.757	0.776	0.788	0.797	0.803	0.808	0.811	0.814
0.05	0.560	0.672	0.720	0.747	0.764	0.775	0.784	0.791	0.796	0.800
	0.592	0.694	0.737	0.760	0.775	0.785	0.793	0.798	0.803	0.806
0.06	0.524	0.645	0.699	0.729	0.749	0.762	0.772	0.780	0.786	0.791
	0.558	0.670	0.718	0.745	0.762	0.774	0.782	0.789	0.794	0.799
0.07	0.493	0.620	0.679	0.713	0.734	0.750	0.761	0.770	0.777	0.782
	0.528	0.648	0.700	0.730	0.749	0.763	0.773	0.780	0.786	0.791
0.08	0.464	0.597	0.660	0.697	0.721	0.738	0.750	0.760	0.768	0.774
	0.501	0.626	0.684	0.716	0.737	0.752	0.763	0.771	0.778	0.784
0.09	0.439	0.576	0.642	0.681	0.707	0.726	0.739	0.750	0.759	0.766
	0.477	0.607	0.667	0.703	0.726	0.742	0.754	0.763	0.770	0.776
0.10	0.417	0.555	0.625	0.666	0.694	0.714	0.729	0.741	0.750	0.757
	0.455	0.588	0.652	0.690	0.714	0.732	0.745	0.755	0.763	0.769

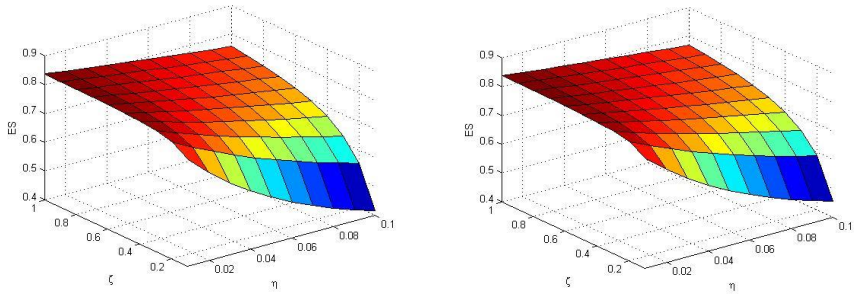

Figure 2

The dependence of *ES* on the parameters η and ζ (first modification on the left, second modification on the right)

Table 3

The mean number of the customers waiting in the queue *EL*

η / ζ	0.10	0.20	0.30	0.40	0.50	0.60	0.70	0.80	0.90	1.00
0.01	1.180	1.236	1.256	1.267	1.273	1.277	1.280	1.282	1.284	1.285
	1.197	1.246	1.263	1.271	1.277	1.280	1.283	1.285	1.286	1.287
0.02	1.076	1.173	1.210	1.229	1.241	1.249	1.255	1.259	1.263	1.265
	1.104	1.190	1.222	1.239	1.249	1.255	1.260	1.264	1.267	1.269
0.03	0.987	1.116	1.167	1.194	1.211	1.222	1.231	1.237	1.242	1.246
	1.024	1.139	1.184	1.207	1.222	1.232	1.239	1.244	1.248	1.252
0.04	0.912	1.064	1.126	1.160	1.182	1.196	1.207	1.215	1.222	1.227
	0.955	1.092	1.148	1.177	1.196	1.209	1.218	1.225	1.230	1.235

0.05	0.846	1.015	1.088	1.128	1.154	1.171	1.184	1.194	1.202	1.209
	0.894	1.049	1.113	1.149	1.171	1.186	1.197	1.206	1.213	1.218
0.06	0.789	0.971	1.052	1.097	1.127	1.147	1.162	1.174	1.183	1.191
	0.840	1.008	1.081	1.121	1.147	1.164	1.177	1.187	1.195	1.202
0.07	0.738	0.930	1.018	1.068	1.101	1.124	1.141	1.154	1.164	1.173
	0.791	0.971	1.050	1.095	1.123	1.143	1.158	1.169	1.178	1.186
0.08	0.693	0.891	0.985	1.040	1.076	1.101	1.120	1.135	1.146	1.156
	0.748	0.935	1.021	1.069	1.101	1.123	1.139	1.152	1.162	1.170
0.09	0.653	0.856	0.955	1.013	1.052	1.079	1.100	1.116	1.128	1.139
	0.709	0.902	0.993	1.045	1.079	1.103	1.121	1.135	1.146	1.155
0.10	0.617	0.823	0.926	0.987	1.029	1.058	1.080	1.097	1.111	1.122
	0.673	0.871	0.966	1.022	1.058	1.084	1.103	1.118	1.130	1.140

The values of the mean number of the customers waiting in the service *EL* are listed in Table 3 and graphically shown in Figure 3. We can see the same character of dependencies as in the case of the performance measure *ES*.

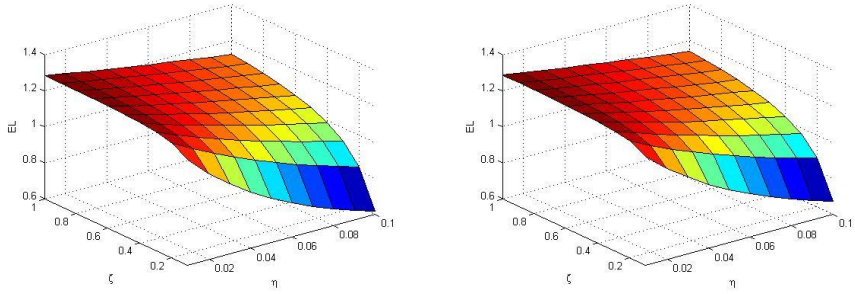

Figure 3

The dependence of *EL* on the parameters η and ζ (first modification on the left, second modification on the right)

The values of the mean number of the broken servers *EF* are listed in Table 4 and graphically shown in Figure 4. It is logical to expect that the measure *EF* should increase with increasing value η and decrease with increasing value of ζ − both expectations were confirmed by reached results. Furthermore, we can check the correctness of reached results using formulas (3) and (5).

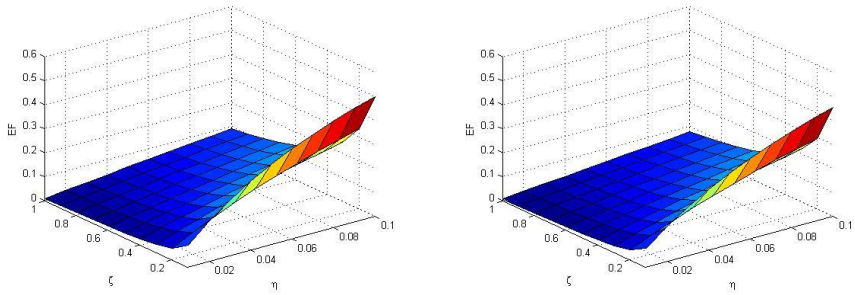

Figure 4

The dependence of *EF* on the parameters η and ζ (first modification on the left, second modification on the right)

Table 4

The mean number of the broken servers *EF*

η / ζ	0.10	0.20	0.30	0.40	0.50	0.60	0.70	0.80	0.90	1.00
0.01	0.091	0.048	0.032	0.024	0.020	0.016	0.014	0.012	0.011	0.010
	0.078	0.041	0.027	0.021	0.017	0.014	0.012	0.010	0.009	0.008
0.02	0.167	0.091	0.063	0.048	0.038	0.032	0.028	0.024	0.022	0.020
	0.144	0.078	0.053	0.041	0.033	0.027	0.024	0.021	0.018	0.017
0.03	0.231	0.130	0.091	0.070	0.057	0.048	0.041	0.036	0.032	0.029
	0.202	0.112	0.078	0.059	0.048	0.040	0.035	0.031	0.027	0.025
0.04	0.286	0.167	0.118	0.091	0.074	0.062	0.054	0.048	0.043	0.038
	0.252	0.144	0.101	0.078	0.063	0.053	0.046	0.040	0.036	0.033
0.05	0.333	0.200	0.143	0.111	0.091	0.077	0.067	0.059	0.053	0.048
	0.296	0.174	0.123	0.095	0.078	0.065	0.057	0.050	0.045	0.040
0.06	0.375	0.231	0.167	0.130	0.107	0.091	0.079	0.070	0.063	0.057
	0.335	0.201	0.144	0.112	0.091	0.077	0.067	0.059	0.053	0.048
0.07	0.412	0.259	0.189	0.149	0.123	0.104	0.091	0.080	0.072	0.065
	0.370	0.227	0.163	0.128	0.105	0.089	0.077	0.068	0.061	0.055
0.08	0.444	0.286	0.211	0.167	0.138	0.118	0.103	0.091	0.082	0.074
	0.401	0.251	0.182	0.143	0.118	0.100	0.087	0.077	0.069	0.063
0.09	0.474	0.310	0.231	0.184	0.153	0.130	0.114	0.101	0.091	0.083
	0.429	0.273	0.200	0.158	0.131	0.111	0.097	0.086	0.077	0.070
0.10	0.500	0.333	0.250	0.200	0.167	0.143	0.125	0.111	0.100	0.091
	0.455	0.294	0.217	0.172	0.143	0.122	0.106	0.094	0.085	0.077

Conclusions

In the paper we discussed two modifications of an $E_r/E_s/1/m$ queuing system subject to disasters which cause loss of all customers in the system and balking all customers incoming to the system while the server is under repair. To solve the

proposed model using Matlab, we developed the one-dimensional system state description, which enabled us to rewrite the linear equation system into the matrix form. After numerically solving the equation system we got the steady-state probabilities we need for computing the performance measures. We focused on three performance measures – *ES*, *EL* and *EF*.

In the experimental part of the paper we presented the dependencies of the performance measures on the parameters of η and ζ defining the failure frequency and the repair rate. Our experiments confirmed that the presented mathematical model can be successfully applied for solving such queuing system. The experiments showed the expected dependencies:

- The increasing value of η decreases the value of *ES* and the increasing value of the parameter ζ increases the value of *ES*. For the same values of η and ζ, the value of *ES* is lower for the operate-independent modification than for the operate-dependent modification.
- The values of *EL* evince the same character of dependency as the values of *ES*.
- The value of *EF* increases with the increasing value of η and decreases with the increasing value of ζ. The values of *EF* are greater for the operate-independent modification than for the operate-dependent modification.

References

[1] B. Krishna Kumar, A. Krishnamoorthy, S. Pavai Madheswari and S. Sadiq Basha "Transient Analysis of a Single Server Queue with Catastrophes, Failures and Repairs", *Queueing Systems*, Vol. 56, No. 3-4, pp. 133-141, 2007

[2] R. Sudhesh "Transient Analysis of a Queue with System Disasters and Customer Impatience", *Queueing Systems*, Vol. 66, No. 1, pp. 95-105, 2010

[3] U. Yechiali "Queues with System Disasters and Impatient Customers when System is Down", *Queueing Systems*, Vol. 56, No. 3-4, pp. 195-202, 2007

[4] N. Plumchitchom and N. T. Thomopoulos "The Queueing Theory of the Erlang Distributed Interarrival and Service Time", *Journal of Research in Engineering and Technology*, Vol. 3, No. 4, pp. 1-14, 2006

[5] K.-H. Wang and H.-M. Huang "Optimal Control of a Removable Server in an $M/E_k/1$ Queueing System with Finite Capacity", *Microelectronics Reliability*, Vol. 35, No. 7, pp. 1023-1030, 1995

[6] S. S. Mishra and D. KumarYadav "Cost and Profit Analysis of $M/E_k/1$ Queueing System with Removable Service Station", *Applied Mathematical Sciences*, Vol. 2, No. 56, pp. 2777-2784, 2008

[7] M. Yu, Y. Tang, Y. Fu and L. Pan "An M/E_k/1 Queueing System with No Damage Service Interruptions", *Mathematical and Computer Modelling*, Vol. 54, No. 5-6, pp. 1262-1272, 2011

[8] M. Binkowski and B. J. McCarragher "A Queueing Model for the Design and Analysis of a Mining Stockyard", *Discrete Event Dynamic Systems: Theory and Applications*, Vol. 9, No. 1, pp. 75-98, 1999

[9] W. L. Pearn and Y. C. Chang "Optimal Management of the N-policy M/E_k/1 Queuing System with a Removable Service Station: a Sensitivity Investigation", *Computers & Operations Research*, Vol. 31, No. 7, pp. 1001-1015, 2004

[10] M. S. El-Paoumy and M. M. Ismail "On a Truncated Erlang Queuing System with Bulk Arrivals, Balking and Reneging", *Applied Mathematical Sciences*, Vol. 3, No. 23, pp. 1103-1113, 2009

[11] D. Yue, C. Li and W. Yue "The Matrix-Geometric Solution of the M/E_k/1 Queue with Balking and State-Dependent Service", *Nonlinear Dynamics and Systems Theory*, Vol. 6, No. 3, pp. 295-308, 2006

[12] A. I. Shawky "The Service Erlangian Machine Interference Model: M/E_r/1/*k*/*N* with Balking and Reneging", *Journal of Applied Mathematics and Computing*, Vol. 18, No. 1-2, pp. 431-439, 2005

[13] I. J. B. F. Adan, W. A. van de Waarsenburg and J. Wessels "Analyzing E_k/E_r/*c* Queues", *European Journal of Operational Research*, Vol. 92, No. 1, pp. 112-124, 1996

[14] M. Jain and P. K. Agrawal "M/E_k/1 Queueing System with Working Vacation", *Quality Technology & Quantitative Management*, Vol. 4, No. 4, pp. 455-470, 2007

[15] K.-H. Wang and M.-Y. Kuo "Profit Analysis of the M/E_k/1 Machine Repair Problem with a Non-Reliable Service Station", *Computers and Industrial Engineering*, Vol. 32, No. 3, pp. 587-594, 1997

[16] V. Vasanta Kumar, B. V. S. N. Hari Prasad and K. P. R. Rao "Optimal Strategy Analysis of an N-policy Two-phase M^x/E_k/1 Gated Queueing System with Server Startup and Breakdowns", *International Journal of Mathematical Archive*, Vol. 3, No. 8, pp. 3016-3027, 2012

[17] MATLAB Version 7.12.0.635 (R2011a) The MathWorks, Inc., Natick, Massachusetts, United States

[18] M. Dorda and D. Teichmann "About a Modification of E_r/E_s/1/*m* Queueing System Subject to Breakdowns", in *Proceedings of the 30th International Conference Mathematical Methods in Economics 2012, Part I.*, pp. 117-122, Karvina, the Czech Republic, September 2012

[19] L. Kleinrock "*Queueing Systems Volume 1: Theory*", Wiley-Interscience, 1975

[20] G. Bolch, S. Greiner, H. de Meer and K. S. Trivedi "*Queueing Networks and Markov Chains: Modeling and Performance evaluation with Computer Science Applications*", John Wiley & Sons, 2006

[21] M. Dorda and D. Teichmann "*The Supplementary Materials*", [online], [accessed: 03.03.2014], available from http://homel.vsb.cz/~dor028/Dorda,Teichmann.htm

[22] I. Adan and J. Resing "*Queueing Theory*", Eindhoven University of Technology, 2002

Fuzzy Logic-based Risk Assessment Framework to Evaluate Physiological Parameters

Edit Tóth-Laufer, Márta Takács, Imre J. Rudas

Óbuda University, Bécsi 96/b, H-1034 Budapest, Hungary
laufer.edit@bgk.uni-obuda.hu, takacs.marta@nik.uni-obuda.hu, rudas@uni-obuda.hu

Abstract: Nowadays the patient monitoring systems are more and more widely used due to the advances in the technical background. These systems can improve the quality of life and by using them, several complications can be avoided in emergency situations. Nevertheless, the proper evaluation of the measured factors is a highly problematic task. The medicine uses a number of parameters, which are difficult to quantify, the boundaries of the examined risk factors cannot be given in a general form, the realistic result is only available from personalized thresholds. For these reasons, user-specific evaluation is required as much as possible, which uses individual characteristics, also the living conditions, habits and the medical recommendations taken into account during the risk calculation. In addition, the complex interactions between the input factors, which are often opaque, can be better handled in a patient-specific way based on the medical history of the patient or previous measurements. We developed a risk assessment framework to meet the above mentioned requirements. This system is flexible with a high degree of adaptive capacity. For the sake of ease of extensibility, and in order to achieve transparency, a generalized, modular system structure is implemented, which is joined with a database to specify the parameters of the configurable subsystems.

Keywords: risk assessment; fuzzy logic; relational database

1 Introduction

Risk management is again becoming more and more the focus of research, due to the economic crisis of recent years the increase in the number of terrorist activity; and extreme environmental and climatic conditions. Additionally, the novel recognizable and measurable risk factors in the field of medical diagnostics needed more efficient risk assessment schemes [1]. The large number of system parameters and the complexity of their context has led to the model's complexity, which should be handled adequately. Both quantitative and qualitative parameters are among the risk factors, therefore a method is needed during the evaluation, which can handle both types of inputs. Soft computing techniques are useful tools

in risk management systems, which are full of uncertainty and subjectivity in the data and in the evaluation process [2]. In this paper, we primarily focus on the system, which examines the physiological parameters. These kinds of systems are integral parts of engineering, natural and social environments and they require generalized, multilevel risk management models.

Nowadays, the beneficial effects of regular exercise in prevention, rehabilitation, and active life are known to everyone. However, basic physical information, including chronic diseases, actual physical status, age, and many other sub-factors, should be considered, in order to keep the practiced sport safe and healthy rather than resulting in the situation becoming worse [3]. To avoid the serious consequences, the implementation of a real-time risk assessment system is justified in order to continuously control the current risk level.

Because of the problem of the aging population in the developed world these monitoring systems mainly focus on elderly people with chronic diseases [4]-[8]. They spend their days often alone and unattended, therefore an emergency frequently occurs unnoticed. However, with the use of monitoring systems, the patients' mortality can be significantly reduced and the course of disease can be better treated and controlled if the problem is detected in time [9]. The sounding of the alarm on time as well the arrival of the right person is of critical importance [10]. The monitoring during sport activity is of similar importance for the emergencies caused by unexpected problems, which can also be eliminated, as well as monitoring whether proper performance is achieved. Due to the large number of input factors and complex interactions between them, most systems examine only one measured parameter and some of its influential parameters [11], [12]. Usually the examined factors are physiological parameters [13], [14] but, in addition, motion detection can also be used [15], [16]. The aim of these systems may differ, they can also be applied as a teaching device in the fields of sports and rehabilitation [17], [18]. The fields of these kinds of systems are the same as the surveillance of the elderly (e.g. basic personal information, chronic diseases), but it should be supplemented by the sport habits (e.g. motion forms, intensity, frequency). Regardless of the measured parameters and the intended use, it can be concluded that these systems evaluate fix parameter combination, independently of the sport type and patient characteristics. In contrast, the novel risk assessment framework is able to work with patient- and sport-specifically defined parameter combinations.

In patient monitoring systems the boundaries of the risk factors, which are predominantly physiological parameters, cannot be given in a general form. There is no general definition of what is considered normal, increased, or perhaps an abnormal value [11]. Although absolute definitions are also used in medicine, the realistic result is only available from personalized thresholds. For these reasons user-specific evaluation is required as much as possible, using individual characteristics. Living conditions and medical recommendations are also taken into account during the risk calculation [19]. In addition to the complex

interactions between the input factors, which are often opaque, can be provided more easily if the medical history of the patient is known or the previous measurements are available. In this case the interactions can also be given in a patient-specific way. The above mentioned requirements, as well as the large number of the considered risk factors, require the development of a robust, flexible risk management system with a high degree of adaptive capacity. For the sake of ease of extensibility, and in order to achieve transparency a generalized, modular system structure should be used, which is joined with a database to specify the parameters of the configurable subsystems [20]. We present our work about a risk assessment framework for physiological parameters, primarily during sport activity but it can be used in other areas (e.g. monitoring of elderly, home rehabilitation) with minor modifications in the database.

The rest of the paper is organized as follows: In Section 2, the basic structure of the fuzzy risk assessment model is described. Section 3 summarizes a hierarchical decision method (AHP). Section 4 and 5 present the evaluation process and the database design behind the framework. In Section 6, the implementation of the proposed risk assessment framework, the test environment and method are described. Finally, the conclusions are drawn.

2 The Model Structure

2.1 The Fuzzy-based Risk Assessment Framework

The risk assessment framework is applied in the authors' sport activity risk calculation model [3], which uses fuzzy logic based decision making in a hierarchical, clustered structure. The aim of the system is to calculate the risk level based on physiological and other personal parameters of the user to control the patient continuously. In the model there are some constant (e.g. sex) and quasi-constant parameters (e.g. age, occupation), which rarely change. The expert can design the personal profile of the patient based on these parameters. This profile, which is realised in a well-structured database, contains the types of activities, which should be monitored for the user, the name of the parameters, which should be measured during the monitoring assigned to the user, and their personal thresholds based on the medical recommendations. Neither the inputs, nor the parameters of the membership functions belonging to them are generally pre-defined, instead, they are found in the personal profile database. The proper operation of the system greatly depends on the applied rule base, which should be patient-specific as far as possible [21]. For this reason, the rule base is formed based on the above factors, and the current risk level is calculated in real-time by evaluating the measured physiological parameters. In the system model structure

the factors are classified based on their nature. The subsystems are formed based on the clusters which belong to different risk groups and they are operated as independent systems, thus the risk assessment framework can be applied for them separately. The model structure is shown in Fig. 1.

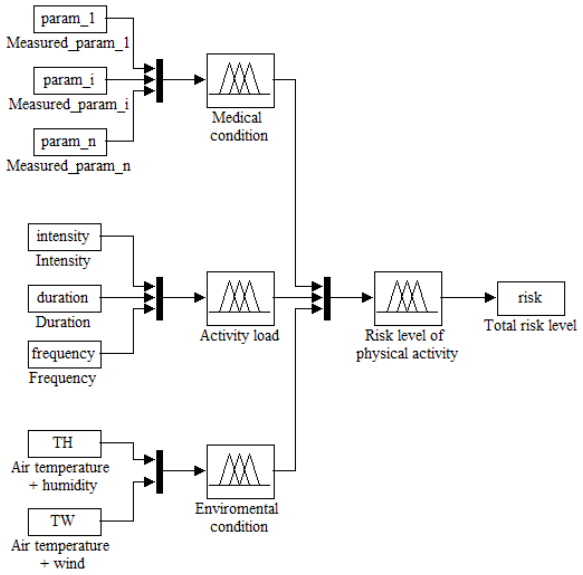

Figure 1
The model structue

The risk assessment framework is used in the first subsystem, which is used to characterize the medical state of the patient and it is called “Medical Condition”. Due to the patient-specific design of the database, the personal characteristics, habits and medical recommendations are built into the system in the rule base and in the membership function design. Consequently, in this group the chronic diseases of the patient, diabetes, cardiovascular diseases, hypertension among others, are taken into account. The basic personal characteristics are also collected in the personal profile, therefore, they are also taken into consideration in this main group. The patient can be identified based on the user ID, which is the social security number (TAJ number in Hungary) of the patient and the personal rule base, the used parameters and the antecedent sets definition is determined by the personal profile in the database. Consequently, general inputs cannot be defined for this subsystem, they can be varied based on the personal profile defined in the database patient-specifically depending on the above factors. After this initialization the real-time parameters, which are assigned to the user, are used to assess the current state of the patient. These parameters are monitored in real-time to control the person continuously.

The second main subsystem is the group "Activity load", which summarizes the characteristics of the patient's sport activity itself. It describes how intensively (intensity), how long per occasion (duration) and how many times per week (frequency) the patient does this activity.

The last main subsystem is the group "Environmental Condition", which is mainly important for outdoor sports. It combines the air temperature with wind (TW) and humidity (TH), these form the two input parameters of this group.

The system's structure allows the expansion and modification of the inference method, which can be performed easily in each subsystem separately, thus the proposed framework can also be applied for each subsystem and organized hierarchically. Since the risk assessment framework is based on a personal database, the evaluation can be updated according to the patient's current health state (e.g. novel personal characteristics, change of the limits) and the current facilities (e.g. novel measuring devices). The modification can be performed by the expert without any programming skills through a user-friendly application.

2.2 Database Design Providing the Flexibility of the Framework

To ensure the appropriate operation of the system, a properly designed database structure is necessary [22], which contains the personal information; the parameters to tune the membership functions; and important information on the conditions.

During the design process it is essential to keep in mind certain principles to obtain an appropriate data model. These are the following [23], [24]:

1 Realistic modeling: the plan must correspond exactly with the specification, i.e. the entity sets, their attributes and the relationships between them should be meaningful.

2 Avoid redundancy: the multiple occurrences has a greater storage requirement, furthermore it can cause modification anomalies, therefore, it should be avoided in the system.

3 Simplicity: Only as many items should be included in the database plan as are really needed.

4 Choosing the right item: During the planning it should be decided whether an item is used as a simply implemented attribute, or as an entity set.

A database structure was designed and implemented, which is used behind the risk assessment framework and it is based on the above requirements as demonstrated in [25]. Usually the first step of the design is to create an entity-relationship (E/R) diagram (keeping in mind the above-described principles in Section 5.1), which provides a graphical representation of data modeling for ease of transparency. The obtained E/R diagram structure is shown in Fig. 2.

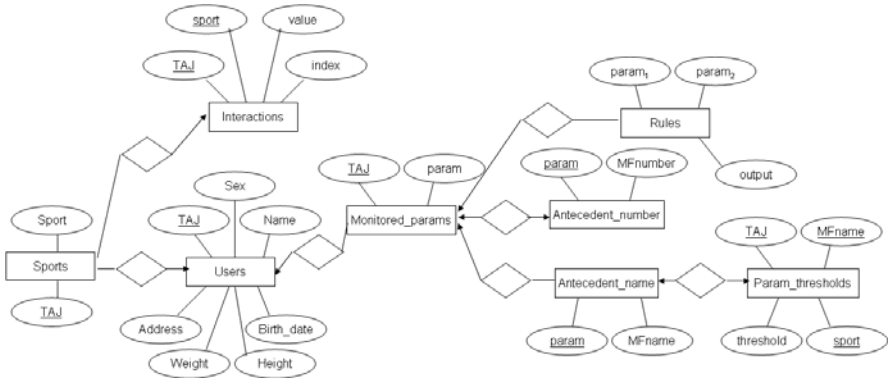

Figure 2
The entity-relationship diagram of the sport activity risk calculation framework's database[1]

Using the data in the model the membership functions can be tuned based on the personal characteristics, and medical recommendations. It can specify the necessary parameters for each user, which should be taken into account during the evaluation, and what types of activities are expected during the monitoring. In the database the number and name of the antecedent sets belonging to each input is given independently from the user, but the input membership function parameters can be adjusted in a patient-specific way. Also as a part of the personal profile, the risk factors' personalized relationship to one another can be defined. The parameters are arranged in pairs and an importance factor can be assigned to them as in the method AHP, whose detailed description can be seen in Section 3. During the rule definition the personal characteristics and medical recommendations can also be taken into account by the personalized rule base, which can be stored for each user separately.

The input parameter set of the system can be expanded dynamically. In this case, the properties of the new factor should be described (the number of the input membership functions and the name of the antecedent sets). The necessary parameters can also be changed per user and the existing parameters can be combined with each other freely according to the personal endowments. Due to the above changes the rule base and the interaction between the input parameters also vary, but the relations can be easily expanded and updated. The expansion,

[1] A : Entity sets: A group of individuals with similar characteristics, it is similar to the class concept, which is used in object-oriented programming languages.
: Attributes: it serves to describe the properties of an individual.
: Relationships: two or more individuals are connected by them. These relationships are bi-directional and they can connect several entity sets. The connection types can be marked using arrows.
Underlined attribute name: Keys: these kinds of attributes or these kinds of attributes' sets, which can clearly identify an entity in the entity set.

the parameter combination, the associated rule base and the comparison matrix can be defined by the expert without programming tasks.

Before the realization of the model, it should be translated into a relational model, which was introduced in the 1970s by Codd [20], but even today it is one of the most effective solutions. Consequently, most of the database management systems are relational [23], in which the data are represented in 2-dimensional tables, in so-called relations, in whose header there are the attribute names that define the meanings of the data in their column (*relation(attributes)*). The queries can be expressed in a high-level language, which significantly increases the efficiency of the database programming [26]. Precise knowledge of the database structure is essential to obtain a well-tuned system therefore the detailed description of the relations is given in the following section at the evaluation steps, where they are used.

3 The Evaluation Process

In this section the preparation and the steps of the evaluation are presented. Before the first-time application of the algorithm the database should be initialized. Otherwise, if any change occurs in the patient's condition (e.g. novel personal characteristics, change of the limits), or in the current facilities (e.g. novel measuring devices) then it should be updated. Failing that, the proper operation of the system cannot be guaranteed.

3.1 Database Initialization

The basic relations, which are applied during the evaluation, are defined in the following basic relations.

Users(TAJ, Name, Address, Birth_date, Sex, Height, Weight). This relation contains basic information of the user and they can be identified based on these values. The key attribute of this table is the *TAJ*, which is the social security number of the patient.

Sports(TAJ, sport). This table contains the possible motion forms, which the person usually performs, i.e. during which the monitoring is expected. The key attribute is *TAJ*.

Antecedent_number(param, MFnumber). Within the input domain different ranges belong to each measured parameter. These ranges form the antecedent sets, which are used in the fuzzy inference system and the number of them depends on the measured parameter characteristics. For example if these ranges define the normal, increased or abnormal response of the measured value then the number of the ranges are three, but is not the same for all the monitored parameters. This relation

is used to define the number of the antecedent sets for each possible parameter. This value does not depend on the patient, it is parameter-specific, therefore the key attribute of this relation is *param*.

Antecedent_name(param, MFname). This relation is closely linked to the relation Antecedent_number, because it is used to define the names belonging to each antecedent set. Therefore, the number of the different antecedent name is equivalent to the number of the antecedent sets, which is defined in the relation Antecedent_number. These names do not depend on the patient, they are parameter-specific, thus here the key attribute is *param*.

3.2 Determination of the Relative Importance of the Factors

Since the input parameters of the system are not equally important during the evaluation process, a need arises for a method, which ensures their weighting. For this purpose the Analytic Hierarchy Process (AHP) is used, which is a hierarchical decision method, which was introduced by Thomas L. Saaty in the 1970s [27]. It is used for organizing and analyzing complex decisions based on a pairwise comparison matrix, which contains the relative importance of all the possible pairs of the examined factors, which are at the same level of the hierarchy. It provides an opportunity to describe both qualitative and quantitative parameters. Let the elements of the $A_{n\times n}$ comparison matrix be X_1, X_2, …, X_n, where a_{ij} is the relative importance of the elements X_i and X_j. Saaty suggested values between 1 and 9 [28], but other values can also be used [29]. If $a_{ij}>1$ then X_i is more important than X_j, consequently the elements in the main diagonal $a_{ii}=1$ and $a_{ji}=1/a_{ij}$ ($i=1,2,...,n$; $j=1,2,...n$), therefore $n(n-1)/2$ comparisons are required for all n-element groups in each level of the hierarchy. If such groups can be formed from the factors, which are more or less independent, then the comparison matrix has a block diagonal matrix form and the computational complexity can be reduced in this way. The blocks are the comparison matrices of the factors of each group and the elements in their main diagonal are 1 because in this case the factor is compared to itself [30].

Let $x=(x_1, x_2 \dots x_n)$ be the input vector, which is the realisation of the actual risk factors $X=(X_1, X_2 \dots X_n)$, then the influence of the pairwise comparison matrix (A) on the actual factors can be described by the transformation $A \cdot x^T$. The aim is to calculate the weights of the factors, and the weighted input vector is to be forwarded to the system. The weight-multiplier λ obtained from the pairwise comparison by $Ax^T = \lambda x^T$.

The λ values can be computed as the real eigenvalues of the comparison matrices as if they exist, otherwise the value $\lambda=1$ is used. If more than one appropriate result can be obtained then the eigenvalue should be chosen, which keeps the input vector in the universe, while it has the most influence on the decision, i.e. which has the highest efficiency.

The above described method should be applied before the decision making process, the weighted input vectors are the system inputs [30], [31]. Due to the particularity of the task, it is a useful tool in structured risk assessment models, such as the authors' risk assessment framework. All of the risk factors and risk levels can be quantitative or given in linguistic form. The rules in the system are described in *IF condition THEN consequent* form. The evaluation of the risk factors and the determination of the decision is obtained by an approximate inference procedure (e.g. Mamdani-type inference system, Mamdani-like structure with discretized output [32]). The system can operate with or without feedback, in the latter case it determines the risk level or it makes a decision depending on the task's nature [33].

3.3 The Steps of the Evaluation

In the following algorithm the steps of the evaluation for a subsystem in the case of the Mamdani-like structure with discretized output detailing the database relations can be seen, which are used in each step to personalize the decision making. If a multilevel, clustered system structure is used then this algorithm should be executed for each subsystem separately.

Step 1 The input parameter combination is not constant, the number of the inputs and the monitored parameters can vary patient- and sport-specifically. The current combination is defined in the personal profile in the relation *Monitored_param(TAJ, sport, param)* according to the health state of the patient and the sport type should also be considered. Consequently, the key attributes are *TAJ* and *sport* together.

The so-defined input values are fuzzified in the case of trapezoidal membership functions by (1)

$$\mu_A(x)=\begin{cases} 0 & x \le a_i \\ \dfrac{x-a_i}{b_i-a_i} & a_i \le x \le b_i \\ 1 & b_i \le x \le c_i \\ \dfrac{d_i-x}{d_i-c_i} & c_i \le x \le d_i \\ 0 & d_i \le x \end{cases} \tag{1}$$

where a_i, b_i, c_i, d_i, are the parameter sets, which can be used to tune the membership functions patient-specifically based on the values defined in the framework's database according to the medical recommendations in the relation *Param_thresholds(TAJ, MFname, thresholds, sport)*. It should be defined for each parameter, which are used to characterize the patient, i.e. which are defined in the table *Monitored_param*. These values define the minimum and maximum values of each range, which

are assigned to each antecedent set. The parameters of the antecedent sets can be obtained from these values, which, apart from the antecedent set, are strongly related to the patient, the type of the monitored sport activity, consequently the key attributes are *TAJ*, *MFname* and *sport* together.

Step 2 The definition of the rule premises (w_i) by (2) from the fuzzified values, which are weighted by the values obtained from the AHP method, whose results are stored in the relation *Interactions(TAJ, sport, index, value)*. This relation defines the relative importance of the parameters in a patient-specific way depending on the type of sport. A default comparison matrix can be defined for each parameter combination, but it can be modified according to the patient's personal characteristics and chronic diseases.

The weighting of the input factors is not ensured in the Mamdani inference based systems, when the product operator is used during the determination of the rule premises. The product operator conceals weighting due to its commutative property, i.e. if different weights are used in different order, so they are assigned to another parameter, the result does not change. Consequently, the basic algorithm should be modified to take into account the different weighting factors.

$$w_i = \begin{cases} \sum_{k=1}^{m} a_k \mu_{A_{kj}}(x_k) & if \quad \mu_{A_{kj}} \neq 0, \forall k \in [1,m] \\ 0 & otherwise \end{cases} \tag{2}$$

where m is the number of the input parameters, a_k is the weight belonging to input k, w_i is the firing strength of the rule premise i.

Step 3 The firing strength obtained in the previous step should be normalized by (3) to ensure the appropriate operation of the system.

$$\overline{w}_i = \frac{w_i}{\sum_{i=1}^{n} w_i} \tag{3}$$

Step 4 The defuzzification of each consequent part happens separately using COG method (4), trapezoidal membership functions can be used again. The consequent parts $(\mu_{D_i}(y))$ belonging to each rule-premise are defined in the database in relation *Rules(param$_1$,…,param$_n$, output)* patient- and sport-specifically. The key attributes of this relation are the parameter combination, which define the rule-premise in step 2.

$$f_i = \frac{\int_{supp\mu_{D_i}} \mu_{D_i}(y) y dy}{\int_{supp\mu_{D_i}} \mu_{D_i}(y) dy} \tag{4}$$

Step 5 The final step of the evaluation is the overall risk level (O) calculation of the subsystem by (5).

$$O = \sum_{i=1}^{n} \overline{w}_i f_i = \frac{\sum_{i=1}^{n} w_i f_i}{\sum_{i=1}^{n} w_i} \tag{5}$$

4 The Risk Assessment Framework Implementation

4.1 Test Environment

The risk assessment framework has been implemented and its performance has been tested in RAD Studio application development environment. This development tool integrates Delphi, C++ Builder and HTML5 Builder, thus allows the broad applicability of the software for multiple devices (PCs, tablets, smart phones) on multiple platforms (iOS, Windows, Mac) in a native form [34]. The testing was performed on a PC using Windows platform. The hardware environment, used to test the model, is Intel® Core™2 Duo CPU T6570 processor with 4GB RAM and Windows7 operating system. The input data are stored in a structured text file, which is based on medical databases.

4.2 The Default Values in the Database

In the case, when there is no detailed personal profile with specified medical recommendations, the program is able to calculate the thresholds of the measured parameters and these thresholds can be used as default values in the database before the personalization. The expert can modify them if it is necessary, but they can be retained, if they characterize the patient properly. In the following section some examples are presented for the measured parameters' default threshold calculation.

4.2.1 The Systolic Blood Pressure (SBP)

A formula (6) was defined to calculate the thresholds of the systolic blood pressure responses for patients. This equation serves as a basis of the membership function parameter calculation.

$$SBP_{limit}(target) = \left(SBP_{limit}^{normal} - SBP_{rest}\right) \cdot zone + SBP_{rest} \tag{6}$$

where *zone* is the center of the recommended zone, *limit* is the range limit, which can be maximum or minimum. The values of $\mathrm{SBP}_{\mathrm{limit}}^{\mathrm{normal}}$ are based on the values defined by Sieira et al. (see Table 1), which are the thresholds of normal systolic blood pressure responses of both sexes with ages between 20 and 79 [11].

Table 1
Normal Systolic Blood Pressure (SBP, [Hgmm]) response

Age	Men		Women	
	SBP_{min}^{normal}	SBP_{max}^{normal}	SBP_{min}^{normal}	SBP_{max}^{normal}
20-29	161	203	136	176
30-39	164	204	138	182
40-49	167	209	144	190
50-59	170	216	153	201
60-69	173	221	162	210
70-79	169	223	160	210

4.2.2 The Heart Rate (HR)

The default heart rate thresholds can be obtained from the predictive maximum heart rate of the patient calculated by Polar training computer [35]. The zones defined by the thresholds can be obtained as a percentage of this value based on the health condition or physical fitness of the patient, which basically determines the allowable intensity of the activity. The zones, which are used in the author's framework, are the modification of the Polar target zones [12], [36], and they are defined in Table 2.

Table 2
Physical fitness and health state zones

Intensity % of HR_{max} (bpm)	Recommended for patients who
<50%	are under: medical treatment/rehabilitation suffer from cardiac disease
50-70%	exercise as prevention are beginners do basic training

Intensity % of HR_{max} (bpm)	Recommended for patients who
<50%	are under: medical treatment/rehabilitation suffer from cardiac disease
70-95%	do sports regularly

4.3 Case Study

In this section a 28 years old male is considered to illustrate the usage of the framework. The relation *Sports* contains the possible motion form for this user.

Table 3
Relation *Sports*

TAJ	Sport
024357942	running
024357942	Cycling

The relation *Monitored_param* (Table 4) defines the input parameter of the *Medical condition* subsystem in the framework. If the patient uses the system during cycling then their heart rate (HR), systolic blood pressure (SBP), and diastolic blood pressure (DBP) should be measured and evaluated; during running heart rate and respiration rate (RR) are considered.

Table 4
Relation *Monitored_param*

TAJ	Sport	Param
024357942	running	(HR, RR)
024357942	cycling	(HR, SBP, DBP)

The number of the antecedent sets assigned to each parameter is stored in the relation *Antecedent_number* (Table 5) and the names of these sets are defined by relation *Antecedent_name* (Table 6). These values are parameter-independent, therefore they are assigned to each parameter generally.

Table 5
Relation *Antecedent_number*

Param	MFnumber
HR	3
SBP	4
DBP	4
RR	3

Table 6
Relation *Antecedent_name*

Param	MFname
HR	(target, mhigh, vhigh)
SBP	(low, normal, increased, abnormal)
DBP	(lower, average, arisen, irregular)
RR	(normal, higher, RRvhigh)

In order to obtain patient-specifically tuned membership functions the relation *Param_thresholds* (Table 7) should be used supplementing the above membership function information.

Table 7
Relation *Param_thresholds*

TAJ	MFname	Threshold	Sport
024357942	Target	0.7	Cycling
024357942	Mhigh	0.85	Cycling
024357942	Low	125	Cycling
024357942	Normal	165	Cycling
024357942	Increased	190	Cycling

Using the obtained data in the case of the 28-year-old male patient, whose HR_{max} is 197 bpm, HR_{rest} is 70 bmp, and he exercises as prevention, the following input membership functions are created.

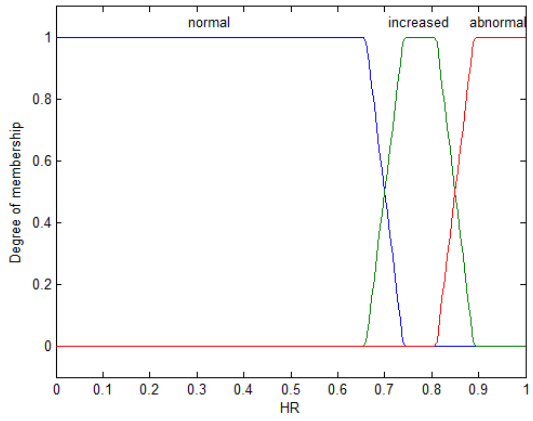

Figure 3
Heart rate membership functions for the 28-year-old male

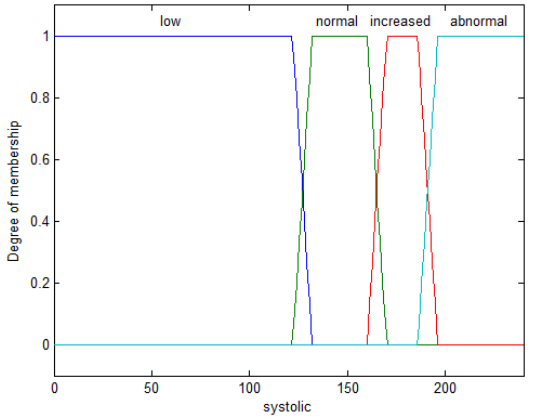

Figure 4
Systolic blood pressure membership functions for the 28-year-old male

There are some examples of obtained risk levels for different input values, which are presented in Table 8. The risk levels are considered in [0,1] interval.

Table 8
Calculated risk levels

HR	Systolic	Diastolic	Risk level
130	140	70	0.16
130	180	90	0.65
170	180	90	0.79
140	150	75	0.26

4.4 The Test Results

The basis of the testing method an AHP-FCE method was [37] to compare the results obtained from weighted input factors. For the sake of comparability, the evaluation was performed for the same patients, utilizing the same input values and the same membership functions in both systems. This condition did not allow the exploitation of the novel model's benefits, but it showed that the results obtained from the comparison are the same. Consequently, the risk assessment framework by Tóth-Laufer, Takács and Rudas was validated.

However, the importance of the presented novel framework lies in the fact that it makes the evaluation more differentiable. Using the appropriate settings the patients with the apparently same parameters can be evaluated differently, over and above the different parameter combinations can be assigned to different sport types. In this way the result is more realistic and patient-specific. In Table 9, the results obtained by using different membership function parameters are shown to illustrate the change in the risk level according to them. These boundaries are

defined in the relation *Parameter_thresholds* according to the medical recommendations, all other inputs are the same as in the case study. The obtained results highlighted that for the more specified values the result is shifted according to the patient's characteristics.

Table 9
Risk levels (Inputs: HR=130 bpm, SBP=180 Hgmm, DBP=90 Hgmm)

Target	Mhigh	Low	Normal	Increased	Risk
0.7	0.85	135	165	190	0.65
0.5	0.6	125	149	155	0.9
0.6	0.7	130	160	170	0.89
0.65	0.75	140	165	180	0.79
0.75	0.9	138	175	198	0.7

Conclusions

In health monitoring systems, the appropriate evaluation process, which provides realistic result, is a highly problematic task. It is the consequence of the high number of input factors, which includes both quantitative and qualitative parameters; the different importance of them; the complex interactions between them; and consequently, the large rule base. Furthermore, for different patients different parameter combinations should be considered and the thresholds of normal, increased or abnormal values cannot be generalized, they should be adjusted is a patient-specific way.

Some of the above problems can be handled by the fuzzy approach, which is able to work with uncertainty, imprecision and subjectivity in the data and in the evaluation process. The large rule base can also be reduced by different fuzzy-based techniques and the membership functions can be tuned according to the patient characteristics, but these kinds of systems are not flexible enough. The parameter combinations cannot be varied, and broadened for each user separately.

A risk assessment framework was designed and implemented, which takes the advantages of the fuzzy approach, while the flexibility, expandability and the adaptive capacity of the system is improved. To ensure the above advantages and to achieve transparency a general, modular system structure is used, which is based on the specifically configurable subsystems. During the evaluation the individual characteristics, living conditions, habits and medical recommendations are considered, which are based on the personal profile, in which different parameter combinations can be defined for each user and these can be modified and broadened user-specifically. In this way the obtained result is more realistic. The results of the proposed model was compared to an AHP-FCE model for the same input values. The results obtained from the comparison are the same, consequently the authors' risk assessment framework was validated.

Acknowledgement

The research was supported by the Hungarian OTKA projects 106392 and 105846, and project of the Vojvodina Academy of Sciences and Arts "Mathematical models of intelligent systems and theirs applications".

References

[1] L. Hanka, "Kockázat becslése numerikus módszerekkel, folytonos eloszlások diszkretizálása", *Műszaki Katonai Közlöny Online* XXII, No. 3, 2012, pp. 55-69

[2] M. Takács, "Multilevel Fuzzy Approach to the Risk and Disaster Management", *Acta Polytechnica Hungarica*, Vol. 7, No. 4, 2010, pp. 91-102

[3] E. Tóth-Laufer, et al., "Current Physical Status Evaluation Subsystem using User-specific tuned Membership Functions in Sport Activity Risk Calculation" in *Proc. of the IEEE 9th International Conference on Computational Cybernetics*, Tihany, Hungary, July 8-10, 2013, pp. 185-190, ISBN: 978-1-4799-0060-2, DOI: 10.1109/ICCCyb.2013.6617585

[4] M. Kozlovszky, J. Sicz-Mesziár, et.al., "Combined Health Monitoring and Emergency Management through Android Based Mobile Device for Elderly People," *Wireless Mobile Communication and Healthcare, Lecture Notes of the Institute for Computer Sciences, Social Informatics and Telecommunications Engineering*, Vol. 83, 2012, pp. 268-364

[5] B. Najafi, K. Aminian, "Measurement of Stand-Sit and Sit-Stand Transitions Using a Miniature Gyroscope and its Application in Fall Risk Evaluation in the Elderly," *IEEE Trans. on Biomedical Engineering*, Vol. 49, No. 8, Aug. 2002, pp. 843-351, doi: 10.1109/TBME.2002.800763

[6] S. Dang, S. Dimmick, G. Kelkar, "Evaluating the Evidence Base for the Use of Home Telehealth Remote Monitoring in Elderly with Heart Failure", *Telemedicine and e-Health*, October 2009, Vol. 15, No. 8, pp. 783-796, doi:10.1089/tmj.2009.0028

[7] M. Pallikonda Rajasekaran, et al., "Elderly Patient Monitoring System Using a Wireless Sensor Network", *Telemedicine and e-Health*, January 2009, Vol. 15, No. 1, pp. 73-79, doi:10.1089/tmj.2008.0056

[8] M. Kozlovszky, Z. Meixner, et al. "Network and Service Management and Diagnostics Solution of a Remote Patient Monitoring System", in *Proc. of the 3rd IEEE International Symposium on Logistics and Industrial Informatics*, Budapest, Hungary, August 25-27, 2011, pp. 61-64, doi: 10.1109/LINDI.2011.6031163

[9] J. Min Kang, T. Yoo, H.Chan Kim, "A Wrist-Worn Integrated Health Monitoring Instrument with Tele-Reporting Device for Telemedicine and Telecare", *IEEE Transactions on Instrumentation and Measurement*, Vol. 55, No. 5, October 2006, pp. 1655-1661, doi: 10.1109/TIM.2006.881035

[10] B. Meade, "Emergency Care in a Remote Area using Interactive Video Technology: A Study in Prehospital Telemedicine", *J. Telemed. Telecare*, Vol. 8, No. 2, Apr. 2002, pp. 115-117

[11] M. C. Sieira, A. O. Ricart, R. S. Estrani, "Blood Pressure Response to Exercise Testing" in *Apunts Med Esport*., Elsevier, 2010, pp. 191-200

[12] K. Hottenrott, "Training with the Heart Rate Monitor", *Meyer and Meyer Verlag*, 2007, ISBN: 9781841262130

[13] F. Rahnman, et al., "Network Approach for Physiological Parameters Measurement," *IEEE Trans. on Instrumentation and Measurement*, Vol. 54, No. 1, Feb. 2005, pp. 337-346, doi: 10.1109/TIM.2004.834595

[14] E. Tóth-Laufer, A. R. Várkonyi-Kóczy, "A Soft Computing-based Hierarchical Sport Activity Risk Level Calculation Model for Supporting Home Exercises", *IEEE Trans. on Instrumentation and Measurement*, Vol. 63, No. 6, 2014, pp. 1400-1411, DOI: 10.1109/TIM.2014.2299523

[15] Y. Koyama, M. Nishiyama, K. Watanbe, "A Motion Monitor Using Hetero-Core Optical Fiber Sensors Sewed in Sportswear to Trace Trunk Motion," *IEEE Trans. on Instrumentation and Measurement*, Vol. 62, No. 4, Apr. 2013, pp. 828-836, doi: 10.1109/TIM.2013.2241534

[16] G. Hache, E. D. Lemaire, N. Baddour, "Wearable Mobility Monitoring Using a Multimedia Smartphone Platform", *IEEE Trans. on Instrumentation and Measurement*, Vol. 60, No. 9, Sept. 2011, pp. 3153-3161, doi: 10.1109/TIM.2011.2122490

[17] A. Karime, M. Eid, J. M. Alja'am, A. E. Saddik, "A Fuzzy-based Adaptive Rehabilitation Framework for Home-Based Wrist Training", *IEEE Trans. on Instrumentation and Measurement*, Vol. 63, No. 1, 2013, pp. 135-144, doi: 10.1109/TIM.2013.2277536

[18] A. Alamri, Cha Jongeun, A. El Saddik, "AR-REHAB : An Augmented Reality Framework for Poststroke-Patient Rehabilitation", *IEEE Trans. on Instrumentation and Measurement*, Vol. 59, No. 10, Oct. 2010, pp. 2554-2563, doi: 10.1109/TIM.2010.2057750

[19] G. Fördős, I. Bosznai, et al., "Sensor-net for Monitoring Vital Parameters Vehicle Drivers", *Acta Polytechnica Hungarica*, Vol. 4, No. 4, 2007, pp. 25-36

[20] E. F. Codd, „A Relational Model for Large Shared Data Banks", *Comm. ACM*, 136, pp. 377-387

[21] Zs. Cs. Johanyák, O. Papp, "A Hybrid Algorithm for Parameter Tuning in Fuzzy Model Identification", *Acta Polytechnica Hungarica*, Vol. 9, No. 6, 2012, pp. 153-165

[22] A. Keszthelyi, „The Role of Data modelling in Information System Efficiency", in *Teaching and learning, 2nd International Conference for Theory and Practice in Education*, 29 May 2009, Budapest, p. 26

[23] J. D. Ullman, J. Widom, „A First Course in Database Systems", *Prentice-Hall*, 2007

[24] S. Sergyán, L. Csink, "Consistency Check of Image Databases", in *Proc. of the 2nd Romanian-Hungarian Joint Symposium on Applied Computational Intelligence*, Timisoara, Romania, May. 12-14, 2005, pp. 201-206

[25] E. Tóth-Laufer, "Database Schema Design for Supporting Sport Activity Monitoring," in *Proc. of the 18th International Conference on Intelligent Engineering Systems*, Tihany, Hungary, July 3-5, 2014, pp. 143-149

[26] A. Keszthelyi, "Remarks on the Efficiency of Information System", in *Acta Polytechnica Hungarica*, Vol. 7, No. 3, 2010, pp. 153-161

[27] T. L. Saaty, "The Analytic Hierarchy Process: Planning, Priority Setting, Resource Allocation", *McGraw-Hill*, 1980, ISBN 0-07-054371-2

[28] T. L. Saaty, L. G. Vargas, "Models, Methods, Concepts and Applications of the Analytic Hierarchy Process", *Kluwer Academic Press*, 2001

[29] L. Mikhailov, "Deriving Priorities from Fuzzy Pairwise Comparison Judgements", *Fuzzy Sets and Systems,* Vol. 134, 2003, pp. 365-385

[30] M. Takács, E. Tóth-Laufer, "The AHP Extended Fuzzy-based Risk Management" in *Proc. of the 10th WSEAS Int. Conference on Artificial Intelligence, Knowledge Engineering and Data Bases*, Cambridge, UK, February 20-22, 2011, pp. 269-272*,* ISBN: 978-960-474-273-8

[31] T. L. Saaty, "Decision Making with the Analytic Hierarchy Process", *Int. J. Services Sciences*, Vol. 1, No. 1, 2008, pp. 83-98

[32] E. Tóth-Laufer, I. J. Rudas, M. Takács, „Operator Dependent Variations of the Mamdani-type Inference System Model to Reduce the Computational Needs in Real-Time Evaluation", *International Journal of Fuzzy Systems,* Vol. 16, No. 1, March 2014, pp. 57-72

[33] J. H. M. Carr, V. Tah, "A Fuzzy Approach to Construction Project Risk Assessment and Analysis: Construction Project Risk Management System", *Advances in Engineering Software*, Vol. 32, No. 10, October, 2001, pp. 847-857

[34] RAD Studio – Embarcadero Technologies Product Documentation, http://docs.embarcadero.com/ products/rad_studio/

[35] Polar RS100 User Manual, http://www.polarusa.com/support_files/us-en/85256F470048B0BC852574730060F559/Polar_RS100_user_manual_English.pdf

[36] Polar RS800CX User Manual, Polar USA, http://www.polar.com/e_manuals/RS800CX/Polar_RS800CX_user_manual_English/manual.pdf

[37] Y. Wu, Y. Ding, H. Xu, ”Comprehensive Fuzzy Evaluation Model for Body Physical Exercise” in Risk Life System Modeling and Simulation Lecture Notes in Computer Science, 2007, Vol. 4689/2007, pp. 227-235, doi: 10.1007/978-3-540-74771-0_26

An ANN-based Speed and Flux Controller of Three-Phase AC Motors with Uncertain Parameters

Hung Linh Le

Faculty of Automation Technology, University of Information and Communication Technology, Thai Nguyen University
Quyet Thang, Thai Nguyen, Vietnam
lhlinh@ictu.edu.vn

Thuong Cat Pham

Institute of Information Technology, Vietnam Academy of Science and Technology
18, Hoang Quoc Viet, Hanoi, Vietnam
ptcat@ioit.ac.vn

Minh Tuan Pham

Space Technology Institute, Vietnam Academy of Science and Technology
18, Hoang Quoc Viet, Hanoi, Vietnam
pmtuan@sti.vast.vn

Abstract: This paper proposes a speed and flux control method of three-phase AC motors using an artificial neural network (ANN) to compensate for uncertain parameters in the motor's dynamic model such as rotor resistance, moment of inertia, friction coefficients, and load changes during system operation. Global asymptotic stability of the overall system is proved by Lyapunov's theory. Matlab simulation results are given to demonstrate the validity of the proposed control method.

Keywords: three-phase AC motor; artificial neural network; speed and flux control; uncertain dynamics

1 Introduction

AC motor speed control has been a popular topic over the past decades, because of uncertain parameters in the system model such as rotor resistance, flux, friction coefficient and variable load [1][2][3][9]. Recently, to estimate motor speed without using speed sensors, many researchers utilize Kalman filters or sliding mode observers [8][9]. These would help reduce production costs. However, the control performance would rely heavily on the estimation algorithm and the accuracy of motor model. The classical control method cannot obtain effective control, when the load of the system changes gradually due to uncertain parameters in the dynamic model of the AC motor. In this case, self-adaptive control [4][5][6][7], on-line identification methods and controllers with neural networks were used.

The main focus of recent research has been to determine a control algorithm and estimate the motor speed based on rotor flux orientation. In this method, the speed of the flux vector is controlled to reach the synchronous speed. Thus, the AC motor speed control is the same as the structure of DC motor control [11][12]. The main objective was to decouple two currents i_{sd}, i_{sq} independently. However, these two currents interact and depend on synchronous speed ω_s. Therefore, this method operates well in static mode and indicates clearly when the system operates in the flux declining domain. This paper proposes a method of speed and flux control for AC motors using an artificial neural network to compensate for uncertain parameters in the dynamic model, such as rotor resistance, moment, friction coefficient as well as a variable load during system operation.

The paper is organized as follows. The second section discusses the speed and flux control models for AC motors. The third section shows the speed and flux control methods with uncertain parameters. The last section presents simulations to verify the efficiency of the proposed method.

2 Speed and Flux Control Model for AC Motors

Table 1

Nomenclature

Notion	Unit	Meaning
M, N, D, Q		Model Matrices
B	Nms/rad	Friction coefficient
J	Nms^2/rad	Inertia moment of rotor
T_L	Nm	Load torque
R_s, R_r	Ω	Stator and rotor resistance

L_s, L_r	H	Stator and rotor inductance
L_m	H	Inductance between stator winding and rotor winding
$\omega_{\text{ref}}, \omega$	Rad/s	Reference angular velocity, rotor angular velocity
$\psi_{r\alpha}, \psi_{r\beta}$	Wb	Horizontal and vertical parts of rotor flux
$i_{r\alpha}, i_{r\beta}$	A	Horizontal and vertical components of rotor current
$u_{r\alpha}, u_{r\beta}$	V	Horizontal and vertical components of rotor voltage

Consider a dynamic model of a three phase motor with a squirrel-cage rotor as follows:

$$\begin{cases} \dfrac{di_{s\alpha}}{dt} = -\left(\dfrac{R_s}{\sigma L_s} + \beta L_m \dfrac{R_r}{L_r}\right) i_{s\alpha} + \beta \dfrac{R_r}{L_r}\psi_{r\alpha} + \beta\omega\psi_{r\beta} + \dfrac{1}{\sigma L_s}u_\alpha \\ \dfrac{di_{s\beta}}{dt} = -\left(\dfrac{R_s}{\sigma L_s} + \beta L_m \dfrac{R_r}{L_r}\right) i_{s\beta} - \beta\omega\psi_{r\alpha} + \beta \dfrac{R_r}{L_r}\psi_{r\beta} + \dfrac{1}{\sigma L_s}u_\beta \\ \dfrac{d\psi_{r\alpha}}{dt} = -\dfrac{R_r}{L_r}\psi_{r\alpha} - \omega\psi_{r\beta} + \dfrac{R_r}{L_r}L_m i_{s\alpha} \\ \dfrac{d\psi_{r\beta}}{dt} = \omega\psi_{r\alpha} - \dfrac{R_r}{L_r}\psi_{r\beta} + \dfrac{R_r}{L_r}L_m i_{s\beta} \end{cases} \tag{1}$$

$$J\frac{d\omega}{dt} + B\omega + T_L = K\left(\psi_{r\alpha} i_{s\beta} - \psi_{r\beta} i_{s\alpha}\right) \tag{2}$$

where $\sigma = 1 - \dfrac{L_m^2}{L_s L_r}$; $\beta = \dfrac{L_m}{\sigma L_s L_r}$; $K = \dfrac{3P}{2}\dfrac{L_m}{L_r}$ is the moment coefficient. L_s, L_r, L_m and R_s rarely change and can be measured accurately. However, rotor resistance R_r often changes in accordance with motor temperature during operation.

The principle goal of this paper is to determine control signals $u_{s\alpha}, u_{s\beta}$ to regulate the speed and flux of the motor reach these desired values $\omega \to \omega_{\text{ref}}$, $\psi_r^2 = \left(\psi_{r\alpha}^2 + \psi_{r\beta}^2\right) \to \psi_{r\,\text{ref}}^2$, where R_r, J, B and T_L are unknown.

Assuming that $i_{s\alpha}, i_{s\beta}$ are known and motor speed ω can be measured or estimated, taking the derivative of equation (2), we obtain:

$$J\ddot{\omega} + B\dot{\omega} + \dot{T}_L = K\left(\dot{\psi}_{r\alpha} i_{s\beta} + \psi_{r\alpha}\dot{i}_{s\beta} - \dot{\psi}_{r\beta} i_{s\alpha} - \psi_{r\beta}\dot{i}_{s\alpha}\right) \tag{3}$$

Substituting equation (1) into (3) and setting $x_1 = \omega$ yields the speed equation:

$$\begin{aligned} J\ddot{x}_1 + B\dot{x}_1 + \dot{T}_L &= -Kx_1\left(\psi_{r\alpha}i_{s\alpha} + \psi_{r\beta}i_{s\beta}\right) \\ &- K\left(\frac{R_s}{\sigma L_s} + \frac{R_r}{L_r}\left(\beta L_m + 1\right)\right)\left(\psi_{r\alpha}i_{s\beta} - \psi_{r\beta}i_{s\alpha}\right) \\ &- K\beta x_1\left(\psi_{r\alpha}^2 + \psi_{r\beta}^2\right) + \frac{K}{\sigma L_s}\left(\psi_{r\alpha}u_\beta - \psi_{r\beta}u_\alpha\right) \end{aligned} \tag{4}$$

By setting $x_2 = \psi_{r\alpha}^2 + \psi_{r\beta}^2$, the flux equation can be written as:

$$\begin{aligned} \ddot{x}_2 &= -2\frac{R_r}{L_r}\dot{x}_2 + 2\left(\frac{R_r}{L_r}\right)^2 L_m\left(i_{s\alpha}^2 + i_{s\beta}^2\right) \\ &-2\frac{R_r}{L_r}L_m\left[\frac{R_s}{\sigma L_s} + \frac{R_r}{L_r}\left(\beta L_m + 1\right)\right]\left(\psi_{r\alpha}i_{r\alpha} + \psi_{r\beta}i_{r\beta}\right) \\ &+2\frac{R_r}{L_r}L_m x_1\left(\psi_{r\alpha}i_{s\beta} - \psi_{r\beta}i_{s\alpha}\right) \\ &+2\beta\left(\frac{R_r}{L_r}\right)^2 L_m x_2 + 2\frac{R_r L_m}{\sigma L_r L_s}\left(\psi_{r\alpha}u_\alpha + \psi_{r\beta}u_\beta\right) \end{aligned} \tag{5}$$

From equation (4) and (5), we obtain a state equation:

$$\ddot{\mathbf{x}} + \mathbf{M}\dot{\mathbf{x}} + \mathbf{N}\mathbf{x} = \mathbf{Q} + \mathbf{D}^{-1}\mathbf{u} \tag{6}$$

where $\mathbf{x} = \begin{bmatrix} x_1 & x_2 \end{bmatrix}^{\mathrm{T}}$; $\mathbf{u} = \begin{bmatrix} u_\alpha & u_\beta \end{bmatrix}^{\mathrm{T}}$

$$\mathbf{M} = \begin{bmatrix} \frac{B}{J} + \frac{R_s}{\sigma L_s} + \frac{R_r}{L_r}\left(\beta L_m + 1\right) & 0 \\ 0 & 2\frac{R_r}{L_r} \end{bmatrix}$$

$$\mathbf{N} = \begin{bmatrix} \frac{B}{J}\left(\frac{R_s}{\sigma L_s} + \frac{R_r}{L_r}\left(\beta L_m + 1\right)\right) & 0 \\ 0 & -2\beta\left(\frac{R_r}{L_r}\right)^2 L_m \end{bmatrix}$$

$$\mathbf{Q} = \begin{bmatrix} \frac{-Kx_1\left(\psi_{r\alpha}i_{s\alpha} + \psi_{r\beta}i_{s\beta}\right)}{J} - \frac{K\beta x_1 x_2}{J} - \left(\frac{R_s}{\sigma L_s} + \frac{R_r}{L_r}\left(\beta L_m + 1\right)\right)\frac{T_L}{J} - \frac{\dot{T}_L}{J} \\ -2\frac{R_r}{L_r}L_m\left[\frac{R_s}{\sigma L_s} + \frac{R_r}{L_r}\left(\beta L_m + 1\right)\right]\left(\psi_{r\alpha}i_{r\alpha} + \psi_{r\beta}i_{r\beta}\right) \\ +2\frac{R_r}{L_r}L_m x_1\left(\psi_{r\alpha}i_{s\beta} - \psi_{r\beta}i_{s\alpha}\right) + 2\left(\frac{R_r}{L_r}\right)^2 L_m\left(i_{s\alpha}^2 + i_{s\beta}^2\right) \end{bmatrix}$$

$$\mathbf{D}^{-1} = \frac{1}{\sigma L_s}\begin{bmatrix} -\frac{K}{J}\psi_{r\beta} & \frac{K}{J}\psi_{r\alpha} \\ 2\frac{R_r L_m}{L_r}\psi_{r\alpha} & 2\frac{R_r L_m}{L_r}\psi_{r\beta} \end{bmatrix}$$

B, J, R_r and variable load T_L are uncertain parameters such as:

$$B = \widehat{B} + \Delta B$$
$$J = \hat{J} + \Delta J$$
$$R_r = \hat{R}_r + \Delta R_r$$

$\hat{B}, \hat{J}, \hat{R}_r$ are known parameters.

$\Delta J, \Delta B, \Delta R_r$ are unknown parameters.

From known parameters, the components of flux $\hat{\psi}_{r\alpha}, \hat{\psi}_{r\beta}$ can be determined following the equation:

$$\begin{cases} \frac{d\hat{\psi}_{r\alpha}}{dt} = -\frac{\hat{R}_r}{L_r}\hat{\psi}_{r\alpha} - \omega\hat{\psi}_{r\beta} + \frac{\hat{R}_r}{L_r}L_m i_{s\alpha} \\ \frac{d\hat{\psi}_{r\beta}}{dt} = \omega\hat{\psi}_{r\alpha} - \frac{\hat{R}_r}{L_r}\hat{\psi}_{r\beta} + \frac{\hat{R}_r}{L_r}L_m i_{s\beta} \end{cases} \tag{7}$$

Matrices in equation (6) can be represented as follows:

$$\begin{aligned} \mathbf{N} &= \hat{\mathbf{N}} + \Delta\mathbf{N}; \quad \mathbf{M} = \hat{\mathbf{M}} + \Delta\mathbf{M} \\ \mathbf{Q} &= \hat{\mathbf{Q}} + \Delta\mathbf{Q}; \quad \mathbf{D} = \hat{\mathbf{D}} + \Delta\mathbf{D} \end{aligned} \tag{8}$$

where $\hat{\mathbf{Q}}, \hat{\mathbf{D}}, \hat{\mathbf{M}}, \hat{\mathbf{N}}$ are known matrices; $\Delta\mathbf{Q}, \Delta\mathbf{D}, \Delta\mathbf{M}, \Delta\mathbf{N}$ are unknown.

$$\hat{\mathbf{M}} = \begin{bmatrix} \frac{\hat{B}}{\hat{J}} + \frac{R_s}{\sigma L_s} + \frac{\hat{R}_r}{L_r}(\beta L_m + 1) & 0 \\ 0 & 2\frac{\hat{R}_r}{L_r} \end{bmatrix}$$

$$\hat{\mathbf{N}} = \begin{bmatrix} \frac{\hat{B}}{\hat{J}}\left(\frac{R_s}{\sigma L_s} + \frac{\hat{R}_r}{L_r}(\beta L_m + 1)\right) & 0 \\ 0 & -2\beta\left(\frac{\hat{R}_r}{L_r}\right)^2 L_m \end{bmatrix}$$

$$\hat{\mathbf{Q}}=\begin{bmatrix} \dfrac{-Kx_1\left(\hat{\psi}_{r\alpha}i_{s\alpha}+\hat{\psi}_{r\beta}i_{s\beta}\right)}{\hat{J}}-\dfrac{K\beta x_1\left(\hat{\psi}_{r\alpha}^2+\hat{\psi}_{r\beta}^2\right)}{\hat{J}} \\ -2\dfrac{\hat{R}_r}{L_r}L_m\left[\dfrac{R_s}{\sigma L_s}+\dfrac{\hat{R}_r}{L_r}\left(\beta L_m+1\right)\right]\left(\hat{\psi}_{r\alpha}i_{r\alpha}+\hat{\psi}_{r\beta}i_{r\beta}\right) \\ +2\dfrac{\hat{R}_r}{L_r}L_m x_1\left(\hat{\psi}_{r\alpha}i_{s\beta}-\hat{\psi}_{r\beta}i_{s\alpha}\right)+2\left(\dfrac{\hat{R}_r}{L_r}\right)^2 L_m\left(i_{s\alpha}^2+i_{s\beta}^2\right) \end{bmatrix}$$

$$\hat{\mathbf{D}}=\frac{\sigma L_s L_r\hat{J}}{2KL_m\hat{R}_r\left(\hat{\psi}_{r\alpha}^2+\hat{\psi}_{r\beta}^2\right)}\begin{bmatrix} -2\dfrac{\hat{R}_r L_m}{L_r}\hat{\psi}_{r\beta} & \dfrac{K}{\hat{J}}\hat{\psi}_{r\alpha} \\ 2\dfrac{\hat{R}_r L_m}{L_r}\hat{\psi}_{r\alpha} & \dfrac{K}{\hat{J}}\hat{\psi}_{r\beta} \end{bmatrix}$$

Let us choose

$$\mathbf{u}=\hat{\mathbf{D}}\left(\mathbf{v}-\hat{\mathbf{Q}}\right) \tag{9}$$

with $\mathbf{v}=\begin{bmatrix} v_\alpha & v_\beta \end{bmatrix}^{\mathrm{T}}$ being an augmented control signal.

Substituting equation (9) into (6) we obtain:

$$\mathbf{v}=\ddot{\mathbf{x}}+\hat{\mathbf{M}}\dot{\mathbf{x}}+\hat{\mathbf{N}}\mathbf{x}+\mathbf{f} \tag{10}$$

with $\mathbf{f}=\ \mathbf{M}\dot{\mathbf{x}}+\ \mathbf{N}\mathbf{x}+\mathbf{D}^{-1}\Delta\mathbf{D}\mathbf{v}+\mathbf{D}^{-1}\Delta\mathbf{D}\hat{\mathbf{Q}}-\Delta\mathbf{Q}$ being an unknown element that can be estimated later.

In summary, the motor control problem becomes determining the control signal $\mathbf{v}$ that regulates motor speed and motor flux reach their respective desired values $\omega\to\omega_{\mathrm{ref}}$, $\psi_r^2=\left(\psi_{r\alpha}^2+\psi_{r\beta}^2\right)\to\psi_{r\,\mathrm{ref}}^2$ where J,B,R_r and changeable load T_{L} are unknown.

3 Speed and Flux Control Method for AC Motors with Uncertain Parameters

We denote:

$$\mathbf{s}=\dot{\mathbf{e}}+\mathbf{C}\mathbf{e} \tag{11}$$

where $\mathbf{C}$ is the positive definite diagonal matrix; $\mathbf{e}=\mathbf{x}-\mathbf{x}_{\mathrm{ref}}$ is the error between the actual value $\mathbf{x}=\begin{bmatrix} x_1 & x_2 \end{bmatrix}^{\mathrm{T}}=\begin{bmatrix} \omega & \psi_r^2 \end{bmatrix}^{\mathrm{T}}$

and the desired value $\mathbf{x}_{\text{ref}} = \begin{bmatrix} x_{1\text{ref}} & x_{2\text{ref}} \end{bmatrix}^{\text{T}} = \begin{bmatrix} \omega_{\text{ref}} & \psi_{r\,\text{ref}}^2 \end{bmatrix}^{\text{T}}$.

Therefore, when $\mathbf{s} \to \mathbf{0}$, then $\mathbf{e} \to \mathbf{0}$.

From equation (10), $\mathbf{f}$ is an unknown function which includes physical motor parameters such as flux, current, voltage and speed. However, in practice the variation of these parameters can be considered bounded and continuous. The motor speed and flux are bounded quantities, so $\mathbf{f}$ is also bounded and continuous: $\|\mathbf{f}\| \le f_{\max}$. The solution is to determine the control signal $\mathbf{v}$ which drives error $\mathbf{e}$ to approach $\mathbf{0}$ when $\lim_{t\to\infty} \mathbf{e}(t) = \mathbf{0}$ without knowing $\mathbf{f}$ exactly. This corresponds to finding the control signal $\mathbf{v}$ assuring $\lim_{t\to\infty} \mathbf{s}(t) = \mathbf{0}$. Applying the universal approximation capacity of artificial neural networks for continuous, bounded unknown nonlinear functions, we can use an artificial neural network with self-adaptation to approximate the unknown parameter $\mathbf{f}$ of system (10) based on known signal $\mathbf{s}(t)$. From [10], the artificial neural network structure is an RBF network. We chose a RBF network as seen in Figure 1 with two inputs, two outputs and three layers to approximate $\mathbf{f}$. The input layer of the neural network consists of the two elements of $\mathbf{s}(t)$ and the output layer has two linear neurons. The hidden layer is composed of two neurons having the following Gauss distribution function:

$$\theta_j = \exp\left(-\frac{\left(s_j - c_j\right)^2}{\lambda_j^2} \right); j = 1,2$$

where c_j, λ_j are the expectation and variance of the Gaussian distribution function that are freely chosen.

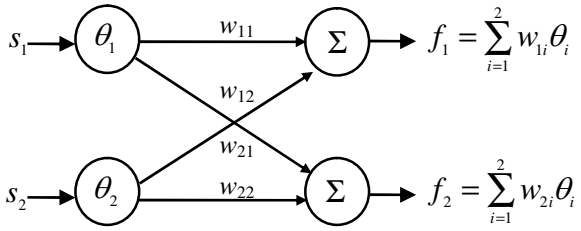

Figure 1
The neural network structure

The form of the neural network:

$$\mathbf{f} = \hat{\mathbf{f}} + \boldsymbol{\varepsilon} = \mathbf{W}\boldsymbol{\theta} + \boldsymbol{\varepsilon} \tag{12}$$

where $\mathbf{W} = \begin{bmatrix} w_{11} & w_{12} \\ w_{21} & w_{22} \end{bmatrix}$ is a weighted matrix;

$\boldsymbol{\theta} = \begin{bmatrix} \theta_1 & \theta_2 \end{bmatrix}^{\mathrm{T}}$ is an output function vector of input neuron;

$\boldsymbol{\varepsilon}$ is a bounded approximation error $\|\boldsymbol{\varepsilon}\| \le \varepsilon_0$.

Therefore, to make $\mathbf{s} \to \mathbf{0}$ and error $\mathbf{e} \to \mathbf{0}$, we need to choose $\mathbf{v}$ and the learning rule for the weighted $\mathbf{W}$ to make the system (10) asymptotically stable.

Theorem: Speed and flux of the AC motor in equation (2) approach the desired values $\omega \to \omega_{\mathrm{ref}}$ and $\psi_r^2 = \left(\psi_{r\alpha}^2 + \psi_{r\beta}^2\right) \to \psi_{r\,\mathrm{ref}}^2$ while J, B, R_r and changeable load T_{L} are unknown if the control signal $\mathbf{v}$ and weighted $\mathbf{W}$ are defined as below:

$$\mathbf{v} = -\mathbf{H}\mathbf{s} + \hat{\mathbf{M}}\dot{\mathbf{x}} + \hat{\mathbf{N}}\mathbf{x} + \ddot{\mathbf{x}}_{\mathrm{ref}} - \mathbf{C}\dot{\mathbf{e}} + \mathbf{v_1} \tag{13}$$

$$\mathbf{v}_1 = (\mu + 1)\mathbf{W}\boldsymbol{\theta} - \gamma \frac{\mathbf{s}}{\|\mathbf{s}\|} \tag{14}$$

$$\dot{\mathbf{w}}_i = -\mu \mathbf{s}\theta_i \tag{15}$$

where $\mathbf{H}$ is a positive definite diagonal matrix, $\mathbf{w}_i$ is the i$^{\mathrm{th}}$ column of the weighted matrix $\mathbf{W}$, $\mu > 0$ and $\gamma = \varepsilon_0 + \rho$ with $\rho > 0$.

Proof:

Applying Lyapunov's stability theory, we chose a positive definite function V such as:

$$V = \frac{1}{2}\mathbf{s}^{\mathrm{T}}\mathbf{s} + \frac{1}{2}\sum_{i=1}^{2} \mathbf{w}_i^{\mathrm{T}}\mathbf{w}_i \tag{16}$$

Taking the derivative of both sides of the equation (16) yields:

$$\dot{V} = \mathbf{s}^{\mathrm{T}}\dot{\mathbf{s}} + \sum_{i=1}^{2} \mathbf{w}_i^{\mathrm{T}}\dot{\mathbf{w}}_i \tag{17}$$

Substituting derivatives $\dot{\mathbf{s}}, \dot{\mathbf{w}}$ into (17) yields:

$$\dot{V} = \mathbf{s}^{\mathrm{T}}\left(\ddot{\mathbf{x}} - \ddot{\mathbf{x}}_{\mathrm{ref}} + \mathbf{C}\left(\dot{\mathbf{x}} - \dot{\mathbf{x}}_{\mathrm{ref}}\right)\right) - \mu \sum_i \mathbf{w}_i^{\mathrm{T}}\theta_i \mathbf{s} \tag{18}$$

From equation (10), (12), (13) and (18), we obtain:

$$\dot{V} = -\mathbf{s}^{\mathrm{T}}\mathbf{H}\mathbf{s} + \mathbf{s}^{\mathrm{T}}\left[\mathbf{v}_1 - (\mu + 1)\mathbf{W}\boldsymbol{\theta} - \boldsymbol{\varepsilon}\right] \tag{19}$$

Substituting equation (14) into (19), results in:

$$\begin{aligned}\dot{V} &= -\mathbf{s}^{\mathrm{T}}\mathbf{H}\mathbf{s} - \gamma\frac{\mathbf{s}^{\mathrm{T}}\mathbf{s}}{\|\mathbf{s}\|} - \mathbf{s}^{\mathrm{T}}\boldsymbol{\varepsilon} \\ &\le -\mathbf{s}^{\mathrm{T}}\mathbf{H}\mathbf{s} - \gamma\|\mathbf{s}\| + \|\mathbf{s}\|.\|\boldsymbol{\varepsilon}\| \le -\mathbf{s}^{\mathrm{T}}\mathbf{H}\mathbf{s} - \gamma\|\mathbf{s}\| + \|\mathbf{s}\|.\varepsilon_0 \\ &= -\mathbf{s}^{\mathrm{T}}\mathbf{H}\mathbf{s} - (\gamma - \varepsilon_0)\|\mathbf{s}\| \le -\mathbf{s}^{\mathrm{T}}\mathbf{H}\mathbf{s} - \rho\|\mathbf{s}\| \le 0\end{aligned} \tag{20}$$

It is clear that $\dot{V} < 0$ when $\mathbf{s} \neq \mathbf{0}$ and $\dot{V} = 0$ if and only if $\mathbf{s} = \mathbf{0}$. Following Lyapunov's theory, we have $\mathbf{s} \to \mathbf{0}$ and error $\mathbf{e} \to \mathbf{0}$. Therefore, $\mathbf{x} \to \mathbf{x}_{\mathrm{ref}}$. In other words, rotor speed and flux converge to their respective desired values with error $\mathbf{e} \to \mathbf{0}$.

Figure 2 shows the overall motor control system.

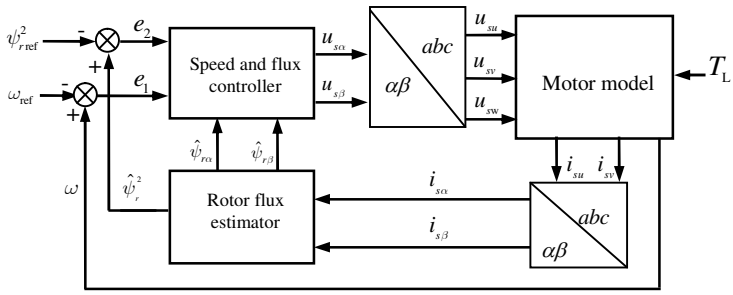

Figure 2
The overall motor control system

4 Simulation

Simulation was conducted using a four-pole squirrel-cage induction motor from LEROY SOMER with the parameters shown in Table 2. The reference angular velocity ω_{ref} varies in a trapezoid shape as seen in Figure 3 with the maximum speed $\omega_{\mathrm{ref}} = 100$ (rad/s) and reference flux $\psi^2_{r\,\mathrm{ref}} = 2.25\left(\mathrm{Wb}^2\right)$.

Table 2
Motor parameters

Rated power	1.5 KW
Rated stator voltage	220/380 V
Rated stator current	6.1/3.4 A
Stator resistance (R_s)	4.58
Rotor resistance (R_r)	4.468
Stator inductance (L_s)	0.253 H
Rotor inductance (L_r)	0.253 H
Mutual inductance (L_m)	0.113 H
Motor inertia (J)	0.023 Nms^2/rad
Viscous coefficient friction (B)	0.0026 Nms/rad

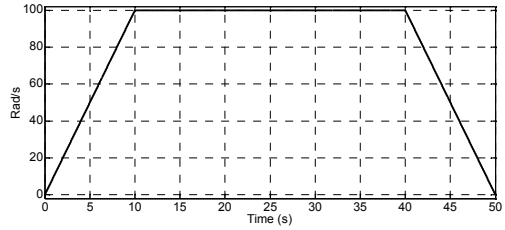

Figure 3
Desired rotor speed ω_{ref}

The motor speed control system was simulated with these assumed uncertain parameters:

$$B = \hat{B} + \Delta B;\ \hat{B} = 0.85B;\ \Delta B = 0.15B \quad (\text{Nms/rad})$$

$$J = \hat{J} + \Delta J;\ \hat{J} = 0.85J;\ \Delta J = 0.15J \quad (\text{Nms}^2/\text{rad})$$

When the unknown changeable load was formulated as

$$T_L = \hat{T}_L + \Delta T_L;\ \Delta T_L = 1.5\sin(2t) + 0.5\sin(50t) \ \text{(Nm)}$$

T_L had an amplitude change over time as seen in Figure 4a) and b).

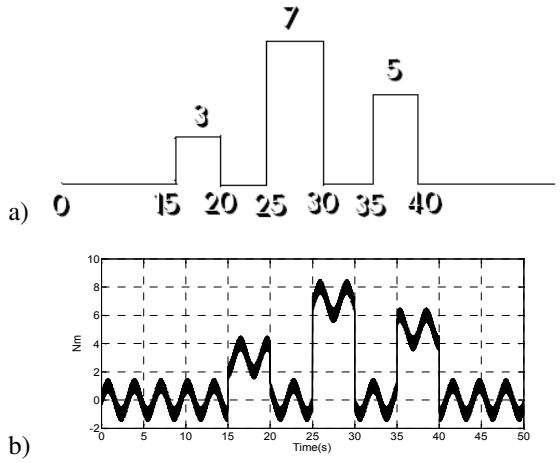

Figure 4
Simulation with control signal using neural networks and direct rotor speed feedback signal:
a) Load changes suddenly; b) Load T_L changes

The coefficients of the neural network were calculated as follows:

$$\mu = 20, \lambda_j = 0.5, c_j = 0.001, \gamma = 300$$

$$\mathbf{H} = \begin{bmatrix} 200 & 0 \\ 0 & 200 \end{bmatrix}, \ \mathbf{C} = \begin{bmatrix} 200 & 0 \\ 0 & 200 \end{bmatrix}$$

The simulation results are shown in Figure 5 to Figure 9.

Based on the simulation results using the neural network shown in Figure 5 to Figure 7, rotor speed and rotor flux were close to the desired values. When the load changed suddenly while the motor was operating normally, speed and rotor flux had a transient period with an error of about 1.6% to rotor angular velocity and 0.1% to rotor flux. Then, they converged rapidly to the desired speed and flux. The results without using the neural network ($\mathbf{v_1 = 0}$) are seen in Figure 8 and Figure 9 which show that rotor speed and flux could not be maintained close to desired values at times when load changed suddenly. Error of rotor angular velocity was about 1.6% and that of the rotor flux about 0.5%.

This proves that the self-adaptive capacity of the system and the efficiency of the proposed control method using ANN with an online learning algorithm compensated for the impact of uncertain parameters and load changes.

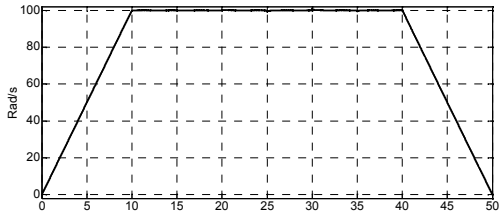

Figure 5
Real rotor speed ω

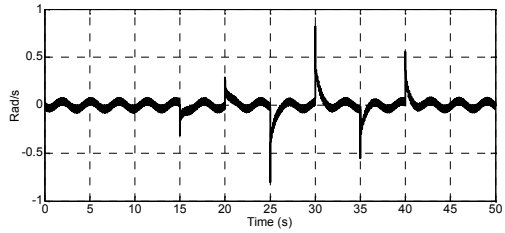

Figure 6
Error e_1 between desired rotor speed ω_{ref} and real rotor speed ω

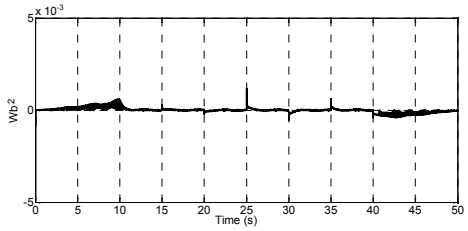

Figure 7
Error e_2 between desired flux $\psi_{r\,\text{ref}}^2$ and estimated flux ψ_r^2

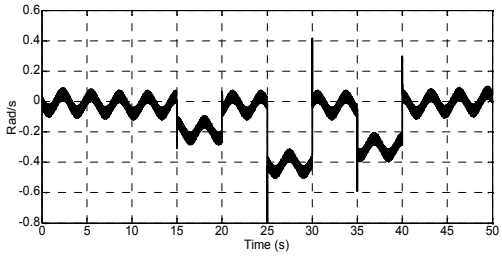

Figure 8
Error e_1 between desired rotor speed ω_{ref} and real rotor speed ω when $\mathbf{v}_1 = \mathbf{0}$

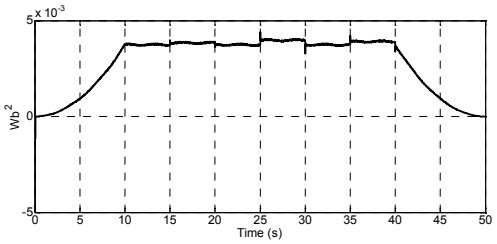

Figure 9

Error e_2 between desired flux $\psi_{r\,\mathrm{ref}}^2$ and estimated flux ψ_r^2 when $\mathbf{v}_1 = \mathbf{0}$

Conclusion

This paper proposes an adaptive, non-decoupling control method based on an ANN, for speed and flux control of AC motors, with uncertain parameters. Global asymptotic stability of the overall control system is proven by Lyapunov's direct method. The proposed speed and flux control method performs well while friction, moment of inertia, unknown rotor resistance and load change significantly in the AC motor dynamic model. The simulation results clearly show the efficiency of the proposed method.

References

[1] W. Leonhard, Control of Electric Drives, Springer Verlag, 2001

[2] P. Krause, Analysis of Electric Machinery, McGrawHill, 1986

[3] R. J. Wai, Robust Decoupled Control of Direct Field-oriented Induction Motor Drive, IEEE Transactions on Industrial Electronics, Vol. 52, No. 3, Jun. 2005

[4] S. Rao, M. Buss, and V. Utkin, An Adaptive Sliding Mode Observer for Induction Machines, Proceedings of the 2008 American Control Conference, Seattle, Washington, USA, Jun. 2008, pp. 1947-1951

[5] R. Marino, S. Peresada, and P. Valigi, Adaptive Input Output Linearizing Control of Induction Motors, IEEE Transactions on Automatic Control, Vol. 38, No. 2, Feb. 1993, pp. 208-221

[6] V. I. Utkin, J. G. Guldner, and J. Shi, Sliding Mode Control in Electromechanical Systems. Taylor & Francis, 1999

[7] K. Halbaoui, D. Boukhetala, and F. Boudjema, A New Robust Model Reference Adaptive Control for Induction Motor Drives Using a Hybrid Controller, Proceedings of the International Symposium on Power Electronics, Electrical Drives, Automation and Motion, Jun. 2008, Italy, pp. 1109-1113

[8] Z. Yan and V. Utkin, Sliding Mode Observers for Electric Machines an Overview, Proceedings of the IECON 02, Vol. 3, No. 2, MeliáLebreros Hotel, Sevilla, Spain, Nov. 2002, pp. 1842-1847

[9] Derdiyok, Z. Yan, M. Guven, and V. Utkin, A Sliding Mode Speed and Rotor Time Constant Observer for Induction Machines, Proceedings of the IECON 01 (The 27th Annual Conference of the IEEE Industrial Electronics Society), Vol. 2, Hyatt Regency Tech Center, Denver, Colorado, USA, Nov. 2001, pp. 1400-1405

[10] N.E Cotter, The Stone-Weierstrass and Its Application to Neural Networks, IEEE Trans. on Neural Networks, Vol. 1, No. 4, 1990, pp. 290-295

[11] P. Marino, M. Milano, F. Vasca, Linear Quadratic State Feedback and Robust Neural Network Estimator for Field-Oriented-Controlled Induction Motors, IEEE Trans. Ind. Electron, Vol. 46, No. 1, 1999, pp. 150-161

[12] Pham Thuong Cat, Le Hung Linh, Pham Minh Tuan, Speed Control of 3-Phase Asynchronous Motor Using Artificial Neural Network, 2010 8th IEEE International on Control and Automation Xiamen, China, June 2010, pp. 832-836

An Integrated Fuzzy Approach to Bidder Selection in Public Procurement: Serbian Government Case Study

Vjekoslav Bobar[1], Ksenija Mandić[2], Boris Delibašić[3], Milija Suknović[3]

[1]Administrative Agency for Common Services of Government Authorities, Nemanjina 22-26, 11000 Belgrade, Serbia, vjekoslav.bobar@uzzpro.gov.rs

[2]Crony d.o.o, Surcinski put 1M, 11070 Belgrade, Serbia, ksenija.mandic@crony.rs

[3]University of Belgrade, Faculty of Organizational Sciences, Jove Ilica 154, 11000 Belgrade, Serbia, boris.delibasic@fon.bg.ac.rs, milija.suknovic@fon.bg.ac.rs

Abstract: Public procurement is one of the most significant activities within the sphere of public administration, whose primary purpose is to achieve maximized cost effectiveness and efficiency for the expenditure of public money. This principle is also known as the principle of "value for money" - meaning to achieve the best possible ratio between the amount paid and the value received. The selection of a suitable bidder within the public procurement procedure assists in our achievement of the aforementioned purpose. In this paper an integrated approach based on the fuzzy Technique for Order Preference by Similarity to Ideal Solution (fuzzy TOPSIS) method and the fuzzy Extent Analysis Method is proposed for utilization within the evaluation and bidder selection processes associated with the process of public procurement. The proposed method objectively allows for the evaluation of bidders without the setting of weights by public procurement committees and in so doing helps to avoid subjectivity in respect to the setting of weights for criteria and or sub-criteria. In order to demonstrate the effectiveness and feasibility of the proposed method and its application in public procurement, a real-life case scenario from the Government of Serbia will be presented in this paper.

Keywords: public procurement; bidder selection; fuzzy extent analysis method; fuzzy TOPSIS

1 Introduction

In brief, public procurement shall mean the procurement of goods, services or works, in the manner and under the conditions as prescribed by the Public Procurement Law [1]. As active participants in this process, there appear two categories of actors, these being: the contracting authorities as procurers and the

economic operators as the bidders. The contracting authority is the government authority or institution from within the public administration sphere. The bidder shall imply a person engaged in the procurement procedure who offers to deliver goods, provide services and or perform works [1]. Public procurement is very important for both the citizens and the economy of any country, and this is no different in the Republic of Serbia. The primary purpose of this process is to achieve cost effectiveness and thereby attain an implicit level of efficiency as regards the expenditure of public money. This principle is also known as the principle of "value for money" - meaning to achieve the best possible ratio between the amount paid and the value received. The importance of this process becomes evident when we consider the fact that in Serbia public procurement accounts for some 10% of gross domestic product (GDP), that in the EU it approximates to 19% of GDP [2] and that globally, public procurement represents around 15% of the world's GDP [3]. The specific characteristic of public procurement is that this process must comply with specific legislative requirements. For example, in the EU this matter is regulated by the 2004/18/EC Directive, also called the Public Procurement Directive [4, 5]. In Serbia, although it is not yet an EU member state, existing EU regulations within the public procurement sphere are transferred into Serbian legislation through the application of Public Procurement Law [1]. In either case, the law's documents establish the need for the application of one of the two following criteria when evaluating potential bids: the Lowest Price offered and the Most Economically Advantageous Tender (MEAT) [1, 4, 5, 6]. In this paper, we will consider the MEAT criterion which is itself based on various elements of those criteria associated with the concept of public procurement. The MEAT criterion usually considers non-price factors together with prices in the evaluation of potential bids [7], the evaluation factors and weights assigned to the criteria or sub-criteria should be publicly announced in advance of the tender [7] and every bid receives a numerical score for each non-price evaluation factor [7]. As opposed to the private sector, in the public sector, we have the awarding committee for public procurement (usually a group of experts selected by a public authority) [4, 6]. This committee consists of a number of decision makers who must adhere to established public procurement principles: Principle of Efficiency and Cost-Effectiveness, Principle of Ensuring Competition, Principle of Transparency in Public Procurement Procedure, Principle of Equality of Bidders and Principle of Environmental Protection and Ensuring [1]. Considering these principles, a public procurement committee needs to treat all potential bidders equally and their selection must be founded on a rigorous ranking system, obtained through the application of transparent decision procedures [4]. For this reason, the method of awarding should have the largest possible degree of objectivity [4]. Therefore, a group decision making process for an alternative selection in public procurement is very useful [8]. Essentially, the process of selecting a bidder within the public procurement can be reduced to the multi-criteria decision making (MCDM) approach [9] which requires that the selection be made from amongst the decision alternatives (potential bidders) in

accordance an evaluation of their inherent attributes (quantitative and qualitative) [10]. In many cases qualitative criteria can be described using linguistic variables. For example, if we have quality as a qualitative criterion, we can define this criteria as bad, good, satisfied, excellent, etc. These variables are able to handle imprecision and also offer us the basis for natural language computation [11]. The linguistic variables are uncertain and in order to make a comparison between the qualitative and quantitative criteria, we can use the Fuzzy Sets Theory. The fuzzy approach performs numerical computation by using linguistic labels stimulated by membership functions [12]. The Fuzzy Sets Theory was introduced by Zadeh [13] as a powerful tool in order to effectively deal with ambiguities, vagueness and uncertainties when dealing with special complexities and or deficiencies in information as concerns the opinions of experts [14]. The major contribution of this theory is its ability to represent vague data; it also allows for mathematical operations and programming to be applied to the fuzzy domain [10, 15, 16, 17].

At this point, we should emphasize that one of the authors of this paper, as a member of public procurement committees, was involved in the realization of more than a hundred public procurements within the Serbian government over the course of the past ten years. During this period a problem was identified in that there exists a high level of subjectivity as concerns the determination of the respective weights assigned to each individual criteria on the part of the public procurement committee. In some instances the weights assigned to certain criteria have a tendency to favor one bidder over another, thus violating the aforementioned public procurement principles. In order to avoid such a scenario, in this paper we propose an approach based on the integration of the fuzzy Extent Analysis Method and the fuzzy TOPSIS method. This integrated model is very objective and allows for the evaluation of bidders without the setting of weights on the part of a potentially subjective public procurement committee. Using this model and taking into consideration the preferences of the public procurement committee, we can determine the respective weights of criteria and sub-criteria in accordance with a process of mathematical calculation.

2 The Public Procurement as MCDM Phenomenon

As we have already stated the process of public procurement implies the sourcing of goods, services and or work by the government authority, in that manner and under those conditions as prescribed by the Public Procurement Law [1]. This process consists of two main stages: the pre-award stage and the post-award stage. The pre-award stage has the sub-stages like call preparation for public procurement, notification, bid submission, bid evaluation and the selecting the most suitable bid. The post-award stage has sub-stages like ordering, invoicing and payment [18]. The bid evaluation and subsequent selection of the most

acceptable bid in the public procurement procedure can be viewed from the perspective of the MCDM phenomenon [9], where a contracting authority must compare the bids against pre-defined criteria, select one of the potential bids or conversely reject all of them. In order to define the bidder selection problem in the public procurement, we need to make introduction a set of bidders $B = \{b_1, b_2, ..., b_m\}$ and a set of conflicting criteria $C = \{c_1, c_2, ..., c_n\}$. Moreover, the different bidders and their bids have to be ranked, taking into account several parameters connected to the bidder's characteristics as also those of the product/service/work features [19]. Accordingly, we associate to each bidder $b_i \in B$ the following n-tuple: $d_{i1}, d_{i2}, ..., d_{in}$ where d_{ij} represents the value of the performance index characterizing the i^{th} bidder with *i=1,..., m* with respect to the j^{th} criterion with *j=1,..., n* [19]. In addition, the input data are collected in an *mxn* decision matrix *DM*, where *m* is the number of available bidders and *n* is the number of criteria on the grounds of which the ranking of bidders is performed [19]. Hence, the generic element d_{ij} of a *DM*, with *i=1,...,m* and *j=1,...,n*, represents the j^{th} performance value the i^{th} alternative bidder b_i [19]. The input data are completed by the criteria importance, i.e., each criterion c_j with *j=1,...,n* is associated to a weight w_j, with $\sum_{j=1}^{n} w_j = 1$ [19]. When the contract is awarded in accordance with the already mentioned MEAT criterion, quantitative and qualitative factors are simultaneously considered [4]. The mentioned EU Directive 2004/18/EC imposes the use of the Linear Weighting technique (when possible) in public tenders to be awarded according to the MEAT criterion [6]. Usage of this technique has its inherent limitations because, when MEAT is used, the public procurement committee can favor a specific bidder by assigning a high weight to a criterion which only that bidder can to fully satisfy [6]. Consequently, this method is oftentimes characterized by subjective choices which have a tendency of enabling corrupt behavior [6]. In the process of applying the Linear Weighting technique in public procurement, the contracting authority needs to fix and publish the importance of the respective weights assigned in advance, before the notification of the public procurement call. In addition, when this awarding arrangement is used, the contracting authority can grant an unfair advantage to a given bidder by assigning a high weight to a criterion that only this competitor can meet fully [4, 6, 20]. In practice, the application of a methodology for the allocation of specific weights to individual criteria is such that it has a tendency to be lacking in objectivity. Moreover, when the weights are subjectively determined, it is still possible to create an unfair evaluation procedure in which too much emphasis is placed on particular evaluation factors, thus favoring, intentionally or otherwise those bidders that score high in the corresponding factors [7].

In order to avoid the aforementioned limitations, this paper will go on to present an integrated fuzzy approach to bidder selection within the public procurement. We will give an example of the application of the fuzzy TOPSIS methodology integrated with the fuzzy Extent Analysis Method in the public procurement process of a Data Storage Hardware System from Serbian government. In this public procurement process, we used the fuzzy Extent Analysis Method to mathematically calculate the weights of each criteria and sub-criteria. In so doing, we excluded the possibility of the subjective assigning of weight to each criterion and sub-criterion which was not the case with the aforementioned Linear Weighting technique which is recognized by the Public Procurement Law both in the EU and Serbia. The obtained weights are used to determine the ranking of the final bid through the application of the fuzzy TOPSIS methodology.

3 The Fuzzy Extent Analysis Method

Chang proposed the fuzzy Extent Analysis Method, which we use in this paper [21]. This method consists of several steps the first of which is the determination of the value of fuzzy synthetic extent with respect to the i^{th} object. This value can be expressed by Eq. (1): $S_i = \sum_{j=1}^{n} M_{g_i}^{j} \otimes \left[\sum_{i=1}^{n} \sum_{j=1}^{m} M_{g_i}^{j} \right]^{-1}$ (1)

In Eq. (1), values $M_{g_i}^{1}, M_{g_i}^{2}, ..., M_{g_i}^{m}$, *i=1,2,..n*, represent triangular fuzzy numbers (TFN). Value g_i is an element from sets of goals $G = \{g_1, g_2, ..., g_m\}$. A TFN is denoted simply as (*l*/*m*, *m*/*u*) or (*l*, *m*, *u*). The parameters *l*, *m* and *u* ($l \leq m \leq u$), respectively, denote the smallest possible value, the most promising value, and the largest possible value that describes a fuzzy event [10, 15, 16]. While there are various operations on TFNs, only the important operations used in this paper are illustrated (addition and multiplication) [15, 16]. If we define two positive TFNs, (l_1, m_1, u_1) and (l_2, m_2, u_2), then the operation of addition we can define as $(l_1, m_1, u_1) + (l_2, m_2, u_2) = (l_1 + l_2, m_1 + m_2, u_1 + u_2)$. Also, the operation of multiplication we can define as $(l_1, m_1, u_1) * (l_2, m_2, u_2) = (l_1 * l_2, m_1 * m_2, u_1 * u_2)$ [15, 16]. In order to get $\sum_{j=1}^{n} M_{g_i}^{j}$ from Eq. (1), we need to perform the operation of fuzzy addition to *m* extent analysis [22, 23, 24, 25] numbers in the matrix as $\sum_{j=1}^{n} M_{g_i}^{j} = \left(\sum_{j=1}^{m} l_j, \sum_{j=1}^{m} m_j, \sum_{j=1}^{m} u_j \right)$. In order to get

expression $\left[\sum_{i=1}^{n}\sum_{j=1}^{m} M_{g_i}^{j}\right]^{-1}$ from Eq. (1), we need to compute the expression $\sum_{i=1}^{n}\sum_{j=1}^{m} M_{g_i}^{j}$ as $\sum_{i=1}^{n}\sum_{j=1}^{m} M_{g_i}^{j} = \left(\sum_{i=1}^{n} l_i, \sum_{i=1}^{n} m_i, \sum_{i=1}^{n} u_i\right)$ and then, we need to take inverse values as $\left[\sum_{i=1}^{n}\sum_{j=1}^{m} M_{g_i}^{j}\right]^{-1} = \left(\frac{1}{\sum_{i=1}^{n} u_i}, \frac{1}{\sum_{i=1}^{n} m_i}, \frac{1}{\sum_{i=1}^{n} l_i}\right)$. The next step is computation the degree of probability of triangular fuzzy numbers $M_2 = (l_2, m_2, u_2)$ and $M_1 = (l_1, m_1, u_1)$ as Eq. (2):

$$V(M_2 \geq M_1) = hgt(M_1 \cap M_2) = \begin{cases} 1, & if \quad m_2 \geq m_1 \\ 0, & if \quad l_1 \geq l_2 \\ \dfrac{l_1 - u_2}{(m_2 - l_2) - (m_1 - l_1)} & otherwise \end{cases} \tag{2}$$

For comparison of two triangular fuzzy numbers M_1 and M_2, we must take both the values of $V(M_1 \geq M_2)$ and $V(M_2 \geq M_1)$ [22, 25, 26, 27]. The next step is computation the degree of probability for a convex fuzzy number as $V(M \geq M_1, M_2, ..., M_k) = \min V(M \geq M_i)$, *i=1,2,..,k*. If we suppose that $d'(A_i) = \min V(S_i \geq S_k), k \neq i$, *k=1,2,..,n,* then the weight vector is computed as

$$W' = (d'(A_1), d'(A_2), ..., d'(A_n))^T \tag{3}$$

where A_i, i=1,2,..,n represents a matrix with *n* elements [22, 25, 26, 27, 28]. At the end, on a process of normalization, we get the normalized weight vectors as $W = (d(A_1), d(A_2), ..., d(A_n))^T$ a fuzzy number *W* is not a fuzzy number [22, 25, 26, 27, 28].

4 The Fuzzy TOPSIS Method

The fuzzy TOPSIS method represents an extension of the classical TOPSIS method. The classical TOPSIS method proposed by [29] seeks to illustrate the ranking of a set of alternatives through their distances from the most optimistic (positive ideal solution) to the most pessimistic (negative ideal solution) points. The reason for the fuzzy extension of the classical TOPSIS method lies in the fact

that the classical TOPSIS method uses precise and crisp values for the weights of criteria and the ratings of alternatives. However, in the public procurement, we use non-crisp values for criteria in solving bidder selection problem. These non-crisp values can be expressed as linguistic variables. For this reason, the fuzzy TOPSIS method is proposed where the weights of criteria and ratings of alternatives are evaluated by linguistic variables represented by fuzzy numbers to deal with the deficiency in the classical TOPSIS [24, 27, 30, 31]. The fuzzy TOPSIS method consists of several steps the first of which is the formation of a committee of decision makers. In this committee that has *K* decision makers, fuzzy rating of each decision maker D_k, *k=1,2,..,K* can be represented as triangular fuzzy number $\tilde{R}_k$, *k=1,2,...,K* with membership function $\mu_{\tilde{R}_k}(x)$ [24, 27, 30, 32, 33]. The next step includes determination of evaluation criteria, selection of appropriate linguistic variables for evaluating criteria and alternatives and aggregation of the weights of evaluation criteria.

If the fuzzy number ratings of all decision makers are described as triangular fuzzy numbers $\tilde{R}_k(a_k, b_k, c_k)$, *k=1,2,...,K* [24, 27], then the aggregated fuzzy rating can be determined as $\breve{R} = (a, b, c)$, *k=1,2,...,K* using expressions $a = \min_k \{a_k\}, b = \frac{1}{K}\sum_{k=1}^{K} b_k, c = \max_k \{c_k\}$ [24, 27]. If the fuzzy rating and importance weight of the k^{th} decision maker are $\tilde{x}_{ij}(a_{ijk}, b_{ijk}, c_{ijk})$ and $\tilde{w}_{ijk}(w_{jk1}, w_{jk2}, w_{jk3})$, *i=1,2,...,m; j=1,2,...,n,* respectively [24, 27, 30, 32, 33], then the aggregated fuzzy ratings $(\tilde{x}_{ij})$ of alternatives with respect to each criterion can be found as $(\tilde{x}_{ij}) = (a_{ij}, b_{ij}, c_{ij})$, [24, 27, 30, 32, 33] which is represented as $a_{ij} = \min_k \{a_{ijk}\}, b_{ij} = \frac{1}{K}\sum_{k=1}^{K} b_{ijk}, c_{ij} = \max_k \{c_{ijk}\}$. In the next step, for each criterion we calculate the aggregated fuzzy weights $(\tilde{w}_{ij})$ as

$$(\tilde{w}_j) = (w_{j1}, w_{j2}, w_{j3}) \tag{4}$$

where $w_{j1} = \min_k \{w_{jk1}\}, w_{j2} = \min_k \{w_{jk2}\}, w_{j3} = \min_k \{w_{jk3}\}$.After this, we create the fuzzy decision matrix as $\breve{D} = \lfloor \breve{x}_{ij} \rfloor_{mxn}$, *i=1,2,...,m; j=1,2,...,n*, [33] and calculate the criteria as $\breve{W} = [\breve{w}_1, \breve{w}_2, ..., \breve{w}_n]$ where $(\tilde{x}_{ij}) = (a_{ij}, b_{ij}, c_{ij})$and $(\tilde{w}_j) = (w_{j1,} w_{j2}, w_{j3})$, *i=1,2,..,m; j=1,2,...,n,* can be approximated by positive triangular fuzzy numbers [24, 27, 33]. After constructing the fuzzy decision matrix, the normalization of fuzzy decision matrix

is accomplished using linear scale transformation [24, 26, 27]. The calculation is made as $\breve{r}_{ij} = \left(\frac{a_{ij}}{c_j^*}, \frac{b_{ij}}{c_j^*}, \frac{c_{ij}}{c_j^*} \right), c_j^* = \max_i c_{ij}$. The normalized fuzzy matrix can be represented as [24, 26, 32, 33] $\breve{R} = \left[\tilde{r}_{ij} \right]_{mxn}$, *i=1,2,...,m; j=1,2,...,n*, where $\tilde{r}_{ij}$ are the normalized values of $\left(\tilde{x}_{ij} \right) = \left(a_{ij}, b_{ij}, c_{ij} \right)$ [26, 32]. In the next step, we create the weighted, normalized fuzzy-decision matrix as

$$\breve{V} = \left[\breve{v}_{ij} \right]_{mxn}, \; i=1,2,...,m; \; j=1,2,...,n \tag{5}$$

where $\breve{v}_{ij} = \breve{r}_{ij}(\bullet)\breve{w}_j$, ($\breve{w}_j$ represents the importance weight of the criterion C_j [24, 27]). According to the weighted, normalized fuzzy decision matrix, a normalized positive triangular fuzzy numbers can also approximate the elements $\breve{v}_{ij}, \forall i, j$ [24, 27, 30, 33]. The computation of fuzzy positive-ideal solution $\left(FPIS, A^* \right)$ and the fuzzy negative-ideal solution $\left(FNIS, A^- \right)$ represents next step. These solutions can be expressed as

$$A^* = \left\{ \breve{v}_1^*, \breve{v}_2^*, ..., \breve{v}_i^* \right\} = \left\{ \max_i v_{ij} \middle| (i = 1,2,..m; \; j = 1,2,..,n) \right\} \tag{6}$$

$$A^- = \left\{ \breve{v}_1^-, \breve{v}_2^-, ..., \breve{v}_i^- \right\} = \left\{ \min_i v_{ij} \middle| (i = 1,2,..m; \; j = 1,2,..,n) \right\} \tag{7}$$

Based on the weighted, normalized fuzzy decision matrix, the ranges belong to the closed interval [0,1] [26, 32]. Therefore, the *FPIS* and *FNIS* can be defined as (1,1,1) and (0,0,0), respectively [18]. After computation of *FPIS* and *FNIS*, we make the computation of the distance of each alternative from *FPIS* and *FNIS* as follows [24, 25, 30, 32, 33]:

$$D_i^* = \sum_{j=1}^{n} d\left(\tilde{v}_{ij}, \tilde{v}_j^* \right), \; i=1,2,..,m \tag{8}$$

$$D_i^- = \sum_{j=1}^{n} d\left(\tilde{v}_{ij}, \tilde{v}_j^- \right), \; i=1,2,..,m \tag{9}$$

The distance measurement between two fuzzy numbers [27,33] $\tilde{a} = \left(a_1, a_2, a_3 \right)$ and $\tilde{b} = \left(b_1, b_2, b_3 \right)$ can be calculated by the Vertex method as $d\left(\tilde{a}, \tilde{b} \right) = \sqrt{\frac{1}{3}\left[\left(a_1 - b_1 \right)^2 + \left(a_2 - b_2 \right)^2 + \left(a_3 - b_3 \right)^2 \right]}$ [24, 26, 27].

In the penultimate step, we make computation of similarities to ideal solution using Eq. (10) [24, 30, 33]:

$$CC_i = \frac{D_i^-}{D_i^* + D_i^-}, \; i=1,2,..,m \tag{10}$$

where CC_i range belongs to the closed interval [0,1] [32]. Finally, the last step includes ranking alternative with maximum CC_i or rank alternative according to CC_i in descending order [23, 26, 33, 34].

5 The Proposed Model of Bidder Selection in Public Procurement

In this paper, we propose the model for bidder selection in the public procurement process which is a hybrid composed of the fuzzy Extent Analysis Method and the fuzzy TOPSIS method. The proposed model consists of three basic steps (see Figure 1):

Step 1: Identification of criteria and bidders and constructing the problem into a hierarchy.

Step 2: Calculation of criteria and bidders with the fuzzy Extent Analysis Method computations.

Step 3: Evaluation of bidders using the fuzzy TOPSIS and final ranking of bidders, according to fuzzy TOPSIS obtained results.

In the first step, after the notification and submission phases have been completed, the bidders, criteria which is to be used in the subsequent evaluation process are determined. After this, we create the decision hierarchy tree which is then approved by public procurement committee. Thereafter follows the second step where weights are assigned to the criteria through the implementation of the fuzzy Extent Analysis Method. In this step, we create fuzzy matrixes of comparison, in order to determine the weights of criteria. The values of the elements of the fuzzy matrixes of comparison can be determined using the public procurement committee's preferences which are based on the scale from Table 1. Then the fuzzy matrixes of comparison for decision criteria and its priority vectors are determined. This is followed by the calculation of the priority vectors for the decision hierarchy and the calculated weight of the criteria are approved by the public procurement committee. At the end of the whole process of calculation, in the last step, the final ranking of the bidders is determined according to CC_i calculated by fuzzy TOPSIS in descending order.

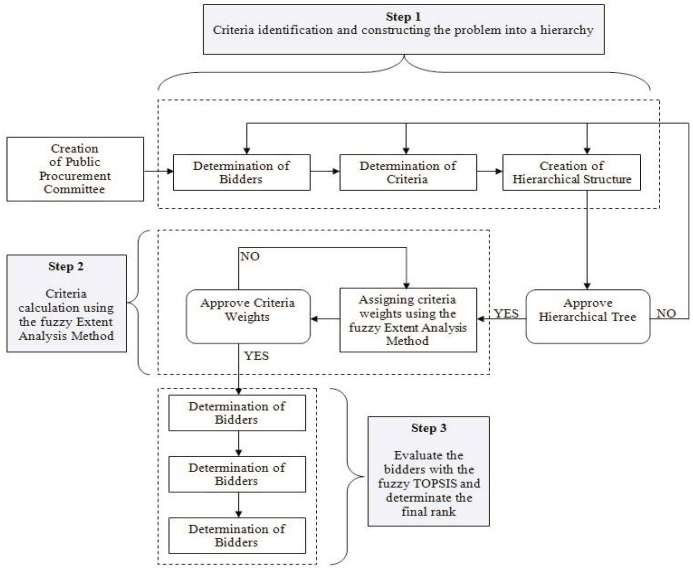

Figure 1
The proposed model of bidder selection in public procurement

In the next sections, we will give a practical application of the described model through a public procurement case study from within a Serbian government organization called the Administrative Agency for Common Services of Government Authorities. This organization has published a call for tender for a Data Storage Hardware System which represents a complex system for the recording (storing) of information (usually Big Data). After the public opening of the bids, the public procurement committee selected three bidders (B_A, B_B, B_C) who met the legal requirements for participation in public procurement.

5.1 Identification of Criteria and Bidders and Constructing the Problem into a Hierarchy

The starting point for the identification of the main criteria for bidder selection was the list of criteria from [1]: Offered price, Current costs, Quality, Technical advantages, Warranty period, Time of delivery, Obligations concerning spare parts, etc. From amongst these criteria, the members of the public procurement committee were asked to identify the most relevant or to propose other criteria without any restriction in the number to be selected. After a round of meetings, the members of the public procurement committee agreed upon the four main criteria and nineteen sub-criteria were linked to the subject matter of the public procurement of a Data Storage Hardware System. The main criteria were as follows: *Technical Features (TF)* with sub-criteria Technical Performance (TP),

Quantities Needed (QU), Time of delivery (TD), Warranty Period (WP), Quality of Packaging (QP) and Quality Certificate (QC); *Bidder Profile (BP)* with sub-criteria Solvency (SO), Market Position (MP), References (RE) and Professional Relations (PR); *Financial Aspect (FA)* with sub-criteria Offered Price (OP), Transport Costs (TC), Customs Fees (CF) and Payment Conditions (PC) and *Support and Services (SS)* with sub-criteria Service (SE), Training Aids (TA), Technical Support (TS), Post-warranty Maintenance (MA) and Obligations concerning spare parts (SP). The hierarchy of the selection criteria and decision alternatives (i.e., bidders) can be seen in Figure 2.

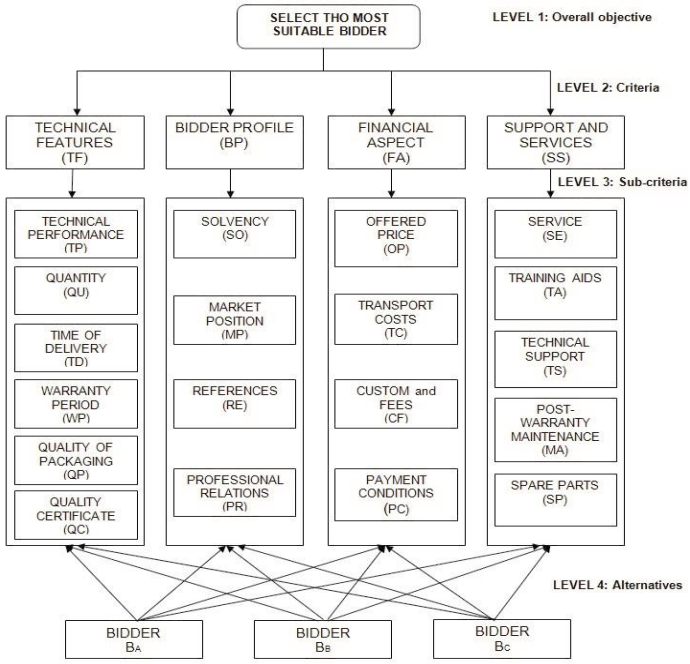

Figure 2
The hierarchy tree

5.2 Calculation of Criteria and Bidders using the Fuzzy Extent Analysis Method

Comparison of criteria, sub-criteria and bidders is facilitated for the experts by means of a Linguistic Importance Scale (see Table 1) [35] and the priority weights are calculated using the fuzzy Extent Analysis method.

The priority weights calculations for essential criteria and sub-criteria are given in Tables 2, 3, 4 and 5.

Table 1
Linguistic scale of importance

Linguistic scale of importance	Triangular fuzzy scale	Triangular fuzzy reciprocal scale
Equal	(1, 1, 1)	(1, 1, 1)
Weak	(1/2, 1, 3/2)	(2/3, 1, 2)
Fairly strong	(3/2, 2, 5/2)	(2/5, 1/2, 2/3)
Very strong	(5/2, 3, 7/2)	(2/7, 1/3, 2/5)
Absolute	(7/2, 4, 9/2)	(2/9, 1/4, 2/7)

Table 2
Priority vectors for the decision hierarchy (TF with sub-criteria)

Level 1 variable (priority)	Level 2 variables (priority)	Level 3 variables (priority)
TF (0.350)	TP (0.296)	B_A(0.325), B_B(0.412), B_C(0.263)
	QU (0.208)	B_A(0.412), B_B(0.263), B_C(0.325)
	TD (0.229)	B_A(0.000), B_B(0.958), B_C(0.042)
	WP (0.005)	B_A(0.412), B_B(0.263), B_C(0.325)
	QP (0.000)	B_A(0.333), B_B(0.333), B_C(0.333)
	QC (0.262)	B_A(0.457), B_B(0.457), B_C(0.086)

Table 3
Priority vectors for the decision hierarchy (BP with sub-criteria)

Level 1 variable (priority)	Level 2 variables (priority)	Level 3 variables (priority)
BP (0.131)	SO (0.306)	B_A(0.272), B_B(0.487), B_C(0.241)
	MP (0.317)	B_A(0.497), B_B(0.158), B_C(0.345)
	RE (0.367)	B_A(0.241), B_B(0.272), B_C(0.487)
	PR (0.010)	B_A(0.487), B_B(0.241), B_C(0.272)

Table 4
Priority vectors for the decision hierarchy (FA with sub-criteria)

Level 1 variable (priority)	Level 2 variables (priority)	Level 3 variables (priority)
FA (0.299)	OP (0.349)	B_A(0.222), B_B(0.418), B_C(0.360)
	TC (0.131)	B_A(0.958), B_B(0.042), B_C(0.000)
	CF (0.258)	B_A(0.228), B_B(0.614), B_C(0.165)
	PC (0.262)	B_A(0.158), B_B(0.497), B_C(0.345)

The results from Tables 2, 3, 4 and 5 shows that the most important criterion is Technical Features, with a total priority value of 0.350.

Table 5
Priority vectors for the decision hierarchy (SS with sub-criteria)

Level 1 variable (priority)	Level 2 variables (priority)	Level 3 variables (priority)
SS (0.220)	SE (0.242)	$B_A(0.421)$, $B_B(0.264)$, $B_C(0.315)$
	TA (0.151)	$B_A(0.239)$, $B_B(0.342)$, $B_C(0.419)$
	TS (0.217)	$B_A(0.264)$, $B_B(0.421)$, $B_C(0.315)$
	MA (0.197)	$B_A(0.145)$, $B_B(0.532)$, $B_C(0.323)$
	SP (0.193)	$B_A(0.421)$, $B_B(0.315)$, $B_C(0.264)$

5.3 Calculation of Criteria and Bidders using the Fuzzy TOPSIS Method

The application of the fuzzy TOPSIS methodology for bidder selection includes a comparison of bidders, calculation of the distance of each bidder from D^* and D^- and calculation of the similarities to an ideal solution. Using a Linguistic Variables for the Ratings (see Table 6), three decision makers have established the decision matrix by comparing bidders under each of the sub-criteria (see Table 7).

Table 6
Linguistic variables for the ratings

Linguistic variable	Very poor	Poor	Medium Poor	Fair	Medium good	Good	Very good
Fuzzy number	(0,0,2)	(1,2,3)	(2,3.5,4)	(4,5,6)	(5,6.5,8)	(7,8,9)	(8,10,10)

Table 7
Decision matrix for sub-criteria by three decision makers from public procurement committee

	Sub-criteria											
	TP			QU			TD			WP		
	B_A	**B_B**	**B_C**	**B_A**	**B_B**	**B_C**	**B_A**	**B_B**	**B_C**	**B_A**	**B_B**	**B_C**
DM_1	G	VG	F	VG	G	G	P	VG	P	G	F	MG
DM_2	MG	G	MG	G	MG	G	VP	VG	VP	G	F	G
DM_3	MG	VG	F	G	MG	G	VP	VG	MP	VG	F	MG
	QP			QC			SO			MP		
	B_A	**B_B**	**B_C**	**B_A**	**B_B**	**B_C**	**B_A**	**B_B**	**B_C**	**B_A**	**B_B**	**B_C**
DM_1	G	G	G	G	G	VP	G	F	MG	VP	MG	G
DM_2	G	G	G	G	G	P	G	F	MG	VP	G	G
DM_3	G	G	G	VG	VG	P	VG	F	MG	VP	G	VG
	RE			PR			QP			TC		
	B_A	**B_B**	**B_C**	**B_A**	**B_B**	**B_C**	**B_A**	**B_B**	**B_C**	**B_A**	**B_B**	**B_C**
DM_1	F	F	MG	G	F	F	MG	F	MG	VP	P	G

DM_2	F	F	VG	G	F	F	G	P	F	VP	P	G
DM_3	MP	F	MG	VG	MP	MG	VG	VP	MG	VP	VP	VG
	CF			PC			SE			TA		
	$\mathbf{B_A}$	$\mathbf{B_B}$	$\mathbf{B_C}$	$\mathbf{B_A}$	$\mathbf{B_B}$	$\mathbf{B_C}$	$\mathbf{B_A}$	$\mathbf{B_B}$	$\mathbf{B_C}$	$\mathbf{B_A}$	$\mathbf{B_B}$	$\mathbf{B_C}$
DM_1	F	F	G	MP	MG	F	VG	MG	MG	MG	MG	G
DM_2	F	P	VG	P	G	F	MG	F	MG	F	MG	MG
DM_3	F	MP	MG	F	MG	F	MG	F	F	F	F	MG
	TS			MA			SP					
	$\mathbf{B_A}$	$\mathbf{B_B}$	$\mathbf{B_C}$	$\mathbf{B_A}$	$\mathbf{B_B}$	$\mathbf{B_C}$	$\mathbf{B_A}$	$\mathbf{B_B}$	$\mathbf{B_C}$			
DM_1	MG	MG	MG	F	MG	MG	MG	MG	F			
DM_2	F	MG	MG	F	G	F	MG	MG	F			
DM_3	MP	MG	F	F	VG	G	MG	F	F			

Using data from Table 6 and Table 7, the fuzzy matrix is created. Using the sub-criterion weights calculated by the fuzzy Extent Analysis Method, the Weighted Normalized Fuzzy Decision Matrix is established with Eq. (5). The results are shown in Table 8.

Table 8

Weighted normalized decision matrix

	Sub-criteria			
Bidder	**TP**	**QU**	**TD**	**WP**
B_A	(0.11,0.16,0.20)	(0.13,0.16,0.18)	(0,0.02,0.06)	(0.09,0.11,0.13)
B_B	(0.16,0.21,0.23)	(0.09,0.13,0.17)	(0.15,0.19,0.19)	(0.05,0.06,0.08)
B_C	(0.09,0.12,0.18)	(0.13,0.15,0.17)	(0,0.03,0.07)	(0.06,0.09,0.12)
	QP	QC	SO	MP
B_A	(0.04,0.05,0.06)	(0.14,0.18,0.2)	(0.2,0.25,0.28)	(0,0,0.05)
B_B	(0.04,0.05,0.06)	(0.14,0.18,0.2)	(0.11,0.14,0.17)	(0.12,0.18,0.22)
B_C	(0.04,0.05,0.06)	(0,0.03,0.06)	(0.14,0.18,0.23)	(0.17,0.21,0.24)
	RE	PR	OP	TC
B_A	(0.1,0.11,0.15)	(0.16,0.19,0.22)	(0.17,0.29,0.35)	(0,0,0.03)
B_B	(0.1,0.12,0.15)	(0.09,0.1,0.13)	(0,0.08,0.21)	(0,0.02,0.04)
B_C	(0.12,0.19,0.25)	(0.09,0.12,0.18)	(0.14,0.21,0.28)	(0.09,0.11,0.13)
	CF	PC	SE	TA
B_A	(0.1,0.13,0.15)	(0.03,0.09,0.16)	(0.12,0.19,0.24)	(0.06,0.08,0.12)
B_B	(0.03,0.09,0.15)	(0.1,0.16,0.21)	(0.1,0.13,0.19)	(0.06,0.09,0.12)
B_C	(0.13,0.21,0.26)	(0.1,0.13,0,16)	(0.1,0.14,0.19)	(0.07,0.1,0.13)
	TS	MA	SP	
B_A	(0.04,0.11,0.17)	(0.02,0.06,0.12)	(0.1,0.13,0.15)	
B_B	(0.11,0.16,0.19)	(0.1,0.16,0.20)	(0.08,0.12,0.15)	
B_C	(0.09,0.13,0.19)	(0.08,0.13,0.18)	(0.08,0.1,0.12)	

After that, we define the fuzzy positive-ideal solution $\left(FPIS, A^*\right)$ as $\tilde{V}_i^* = (1,1,1)$ for benefit sub-criterion and $\tilde{V}_i^* = (0,0,0)$ for the cost sub-criterion. Also, we define the fuzzy negative-ideal solution $\left(FNIS, A^-\right)$ as $\tilde{V}_i = (0,0,0)$ for benefit sub-criterion and $\tilde{V}_i^- = (1,1,1)$ for the cost sub-criterion. In this case study, OP, TC and CF are cost sub-criteria, whereas the other sub-criteria are benefiting criteria.

The distance of each bidder from D^* and D^- is calculated by using Eq. (8), (9). The results are shown in Table 9.

Table 9
Rank of bidders

Bidders	D_i^*	D_i^-	CC_i	Rank
B_A	14.483	4.653	0.243	2
B_B	14.119	4.993	0.261	1
B_C	14.593	4.610	0.240	3

Finally, the similarities to an ideal solution are calculated by using Eq. (10). The results of fuzzy TOPSIS analysis are summarized in Table 9. Based on CC_i values, the ranking of the bidders is descending order are B_B (0.261), B_A (0.243), B_C (0.240). The results of the proposed model indicate that B_B is the most suitable bidder with a value of 0.261. Analysis of results from Tables 2, 3, 4 and 5 shows that B_B has the highest priority value for Technical Features (especially for Technical Performance), Financial Aspect (especially Offered Price), Support and Services (especially Technical Support and Post-Warranty Maintenance). This is very significant because criteria and sub-criteria mentioned above are more important for government contract authority than others.

Conclusions

A suitable bidder selection procedure within the public procurement process is a strategic decision undertaken by all governments which provide economical, transparent and non-discriminatory work for every government authority. The objective of the government is to carefully assess and select an appropriate bidder able to provide the required product or service, at a specified time and of acceptable price and quality. In this respect, bidder selection in public procurement is a multi-criteria decision problem on account of the fact that the process has many evaluation criteria and alternatives (bidders).

This paper advocates a multi-criteria decision approach in fuzzy environment to bidder selection problem in public procurement in Serbia. In a decision-making

process concerning public procurement, the use of linguistic variables is highly beneficial when performance values cannot be expressed by means of numerical values. Naturally, bidder evaluation and selection problems within the sphere of public procurement have a determined degree of uncertainty. Therefore, the fuzzy set theory helps convert a decision maker's preferences and experiences into meaningful results by applying linguistic values for measuring each criterion with respect to every bidder. An integrated fuzzy Extent Analysis Method and fuzzy TOPSIS approach for choosing the most suitable bidder for a Data Storage Hardware System has been used for this study. Four essential criteria and nineteen sub-criteria have been analyzed for three bidders. Essential criteria and sub-criteria have been determined by means of the existing Public Procurement Law and in cooperation with the public procurement committee. In order to avoid subjectivity in the determination of weights for criteria and sub-criteria, the fuzzy Extent Analysis Method was used to calculate the weights of criteria, while fuzzy TOPSIS was used to rank bidders in public procurement. Actually, the weights obtained from the fuzzy Extent Analysis Method have been included in the decision-making process as they are used in fuzzy TOPSIS calculations. The proposed model yielded very precise results and for that reason, it can be very useful for practical application in all public procurement procedures where we have a combination of quantitative and qualitative evaluation criteria.

Future research in this field could include more methods of multi-criteria analysis like the fuzzy PROMETHEE and fuzzy ELECTRE and furthermore on building a model by combining multiple methods of multi-criteria analysis in order to attain a higher degree of objectivity within public procurement procedures. At the same time, future research in the field of public procurement bidder selection in Serbia could include the design and implementation of an electronic decision support system for a Serbian public procurement web portal which would be based on the integrated model proposed in this paper.

Acknowledgement

This work was supported by the Administrative Agency for Common Services of Government Authorities which is the government authority for centralized public procurement in Serbia. In addition, the authors are very grateful to the anonymous reviewers for their excellent suggestions and comments that led to an improved version of this paper.

References

[1] National Assembly of the Republic of Serbia: Public Procurement Law, Official Gazette, No. 124/12, pp. 60-61, 2012

[2] European Commission: A strategy for e-Procurement, MEMO/12/201. http://trade.ec.europa.eu/doclib/docs/2012/march/tradoc_149242.pdf, 2012. Last visited on 25.03.2014

[3] P. Bajari, G. Lewis: Procurement Contracting with Time Incentives: Theory and Evidence, Quarterly Journal of Economics, Vol. 126, pp. 1173-1211, 2011

[4] M. Falagario, F. Sciancalepore, N. Costantino, R. Pietroforte: Using a DEA-Cross Efficiency Approach in Public Procurement Tenders, European Journal of Operational Research, Vol. 218, No. 2, pp. 523-529, 2012

[5] European Parliament and Council Directive 2004/18: Concerning the Co-ordination of Procedures for the Award of Public Works, Contracts, Public Supply Contracts and Public Service Contracts, 31 March 2004

[6] F. Sciancalepore, M. Falagario, N. Constantino, R. Pietroforte: Multi-Criteria Bid Evaluation of Public Projects. In: Proceedings of the International Conference on ''Management and Innovation for a Sustainable Built Environment'', 19-23 June, Amsterdam, Netherlands, 2011; Online on http://misbe2011.fyper.com/proceedings/documents/185.pdf. Last visited on 24.04.2014.

[7] P. L. Lorentziadis: Post-Objective Determination of Weights of the Evaluation Factors in Public Procurement Tenders, European Journal of Operational Research, Vol. 200, pp. 261-267, 2010

[8] B. D. Rouyendegh: A Hybrid Intuitionistic MCDM Model for Supplier Selection. In: Proceedings of the 5th International Conference on ''Agents and Artificial Intelligence'' - ICAART 2013, Vol. 2, pp. 519-522, Barcelona, Spain, 2013

[9] V. Bobar: Methodology of Concept Application for Multicriteria Decision Making in the Public e-Procurement Process, Metalurgia International, Vol. 18, No. 4, pp. 128-142, 2013

[10] B. D. Rouyendegh, T. E. Erkan: An Application of the Fuzzy ELECTRE Method for Academic Staff Selection, Human Factors and Ergonomics in Manufacturing & Service Industries, Vol. 23, No. 2, pp. 107-115, 2013

[11] T. Galli, F. Chiclana, J. Carter, H. Janicke: Modelling Execution Tracing Quality by Means of Type-1 Fuzzy Logic, Journal of Acta Polytechnica Hungarica, Vol. 10, No. 8, pp. 49-67, 2013

[12] L. Bessissa, L. Boukezzi, Dj. Mahi: A Fuzzy Logic Approach to Model and Predi t HV Calbe Insulation Behaviour under Thermal Aging, Journal of Acta Polytechnica Hungarica, Vol. 11, No. 3, pp. 107-123, 2014

[13] L. A. Zadeh.: Fuzzy Sets, Information and Control, Vol. 8, No. 3, pp. 338-353, 1965

[14] P. Rezaei, K. Rezaei, S. Nazari-Shirkouhi, M. R. J. Tajabadi: Application of Fuzzy Multi-Criteria Decision Making Analysis for Evaluationg and

Selecting the Best Location for Construction of Underground Dam, Journal of Acta Polytechnica Hungarica, Vol. 10, No. 7, pp. 187-205, 2013

[15] B. D. Rouyendegh: Evaluating Projects Based on Intuitionistic Fuzzy Group Decision Making, Journal of Applied Mathematics, Vol. 2012, pp. 1-16, 2012

[16] B. D. Rouyendegh, S. Erol: The DEA – FUZZY ANP Department Ranking Model Applied in Iran Amirkabir University, Journal of Acta Polytechnica Hungarica, Vol. 7, No. 4, pp. 103-114, 2010

[17] B. D. Rouyendegh, T. E. Erkan: Selection of Academic Staff Using Fuzzy AHP : Pilot Study, Technical Gazette, Vol. 19, No. 4, pp. 923-929, 2013

[18] V. Bobar: Concept of Implementation Public Electronic Procurement in Serbia: Challenges and Risks, InfoM, Vol. 47, pp. 10-15, 2013

[19] N. Costantino, M. Dotoli, M. Falagario, M.P. Fanti: Fuzzy Logic Based Vendor Selection for the Public Procurement Sector: a Case Study; Proceedings of SIGEF 2006, 13th Congress of the International Association for Fuzzy Set Management and Economy, 30 November – 2 December 2006, Hammamet, Tunisia, 2006. Online at http://dee.poliba.it/LabControlli/file_pdf/SIGEF_2006.pdf. Last visited on 24.04.2014.

[20] T. Søreide: Corruption in Public Procurement. Causes, Consequences and Cures, Bergen, Norway: Chr. Michelsen Institute, 2002

[21] D. Y. Chang: Applications of the Extent analysis Method on Fuzzy AHP, European Journal of Operational Research, Vol. 95, pp. 649-655, 1996

[22] G. Büyüközkan, T. Ertay, C. Kahraman, D. Ruan: Determining the Importance Weights for the Design Requirements in the House of Quality using the Fuzzy Analytic Network Approach, International Journal of Intelligent Systems, Vol. 19, No. 5, pp. 443-461, 2004

[23] R. Rostamzadeh, S. Sofian: Prioritizing effective 7Ms to Improve Production Systems Performance using Fuzzy AHP and Fuzzy TOPSIS (case study), Expert Systems with Applications, Vol. 38, No. 5, pp. 5166-5177, 2011

[24] I. Alavi, H. Alinejad-Rokny: Comparison of Fuzzy AHP and Fuzzy TOPSIS Methods for Plant Species Selection (Case study: Reclamation Plan of Sungun Copper Mine; Iran), Australian Journal of Basic & Applied Sciences, Vol. 5, No.12, 2011

[25] G. Tuzkaya, B. Gülsün, C. Kahraman, D. Özgen: An Integrated Fuzzy Multi-Criteria Decision Making Methodology for Material Handling Equipment Selection Problem and an Application, Expert Systems with Applications, Vol. 3, No. 4, pp. 2853-2863, 2010

[26] A. Yazdani-Chamzini, A., S. H. Yakhchali: Tunnel Boring Machine (TBM) Selection using Fuzzy Multicriteria Decision Making Methods, Tunnelling and Underground Space Technology, Vol. 30, pp. 194-204, 2012

[27] İ. Ertuğrul, N. Karakaşoğlu: Comparison of Fuzzy AHP and Fuzzy TOPSIS Methods for Facility Location Selection, The International Journal of Advanced Manufacturing Technology, Vol. 39, No. 7-8, pp. 783-795, 2008

[28] N. E. Rezaee, S. H. Zegordi, A. Nazari, M. Sakawa, F. H. Choobar: A Combined Fuzzy Analytic Network Process and Fuzzy-TOPSIS Model for Project Risk Assessment, International Journal of Modeling and Optimization, Vol. 1, No. 4, pp. 275-28, 2011

[29] C. L. Hwang, K. P. Yoon: Multiple Attributes Decision Making Methods and Applications, Berlin: Springer, 1981

[30] İ. Ertuğrul: Fuzzy Group Decision Making for the Selection of Facility Location, Group Decision and Negotiation, Vol. 20, No. 6, pp. 725-740, 2011

[31] X. Zhang, L. Gao, D. Barrett, Y. Chen: Evaluating Water Management Practice for Sustainable Mining, Water, Vol. 6, No. 2, pp. 414-433, 2014

[32] C. N. Liao, H. P. Kao: An Integrated Fuzzy TOPSIS and MCGP Approach to Supplier Selection in Supply Chain Management, Expert Systems with Applications, Vol. 38, No. 9, pp. 10803-10811, 2011

[33] C. T. Chen, C. T. Lin, S. F. Huang: A Fuzzy Approach for Supplier Evaluation and Selection in Supply Chain Management, International Journal of Production Economics, Vol. 102, No. 2, pp. 289-301, 2006

[34] M. Dağdeviren, S. Yavuz, N. Kılınç: Weapon Selection using the AHP and TOPSIS Methods under Fuzzy Environment, Expert Systems with Applications, Vol. 36, No. 4, pp. 8143-8151, 2009

[35] O. Kilincci, S. A. Onal: Fuzzy AHP Approach for Supplier Selection in a Washing Machine Company, Expert Systems with Applications, Vol. 38, pp. 9656-9664, 2011

Resistivity-induced Polarization Receiver/Transmitter Design and PC-assisted Data Analysis

Abdülkadir Çakır[1], Seyit Akpancar[2]

[1]Department of Electrical and Electronics Engineering, Faculty of Technology, Suleyman Demirel University, Isparta, Turkey
E-mail: abdulkadircakir@sdu.edu.tr

[2]Department of Computer Programming, Atabey Vocational School, Suleyman Demirel University, Isparta, Turkey
E-mail: seyitakpancar@sdu.edu.tr

Abstract: Resistivity-induced polarization is a method that is used to identify underground layers by resistivity. In this study, a resistivity induced polarization receiver/transmitter device was designed using the CCS C programming language and tested. The most outstanding feature of the implemented system is that the connection between the receiver and the transmitter were enabled by wireless bluetooth. The data obtained by this system were sent to a PC via wireless bluetooth connection and the data were analyzed after being processed by a program in C# language. The system has 55 volt, 110 volt, 220 volt output amplitudes, as direct or alternating current. The frequency of the current used in the system is 0.1 Hz, 0.3 Hz, 1 Hz, and 3 Hz, and the signals follow the square wave amplitude form. The system was designed to be user-friendly by LCD monitors, which were used to detect the amplitude and frequency of the current sent to the underground.

Keywords: Resistivity IP; geological structure; resistivity; bluetooth

1 Introduction

Even today, many countries in the world intensively experience geological formations. This dynamic structure of the underground causes landslides and underground clearance. It is crucial for today's technological world to forsee these geological formations in order to identify the locations that are suitable for residential areas.

Underground research is not conducted solely for predicting earthquakes. For instance, in agriculture, which plays a vital role in many economies around the world, watering is critically important. Considering that surface water agricultural opportunities are limited in many countries around the world, this surface water

shortage necessitates utilizing underground water supplies. Accordingly, identifying the water supplies and productive location underground is extremely significant regarding economics and labour force.

2 Underground Research Systems

Geophysics engineering, which studies the issues of identifying and examining the locations of mines, minerals, fuel, natural gas, or water underground has specific research and measuring methods. The methods used in this engineering area are seismic, gravity, electrical-electro-magnetic, magnetic, thermal, radioactive, and remote sensing. In the research of underground mineral resources, geophysical methods research practices on the differences between the physical features of minerals and the physical features of the location where these minerals are located (density, wave velocity, electrical conductivity, and magnetic sensitivity).

The method or methods to be used in underground research is crucial for the reliability of the results. Considering the theoretical application capacity, field condition adeptness, and expenditure of the methods, the geoelectrical resistivity method appears to be the most appropriate method.

Every substance in the world has specific parameters such as resistivity, density, and specific heat. Resistivity maps of the mineral layers underground are drawn via the electrical resistivity method, which calculates the resistivity of the substances, which are located as layers underground, to an electric current. These maps illustrate water resources, fuel, or various metal reservoirs underground [1].

Today, the developments in electrical resistivity systems require employing computational methods in the phase of the evaluation of the data. In particular, the basic algorithms, in which forward and inversion modelling are used in the evaluation of geophysical data, require computational assessment. A direct formula is the basic evaluation approach of geophysics, which is described as the assessment of the reaction caused by a model, starting from an underground model with known parameters [2].

Finite differences and elements methods are becoming the most popular computational methods in forward modelling. These developments in computational assessments enable point and two-dimensional electronic data assessments to be realized to facilitate electrode permutation.

2.1 Electrical Resistivity

Underground geological substances have characteristic features such as resistivity, acoustical impedance, magnetic sensitivity, and density. In the chemical structure of the substance, resistivity differs according to the types and strength of the

fastening points of atomic bonds. The bonding strength of the atomic bonds reveal electrical resistivity, which is specific to the substance, according to the reactive resistivity that the substance shows towards the current [3]. Table 1 shows the electrical resistivity of some substances in the ground.

Table 1
Electrical resistivity of some of the substances

Element	Resistivity (Ωm)	Element	Resistivity (Ωm)
Chalcopyrite	$1{,}5x10^{-5}$ - $3x10^{-1}$	Soil (Top)	250 - 1700
Pyrite	$2{,}9x10^{-5}$ - 1,5	Dry Sandy Soil	80 - 1050
Hematite	$3{,}5x10^{-3}$ - 10^{7}	Sand and Gravel	30 - 225
Limonite	10^{3}-10^{7}	Silt (Dry)	1400
Ilmenite	10^{-3} - 5x10	Silt (Saturated)	100
Rock Salt	$3x10^{2}$ - 10^{13}	Marble	10^{2} - $2{,}5x10^{8}$
Hard Coal	10^{-3} - $2x10^{5}$	Sandstone	1 - $7{,}4x10^{8}$
Granite	$3x10^{2}$ - 10^{6}	Limestone	5x10 - 10^{7}
Sand(40%shale)	8	Dolomite	$3{,}5x10^{2}$ - $5x10^{3}$
Sea Water	$3x10^{-1}$	Alluvium and Sand	10 - $8x10^{2}$
Lignite	9 - $2x10^{2}$	Pure Ground Water	10 - 100

3 Geoelectrical Methods Used in Underground Research

Underground resistivity dispersion is identified via surface measurements. In surface measurements, in order to measure the potential difference of the current produced by two conductive electrodes, which are used to transmit electricity underground, resistivity dispersion underground is identified with two potential electrodes [4].

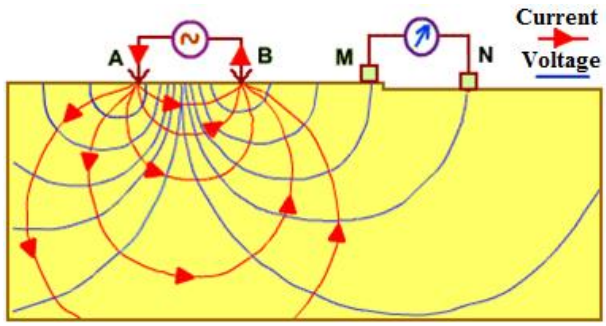

Figure 1
Electricity resistivity method

Figure 1 shows the distribution of current lines that are produced by the electrodes shown with the rows in the A-B range and as a result of this current, the distribution of the electrical stress (electrical potential) created in M-N range current lines [5].

Underground resistivity distribution depends on the type and form of the resource, type of the current transmitted underground, and on the distance between the resource and the receiver [6]. Therefore, it is critical to decide the most convenient one between the self-potential and induced polarization geoelectrical methods according to the geological structure.

3.1 Self-Potential Method

The self-potential method is based on the measurement of the potential variation of the resistance between two points in the earth. It is the only geoelectrical method that allows the opportunity to implement the method without transmitting an electrical current underground. This feature of the self-potential method makes its usage easy and its implementation simple. This method measures the natural electricity current underground [7]. Especially, this method is successfully used in the identification of sulfa-minerals, which can be oxidized such as pyrite, chalcopyrite, galena, molybdenite, and their extensions and horizontal locations.

Generally, metallic stakes are used in order to measure the potential difference between two points. However, in the measurement of self-potential, using metallic stakes is not a reliable method. This is one of the critical disadvantages of the self-potential method. A variable electrolytic potential difference exists between the metallic electrode driven in the ground and the ground. In particular, this situation is distinctly observable when the ground is wet. Additionally, these induced potentials which occur between electrodes and the ground are erratic and vary according to the location and time. Therefore, self-potential measurements should be realized with the electrodes that are not polarized instead of metallic stakes [8].

3.2 Induced Polarization Method

In the resistivity method, an electricity current is transmitted underground with the help of two electrodes that are connected to a power plant or battery system. In order to measure the reaction of the ground when the voltage variation is examined from a different point with an electrode, a delay is observed in the reactions of the ground. In particular, when the welding current is shut instantly, the voltage value does not drop to zero. This impact is called induced polarization.

There are two different ways to carry current between two electrodes placed in points A-B in Figure 1, called faradaic and non-faradaic currents (Figure 2). With the transmission of a faradaic current the result is an electrochemical reaction of some ions and the spread of those ions in the underground interfacial layers. The current is physically carried through electron transfer from the interfacial layer.

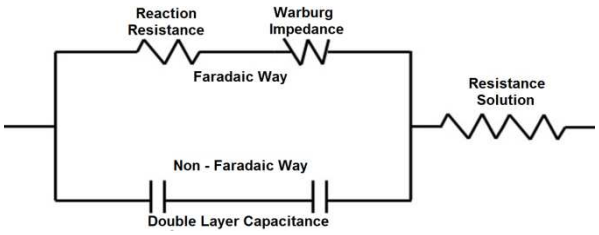

Figure 2
The path of current in the ground

A significant amount of the current above 1000 Hz is carried through the interfacial layer in a non-faradaic way. Therefore, it changes according to internal resistivity frequency of interface. As the frequency is lowered, more current transmits through faradaic way [9]. Consequently, frequency and wave form of the current sent underground have the utmost importance in the induced polarization method.

Induced polarization used in geophysics is measured through voltage variation in time or frequency impact. These two induced polarization methods are essentially similar to each other.

Time setting measurements: When the current sent underground is terminated in an instant, the voltage rate creates a damping or discharge curve (Figure 3).

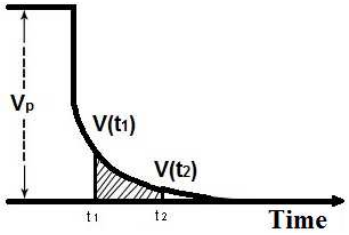

Figure 3
Voltage damping graphic in time setting measurements

Transferring and breaking current times are called “current on” and “current off”. This transaction is repeated several times in order to clear the voltage rate on the substance underground, which is created by the current sent to the underground, from the noise [10]. The ΔV voltage, shown in the fields of Figure 3 is calculated, generally, when the square wave current is sent underground for 3 seconds on, and 3 seconds off, and the integral time is 0.5 and 1.5 seconds.

Accuracy in several implementations of the current transmissions to the underground in very short time spans has a critical impact on the results. Consequently, it is important for the measuring instruments be highly sensitive towards the data produced within the time spans of “current on” and “current off”.

This method is fully accomplished by the identification of sulphuric mineral strata, and underground water, and ground studies.

Frequency environment measurement: Induced polarization impacts are observed in frequency environments as well. By and large, measurements realized in the frequency environment are below 10 Hz. The current is transmitted underground at two different frequencies. The frequency of the first current should be rather low (close to direct current). The visible resistance values in these two frequencies are called frequency effect (FE). Frequency effect is calculated with equation 1.

$$FE = \frac{[\rho_{DC} - \rho_{AC}]}{\rho_{AC}} \quad (1)$$

FE: Frequency effect

ρ_{AC}: Visible resistivity value at high frequency

ρ_{DC}: Visible resistivity value at low frequency

In practice, the value of one frequency is ten times higher than the value of other frequency, such as f1=0.1 Hz, f2=1.

Frequency effect is also called frequency effect percentage (FEP) as in equation 2.

$$FEP = 100 \times FE \quad (2)$$

FEP: Frequency effect percentage

FE: Frequency effect

Another parameter used in the frequency setting method is metallic factor. The metallic factor is proposed in order to minimize the effects of the parameters, such as, electrolyte, heat, and pore size. The metallic factor is calculated through equation3 [10].

$$MF = \frac{FEP}{\rho_{DC}} \times 2\pi \times 10^3 \quad (3)$$

MF: Metallic factor

FEP: Frequency effect percentage

ρ_{DC}: Visible resistivity value at lower frequencies

In frequency setting measurements, by examining the changes of the values of visible resistivity and the metallic factor, the location of the mineral stratum is ascertained. This process usually depends on the principle that as the frequency of the current sent underground increases, the resistance of the rocks underground decreases. The induced polarization effect is mostly seen between the frequencies of 0.1 and 20 Hz [9]. Higher frequencies are not preferred because of their high electromagnetic induction effect.

4 Description of System

The system proposed in this study consists of three basic parts (Figure 4). These include:

- Transmitter unit
- Receiver unit
- Evaluation Program

The transmitter and receiver units can operate in correlation with each other or independently from each other. The software developed for the evaluation of the data is designed in a way that it can operate independently from these two units, likewise.

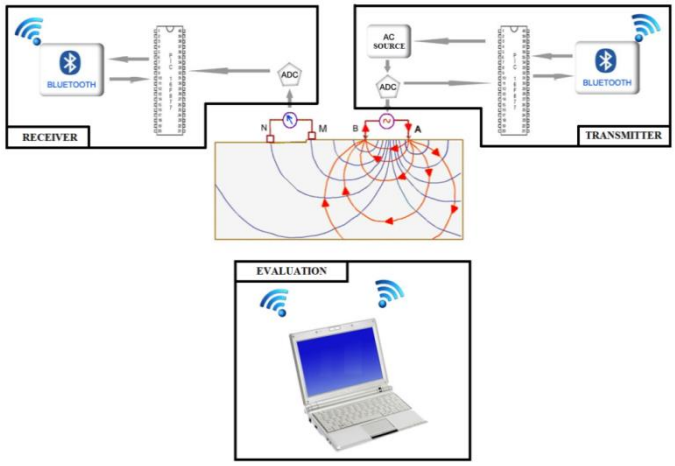

Figure 4
The block diagram of the resistivity IP system proposed in this study

4.1 Transmitter Unit

The transmitter unit designed and developed for this study produces the current to be transmitted underground and measures the current absorbed underground as well.

As is pictured in Figure 5 in a block diagram, the transmitter unit consists of four parts: power stage, frequency stage, control stage, and PC connection stage.

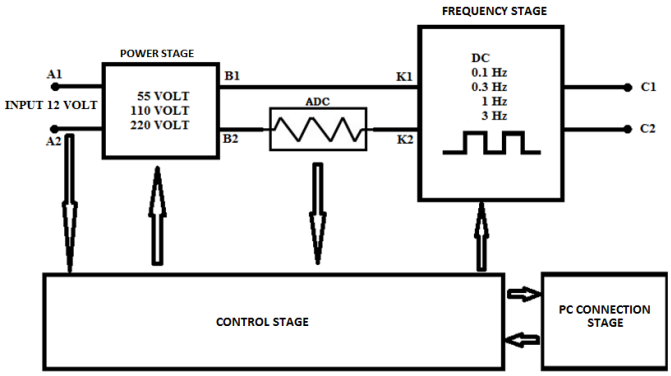

Figure 5

Block diagram of the transmitter unit

A 12 volt amplitude direct current is applied through A1 and A2 points via the transmitter unit. After the amplitude is increased to 55 volts, 110 volts, or 220 volt at the power stage, it is sent to points B1 and B2. The current transmitted through point B2 is measured with a PIC analog digital converter at the control stage, then enters to the frequency stage from points K1 and K2. After converted to 0.1 Hz, 0.3 Hz, 1 Hz, or 3 Hz square wave or as unconverted, the direct current that enters the frequency stage from points K1 and K2 is sent to points C1 and C2, which are the last steps of the process of the transmission of the current underground.

4.1.1 Power Stage

This study designed and developed the circuit as it is pictured in Figure 6, which increases the 12 volt current applied from points A1 and A2 of the transmitted unit to 55 volts, 110 volts, or 220 volts and converts the current into accurate direct current through filtering [11].

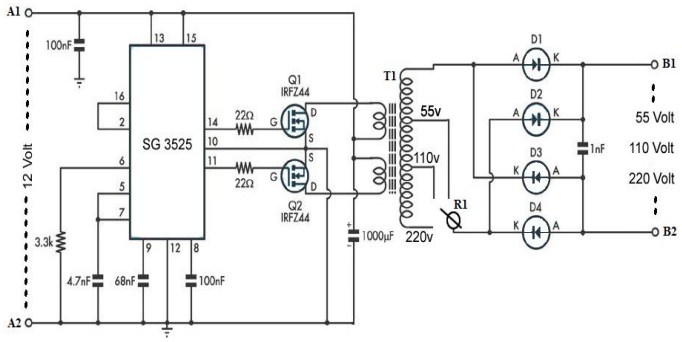

Figure 6

Power stage circuit diagram of the transmitter unit

In the circuit, a 100 Hz square wave signal, which is produced through a SG3525 integrated unit, is applied to the primary windings of the T1 transformator through Q1 and Q2 power MOSFETs (metal oxide semiconductor field effect transistors).

The MOSFETs used in the circuit are resistant up to a 50 ampere current [12].In order to prevent the MOSFETs from being destroyed in the case that they overheat when a high current is drawn, MOSFETs are looped to heatsinks.

A 12 volt voltage applied from the primary winding of the T1 transformator is converted to 55 volt, 110 volt, and 220 volt at the secondary winding. The R1 relay is responsible for selecting the transformed voltages. A 100 Hz voltage alternating current chosen by the R1 relay is transformed into a direct current through diodes D1, D2, D3, and D4 and sent to points B1 and B2.

4.1.2 Frequency Stage

DC current in the power stage is used to convert 0.1 Hz, 0.3 Hz, 1 Hz or 3 Hz square wave by the circuit in Figure 7.

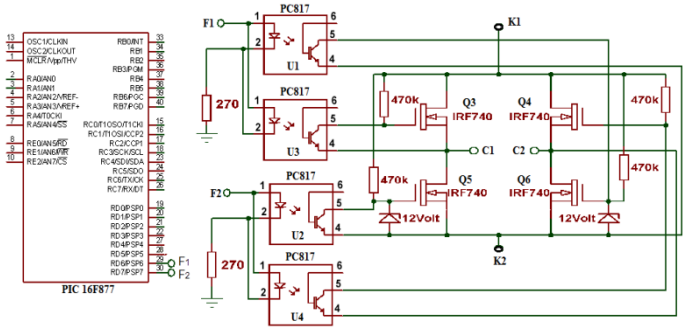

Figure 7

Frequency stage circuit diagram of the transmitter unit

The 0.1 Hz, 0.3 Hz, 1 Hz, or 3 Hz frequency signal is generated by using the CCS C programming language in the PIC16F877 microcontroller and inverter circuit, as shown in Figure 7.

When point F1 of the inverter circuit is logic-1, the Q3 and Q6 MOSFETs are switched; when point F2 is logic-1, the Q4 and Q5 MOSFETs are switched. The direct current derived from the power stage, which is looped to points K1 and K2, is transformed into the square wave form at the C1 and C2 collector points through the double cross switching of the MOSFETs. The waveforms in Figure 8 are the square wave forms, which are observed through the oscilloscope at the C1and C2 collector points.

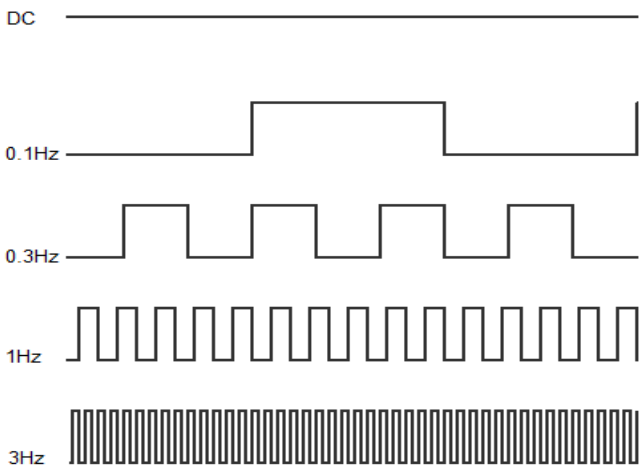

Figure 8
Wave forms of C1 - C2 collectors in the transmitter unit

4.1.3 PC Connection Stage (Bluetooth)

It is extremely important to obtain the value of the current sent to the underground through C1 and C2 collector points of the transmitter unit carried out in this study, as well as to transfer the related data to the computer where the data to be evaluated. After the current data, which is received as analogue, is processed in PIC and transformed into digital data, it is sent to the computer via the bluetooth module circuit in Figure 9.

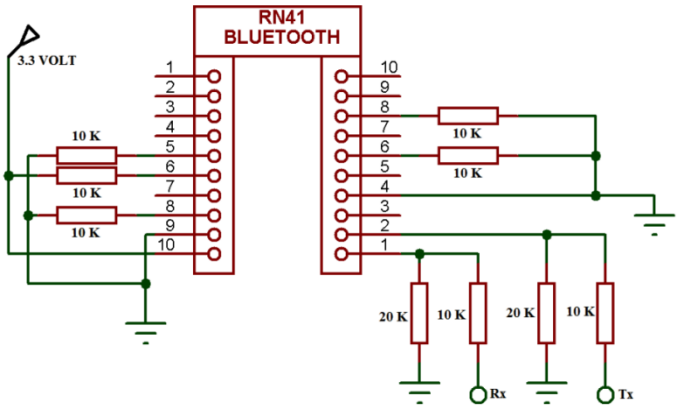

Figure 9
Connection stage circuit diagram of the transmitter unit

The circuit in Figure 9 was designed and activated for the RN41 bluetooth module, which connects the transmitter unit, PC, and the receiver unit.

The connection between the transmitter unit, receiver unit, and the PC is achieved through connecting the Rx and Tx points in the circuit with C6 and C7 pins, respectively, of PIC in the control stage. The top view of the bluetooth module is seen in Figure 10.

Figure 10
RN41 bluetooth module for PC connection

4.1.4 Control Stage

The designed control stage executes all the administrative functions of the transmitter unit. The PIC in Figure 11 which constitutes the base of the control stage, measures charge of the transmitter unit source in percentage shown on the LCD monitor. Voltage and frequency choices can be seen on the LCD monitor menu, and the values are arranged through operating relays connected to the D6 and D7 pins of the PIC according to the choices of the user. Additionally, via communication with the bluetooth kit, the transaction of sending the current and frequency data is received from the receiver unit by the PC.

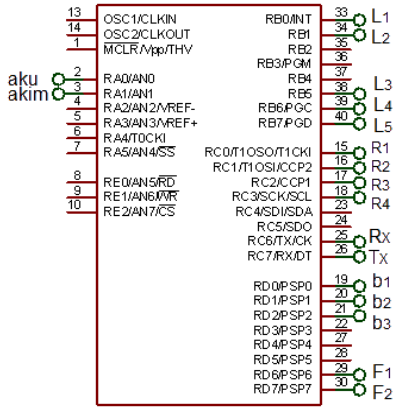

Figure 11
Control PIC of the transmitter unit

The top view of the transmitter unit is seen in Figure 12.

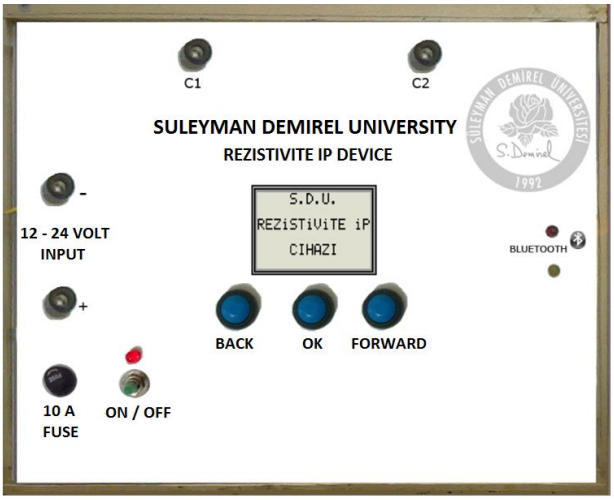

Figure 12
Topview of the transmitter unit

4.2 Receiver Unit

The receiver unit monitors the voltage value on the underground substance, which is produced by the current sent underground.

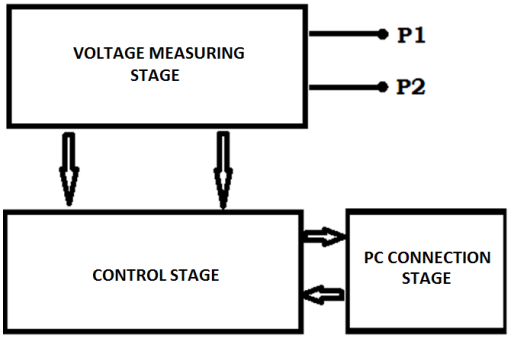

Figure 13
Block diagram of the receiver unit

In order to measure the voltage on the substance underground, a circuit that is sensitive to different frequencies was designed. The Figure consists of three main parts as shown in Figure 13. These consist of the voltage measuring stage, control stage, and PC connection stage. The PC connection stage has the same function and circuit with the PC connection stage of the transmitter unit.

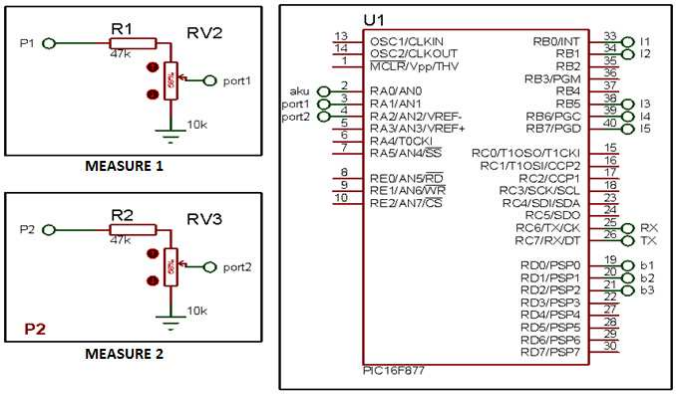

Figure 14

Circuit diagram of the voltage measuring stage of the receiver unit

The A1 and A2 ADC input of the PIC16F877 microcontroller used in the receiver unit circuit, which is pictured in Figure 14, is designed in a way that it receives voltage data in an analogue format from underground. The voltage value received from underground is sent to a PC via the PC connection stage, which is connected to the PIC.

A topview of the receiver unit is seen in Figure 15.

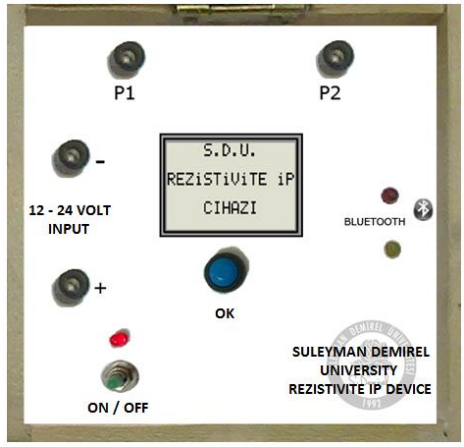

Figure 15

Topview of the receiver unit

4.3 Computer Software

Visual Studio editor software was used to evaluate the data received from the transmitter and receiver units.

4.3.1 Operating the Software and Interpreting the Data

The main format of the program is seen in Figure 16.

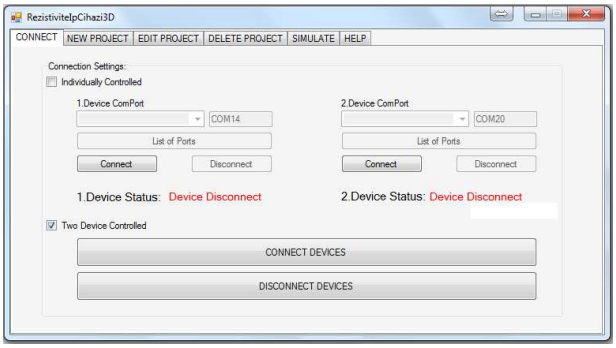

Figure 16

Connection window with transmitter and receiver units

The program used in this study realizes the connection between the transmitter and receiver units, and the connection of these two units with the computer via bluetooth. The program provides the opportunity to control these two units from the computer simultaneously, as well as separately.

It has another significant advantage in that the program evaluates the data received from the transmitter and receiver units; it also possesses a database. Recording the data received from the units in the database provides the opportunity to revise the previous studies.

In the process of receiving data from the transmitter and receiver units, the form in Figure 17 was used.

Figure 17

The screen shows the chart in which the data from the transmitter and receiver units are to be saved

The form in Figure 17 is the screen that shows the current and voltage data measured vertically from a single point underground. Frequency, and current and voltage data received from the transmitter and receiver units arrive in a string, and the related parts in the form screen are completed, then saved. This process is repeated for every point to be measured vertically from ground to underground.

5 Results and Discussion

The comparison of the data recorded in the Beşirli Region of the Trabzon Province in Turkey using the proposed study system/device and the RVA-1 brand system/device is provided in Table 2.

Table 2
Measured Rhoa values

AB/2	MN/2	Other device (Rhoa)	Proposed study device (Rhoa)
2	0.5	7.7	7.83
3	0.5	7.12	6.98
4	0.5	6.64	6.47
5	0.5	7.16	7.08
6	0.5	6.58	6.4
5	1	6.3	6.3
6	1	5.82	5.9
8	1	7	7.1
10	1	8.8	8.5
15	1	9.2	9.34
20	1	9.34	9.34
25	1	9.9	10.08
30	1	10.6	10.3
25	5	11	10.9
30	5	11.7	11.5
35	5	12.7	12
40	5	13.5	13.5
50	5	13.8	13.7

The data obtained with these two systems were roughly similar. Using the data in Table 2, graphs were drawn for the vertical electrical sounding (VES) curves of the measured points. These VES curves are shown in Figure 18a and 18b.

It can be seen that the VES curves of the graphs in Figure 18a and 18b are of the same character.

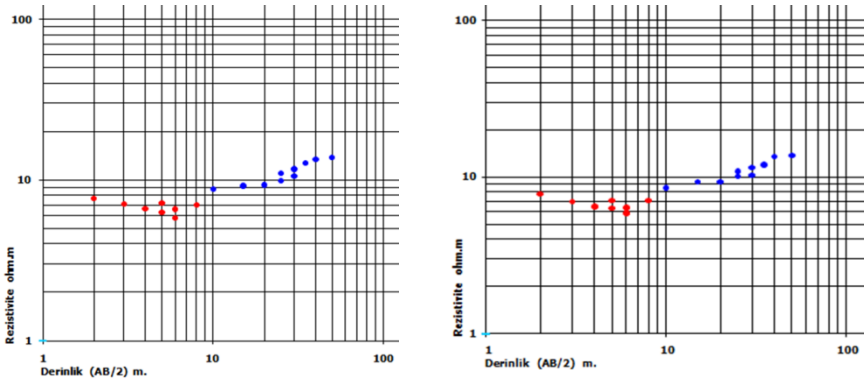

(a) (b)

Figure 18

a: VES curve of the RVA-1 system, b: VES curve of the proposed study system

The graphs in Figure 19 (Rhoa1, Rhoa2, the frequency effect, and the frequency effect percentage) are 3-dimensional representations that use shades of black to illustrate the shapes formed by the underground layers.

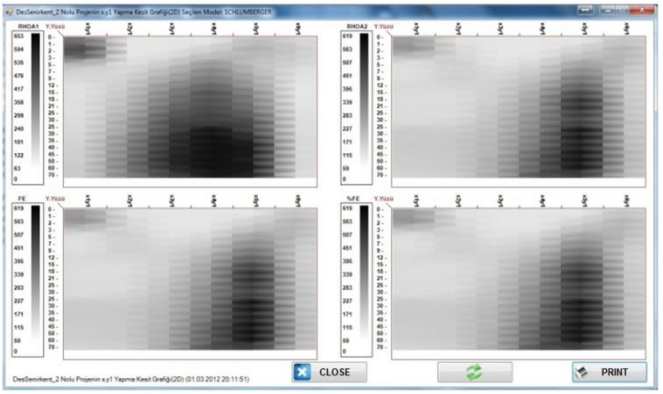

Figure 19

2D Simulative profile graphic

Conclusions

In this study, in order to identify the physical and chemical features underground, a resistance device that sends direct or alternating current underground, as well as transfers the current sent underground, and the resulting voltage that is released to the PC through a wireless process, was designed and implemented. In an attempt to identify the nature of the substances underground, the current sent from the power stage of the system should be strong; it affects the accuracy of the results to a large extent.

The most significant advantage of this system is that the transmitter and the receiver units are not integrated and these two units can connect to computer wirelessly. A wireless connection provides significant savings from the cable cost and relieves the users from cable confusion.

A system was generated in C# programming language, which enables a bluetooth connection between the receiver unit, transmitter unit, and PC for the graphic interpretation of the data received through the system. It also saves and interprets the data on the database. The software saves the data from the DES model and simulative profile model, as well as draws the graphics.

The fact that the number of studies regarding the development of geophysics devices is very limited, as well as the fact that there is very little information available on the operating rationale of such systems, have led to considerable difficulties during the development of the study device/system. Taking into consideration the development processes for technologies in general, the authors hope that this study will serve as a basis for the use of more advanced microprocessors and computers within the study system, which will ensure creation of systems that provide more accurate data.

References

[1] S. Akpancar: "Rezistivite-IP Alıcı / Verici Tasarımı ve PC'de Verilerin Analizi", Suleyman Demirel University Graduate School of Natural and Applied Sciences Department of Electronic and Computer Education M.Sc. Thesis, Isparta, Turkey, 2012

[2] F. Ergüder, L. Karaoğlu: "Yeraltı Yapılarının Özdirenç Yöntemiyle Saptanması ve Uygulamaları", Turkey 5 coal Congres, 10p, 1983

[3] A. Uluğ: "Jeofizikte Veri İşlem", Dokuz Eylul University Faculty of Engineering and Architecture Lecture Notes, 1988

[4] M. A. Berge: "Iki Boyutlu Özdirenç Ters Çözüm Modellemesi", Dokuz Eylul University Faculty of Engineering Department of Geophysical Engineering M.Sc. Thesis, 2005

[5] M. E. Candansayar: "Doğru Akım Özdirenç Yönteminde Modelleme Ve İki Boyutlu Sığ Yapıların Aranmasında Elektrot Dizilimlerinin Ayrımlılıklarının Karşılaştırılması", Ankara University Institute of Science M.Sc. Thesis, 1997

[6] A. Çakır: "Genliği Ve Frekansı Ayarlanabilen Konvertör Tasarımı Ve Yapımı", Gazi University Institute of Science M.Sc. Thesis, 1997

[7] Ş. Yıldız, E. Ölmez, F. Ataselim: "Odayeri Katı Atık Düzenli Depolama Sahası Depo Gövdesindeki Su Muhtevasının Doğal Potansiyel Ve Elektrik Özdirenç Yöntemleri Kullanılarak Tespiti", Symposium on Solid Waste Management in Turkey, 5p, 2009

[8] A. Kara: "Genel Jeofiziğe Giriş", Suleyman Demirel University Faculty of Engineering and Architecture Lecture Notes, 36p, 2010

[9] N. Coşkun: "Yer Elektrik Yöntemleri III: İndüksiyon Polarizasyonu (IP) Yöntemi", Karadeniz Technical University Faculty of Engineering Lecture Notes, 2009

[10] A. T. Başokur: Maden Aramalarında Elektrik ve Elektromanyetik Yöntemler, Ankara University Faculty of Engineering Department of Geophysical Engineering, 43p, 2003

[11] J. Dudrik, J. Oetter, High-Frequency Soft-Switching DC-DC Converters for Voltage and Current DC Power Sources, Acta Polytechnica Hungarica, Vol. 4, No. 2, 2007, pp. 29-46

[12] Datasheetcatalog: [Online]. Available: http://www.datasheetcatalog.org/ datasheets/166/373875_DS.pdf, 2012

Sturm–Liouville problem and *I*–Bessel sampling

Dragana Jankov Maširević

Department of Mathematics, University of Osijek, Trg Lj. Gaja 6, 31000 Osijek, Croatia
e-mail: djankov@mathos.hr

Abstract: *The main aim of this article is to establish summation formulae in form of the sampling expansion series building the kernel function by the samples of the modified Bessel function of the first kind I_ν, and to obtain a sharp truncation error upper bound occurring in the derived sampling series approximation. Summation formulae for functions $I_{\nu+1}/I_\nu, 1/I_\nu, I_\nu^2$ and the generalized hypergeometric function ${}_2F_3$ are derived as a by–product of these results.*

The main derivation tools are the Sturm–Liouville boundary value problem and various properties of Bessel and modified Bessel functions.

Keywords: *Bessel function of the first kind J_ν, modified Bessel function of the first kind I_ν, sampling series expansions, Sturm–Liouville boundary value problems, generalized hypergeometric function ${}_2F_3$, Fox-Wright generalized hypergeometric function ${}_p\Psi_q^*$, sampling series truncation error upper bound.*

1 Introduction and motivation

The historical background of sampling theorems, various applications in many branches of science and engineering, especially in signal analysis and reconstruction and/or its up-to-date results in different areas of mathematics like approximation theory and interpolation are well–covered among others by Jerri's "IEEE 1977 paper" [13], by survey articles of Khurgin–Yakovlev [14] and Unser [24], by the monographs of Higgins [9], an edited monograph by Higgins and Stens [10], the book by Seip [22] and numerous references therein. Thus, by skipping an outline of the facts from the aforementioned references we can focus on our main goal – establishing the *I*–Bessel sampling expansion result *via* the appropriate Strum–Liouville boundary value problem and the related sampling expansion series truncation upper bound, which yields the precise convergence rate in this kind of approximation procedures.

Here and in what follows *$\mathscr{B}$–Bessel sampling* is called a sampling expansion procedure for some input function f, when the underlying sampling kernel function is built up in terms of samples of $\mathscr{B}$ being a Bessel or modified Bessel function, and the sampling nodes correspond to the zeros b_k of $\mathscr{B}$ used in the expansion formula.

For instance, Kramer considered J–Bessel sampling as an illustrative example for his theorem [17] which generalized the Whittaker–Shannon–Kotel'nikov (WKS) sampling theorem [30]. More precisely, Kramer derived the following summation formula:

$$f(t) = 2J_m(t) \sum_{k\in\mathbb{Z}} \frac{j_{m,k} f(j_{m,k})}{(j_{m,k}^2 - t^2) J_{m+1}(j_{m,k})}, \qquad J_m(j_{m,k}) = 0\,.$$

Before Kramer, we have to mention Weiss [29] who arrived at the same result for $k = 2$, and also Whittaker who first discussed a very similar sampling expansion [30]; see also [31, p. 439, Eq. (17)]:

$$f(t) = \frac{2\sqrt{t}}{\pi} J_\nu(\pi t) \sum_{k\geq 1} \frac{\sqrt{t_k} f(t_k)}{J_{\nu+1}(\pi t_k)(t_k^2 - t^2)}, 0 < t < \infty,$$

where $\{\pi t_k\}$ are positive zeros of $J_\nu(\pi t)$, $\nu \geq \frac{1}{2}$. It is worth mentioning that a recent article by Jankov Maširević *et al.* [12] is devoted mainly to Y–Bessel sampling, where Y stands for the Bessel function of the second kind.

On the other hand, the sampling theorem is related to Sturm–Liouville boundary value problems (see e.g. [5, 25, 27]). Motivated essentially by that connection, our main objective is to establish a new I–Bessel sampling expansion formula which will be presented in the next section, together with a set of corresponding expansion results for I_ν, I_ν^2 and for the generalized hypergeometric function ${}_2F_3$, where the sampling reproduction kernel consists of the Fox-Wright generalized hypergeometric function ${}_p\Psi_q^*$.

The results about truncation error upper bounds for J–Bessel sampling for the band–limited Hankel transform can be found in [8, 31]. Recent progress was also made by Knockaert [16] with respect to the J–Bessel truncation procedure and Jankov Maširević *et al.* [12] in the case of Y–Bessel sampling. Thus, the last section is devoted to establishing sharp truncation error upper bounds for a newly derived truncated sampling series of modified Bessel functions I_ν.

2 I–Bessel sampling expansions and Sturm–Liouville differential equation

The main aim of this section is to establish a new Bessel–sampling expansion formula for a function which possesses an integral representation in terms of the modified Bessel function of the first kind I_ν. The derivation is based on the Sturm–Liouville differential equation. After that, we apply the obtained expansion to derive another Bessel sampling formulae for $I_{\nu+1}/I_\nu$, $1/I_\nu$, I_ν^2 and for a generalized hypergeometric function ${}_2F_3$ as well.

Firstly, the modified Bessel function of the first kind I_ν of the order ν is a particular solution of the Bessel–type differential equation

$$x^2 y''(x) + xy'(x) - (x^2 + \nu^2) y(x) = 0, \qquad x \in (0,\infty)\,,$$

which can be presented in the Sturm–Liouville form:

$$-(xy'(x))' + \frac{\nu^2}{x} y(x) = -xy(x), \qquad x \in (0,\infty).$$

This in turn implies [4] that $\sqrt{x} I_\nu(x\sqrt{\lambda})$ satisfies the Sturm–Liouville differential equation

$$y''(x) - (\nu^2 - 1/4)x^{-2} y(x) = \lambda y(x), \qquad x \in (0,\infty).$$

We notice that this is in fact a singular Sturm–Liouville problem.

In order to state our next auxiliary result, which we require to perform our results in this section, we mention some preliminary facts. In [26, p. 581], Zayed stated that if $\phi(x) = \phi(x,\lambda)$ and $\theta(x) = \theta(x,\lambda)$ are the solutions of the singular Sturm–Liouville boundary value problem such that

$$\begin{aligned} &\phi(0) = \sin\alpha, \quad \phi'(0) = -\cos\alpha, \\ &\theta(0) = \cos\alpha, \quad \theta'(0) = \sin\alpha, \end{aligned}$$

then it is known [23] that there exists a complex valued function m such that for every nonreal λ the appropriate Sturm–Liouville differential equation has a solution

$$\psi(x,\lambda) = \theta(x,\lambda) + m(\lambda)\phi(x,\lambda) \in L^2(0,\infty). \tag{1}$$

Throughout this section m will denote a meromorphic function that is real–valued on the real axis and whose singularities are simple poles on $\mathbb{R}$. The poles of m will be denoted by $\{\lambda_k\}_{k\in\mathbb{N}_0}$.

Theorem A. [26, p. 582, Theorem 3.1] Consider the singular Sturm–Liouville problem

$$\begin{aligned} &y'' - q(x)y = -\lambda y, \qquad x \in [0,\infty), \\ &y(0)\cos\alpha = -y'(0)\sin\alpha, \end{aligned}$$

where $q(x) \in \mathrm{C}[0,\infty)$. Assume that m is a meromorphic function that is real–valued on the real axis and whose only singularities are simple poles $\{\lambda_k\}_{k\in\mathbb{N}_0}$ on the non-negative real axis, and λ_0 will be reserved for the eigenvalue zero.

Let p be the smallest integer for which the series $\sum_{k\geq 1}(\lambda_k)^{-p-1}$ converges.

(a) If none of λ_k is zero, set

$$G(\lambda) = \begin{cases} \displaystyle\prod_{k\geq 0}\left(1 - \frac{\lambda}{\lambda_k}\right) \exp \sum_{j=1}^{p} \frac{1}{j}\left(\frac{\lambda}{\lambda_k}\right)^j, & p \in \mathbb{N} \\ \displaystyle\prod_{k\geq 0}\left(1 - \frac{\lambda}{\lambda_k}\right), & p = 0 \end{cases};$$

(b) If one λ_k is zero, say $\lambda_0 = 0$, set

$$G(\lambda) = \begin{cases} \lambda \prod_{k\geq 1} \left(1 - \frac{\lambda}{\lambda_k}\right) \exp \sum_{j=1}^{p} \frac{1}{j} \left(\frac{\lambda}{\lambda_k}\right)^j, & p \in \mathbb{N} \\ \lambda \prod_{k\geq 1} \left(1 - \frac{\lambda}{\lambda_k}\right), & p = 0 \end{cases}.$$

Let $\Phi(x,\lambda) = G(\lambda)\psi(x,\lambda)$, $g(x) \in L^2(0,\infty)$ and

$$f(\lambda) = \int_0^\infty g(x)\,\Phi(x,\lambda)\,\mathrm{d}x.$$

Then f is an entire function that admits the sampling representation

$$f(\lambda) = \sum_{k\geq 0} f(\lambda_k) \frac{G(\lambda)}{(\lambda - \lambda_k)\,G'(\lambda_k)},$$

where the series converges uniformly on compact subsets of the complex λ–plane.

Now, we establish our main result in this section.

Theorem 1. *If for some $g \in L^2(0,a), a > 0$, the function F has an integral representation*

$$F(\lambda) = \frac{2^\nu\,\Gamma(\nu+1)}{\lambda^{\frac{\nu}{2}}\,a^{\nu+\frac{1}{2}}} \int_0^a g(x)\sqrt{x} I_\nu(x\sqrt{\lambda})\,\mathrm{d}x, \tag{2}$$

then the following sampling representation holds

$$F(\lambda) = \frac{2I_\nu(a\sqrt{\lambda})}{a\,\lambda^{\frac{\nu}{2}}} \sum_{k\geq 1} \frac{\lambda_k^{(\nu+1)/2} F(\lambda_k)}{(\lambda - \lambda_k) I'_\nu(a\sqrt{\lambda_k})}, \tag{3}$$

where $\lambda_k = -a^{-2} j_{\nu,k}^2$, $k \in \mathbb{N}$; $\nu > -1$ and the series converges uniformly on compact subsets of the complex λ–plane.

Moreover, let $g \in L^2(0,1)$ and assume that a function f possesses an integral expression, which reads as follows

$$f(t) = \int_0^1 g(x)\sqrt{x} I_\nu(tx)\,\mathrm{d}x. \tag{4}$$

Then the related sampling representation is

$$f(t) = 2I_\nu(t) \sum_{k\geq 1} \frac{t_k f(t_k)}{I_{\nu+1}(t_k)\left(t^2 - t_k^2\right)}, \tag{5}$$

where $\nu > -1$ and $t_k = -\mathrm{i}\, j_{\nu,k}$ is the kth zero of I_ν.

Proof. In order to derive summation formula (3) we set $\phi(x,\lambda)$, $\theta(x,\lambda)$ and $\mu(\lambda)$ as

$$\begin{aligned}
\phi(x,\lambda) &= \sqrt{ax}\left(I_\nu(a\sqrt{\lambda})K_\nu(x\sqrt{\lambda}) - I_\nu(x\sqrt{\lambda})K_\nu(a\sqrt{\lambda})\right)\\
\theta(x,\lambda) &= \sqrt{a\lambda x}\left(I'_\nu(a\sqrt{\lambda})K_\nu(x\sqrt{\lambda}) - I_\nu(x\sqrt{\lambda})K'_\nu(a\sqrt{\lambda})\right) + \frac{\phi(x,\lambda)}{2a}\\
m(\lambda) &= -\sqrt{\lambda}\,\frac{I'_\nu(a\sqrt{\lambda})}{I_\nu(a\sqrt{\lambda})} - \frac{1}{2a}\,.
\end{aligned}$$

Now, from (1) we have that

$$\psi(x,\lambda) = \sqrt{a\lambda x}\left(\frac{I'_\nu(a\sqrt{\lambda})I_\nu(x\sqrt{\lambda})K_\nu(a\sqrt{\lambda})}{I_\nu(a\sqrt{\lambda})} - I_\nu(x\sqrt{\lambda})K'_\nu(a\sqrt{\lambda})\right)$$

i.e.

$$I_\nu(a\sqrt{\lambda})\,\psi(x,\lambda) = \sqrt{\frac{x}{a}}\,I_\nu(x\sqrt{\lambda})\,, \tag{6}$$

involving the Wronskian $\mathscr{W}[\cdot,\cdot]$ of the modified Bessel functions I_ν and K_ν [28, p. 80]

$$\mathscr{W}(K_\nu,I_\nu)(a\sqrt{\lambda}) = I'_\nu(a\sqrt{\lambda})K_\nu(a\sqrt{\lambda}) - I_\nu(a\sqrt{\lambda})K'_\nu(a\sqrt{\lambda}) = \frac{1}{a\sqrt{\lambda}}\,.$$

From the definition of m and the well–known identity $I_\nu(t) = \mathrm{i}^{-\nu}J_\nu(\mathrm{i}t)$, we find that $\lambda_k = -a^{-2}\,j_{\nu,k}^2$, $k\in\mathbb{N}$, where $j_{\nu,k}$ is the kth positive real zero of the Bessel function J_ν. Let us also mention that the zeros $j_{\nu,k}$, $k\in\mathbb{N}$ are positive real numbers for all $\nu > -1$ and there also holds [28, p. 479]

$$0 < j_{\nu,1} < j_{\nu+1,1} < j_{\nu,2} < j_{\nu+1,2} < j_{\nu,3} < \cdots\,.$$

Further, by Theorem A we conclude that

$$G(\lambda) = \prod_{k\geq 1}\left(1 + \frac{\lambda a^2}{j_{\nu,k}^2}\right). \tag{7}$$

Now, with the help of the formula [28, p. 498]

$$J_\nu(z) = \frac{\left(\frac{z}{2}\right)^\nu}{\Gamma(\nu+1)}\prod_{k\geq 1}\left(1 - \frac{z^2}{j_{\nu,k}^2}\right), \qquad \Re\{\nu\}\notin\mathbb{Z}^-\,,$$

which by virtue of substitution $z\mapsto \mathrm{i}z$ becomes

$$I_\nu(z) = \frac{\left(\frac{z}{2}\right)^\nu}{\Gamma(\nu+1)}\prod_{k\geq 1}\left(1 + \frac{z^2}{j_{\nu,k}^2}\right),$$

we can rewrite relation (7) as

$$G(\lambda) = \frac{2^{\nu}\Gamma(\nu+1)\, I_{\nu}(a\sqrt{\lambda})}{(a\sqrt{\lambda})^{\nu}}. \tag{8}$$

Now, from (6) and (8) we have

$$\Phi(x,\lambda) = G(\lambda)\,\psi(x,\lambda) = \frac{2^{\nu}\Gamma(\nu+1)}{(a\sqrt{\lambda})^{\nu}}\,\sqrt{\frac{x}{a}}\,I_{\nu}(x\sqrt{\lambda}).$$

The desired formula (3) readily follows by previous results and Theorem A.

Now, transforming integral representation (2) and the sum in (3) by taking $\lambda = t^2$, $\lambda_k = t_k^2$ and $a = 1$, being $I_{\nu}'(t) = I_{\nu+1}(t) + \frac{\nu}{t} I_{\nu}(t)$, we deduce that if for some $g \in L^2(0,1)$ the function F has an integral representation

$$F(t) = \frac{2^{\nu}\Gamma(\nu+1)}{t^{\nu}} \int_0^1 g(x)\sqrt{x} I_{\nu}(xt)\,\mathrm{d}x, \tag{9}$$

then the related sampling representation is

$$F(t) = \frac{2\,I_{\nu}(t)}{t^{\nu}} \sum_{k\geq 1} \frac{t_k^{\nu+1} F(t_k)}{(t^2 - t_k^2) I_{\nu+1}(t_k)}, \tag{10}$$

where $\nu > -1$ and $t_k = -\mathrm{i}\, j_{\nu,k}$ is the kth zero of $I_{\nu}(t)$.

Equivalently, if $f(t) := \dfrac{t^{\nu}F(t)}{2^{\nu}\Gamma(\nu+1)}$, from formulas (9) and (10) we can immediately deduce that if the function f has an integral representation (4), then the appropriate sampling representation is given by (5). □

Remark 1. Zayed [26, p. 592] obtained summation formulae analogous to (3) and (5) for the Bessel function of the first kind J_{ν}.

Also, a special case of the sampling representation formula (3), when $a = 1$, was derived by Ismail and Kelker (see [11, Theorem 6.4, p. 899]), where they assumed that F is a single–valued entire function with the asymptotic behavior $F(\lambda) = O(\lambda^{-\nu/2-1/2}\mathrm{e}^{\sqrt{\lambda}})$, as $|\lambda| \to \infty$ uniformly in every sector $|\arg\lambda| \leq \pi - \varepsilon$, $0 < \varepsilon < \pi$.

Now, we present three summation formulae for a modified Bessel function I_{ν}.

Corollary 1.1. *For $\nu > -1$ we have*

$$\frac{I_{\nu+1}(t)}{I_{\nu}(t)} = 2t \sum_{k\geq 1} \frac{1}{t^2 - t_k^2} = 2t \sum_{k\geq 1} \frac{1}{t^2 + j_{\nu,k}^2}. \tag{11}$$

Moreover, there holds

$$\pi \coth(\pi t) = 2t \sum_{k\geq 1} \frac{1}{t^2 + k^2} + \frac{1}{t}, \qquad t \neq 0.$$

Proof. By rewriting the integral expression [6, p. 668, Eq. 6.561.7]

$$t^{-1}I_{\nu+1}(t) = \int_0^1 x^{\nu+1} I_\nu(tx)\,\mathrm{d}x, \qquad \nu > -1\,,$$

into

$$t^{-1}I_{\nu+1}(t) = \int_0^1 x^{\nu+\frac{1}{2}} \sqrt{x} I_\nu(tx)\,\mathrm{d}x\,,$$

we recognize that

$$g(x) = x^{\nu+1/2} \in L^2(0,1), \text{ for all } \nu > -1 \qquad \text{and} \qquad f(t) = t^{-1}I_{\nu+1}(t)\,.$$

Now, from (5) we can immediately get (11). Using the well–known identities

$$I_{\frac{1}{2}}(z) = \sqrt{\frac{2}{\pi}}\,\frac{\sinh z}{\sqrt{z}}, \qquad I_{\frac{3}{2}}(z) = \sqrt{\frac{2}{\pi}}\,\frac{z\cosh z - \sinh z}{z^{3/2}}$$

and bearing in mind that zeros of $J_{\frac{1}{2}}$ are of the form $j_{\frac{1}{2},k} = k\pi$, $k \in \mathbb{N}$, for $\nu = 1/2$ equation (11) becomes

$$\frac{\cosh t}{\sinh t} - \frac{1}{t} = 2t \sum_{k\geq 1} \frac{1}{t^2 + (k\pi)^2}, \qquad t \neq 0$$

and this expression is equivalent to the hyperbolic cotangent sum. □

Remark 2. Equality (11) is already known as a Mittag–Leffler expansion [3, Eq. 7.9.3].

The formula

$$\sum_{k\geq 1} \frac{1}{t^2 + k^2} = \frac{\pi}{2t}\coth(\pi t) - \frac{1}{2t^2}, \qquad t \neq 0$$

was considered by Hamburger [7, p. 130, Eq. (C)] in a slightly different form

$$1 + 2\sum_{k\geq 1} \mathrm{e}^{-2\pi k t} = \mathrm{i}\cot \pi \mathrm{i} t = \frac{1}{\pi t} + \frac{2t}{\pi}\sum_{k\geq 1}\frac{1}{t^2+k^2}, \qquad t \neq \mathrm{i}k\,.$$

Also, subsequent complex analytical generalizations of Hamburger's formula can be found in [2].

Corollary 1.2. *For* $\nu \in (-1,1)\backslash\{0\}$ *it holds*

$$\frac{1}{I_\nu(t)} = \frac{2^\nu \Gamma(\nu)}{t^{\nu-1}}\left(\frac{\nu}{t} - \frac{t}{2^{\nu-1}\Gamma(\nu)}\sum_{k\geq 1}\frac{j_{\nu,k}^{\nu-1}}{J_{\nu+1}(j_{\nu,k})\,(t^2 + j_{\nu,k}^2)}\right). \tag{12}$$

Proof. From the recursive relation

$$t\,I_{\nu-1}(t) - t\,I_{\nu+1}(t) = 2\nu\,I_\nu(t)$$

and equality (11) we can conclude that

$$\frac{I_{\nu-1}(t)}{I_\nu(t)} = \frac{I_{\nu+1}(t)}{I_\nu(t)} + \frac{2\nu}{t} = 2t \sum_{k\geq 1} \frac{1}{t^2 + j_{\nu,k}^2} + \frac{2\nu}{t}, \quad \nu > -1. \tag{13}$$

Now, by using the integral expression [6, p. 668, Eq. 6.561.11]

$$t^{-1} I_{\nu-1}(t) - \frac{t^{\nu-2}}{2^{\nu-1}\Gamma(\nu)} = \int_0^1 x^{1-\nu} I_\nu(tx)\,\mathrm{d}x,$$

where we recognize that $g(x) = x^{1/2-\nu} \in L^2(0,1)$ for all $\nu < 1$ and $f(t) = t^{-1} I_{\nu-1}(t) - \frac{t^{\nu-2}}{2^{\nu-1}\Gamma(\nu)}$, from (5) we can conclude that

$$\frac{I_{\nu-1}(t)}{I_\nu(t)} - \frac{t^{\nu-1}}{2^{\nu-1}\Gamma(\nu) I_\nu(t)} = 2t \sum_{k\geq 1} \frac{1}{t^2 + j_{\nu,k}^2} \left(1 - \frac{t_k^{\nu-1}}{2^{\nu-1}\Gamma(\nu) I_{\nu+1}(t_k)}\right).$$

Combining the previous expression and (13) we get

$$\frac{t^{\nu-1}}{2^{\nu-1}\Gamma(\nu) I_\nu(t)} = \frac{2\nu}{t} + \frac{2t}{2^{\nu-1}\Gamma(\nu)} \sum_{k\geq 1} \frac{t_k^{\nu-1}}{I_{\nu+1}(t_k)\,(t^2 + j_{\nu,k}^2)},$$

which immediately gives the desired summation formula (12). Here, we also assumed that $\nu \neq 0$, because $\Gamma(0) = (-1)! = +\infty$. □

Remark 3. A result similar to (12) was deduced by Ismail and Kelker (see [11, Theorem 4.10, p. 896]). They proved that

$$\frac{t^{\nu/2}}{I_\nu(\sqrt{t})} = -2 \sum_{k\geq 1} \frac{j_{\nu,k}^{\nu+1}}{(t + j_{\nu,k}^2) J_\nu'(j_{\nu,k})}, \; \nu > -1.$$

Corollary 1.3. *For $\nu > 0$ we have*

$$I_\nu^2\left(\frac{t}{2}\right) = 2(-1)^{-\nu} t^\nu I_\nu(t) \sum_{k\geq 1} \frac{j_{\nu,k}^{1-\nu} I_\nu^2\left(\frac{\mathrm{i}}{2} j_{\nu,k}\right)}{(t^2 + j_{\nu,k}^2) J_{\nu+1}(j_{\nu,k})}. \tag{14}$$

Proof. Using the same procedure as above, with the help of the integral representation [6, p. 672, Eq. 6.567.12]

$$2^{-\nu-1}\sqrt{\pi} t^{-\nu} \Gamma\left(\nu + \tfrac{1}{2}\right) I_\nu^2\left(\tfrac{t}{2}\right) = \int_0^1 x^\nu (1-x^2)^{\nu-1/2} I_\nu(tx)\,\mathrm{d}x,$$

where the kernel function $g(x) = (x - x^3)^{\nu-1/2}$ is in $L^2(0,1)$ for all $\nu > 0$, setting $f(t) = 2^{-\nu-1}\sqrt{\pi} t^{-\nu} \Gamma\left(\nu + \frac{1}{2}\right) I_\nu^2\left(\frac{t}{2}\right)$, by virtue of (5) and using the identities $I_\nu(z) = \mathrm{i}^{-\nu} J_\nu(\mathrm{i}z)$, $I_\nu(-z) = (-1)^\nu I_\nu(z)$ we arrive at (14). □

Finally, by using Theorem 1, we derive the sampling expansion formula for a generalized hypergeometric function ${}_2F_3$. Firstly, the *generalized hypergeometric function* ${}_pF_q[z]$ with p numerator parameters $a_1,\cdots,a_p$ and q denominator parameters $b_1,\cdots,b_q$ is defined as the series [20]

$$ {}_pF_q[z] = {}_pF_q\left[\begin{array}{c} a_1,\cdots,a_p \\ b_1,\cdots,b_q \end{array}\middle| z\right] = \sum_{n\geq 0} \frac{\prod_{j=1}^{p}(a_j)_n}{\prod_{j=1}^{q}(b_j)_n}\frac{z^n}{n!}, $$

where $(a)_n$ denotes the Pochhammer symbol (or the shifted factorial) [19]

$$ (a)_n \equiv \frac{\Gamma(a+n)}{\Gamma(a)} = a(a+1)\cdots(a+n-1). $$

When $p \leq q$, the generalized hypergeometric function converges for all complex values of z; thus, ${}_pF_q[z]$ is an entire function. When $p > q+1$, the series converges only for $z=0$, unless it terminates (as when one of the parameters a_i is a negative integer) and in that case it is just a polynomial in z. When $p = q+1$, the series converges in the unit disk $|z|<1$, and also for $|z|=1$ provided that $\Re\left\{\sum_{j=1}^{q} b_j - \sum_{j=1}^{p} a_j\right\} > 0$.

Further, we need the Fox-Wright generalized hypergeometric function ${}_p\Psi_q^*[\cdot]$ with p numerator parameters $a_1,\cdots,a_p$ and q denominator parameters $b_1,\cdots,b_q$, which is defined by [15, p. 56]

$$ {}_p\Psi_q^*\left[\begin{array}{c} (a_1,\rho_1),\cdots,(a_p,\rho_p) \\ (b_1,\sigma_1),\cdots,(b_q,\sigma_q) \end{array}\middle| z\right] = \sum_{n=0}^{\infty} \frac{\prod_{j=1}^{p}(a_j)_{\rho_j n}}{\prod_{j=1}^{q}(b_j)_{\sigma_j n}}\frac{z^n}{n!}, \tag{15} $$

where $a_j, b_k \in \mathbb{C}$ and $\rho_j, \sigma_k \in \mathbb{R}_+$, $j=1,\cdots,p$; $k=1,\cdots,q$. The defining series in (15) converges in the whole complex z-plane when

$$ \Delta := \sum_{j=1}^{q}\sigma_j - \sum_{j=1}^{p}\rho_j > -1; $$

when $\Delta = 0$, the series in (15) converges for $|z| < \nabla$, where

$$ \nabla := \left(\prod_{j=1}^{p}\rho_j^{-\rho_j}\right)\left(\prod_{j=1}^{q}\sigma_j^{\sigma_j}\right). $$

Corollary 1.4. *For all* t,λ,ν,μ *such that* $\min\left(t,\lambda-1,\nu+1,\mu-\frac{1}{2}\right) > 0$ *we have*

$$ \begin{aligned} &{}_2F_3\left[\begin{array}{c} \frac{1}{2}(\nu+\lambda), \quad \frac{1}{2}(\nu+\lambda+1) \\ \nu+1, \frac{1}{2}(\nu+\lambda+\mu), \frac{1}{2}(\nu+\lambda+\mu+1) \end{array}\middle| \frac{t^2}{4}\right] \\ &\quad = \frac{2I_\nu(t)}{t^\nu}\sum_{k\geq 1}\frac{j_{\nu,k}^{\nu+1}\,{}_1\Psi_2^*\left[\begin{array}{c} (\nu+\lambda,2) \\ (\nu+1,1),(\nu+\lambda+\mu,2) \end{array}\middle| \frac{-j_{\nu,k}^2}{4}\right]}{(t^2+j_{\nu,k}^2)J_{\nu+1}(j_{\nu,k})}. \end{aligned} \tag{16} $$

Proof. Consider the integral representation formula [6, p. 673, 6.569] derived for J_ν. Its corresponding modified Bessel I_ν–variant reads as follows:

$$\int_0^1 x^{\lambda-1}(1-x)^{\mu-1} I_\nu(tx)\,\mathrm{d}x = \frac{2^{1-2\nu-\lambda-\mu}\sqrt{\pi}\,t^\nu\,\Gamma(\nu+\lambda)\Gamma(\mu)}{\Gamma(\nu+1)\Gamma\left(\frac{\nu+\lambda+\mu}{2}\right)\Gamma\left(\frac{\nu+\lambda+\mu+1}{2}\right)} \times {}_2F_3\left[\begin{matrix}\frac{1}{2}(\nu+\lambda), & \frac{1}{2}(\nu+\lambda+1)\\ \nu+1, \frac{1}{2}(\nu+\lambda+\mu), & \frac{1}{2}(\nu+\lambda+\mu+1)\end{matrix}\,\middle|\,\frac{t^2}{4}\right],$$

and it is valid for $\min(t,\lambda,\nu+\lambda,\mu)>0$. Choosing $g(x)=x^{\lambda-\frac{3}{2}}(1-x)^{\mu-1}\in L^2(0,1)$ for $\mu>\frac{1}{2}$ and $\lambda>1$ and then applying Theorem 1 we arrive at

$$\begin{aligned} &t^\nu\,{}_2F_3\left[\begin{matrix}\frac{1}{2}(\nu+\lambda), & \frac{1}{2}(\nu+\lambda+1)\\ \nu+1, \frac{1}{2}(\nu+\lambda+\mu), & \frac{1}{2}(\nu+\lambda+\mu+1)\end{matrix}\,\middle|\,\frac{t^2}{4}\right]\\ &\quad= 2I_\nu(t)\sum_{k\geq 1}\frac{j_{\nu,k}^{\nu+1}\,{}_2F_3\left[\begin{matrix}\frac{\nu+\lambda}{2}, & \frac{\nu+\lambda+1}{2}\\ \nu+1, \frac{\nu+\lambda+\mu}{2}, & \frac{\nu+\lambda+\mu+1}{2}\end{matrix}\,\middle|\,\frac{-j_{\nu,k}^2}{4}\right]}{(t^2+j_{\nu,k}^2)J_{\nu+1}(j_{\nu,k})}. \end{aligned} \tag{17}$$

Now, with the aid of the property of the Pocchammer symbol

$$(x)_{2n}=2^{2n}\left(\frac{x}{2}\right)_n\left(\frac{1+x}{2}\right)_n,$$

we have that

$$\begin{aligned} &{}_2F_3\left[\begin{matrix}\frac{\nu+\lambda}{2}, & \frac{\nu+\lambda+1}{2}\\ \nu+1, \frac{\nu+\lambda+\mu}{2}, & \frac{\nu+\lambda+\mu+1}{2}\end{matrix}\,\middle|\,\frac{-j_{\nu,k}^2}{4}\right]\\ &\quad=\sum_{n\geq 0}\frac{(\nu+\lambda)_{2n}}{(\nu+1)_n(\nu+\lambda+\mu)_{2n}}\frac{(-j_{\nu,k}^2)^n}{4^n\,n!}\\ &\quad={}_1\Psi_2^*\left[\begin{matrix}(\nu+\lambda,2)\\ (\nu+1,1),(\nu+\lambda+\mu,2)\end{matrix}\,\middle|\,\frac{-j_{\nu,k}^2}{4}\right]. \end{aligned} \tag{18}$$

Summing (17) and (18) we obtain the summation formula (16). □

3 Truncation error upper bounds in I–Bessel sampling expansions

In this section our aim is to derive a uniform upper bound for the truncation error for the Bessel–sampling expansion (5).

The truncated sampling reconstruction sum of the size $N\in\mathbb{N}$ for the Bessel–sampling formula (5) is defined as

$$\mathscr{S}_N^I(f;t)=2I_\nu(t)\sum_{k=1}^N\frac{t_k f(t_k)}{I_{\nu+1}(t_k)\left(t^2-t_k^2\right)},$$

where $t \in \mathbb{R}$, $t_k = -\mathrm{i}\, j_{\nu,k}$ is the kth zero of I_ν, $\nu > -1$ and the function f has a band–region contained in $(0,1)$. Let us also define the truncation error of the order N as the quantity

$$\mathscr{T}_N^I(f;t) = \left|f(t) - \mathscr{S}_N^I(f;t)\right| = \left|2I_\nu(t) \sum_{k\geq N+1} \frac{t_k f(t_k)}{I_{\nu+1}(t_k)\left(t^2 - t_k^2\right)}\right|.$$

We are looking for an upper bound for the truncation error $\mathscr{T}_N^I(f;t)$ in the case when the input function possesses a polynomially decaying upper bound like

$$|f(t)| \leq A\,|t|^{-(r+1)}, \qquad A > 0,\, r > 0\,, t \neq 0.$$

Thus, for all $\nu > -1$ we have

$$\mathscr{T}_N^I(f;t) \leq 2A \sum_{k\geq N+1} \frac{|I_\nu(t)|}{j_{\nu,k}^r (t^2 + j_{\nu,k}^2)\,\left|J_{\nu+1}(j_{\nu,k})\right|},$$

because of the identity $I_\nu(t) = \mathrm{i}^{-\nu} J_\nu(\mathrm{i}t)$ and the fact that all zeros $j_{\nu,k}$ are positive for $\nu > -1$.

Using an integral representation [28, p. 181, Eq. (4)]

$$I_\nu(z) = \frac{1}{\pi}\int_0^\pi \mathrm{e}^{z\cos t}\cos \nu t\,\mathrm{d}t - \frac{\sin(\nu\pi)}{\pi}\int_0^\infty \mathrm{e}^{-z\cosh t - \nu t}\,\mathrm{d}t, \quad \nu > 0$$

we can conclude that

$$|I_\nu(t)| \leq I_0(t) + \frac{1}{\pi}\int_0^\infty \mathrm{e}^{-t\cosh x}\,\mathrm{d}x = I_0(t) + \frac{1}{\pi}K_0(t), \qquad t > 0,$$

thus

$$\sup_{\nu<t<y_{\nu,2}} |I_\nu(t)| = I_0(y_{\nu,2}) + \frac{1}{\pi}K_0(\nu) := H_1\,. \tag{19}$$

Using (19) and the particular value of the Rayleigh function [28, p. 502]

$$\sigma_\nu^{(r)} = \sum_{k\geq 1} \frac{1}{j_{\nu,k}^{2r}}, \qquad r \in \mathbb{N},$$

for $r = 1$, that is $\sigma_\nu^{(1)} = (4(\nu+1))^{-1}$ bearing in mind that $|t| > 0$, it holds

$$\begin{aligned}\mathscr{T}_N^I(f;t) &< \frac{2A\,H_1}{\min\limits_{k\geq N+1} j_{\nu,k}^r\,|J_{\nu+1}(j_{\nu,k})|} \sum_{k\geq 1}\frac{1}{j_{\nu,k}^2} \\ &= \frac{A\,H_1}{2(\nu+1)\min\limits_{k\geq N+1} j_{\nu,k}^r\,|J_{\nu+1}(j_{\nu,k})|}\,.\end{aligned} \tag{20}$$

It remains to minimize the expression in the denominator of (20). For that purpose we exploit Krasikov's bound [18, p. 84, Theorem 2]:

$$J_\nu^2(x) \geq \frac{4\left(x^2 - (2\nu+1)(2\nu+5)\right)}{\pi\left((4x-\nu)^{\frac{3}{2}} + \mu\right)}, \qquad x > \frac{1}{2}\sqrt{\mu + \mu^{\frac{3}{2}}},$$

where

$$\mu = (2\nu+1)(2\nu+3), \qquad \nu > -\tfrac{1}{2}.$$

In [18] Krasikov pointed out that this lower bound is poor in the transition region around zeros $j_{\nu,k}$, while it fits well the Bessel function of the first kind $J_\nu(t)$ in the oscillatory region. Since we have to estimate $J_{\nu+1}(j_{\nu,k})$, these values are obviously separated from zero as $j_{\nu+1,k}$ and $j_{\nu,k}$ interlace and the latter zero belongs to the oscillatory region of $J_{\nu+1}(t)$. Hence

$$\left|J_{\nu+1}(j_{\nu,k})\right| \geq \frac{2}{\sqrt{\pi}} \left\{ \frac{j_{\nu,k}^2 - (2\nu+3)(2\nu+7)}{(4j_{\nu,k} - \nu - 1)^{\frac{3}{2}} + \mu^*} \right\}^{\frac{1}{2}}, \tag{21}$$

where

$$\mu^* = \frac{2\nu+5}{2\nu+1}\,\mu > 15.$$

The range of validity of (21) is

$$x = j_{\nu,N+1} > \frac{1}{2}\sqrt{\mu^* + (\mu^*)^{\frac{3}{2}}} \approx 4.27447. \tag{22}$$

Thus, for N large enough, applying the MacMahon asymptotics for the zeros of the cylinder functions [28, p. 506] (see also Schläfli's footnote [21, p. 137])

$$y_{\nu,N} = \left(N + \tfrac{\nu}{2} - \tfrac{1}{4}\right)\pi + \mathscr{O}(N^{-1}), \qquad N \to \infty, \tag{23}$$

and the well–known interlacing inequalities for the positive zeros $j_{\nu,k}, j'_{\nu,k}, y_{\nu,k}$ and $y'_{\nu,k}$ of Bessel functions $J_\nu(t), J'_\nu(t), Y_\nu(t)$ and $Y'_\nu(t)$, respectively [1, p. 370],

$$\nu \leq j'_{\nu,1} < y_{\nu,1} < y'_{\nu,1} < j_{\nu,1} < j'_{\nu,2} < y_{\nu,2} < \cdots,$$

we have that the solution of (22) in N for the range $\nu > 0$ becomes:

$$N + \mathscr{O}(N^{-1}) > \frac{1}{2\pi}\sqrt{15 + 15^{\frac{3}{2}}} + \frac{1-2\nu}{4} \approx 1.61061 - \frac{\nu}{2}.$$

Thus, (22) is not redundant for

$$\nu \leq \frac{1}{\pi}\sqrt{15 + 15^{\frac{3}{2}}} - \frac{3}{2} =: \nu^* \approx 1.22141.$$

Now, bearing in mind that $\nu \in (0, \nu^*]$, by (21) we deduce

$$j_{\nu,k}^r \left|J_{\nu+1}(j_{\nu,k})\right| \geq \frac{2}{\sqrt{\pi}}\, j_{\nu,k}^r \left\{ \frac{j_{\nu,k}^2 - (2\nu+3)(2\nu+7)}{(4j_{\nu,k} - \nu - 1)^{\frac{3}{2}} + \mu^*} \right\}^{\frac{1}{2}} =: L_k(\nu).$$

It is not hard to see that the function

$$x \mapsto x^r \left\{ \frac{x^2 - (2\nu+3)(2\nu+7)}{(4x - \nu - 1)^{\frac{3}{2}} + \mu^*} \right\}^{\frac{1}{2}}$$

monotonically increases in its domain, thus

$$\min_{k\geq N+1} j_{\nu,k}^{r}\,|J_{\nu+1}(j_{\nu,k})| \geq L_{N+1}(\nu)\,,$$

where we assume $N \geq 2$, because of positivity of the expression in the numerator of $L_{N+1}^2(\nu)$. Thus, we proved the result given in the following theorem.

Theorem 2. *Let $\nu \in (0,\nu^*]$, where*

$$\nu^* = \frac{1}{\pi}\sqrt{15+15^{\frac{3}{2}}} - \frac{3}{2}.$$

Then for all $t \in (\nu, y_{\nu,2})$, $\min(A,r) > 0$ and all $N \geq 3$ there holds the truncation error upper bound

$$\mathscr{T}_N^I(f;t) < \frac{A\,H_1}{2(\nu+1)\,L_N(\nu)} := U_N^I(t), \tag{24}$$

where

$$H_1 = I_0(y_{\nu,2}) + \frac{1}{\pi}K_0(\nu),$$

$$L_N(\nu) = \frac{2}{\sqrt{\pi}}\,j_{\nu,N}^{r}\left\{\frac{j_{\nu,N}^2-(2\nu+3)(2\nu+7)}{(4j_{\nu,N}-\nu-1)^{\frac{3}{2}}+\mu^*}\right\}^{\frac{1}{2}}.$$

Moreover, for N large enough the asymptotics of the truncation error is

$$\mathscr{T}_N^I(f;t) = \mathscr{O}\left(N^{-r-\frac{1}{4}}\right).$$

Proof. As already proved, an upper bound (24), it remains to show the asymptotics of the truncation error $\mathscr{T}_N^I(f;t)$. Thus, for fixed t and N large enough, again by applying (23) we have

$$\mathscr{T}_N^I(f;t) = \mathscr{O}\left(U_N^I(t)\right) = \mathscr{O}\left(\frac{1}{L_N(\nu)}\right) = \mathscr{O}\left((j_{\nu,N})^{-r-\frac{1}{4}}\right) = \mathscr{O}\left(N^{-r-\frac{1}{4}}\right),$$

which completes the proof. □

In addition, we will consider an example which includes the results obtained in Corollary 1.3 to demonstrate the Bessel–sampling approximation behavior.

Example 1. Let us denote

$$h(t) = \frac{(-1)^{\nu}I_{\nu}^2\left(\frac{t}{2}\right)}{2t^{\nu}I_{\nu}(t)}, \qquad \mathscr{S}_N^I(h;t) = \sum_{k\geq 1}\frac{j_{\nu,k}^{1-\nu}I_{\nu}^2\left(\frac{\mathrm{i}}{2}\,j_{\nu,k}\right)}{(t^2+j_{\nu,k}^2)J_{\nu+1}(j_{\nu,k})}\,.$$

In Fig. 1 we present the input function h and the truncated sampling I–Bessel sampling approximation sums $\mathscr{S}_N^I(h;t)$ for $N = 15, 150, 3000$, respectively, on the t–domain $[0, j_{0,1}] \approx [0, 2.40483]$ in case $\nu = 0$.

ACKNOWLEDGEMENT

The author wishes to thank Tibor Pogány for his very kind and continuous help in preparing, improving and finishing the manuscript of this article and also Árpád Baricz for his valuable observations and suggestions.

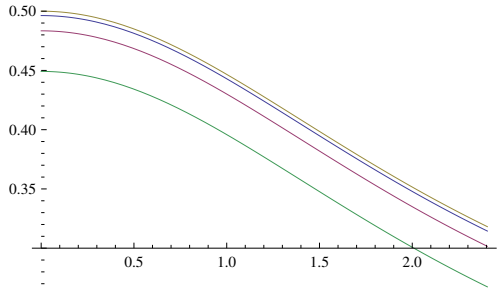

Figure 1
I–Bessel–sampling approximation patterns associated with Eq. (14) in Corollary 1.3. Legend: $h(t)$ – yellow, $\mathscr{S}^I_{15}(h;t)$ – green, $\mathscr{S}^I_{150}(h;t)$ – violet and $\mathscr{S}^I_{3000}(h;t)$ – blue.

References

[1] M. ABRAMOWITZ, I. A. STEGUN, Editors, *Handbook of Mathematical Functions with Formulas, Graphs and Mathematical Tables*, Applied Mathematics Series 55, National Bureau of Standards, Washington, D. C., 1964; Reprinted by Dover Publications, New York, 1965.

[2] B. BERNDT, P. LEVY, Problem 76–11. A Bessel function summation, *SIAM Rev.*, **27(3)**, 446, 1985, In: M. Klamkin, Editor, Problems in Applied Mathematics: Selections from SIAM Review, *Society for Industrial and Applied Mathematics (SIAM)*, Philadelphia, PA, 179–180, 1990.

[3] A. ERDÉLYI, W. MAGNUS, F. OBERHETTINGER, F. TRICOMI, *Higher Transcendental Functions, Vol. 2*, McGraw-Hill, New York, 1954.

[4] W. N. EVERITT, *A catalogue of Sturm–Liouville differential equations*, In: W. O. Amrein, A. M. Hinz, D. B. Pearson, Editors, *Sturm-Liouville Theory, Past and Present*, 271–331, Birkhäuser Verlag, Basel, 2005.

[5] W. N. EVERITT, G. NASRI–ROUDSARI, J. REHBERG, A note on the analytic form of the Kramer sampling theorem, *Results Math.*, **34(3–4)** (1998), 310–319.

[6] I. GRADSHTEYN, I. RYZHIK, *Tables of Integrals, Series and Products*, Sixth ed., Academic Press, New York, 2000.

[7] H. HAMBURGER, Über einige Beziehungen, die mit der Funktionalgleichung der Riemannschen ζ–Funktion äquivalent sind, *Math. Anal.*, **85** (1922), 129–140.

[8] H. D. HELMS, J. B. THOMAS, On truncation error of sampling theorem expansion, *Proc. IRE*, **50** (1962), 179–184.

[9] J. R. HIGGINS, *Sampling Theory in Fourier and Signal Analysis*, Clarendon Press, Oxford, 1996.

[10] J. R. HIGGINS, R. L. STENS, Editors, *Sampling Theory in Fourier and Signal Analysis: Advanced Topics*, Oxford University Press, 67–95, 1999.

[11] M. E. H. ISMAIL, D. H. KELKER, Special functions, Stieltjes transforms and infinite divisibility, *SIAM J. Math. Anal.*, **10(5)** (1979), 884–901.

[12] D. JANKOV MAŠIREVIĆ, T. K. POGÁNY, Á. BARICZ, A. GALÁNTAI, Sampling Bessel functions and Bessel sampling, *Proceedings of the 8th International Symposium on Applied Computational Intelligence and Informatics*, May 23-25, 2013, Timisoara, Romania, 79–84.

[13] A. J. JERRI, The Shannon sampling theorem – its various extensions and applications: A tutorial review, *Proc. IEEE*, **65(11)** (1977), 1565–1596.

[14] YU. I. KHURGIN, V. P. YAKOVLEV, Progress in the Soviet Union on the theory and applications of bandlimited functions, *Proc. IEEE*, **65(5)** (1977), 1005–1028.

[15] A. A. KILBAS, H. M. SRIVASTAVA, J. J. TRUJILLO, *Theory and Applicatios of Fractioal Differential Equatios; North–Holland Mathematical Studies*, Vol. 204, Elsevier (North–Holland) Science Publishers, Amsterdam, London and New York, 2006.

[16] L. KNOCKAERT, A Class of Scaled Bessel Sampling Theorems, *IEEE Trans. Signal Process.*, **59(10)** (2011), 5082–5086.

[17] H. P. KRAMER, A generalized sampling theorem, *J. Math. Phys.*, **38** (1959), 68–72.

[18] I. KRASIKOV, Uniform bounds for Bessel functions, *J. Appl. Anal.*, **12(1)** (2006), 83–91.

[19] Y. L. LUKE, *The Special Functions and Their Approximations*, Vol. 1, Academic Press, New York, 1969.

[20] A. R. MILLER, On Mellin transform of products of Bessel and generalized hypergeometric functions, *J. Comput. Appl. Math.*, **85** (1997), 271–286.

[21] L. SCHLÄFLI, Über die Convergenz der Entwicklung einer arbiträren Funktion $f(x)$ nach den Bessel'schen Funktionen

$$\overset{a}{J}(\beta_1 x), \overset{a}{J}(\beta_2 x), \overset{a}{J}(\beta_3 x), \cdots\cdots$$

wo $\beta_1, \beta_2, \beta_3, \ldots$ die positiven Wurzeln der Gleichung $\overset{a}{J}(\beta) = 0$ vorstellen, *Math. Ann.*, **10** (1876), 137–142.

[22] K. SEIP, *Interpolation and sampling in spaces of analytic functions*, University Lecture Series 33, American Mathematical Society, Providence, RI, 2004.

[23] E. TITCHMARCH, *Eigenfunction Expansions Associated with Second–Order Differential Equations, Part I*, Second ed., Clarendon Press, Oxford, 1962.

[24] M. UNSER, Sampling—50 years after Shannon, *Proc. IEEE*, **88(4)** (2000), 569–587.

[25] A. I. ZAYED, *Advances in Shannon's Sampling Theory*, CRC Press, New York, 1993.

[26] A. I. ZAYED, On Kramer's sampling theorem associated with general Sturm-Liouville problems and Lagrange interpolation, *SIAM J. Appl. Math.*, **51** (1991), 575-604.

[27] A. ZAYED, G. HINSEN, P. BUTZER, On Lagrange interpolation and Kramer-type sampling theorems associated with Sturm-Liouville problems, *SIAM J. Appl. Math.*, **50** (1990), 893–909.

[28] G. N. WATSON, *A treatise on the theory of Bessel functions*, Cambridge University Press, Cambridge, 1958.

[29] P. WEISS, Sampling theorems associated with the Sturm–Liouville systems, *Bull. Amer. Math. Soc.*, **163** (1957), 242.

[30] J. M. WHITTAKER, *Interpolatory Function Theory*, Cambridge University Press, Cambridge, 1935.

[31] K. YAO, Application of reproducing kernel Hilbert spaces – band-limited signal models, *Inf. Contr.*, **11** (1967), 427–444.